Pharmacometric Modelling of Processes in the Haematopoietic System and Blood: Leukocyte Progenitor Proliferation and Maturation In Vitro and in Cancer Patients and Erythrocyte Ageing in Diabetic Patients

Dissertation

zur Erlangung des akademischen Grades des
Doktors der Naturwissenschaften (Dr. rer. nat.)

eingereicht im Fachbereich Biologie, Chemie, Pharmazie
der Freien Universität Berlin

vorgelegt von

Valerie Christine Nock

aus Biberach an der Riß

2013

Die folgende Arbeit wurde von 2009 bis 2012 unter der Leitung von
Frau Professor Dr. Charlotte Kloft
am Institut für Pharmazie
der Martin-Luther-Universität Halle-Wittenberg und
der Freien Universität Berlin erstellt.

1. Gutachter: Frau Prof. Dr. Charlotte Kloft
2. Gutachter: Herr Prof. Dr. Christoph Ritter

Disputation am 08. Mai 2013

Für meine Familie,
Onkel Reinhard
und Tante Renate.

Contents

Abbreviations and Symbols

Abbreviation	Definition
a_N	Amount of drug in the N-th transit compartment
AAG	α_1-acid glycoprotein
AGE	Age
AIC	Akaike information criterion
ALB	Albumin
ALT	Alanine transaminase
ASCR	Autologuous stem cell rescue
AST	Aspartate transaminase
AUC	Area under the curve
B1, B2, B3	Baseline estimation method 1, 2 and 3
Bcl-2	B-cell lymphoma 2
BMI	Body mass index
BSA	Body surface area
C	Carboplatin
C_{INI}	Estimated concentration of cells describing the initial increase in leukocyte concentrations
C(t)	Concentration at time t
CFU	Colony-forming unit
CFU-GM/Mk/E	Colony-forming unit granulocytes macrophages/ megakaryocytes/erythrocytes
Circ(t)	Predicted concentration of circulating cells at time t
Circ(t_0)	Predicted concentration of circulating cells before therapy
Circ($t_{0,i}$)	Individual predicted concentration of circulating cells before therapy
Circ($t_{0,i,obs}$)	Individual observed concentration of circulating cells before therapy
CL	Clearance
CLCR	Creatinine clearance
C_{max}	Maximal drug concentration

continued...

Abbreviation	Definition
CMT	Compartment
COV	Covariate
CREA	Serum creatinine
CV	Coefficient of variation
CWRES	Conditional weighted residuals
CYP	Cytochrome P_{450}
ΔOFV	Difference in the objective function value
D	Day
DEXA	Dexamethasone
df	Degrees of freedom
DLCO	Diffusion capacity for carbon monoxide
DNA	Deoxyribonucleic acid
E	Etoposide
$E_{A,B}$	Joint drug effect of drug A and B
$E_{drug}(t)$	Drug effect at time t
E_{max}	Maximal effect
E_{50}	Potency of the drug combination
	at a given combination of the drugs' concentrations
EBE	Empirical Bayes estimate
$EC_{50/70/90}$	Concentration at half (70%, 90%) of the maximal effect
EMA	European Medicines Agency
EPO	Erythropoietin
EVID	Event identifier
F	Bioavailability
FAAS	Flameless atomic absorption spectrometry
FDA	Food and Drug Administration
FO	First-order
FOCE	First-order conditional estimates
FOCE+I	First-order conditional estimates with interaction
FPG	Fasting plasma glucose
G-CSF	Granulocyte colony-stimulating factor
GFR	Glomerular filtration rate
GGT	Gamma-glutamyltransferase

continued...

Abbreviation	Definition
GLP-1	Glucagon-like peptide 1
GOF	Goodness of fit
HDCT	High-dose chemotherapy
HPLC	High-performance liquid chromatography
H_3PO_4	Phosphoric acid
HbA_{1c}	Glycated haemoglobin
HT	Height
I	Ifosfamind
IC	Inhibitory concentration
ID	Individual identifier
IIV	Interindividual variability
INI_{DEXA}	Compartment for the description of the initial increase in leukocyte concentrations
IOV	Interoccasion variability
i.v.	Intravenous
IPRED	Individual predictions
IWRES	Individual weighted residuals
k_a	Absorption rate constant
k_{el}	Elimination rate constant of leukocytes
k_{GL}	Glycation rate constant
k_{GL2}	Glycation rate constant of the second glycation pathway
k_{in}	Production rate constant of FPG
k_{INH}	Release rate of erythrocytes from the bone marrow
k_{INI}	Transition rate constant describing the inital increase in leukocyte concentrations
k_{out}	Elimination rate constant of FPG
k_{prol}	Proliferation rate constant of leukocytes and neutrophils
k_{SCR}	Transition rate constant for the ASCR
k_{tr}	Transition rate constant
$k_{12/21}$	Mirco-constants describing drug distribution from and to the central volume of distribution, respectively
LLP	Log likelihood profiling
ln	logarithmic (natural logarithm)

continued...

Abbreviation	Definition
LLOQ	Lower limit of quantification
M	Molar
MDV	Missing dependent variable
MMT	Mean maturation time
MRT	Mean residence time
MTT	(3-(4,5-Dimethylthiazol-2-yl)-2,5-diphenyltetrazolium bromide
MT_{SCR}	Mean time associated with the autologuos stem cell rescue (homing of cells)
MT_{INI}	Mean time associated with the description of the initial increase in leukocyte concentrations
n	Number of transitions
N	Number of transit compartments
Na_2HPO_4	Disodium monohydrogenphosphate
NA	Not available
NLME	Nonlinear mixed-effects
NR	Not reported
OF_{ELS}	Extended least square objective function
OFV	Objective function value
PD	Pharmacodynamic
PK	Pharmacokinetic
PPG	Postprandial glucose
PRED	Population predictions
Prol	Compartment of proliferating cells in the bone marrow
p.o.	Per oral
PsN©	Pearl-speaks-NONMEM
Pt	Platinum
Q	Intercompartmental clearance
RSE	Relative standard error
RV	Residual variability
s.c.	Subcutaneous
SCM	Stepwise covariate modelling
SCR	Compartment for the autologuous stem cell rescue
SD	Standard deviation

continued...

Abbreviation	Definition
SI	Survival Index
SL	Slope of linear relation between drug effect and concentration
T	Thiotepa
T1, T_N	Transit compartment 1 and N
TT	Mean transition time
TALD	Time after last dose administration
t	Time
TNF-α	Tumour necrosis factor-alpha
Transit SCR	Transit compartment associated with the stem cell rescue
U_A, U_B	Transformed drug concentrations of drug A or B ($C_{A \text{ or } B} \cdot SL_{A \text{ or } B}$)
V	Volume of distribution
$V_{cen/per}$	Central/Peripheral volume of distribution
VPC	Visual predictive check
WRES	Weighted residuals
WT	Weight
-2LL	Minus two times the log likelihood

end

Symbol	Definition
$E(y_i)$	Vector of expectations for y_i
ϵ	Random effect parameter describing deviation between individual predicted and observed measurement
$\epsilon_{add,ij}$	Additive residual variability for the j-th observation in the i-th individual
$\epsilon_{prop,ij}$	Proportional residual variability for the j-th observation in the i-th individual
η	Individual random-effects parameter estimate
η_i	Vector of individual random effects
Ω	Variance-covariance matrix of η
ω^2	Variance of η
P_{ki}	k-th model parameter of the i-th individual
ϕ_i	Model parameters of the i-th individual
Σ	Variance-covariance matrix of ϵ
σ^2	Variance of ϵ
θ	Typical population parameter estimate; (vector of) fixed-effects parameter
$var(y_i)$	Variance-covariance matrix of y_i
X_{ij}	Design variables for the j-th observation in the i-th individual
y_i	Vector for observations
y_{ij}	j-th observation of the i-th individual
z_i	Vector containing covariate information for the i-th individual
z_{ij}	Design variables for the j-th observation in the i-th individual

end

1 Introduction

1.1 Pharmacometric drug-disease modelling and simulation

1.1.1 History and overview

In 1937, the concept of compartmental analysis was introduced by Teorell who described the disposition of xenobiotics applying first-order kinetic equations which had long been used to describe chemical reactions[1,2]. Dost introduced the concepts of pharmacokinetics in his book "Der Blutspiegel - Kinetik der Konzentrationsabläufe in der Kreislaufflüssigkeit" in 1953[3] which were further characterised by Nelson[4] who first reviewed the basic elements of pharmacokinetics in 1961: absorption, distribution, metabolism and excretion, which still form the basis of modern pharmacokinetic (PK) data analysis. In compartmental analysis PK models typically describe the number of phases in the concentration-time profile after a single drug administration by the corresponding number of compartments[5]. The accurate assessment of the PK behaviour of a drug is of particular importance if the drug is showing a narrow therapeutic range, e.g. drugs in oncology. Whilst the PK describes the fate of a compound in the body, the pharmacodynamic (PD) characterises the biochemical, physiological and pharmacological effects of a substance on the body, microorganisms and parasites[6]. Holford and Sheiner defined PD as the "relationship between drug concentrations at the site of action and drug effects, and factors influencing this relationship"[7]. In their paper from 1982, they defined various PD models describing the effect of a drug in dependency of its concentration by models that might be as simple as linear ones, up to more complex, mechanistic models. The variety of PK and PD models is multifarious, comprising models of more empirical nature ("models of data") and mechanistically motivated ones which include information about the underlying physiological system ("models of system")[8]. PK/PD modelling describes the drug effect over time and can help to assess the efficacy of a drug or relate drug exposure to a clinical outcome or an adverse event. The modelling and simulation approach has been increasingly recognised in preclinical and clinical research and developed to a discipline of its own: "Pharmacometrics", the science of quantitative pharmacology. Williams and Ette defined it more formally as "the science of developing and applying mathematical and statistical methods to characterize, understand, and predict a drug's pharmacokinetic, pharmacodynamic, and biomarker-outcomes behavior"[9].

1.1.2 The population approach

The population PK/PD analysis is the application of a model to describe data from a group of individuals[10]. It allows the description of the typical PK and/or PD profile and, at the same time, the quantification of variability in drug concentration or PD response within a population even when the study design and therefore the sampling varies considerably between individuals. Hence, it is a powerful tool to summarise and characterise large amounts of data. As data from many individuals enter the analysis, complex processes can be identified, which might not always be distinct in analysis of individual patients. More mechanistically motivated models can be developed which allow for extrapolations beyond conditions that have been investigated in the original study. One of the main benefits of population analysis is the investigation of covariates, i.e. patient-specific characteristics, and their relations to model parameters that explain the variability within the population to some extent. In 1984, Steimer et al.[11] reviewed different approaches for the estimation of population parameters. Among them were:

- Naive pooling: Model parameters are estimated based on an analysis that pools all available data neglecting the fact that the data originated from more than one individual. This procedure enables the calculation of point estimates for the model parameters[12].

- Standard two-stage approach: In a first step, model parameters are estimated based on data from each individual. The second step then comprises the characterisation of the distribution of the estimated parameters in the investigated study population by descriptive statistics. Variability can be assessed on the individual level, but the source of variability (interindividual or residual) is neglected resulting in an overestimation of variability in the model parameters[13].

- Nonlinear mixed-effects (NLME) modelling: Data of all individuals is analysed simultaneously taking information from each individual into account, thus, providing distributions for model parameters that can be used to characterise each individuals' model parameters. Sources of variability, including residual variability, can be differentiated and as the information in the data on an individual level is contained, imbalances and confounding correlations can be accounted for[12]. As this approach was applied for the analyses presented in this thesis it will be explained in more detail in the following section.

1.1.3 Nonlinear mixed-effects modelling

The NLME approach provides more accurate estimates of the variability in a population[12–14] and shows several advantages over the standard two-stage approach. For one, the NLME approach is applicable for analysis of unbalanced, rich and sparse data situations, enabling the application of quite complex models, whereas data analysis on an individual level is potentially limiting the model complexity. The possibility of handling sparse data situations allows taking samples at regular visits to the clinic during a study or analyse data from clinical routine without the need for extra sampling time points. Moreover, data from populations that are difficult to study from an ethical point of view such as children, elderly, severely ill patients can be investigated. Unbalanced data, e.g. resulting from studies with different dosing regimens, sampling schemes and administration routes, does not limit the pooling of studies. The term "mixed-effects" refers to the simultaneous estimation of fixed-effects (estimates for structural parameters and covariate effects) as well as random-effects (variability between individuals and residual variability) in one model. The influence of patient-specific characteristics as well as the remaining unexplained variability can be quantified. This enables the identification of subgroups of patients that are inadequately treated or at risk of suffering from adverse events due to a too low or high drug exposure, respectively. With the help of covariates, therapy regimens can be adjusted e.g. in terms of dose, thereby increasing the benefit/risk ratio.
The term "nonlinear" denotes the nonlinear regression used to estimate model parameters. Among many different algorithms that fit a mathematical function to a given set of observations, i.e. estimate values of model parameters, the most widely used is the maximum likelihood estimation method[15]. For the approximation of the likelihood, different algorithms are applied that maximise the likelihood by iteratively changing the values of the model parameters.

Software In the early 1980's, Sheiner and Beal introduced NONMEM® as the first regression program which was specialised in nonlinear systems enabling the estimation of population parameters[12,13,16]. Other approaches exist and some of them were summarised by Aarons[17], including a nonparametric maximum likelihood method, Bayesian methods and variants of the NLME modelling approach. However, over the years NONMEM® has become the by far most common used software in the field of population PK/PD modelling although today several software packages exist (NLME in S-Plus, NLMIX in SAS and R, Phoenix NMLE, Adapt II, etc.) and, lately, MONOLIX is gaining popularity.

1.1.4 Application of PK/PD analysis

The application for modelling and simulation in drug development and clinical research is a broad field. Modelling analyses describe and characterise the data, quantify variability between patients (interindividual variability, IIV) and within a patient (intraindividual/residual variability) and establish relations between drug exposure and clinical outcome, thereby supporting the evaluation and optimisation of drug therapy. The identification of covariates assists in the selection of dosing strategies for individual or subgroups of patients and enables the application of therapeutic drug monitoring.
In 1997, Sheiner introduced the concept of repetitive circles of "learning and confirming" to clinical drug development[18]. The learning step comprises retrospective data analysis or analysis from earlier stages of drug development which then can be used to generate hypotheses that are tested (confirmed) in larger studies, enhancing the efficiency in drug development. Hypotheses can be generated seeking to answer "what if" questions for the optimal dose and the best dosing interval by means of simulations to achieve the desired outcome or minimise the risk of an adverse event[10]. Simulations can also be used to select the most informative and efficient study design by applying optimal design techniques and simulating clinical trials[5].

Population PK/PD modelling in oncology Therapeutic drug monitoring becomes very important when drugs exhibit narrow therapeutic ranges whilst the exposure is related to the clinical outcome, which is, for example, the case in oncology. Population PK/PD analysis can assist in the selection of individual doses, yielding safe and effective dosing regimens with optimal outcome and without causing life-threatening adverse events. However, in oncology, population analyses are faced with special challenges: Toxicity scores and response rates are, in most cases, categorical, sparse, subject to the observer and not seldom a result of cumulative treatment[19]. One exception are haematological data, which are continuous and samples are taken on a continuous time scale. PK/PD modelling has been widely used to characterise myelosuppression, which is one of the most important dose-limiting adverse events in many anticancer regimens.

1.2 Haematopoiesis and lifespans of blood cells

The proliferation, differentiation and maturation processes of haematopoietic progenitor cells in the bone marrow and the survival of the mature cells in the blood share a common element:

a defined period of time or a "lifespan" that they spend in each of these stages. The need of blood cells is high and each year 200 - 300 kg blood cells are produced to maintain steady state in the circulation[20]. Haematopoiesis - the process of blood cell formation - in adults is mainly located in the bone marrow of the flat bones of the pelvis, cranium, ribs and vertebra as well as the proximal ends of femur and humerus. The haematopoietic system consists of a hierarchy of cells which originate from a pool of pluripotent haematopoietic stem cells that can be found in the bone marrow and, to a small extent, in the peripheral blood. Approximately one in 10^5 bone marrow cells is a pluripotent haematopoietic stem cell[21] which gives rise to different types of highly specialised circulating blood cells[22,23]. The pluripotent heamatopoietic stem cells themselves are unspecialised precursor cells which are capable of self-renewal to sustain the stem cell pool and capable of limited differentiation towards the more determined lymphoid stem cell or the multipotent myeloid stem cell[24]. Whilst the pluripotent heamatopoietic stem cells are believed to be dormant and only stochastically awakened to enter the cell cycle, the lineage-specific precursor cells show a high mitotic activity and only little self-renewal capacity. The bone marrow comprises mostly lineage-specific precursor cells which develop into different cell lines dependent on cell-cell interaction and a network of lineage-specific growth factors such as granulocyte colony-stimulating growth factor (G-CSF) or erythropoietin which effect the process of haematopoiesis on multiple levels, acting synergistically with other factors such as cytokines and extracellular matrix components[20]. The lymphoid stem cells give rise to T- and B-lymphocytes whereas erythrocytes, granulocytes, thrombocytes and monocytes arise from the multipotent myeloid stem cell. Leukocytes, or white blood cells, comprise five types of different cell lines: granulocytes (neutrophil, eosinophil, basophil) and agranulocytes (lymphocytes, monocytes). The neutrophil fraction of the granulocytes constitutes 60% to 70% of the total leukocyte count whereas lymphocytes, monocytes, eosinophils and basophils cover approximately 30%, 5%, 2% and less than 1%, respectively[20]. In the human body the cells fulfil a large variety of tasks, reaching from transport of oxygen (erythrocytes), blood haemostasis (thrombocytes) to multi-level response of the immune system (leukocytes). In this thesis the system of leukopoiesis and its impairment during high-dose chemotherapy (HDCT) is characterised. The formation of granulocytes, representing the largest fraction of leukocytes, is schematically depicted in Figure 1.1 as an example for leukopoiesis. Starting from a slowly proliferating pluripotent haematopoietic stem cell, which differentiates into the determined multipotent myeloid stem cell, the cells reach the highly proliferative stages of myeloblasts, promyeloblasts and myelocytes ("lineage specific precursor cells") in which they stay for about 5.5 d. Following these stages, pure maturation processes take place dur-

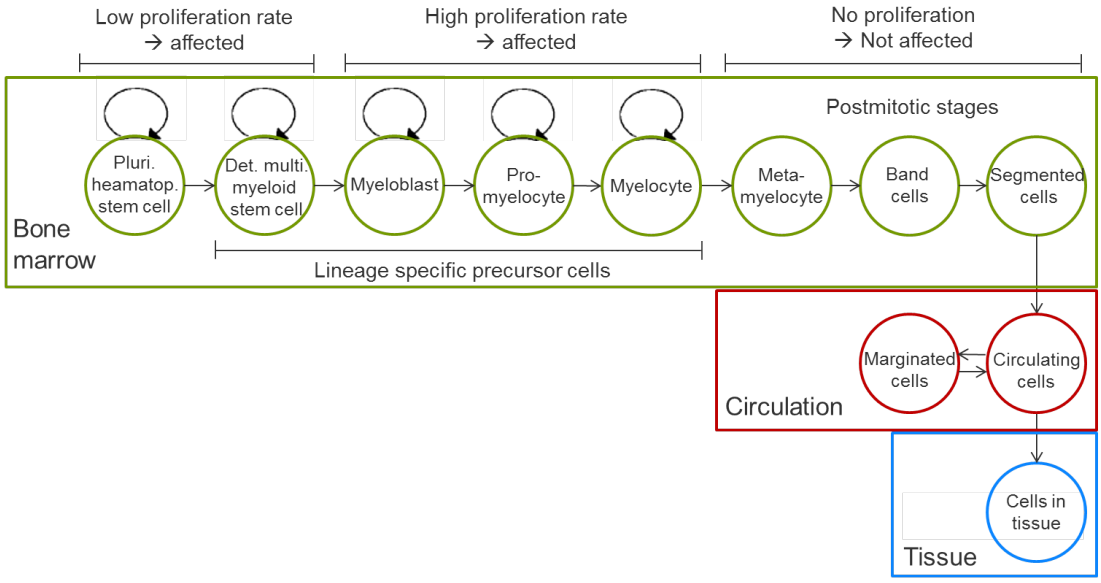

Figure 1.1 Schematic illustration of granulocytopoiesis using the example of neutrophil development. Modified from Friberg and Karlsson[20]. Pluri. haematop.: pluripotent haematopoietic; Det. multi.: determined multipotent.

ing which the cells differentiate through postmitotic stages for a time period of approximately 6.6 d. After that, the mature cells enter the circulation from where they migrate into the tissues with a half-life of 6.7 h to then undergo apoptosis within the next few days[25]. The pool of circulating granulocytes is divided into two equally large parts which are in a rapid equilibrium, consisting of circulating granulocytes and those marginated along the vessel walls. Granulocytopoiesis in general is highly regulated by growth factors such as G-CSF and cytokines, e.g. interleukin 6, which both increase the proliferative activity of the lineage specific precursor cells, shorten the maturation time of cells in the bone marrow and mobilise granulocytes from the marginated pool[26]. TNF-α (tumour necrosis factor-alpha) on the other hand suppresses haematopoiesis by inducing apoptosis.

Due to the highly proliferative activity and, hence, a rapid turnover, the haematopoietic system has the capacity to respond quickly to an increased demand due to e.g. blood loss or infection[21]. The same enormous production capacity, which is able to increase granulocytopoiesis under stress up to a factor at least 10, makes the highly proliferative cells in the bone marrow vulnerable towards cytotoxic drugs[27]. However, despite being a severe adverse event, haematotoxicity is accepted in chemotherapy, as it is necessary to obtain the closely related desired clinical benefits, i.e. destruction of tumour cells.

Besides the characterisation of the leukopoietic system under chemotherapy and the effect of cytotoxic compounds, the lifespan of erythrocytes was investigated in this thesis (for more details on erythrocytes and their lifespan see section 1.6). With 4.8 - 5.4 $\cdot 10^{12}$ cells/L erythrocytes are the most common type of blood cells[28]. Every day, 200 billion erythrocytes are released into the circulation after a mean production time of seven days where they survive for a mean time of 120 days[29,30].
As diverse as the different cell lines are, as various are the effects of xenobiotics on their production or other endogenous processes involving blood cells. In this thesis, special attention was drawn to the impairment of the haematopoietic system in patients undergoing HDCT and the cytotoxic effect of chemotherapeutics on proliferative haematopoietic precursor cells *in vivo* and *in vitro*. Therefore, proliferation and maturation processes of progenitor cells in the bone marrow were assessed and regulatory processes as well as influential factors of the therapy regimen (e.g. concomitant medication) were investigated. Additionally, the endogenous process of glycation of haemoglobin in erythrocytes was investigated in a population of diabetes mellitus type 2 patients.

1.3 Carcinomas and (high-dose) chemotherapy

Cancer is a generic term comprising more than 100 different types of diseases which are characterised by a rapid, uncontrolled division of abnormal cells, which can invade adjoining tissues and spread to other parts of the body via the blood and the lymphatic system. Worldwide, cancer is one of the leading causes of death with 7.6 million deaths in 2008 (13% of all deaths) and an expected estimate of 13.2 million deaths in 2030[31]. In Germany, the incidence for non-melanotic cancers in 2008 was around 165,000 with a median age of onset of 69 years[32]. Due to an increasing life expectancy cancer is gaining further importance in the health care system as more patients are likely to be affected by cancer due to impaired apoptosis of and repair mechanisms in the cells. The most frequent cancer types causing death every year are lung cancer, breast cancer, colon cancer, pancreatic cancer, prostate cancer and stomach cancer whose occurrences differ between men and women[31,32]. Treatment concepts consist of interdisciplinary approaches comprising surgery, radiotherapy and chemotherapy and depend on the tumour type and stage. The use of intense polychemotherapy in combination with surgery and/or radiotherapy enabled to improve the prognosis in certain tumour types, e.g. depending on the stage the cure rate for testicular cancer could be raised up to 90%[33]. In

general and depending on the type of malignancy, progression of disease, prognosis and the status of the patient, two treatment options can be classified:

- Curative treatment, with the goal of curing of cancer or a long-term disease free survival with good prognosis, e.g. 40% to 80% for acute lymphoblastic leukemia in children, or testicular cancer. Hence, it can be defined as "the proportion of patients who survive beyond the time after which the risk of treatment failure approaches zero, i.e. the disease-free survival plateau"[34].

- Palliative treatment aims at symptom relief resulting in the improvement of "quality of life for the patients and their families [...] through the prevention and relief of suffering [...] and treatment of pain and other problems,[e.g.] physical, psychosocial and spiritual", World Health Organisation (WHO)[31].

1.3.1 Chemotherapy in cancer

Chemotherapy, i.e. the use of cytotoxic agents for the destruction of autonomously and progressively growing abnormal tumour cells, is an important part of cancer therapy. It can be applied to cure, prolong the lifetime of a patient or, in the palliative treatment, for symptom relief. Chemotherapy is also used to decrease the tumour load before (neoadjuvant) or after (adjuvant) surgery or radiotherapy to prevent metastasis by cells that might have spread in the body or were not removed during surgery and/or radiotherapy. Solid tumours are rarely curable by chemotherapy alone, with success rates of 10% to 15%[33]. In contrast to this, haematological malignancies including acute myeloid leukaemia are curable using chemotherapy alone[35]. In general it is believed that the higher the drug exposure, the better the effect of the treatment on the tumour. High doses are associated with adverse events, which, in reverse, can be dose-limiting due to tolerability. Combinatorial regimens can be applied to circumvent resistances of tumour cell populations by (empirically) combining drugs with different modes of action which might, in addition, achieve a synergistic effect on the tumour cells. To avoid additive effects with respect to adverse events, the drugs used in combination therapy should show differing spectra of adverse events. The intensity of the desired and adverse effects depends on the dose, the PK profile of the drug as well as the sensitivity of the cells in the individual patient. Due to high variability in the response to chemotherapy and the occurrence of adverse events the optimisation of anticancer treatment is desirable. One approach for the optimisation of cancer therapy, besides the development of new drugs and therapy regimens, is the individualisation of doses[36,37]. With regard to adverse events, the type of treatment and

the goal of the therapy play an important role. For a curative treatment option the occurrence of adverse events is tolerated whereas in palliative treatment the benefits and symptom relief have to be weighted against the adverse events of a treatment.

1.3.2 Testicular cancer and treatment strategies

In 2008, a total of 3,970 patients in Germany were diagnosed with testicular cancer accounting for only 1.6% of all cancer types in men. However, it is the most common solid tumour in male patients between 15 and 34 years of age[32]. Due to improvements in the therapeutic regimens, the mortality rate has been declining over the past 40 years although the overall incidence has more than doubled[38]. With a relative 5-year survival rate of 96%, testicular cancer belongs to the cancers with the most favourable prognosis of malignant neoplasms[32]. Approximately 90% of the patients with a good prognosis and the majority of patients with an advanced disease are cured with conventional (cis-)platinum-based chemotherapy. The current standard of care for patients with advanced disease and a poor prognostic is a combination chemotherapy consisting of four cycles of cisplatin, etoposide and bleomycin resulting in a 5-year overall survival rate of less than 60% in this group[39,40]. Second- and third-line treatment options still offer a cure and include the combination of cisplatin and ifosfamide with either paclitaxel[41] or vincristine[42] with response rates of 63%. Another approach is the use of HDCT comprising an autologuous stem cell rescue (ASCR) which is described in more detail in the next paragraph.

1.3.3 High-dose chemotherapy

In the 1980's, first trials for the treatment of solid tumours with HDCT were undertaken. Inclusion of patients suffering from testicular cancer into those studies was a logical step due to the relatively high sensitivity of the tumour against cytotoxic drugs, drug combinations with synergistic drug interaction, only rare occurrence of bone marrow metastasis and the population being young with a low incidence of comorbidities[43]. Since then, HDCT including an autologuous bone marrow support was increasingly used as a potentially curative treatment option for patients with solid tumours and an advanced disease status[44]. The use of HDCT is based on the hypothesis that the higher the doses, the more tumour cells are destroyed. Another assumption is that by escalating the dose resistances can be overcome. According to theoretical assumptions, a dose escalation by a factor of at least 5 to 8 is necessary to treat a tumour curatively which only partially responded to conventional chemotherapy[34]. However, the drugs used in HDCT need to meet specific prerequisites, comprising a broad cytotoxic activity even at conventional doses, a steep dose-response relation and non-haematological

adverse events which are not overlapping. These conditions have to be met to enable the administration of full doses of the drugs in combinatorial regiments without additive effects for each of the drugs' toxicity profile[45]. Ideally, the concentrations reached by the administered doses are in the linear part of the dose-response curve to guarantee a higher effect with a higher dose without reaching the plateau of the curve. Moreover, the dominant dose-limiting adverse event even at high doses has to be myelosuppression which can be modulated by an ASCR with or without additional administration of growth factors.

HDCT in testicular cancer HDCT as a treatment option offers a chance for testicular cancer patients with an incomplete response to first-line therapy. These patients either show cisplatin refractoriness, multiple relapses or an advanced stage at the initial diagnosis[46]. The benefit of a HDCT with ASCR in the first-line treatment of patients with poor prognosis could not be proven. Hence, HDCT is reserved as a salvage treatment option[43]. Although cisplatin shows high response rates when used in conventional chemotherapy of testicular cancer its toxic profile makes it useless for HDCT as nephrotoxicity limits the dose escalation to only a factor of 1.7, compared to a desired factor of 5 to 8 (section 1.3.3). As a platinum-based drug with a more favourable profile of adverse events, carboplatin, in combination with etoposide, was introduced to HDCT in 1989 by Nichols et al.[47] who described a response rate of 44% and a long-term remission rate of 12% over 12 months for patients with refractory disease. With the routine use of ASCR and the administration of growth factors as well as improvements in supportive care treatment, the HDCT-related mortality was reduced to less than 3% in the past years[48]. Until today, carboplatin and etoposide remain the backbone of HDCT regimens with or without additional agents such as cyclophosphamide, ifosfamide or paclitaxel. The benefit of intensification of HDCT by adding of thiotepa could not be proven and neither response nor survival rates were increased. In addition, serious polyneuropathies added to a poorer spectrum of adverse events compared to other HDCT regimens[49].

1.3.3.1 Autologuous stem cell rescue

The immense dose escalation which is necessary for a successful use of HDCT was first possible through the addition of a bone marrow support to the regimen which modulated the occurrence of myelosuppression[50,51]. By the autologuous retransfusion of peripheral stem cells (autologuous stem cell rescue, ASCR) recovery of the haematopoietic system in a clinical tolerable time frame can be achieved[52]. The performance of an ASCR was first introduced into clinical practice in the late 1980's and ever since then became the method of choice for

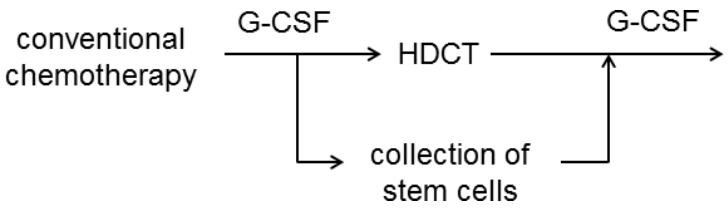

Figure 1.2 Schematic illustration of an autologuos stem cell retransfusion following high-dose chemotherapy (HDCT). G-CSF: granulocyte colony-stimulating factor. Modified from Bokemeyer and Kanz[51]

a haematopoietic support in HDCT regimens. By 1996, 90% - 95% of all HDCT included an ASCR which proved to be superior compared to a bone marrow transplantation due to several advantages: Stem cells from the peripheral blood can be harvested without the need of general anesthesia and can be used in patients having inadequate bone marrow for harvesting[53]. However, the more important argument is the more rapid haematopoietic recovery due to the larger part of more mature progenitor cells which develop and differentiate faster into functional blood cells in comparison to their counterparts harvested from bone marrow. The duration of neutropenia and thrombocytopenia was shown to be much shorter being reduced to two weeks for an ASCR in comparison to a full haematopoietic recovery after 20 - 30 days in patients receiving an autologuous bone marrow transplantation[53], however no difference in the overall and event free survival was found[54,55]. Another advantage of ASCR or an autologuous bone marrow transplantation is that donor and recipient of the stem cells/bone marrow transplant are identical and therefore graft-rejection reactions are avoided.
Figure 1.2 illustrates the performance of an ASCR. Among other cells pluripotent haematopoietic stem cells and lineage specific precursor cells are mobilised from the bone marrow by administration of growth factors, interleukines and/or the use of a stem cell mobilising chemotherapy prior to HDCT. The cells are harvested from the blood via leukoapharesis, cryopreserved in liquid nitrogen and retransfused after the end of HDCT taking the PK of the drugs into account.

Depending on the HDCT regimen an amount of 1 - 4$\cdot$ 10^6 $CD34^+$ cells/kg was reported to be sufficient to reach haematopoietic recovery[56]. In a survey evaluating 162 questionnaires the usage of 1 - 5 $\cdot 10^6$ $CD34^+$ cells/kg was reported with two thirds of the questioned hospitals aiming for an amount of $2 \cdot 10^6$ $CD34^+$ cells/kg[53]. Weaver et al.[57] investigated 692 patients receiving HDCT and found an amount of $\geq 5 \cdot 10^6$ $CD34^+$ cells/kg to be optimal to ensure a rapid recovery from neutropenia and thrombocytopenia whilst a transplantation of $\geq 2.5 \cdot 10^6$

$CD34^+$ cells/kg yielded satisfying results with regard to haematological recovery (defined as absolute neutrophile count > $0.5{\cdot}10^9$/L for 2 consecutive days).

1.3.3.2 Granulocyte colony-stimulating factor

Granulocyte colony-stimulating factor (G-CSF) is one of the most important regulators of granulocytopoiesis. In oncology, G-CSF is used to accelerate the time to recovery from leukopenia after chemotherapy as patients are prone to severe infections and sepsis due to low concentrations of leukocytes in the circulation. The efficacy of using G-CSF in HDCT regimens including ASCR was proven in various studies which were reviewed by Voss et al.[43] and Klumpp et al.[58] Comparing two HDCT studies including bone marrow transplantation the additional administration of G-CSF reduced the duration of grade 3 neutropenia ($< 0.5 \cdot 10^9$ cells/L) from 20 to 11 days[59]. Unfortunately no information on the administered amount of G-CSF and the dosing regimen were provided in the publication.
Moreover, the administration of G-CSF following ASCR has shown to shorten hospitalisation and reduce the days of non-prophylactic antibiotic treatment[58]. Prior to HDCT G-CSF is used to mobilise stem cells from the bone marrow for harvesting cells for the performance of an ASCR. G-CSF administration was reported to result in an dose-dependent increase in circulating haematopoietic progenitor cells up to 100 to 500-fold compared to pretreatment values[51,60]. For example, for a dose of 12 μg/kg/d for 6 days a 58-fold increase in circulating granulocyte-macrophage progenitors was observed[61]. Upon G-CSF administration, cells of all maturation stages are released from the bone marrow and demargination of the cells from the walls of the blood vessels is stimulated resulting in a fast and transient increase in neutrophil concentrations[62]. A more sustained increase in the number of circulating cells due to G-CSF treatment caused by the increase in proliferation of the haematopoietic progenitor cells in the bone marrow and shortening of cell maturation processes was observed in mice (dose: 125 μg/kg)[63] and healthy volunteers (dose: 30 - 300 μg/d,)[64] and the enhancement of cell survival of bone marrow cells was shown *in vitro*[65]. Although production and maturation processes are enhanced, the functionality and also the half-life of the cells in the blood remain unchanged[62,64,66].
Endogenously, G-CSF is produced by monocytes, fibroblasts, endothelial cells and by haematopoietic cells which stimulate production in stromal cells in the bone marrow[62,67]. Its elimination is mediated by mature neutrophils which express G-CSF receptors that are internalised after G-CSF binding. Hence, a physiological feedback mechanism exists, linking the number of circulating neutrophils to the amount of available G-CSF[68,69] and therefore cell proliferation

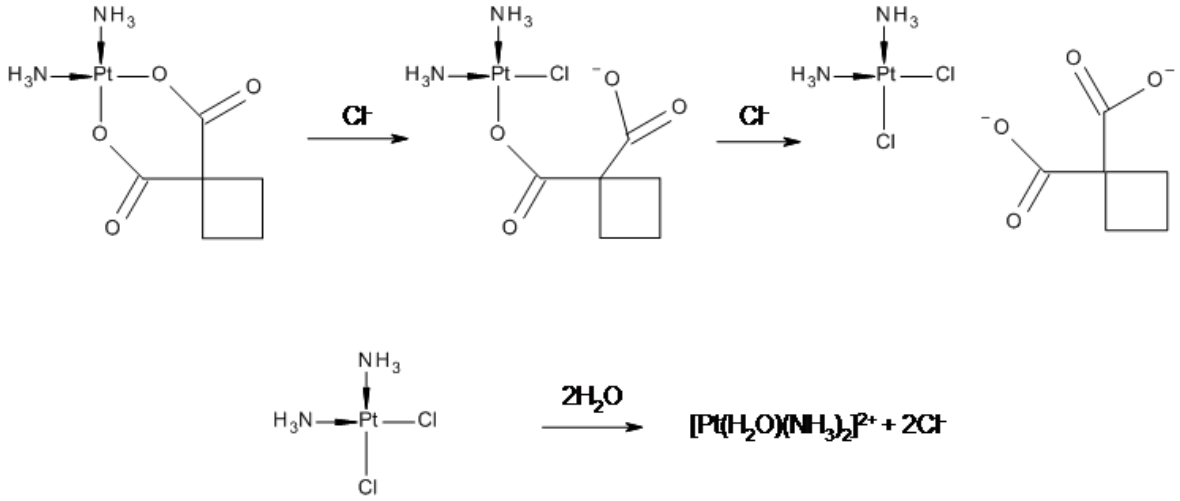

Figure 1.3 Activation of carboplatin (solvent pathway). From Ciancetta et al.[71].

and maturation. Administration of glucocorticoides enhances endogenous G-CSF production. For example, the administration of dexamethasone (DEXA) has shown to enhance G-CSF concentrations in healthy male volunteers up to 240% - 871% in a dose-dependent way[70].

1.3.4 Chemotherapeutic agents of interest in this thesis

Carboplatin Carboplatin was introduced to the clinics in the late 1980's and has gained popularity due to its favourable spectrum of adverse events compared to its parent compound cisplatin. The exact mode of action is unknown, although the platinisation of deoxyribonucleic acid (DNA) represents a key element. Platinum (Pt) agents need to be activated by a ligand exchange of the leaving group through nucleophiles. The potency of the substances is determined by the reactivity and stability of the resulting aqua complex. Carboplatin is most probably activated by the so-called solvent pathway (see Figure 1.3), characterised by an exchange of its ligand (cyclobutane-1,1-dicarboxylate) with chloride ions which are, in return, substituted by water atoms (Figure 1.3). However, this aquation reaction is very slow and therefore an alternative reaction pathway, indicating a direct nucleophilic substitution of the ligand, was discussed[72]. In 1996, the attack of methionine (a thioether) followed by a more rapid substitution of the monodentate bound ligand by nucleophiles was postulated[73].
The active aqua complex platinises the DNA, preferentially at the N7 atoms of guanine[74], leading to cross-linking of inter- and intra-DNA strands. This causes a significant change in the three dimensional structure of the DNA including weakening of hydrogen bonds. In the

area of cross-linkage the DNA is bent in the direction of the major groove, shielding DNA repairing enzymes. Replication and transcription processes of the DNA are impeded or suppressed and cell death occurs. Additionally, a damage of the cell membrane contributes to the cytotoxic effect due to binding of Pt to ribonucleic acid, amino acids and proteins[75].
Carboplatin is used in the treatment of ovarian, cervical and small-cell lung carcinoma as well as head and neck cancer and testicular cancer. Together with etoposide it forms the backbone of many high-dose anticancer regimens[43] (see also section 1.3.2). In general, carboplatin is administered as a short intravenous (i.v.) infusion or, in the case of ovarian cancer, as an intraperitoneal infusion. Rather than the earlier customary dose adjustment based on body surface area (BSA), the target AUC-concept using the Calvert formula[76] should be used if the actual glomerular filtration rate (GFR) is available[43]. If the GFR needs to be estimated based on serum creatinine (CREA) the Food and Drug Administration (FDA) recommends to cap the dose at a GFR of 125 mL/min to achieve the desired exposure in terms of AUC and to avoid overdosing. However, in HDCT the dose is often overestimated if it is calculated based on BSA or GFR. In 2002, Kloft et al. proposed an individualisation of the dosing strategy for high-dose carboplatin based on patient-specific factors[77].
After administration of the drug a distribution to nearly all tissues was shown, with highest concentrations in the liver, tumour tissue, kidney and pleura[78,79]. The transport through membranes is passive, although an active and facilitated transport of reaction products with thioethers and nucleobases is discussed[80]. The plasma protein binding is moderate due to the rather stable leaving group and is changing over time. Two hours after drug administration a fraction of 5% of the administered dose was reported to be bound to plasma proteins *in vitro* which increased to 40% - 50% after 24 h[81,82]. Only the unbound fraction of Pt is pharmacodynamically active, as Pt is irreversibly bound to proteins and can therefore not penetrate cell membranes. Hence, a differentiation between total and unbound Pt needs to be made to characterise its PD effect. Ultrafilterable Pt comprises unbound Pt as well as intact carboplatin, thus, all species which are responsible for the anti-tumour and adverse effects[82–84]. At conventional doses (around 400 mg/m^2 BSA[51]) the dose-limiting adverse event is myelosuppression, in particular thrombocytopenia, making carboplatin a candidate for the use in HDCT (section 1.3.3). Compared to cisplatin, nephrotoxicity is less severe but becomes dose-limiting once myelosuppression is modulated by myelosupportive treatment during HDCT. In HDCT with ASCR the safe use of doses up to 1800 mg/m^2 BSA were reported[85], whilst linear pharmacokinetics (drug concentrations increase proportionally to the administered dose) were confirmed for doses up to 1500 mg/m^2 BSA[78,83].

Etoposide Etoposide is a semi-synthetic derivate of podophyllotoxin, a lignan which can be found in *Podophyllum peltatum* and *Podophyllum emodi*. Podophyllotoxin is a constituent of podophyllin which can be extracted via ethanolic extraction from the dried rhizomas. In 1861, podophyllin was first described in the context of treatment of skin cancer[86]. Etoposide is the 4'',6''-acetal of the 4'-Demethyl-4-O-β-D-glycolsyl-epipodophyllotoxin. It is not soluble in water which requires the use of solvents such as ethanol or polysorbate for the formulation of solutions for i.v. administration. Etoposide is applied in different amounts in mono- or combinatory therapy regimens in the treatment of lung cancer, leukemia, (non-) Hodgkin's lymphoma, testicular cancer, ovarian and chorion carcinoma as well as brain tumours[87]. Etoposide is a phase specific cytotoxic agent with high activity in the S- and G2-phase of the cell cycle, causing single and double strand breaks of the DNA. Its cytotoxic effect lies in the interaction with topoisomerase II which belongs to a group of enzymes that cut both DNA strands, pass an unbroken DNA helix through it and reanneal the cut strand, thereby changing the topology of the DNA[88]. The cytotoxic effect is not due to inhibition of the enzyme but the stabilisation of the cleavable complex which consists of topoisomerase II covalently bound to DNA. During replication of the DNA, these transient breaks can become permanent resulting in apoptosis after cumulation of strand breaks[89]. Additionally, the creation of free radicals is discussed to further enhance apoptosis. Also, the metabolism towards the ortho-chinon (Figure 1.4) results in reactive species with high *in vitro* binding to DNA[90].

Etoposide can be administered in form of an i.v. or per oral (p.o.) formulation. The plasma protein binding is high, between 94% to 98%[91,92] with etoposide mostly being bound to albumin. Due to pathological changes of albumin concentrations in cancer patients, an altered protein binding was observed resulting in a unbound fraction of 13.9% $\pm$ 9.9%[93], whilst others reported a range of 1.9% - 15.6% for cancer patients[94] and even 21% at the end of an infusion of high-dose etoposide (35 - 60 mg/kg)[95]. This is important as only unbound drug can interact with target structures, resulting in the anti-tumour effect as well as adverse events.

About 30% to 40% of etoposide is excreted unchanged via the kidneys. Additionally to the CYP3A4 (CYP: Cytochrome P_{450}) mediated metabolism to its catechol, the ring opening of the lacton ring (Figure 1.4, 2) yields to the trans- and cis-hydroxy acids as further metabolites[96–98]. Furthermore, glucuronidation of the phenolic hydroxy group (Figure 1.4, 3) and the hydroxy group of the glucose takes place in the liver.

For conventional chemotherapy, the dose-limiting toxicity is myelotoxicity, in particular the occurrence of neutropenia. In the setting of HDCT mucositis becomes the dose-limiting adverse event as the ASCR with or without G-CSF administration modulates the magnitude and

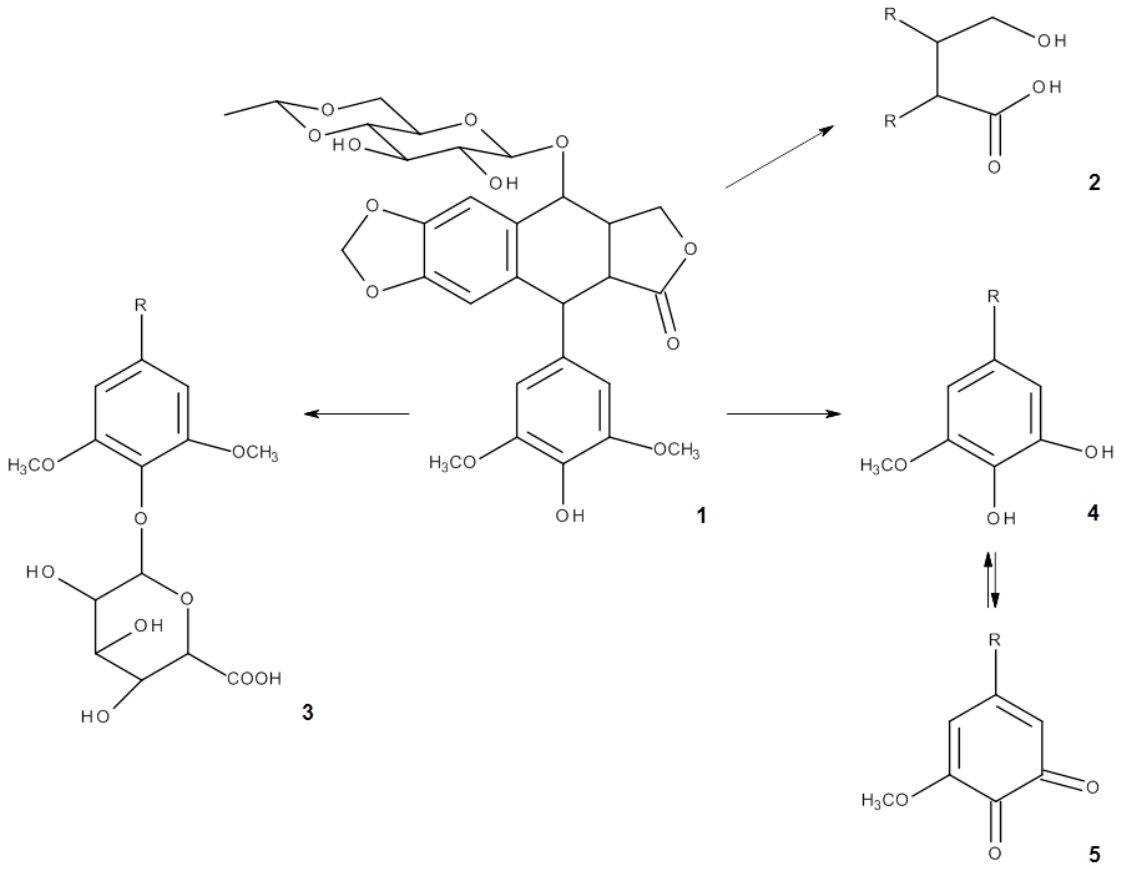

Figure 1.4 Metabolism of etoposide (1). Opening of the lacton ring (2), glucoronidation of the phenolic hydroxy group (3), CPY3A4-mediated metabolism to its catechol (4) and o-chinon (5). From Haim et al.[99], Van-Maanen et al.[90]and Hande et al.[100]

time course of neutropenia[101]. Conventional chemotherapy regimens comprise an i.v. dose of 50 - 100 mg/m^2 BSA on five consecutive days or a dose of 120 - 150 mg/m^2 on day one, three and five[102]. As a p.o. formulation, etoposide is dosed at 50 - 100 mg/d for the duration of 2 - 3 weeks. For the administration in combinatorial regimens, the dose depends on the respective regimen and therapy protocols which proved to be effective in the treatment of the respective tumour. The fractionated administration reflects the phase-specificity of etoposide and the repeated administrations result in more cells that are in a sensitive state[103]. Wolff et al.[104] and Siegert et al.[105] reported safe doses up to 2400 mg/m^2 BSA for the setting of HDCT and Fields et al.[85] described a safe dosing up to 3000 mg/m^2 BSA. These high doses request the usage of solvents for the i.v. formulation which might be the reason for allergic reactions and hypotensions related to HDCT comprising etoposide[106–108]. Moreover, due to limited solubility, etoposide is injected without being diluted[109,110] causing the breaking of infusion sets[111] which was the case during one administration in the investigated study (section 2.2).

Thiotepa The first use of thiotepa in cancer therapy was reported in 1952[112]. It has been used systemically in combination with other chemotherapeutic drugs for the treatment of ovarian cancer, (metastatic) breast cancer, brain cancer and, as intravesical chemotherapy, in superficial bladder cancer. In 2010, it was authorised by the European Medicines Agency (EMA) as an orphan drug for the conditioning treatment prior to haematopoietic progenitor cell transplantation and the treatment of solid tumours when HDCT with ASCR is appropriate.
Thiotepa is a small, lipophilic and highly reactive molecule belonging to the group of ethyleniminderivates (aziridine) which is related to the nitrogen mustard derivates. It is a polyfunctional alkylating agent which causes inter- and intra strand cross-linking of the DNA by reacting with the nitrogen of different DNA bases. Another postulated mode of action is its function as a prodrug for aziridine, a highly reactive molecule with high alkylating potency, which is released intracellularly by hydrolysis of thiotepa. Aziridine reacts, in turn, with the DNA resulting in DNA chain scission. Which pathway represents the mechanism of action remains unclear, although both pathways were identified *in vitro* and *in vivo*[113]. Its main, active, metabolite TEPA (Figure 1.5) is formed by an enzymatic reaction catalysed by the isoenzymes cytochrom P_{450} (CYP) 2B1 and CYP2C11[113]. TEPA interacts with the DNA in a different way, causing DNA lesions comparable to those of a monofunctional alkylating agent without observable cross-linking of the DNA strands.
Thiotepa is extensively and evenly distributed throughout the body tissues with exception of the liver which reveals only 10% of the concentration present in the other organs[114]. Also,

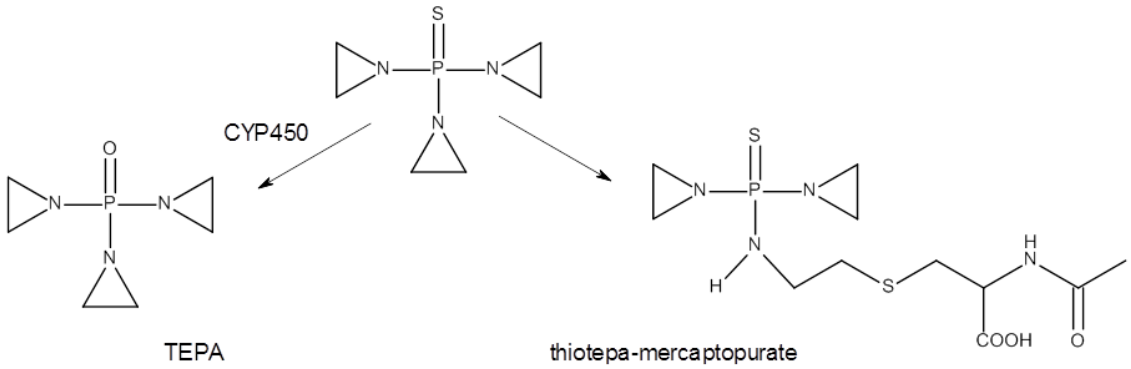

Figure 1.5 Thiotepa and its major metabolites TEPA and thiotepa-mercaptopurat. From Maanen et al.[116]

concentrations in the liquor are comparable to plasma concentrations making an intrathecal application unnecessary[115]. Plasma protein binding of albumin is low with 10% to 30% being bound to albumin.

The metabolism of thiotepa is quite complex. Besides metabolism to TEPA, the conjugation to glutathion[113] with subsequent separation of the glutamyl and glycine moieties as well as N-acetylation to thiotepamercaptopurat is observed (Figure 1.5). This conjugation is catalysed by the glutathione S-transferase isoenzymes. In resistant tumour cells high levels of these enzymes are found and believed to cause the resistance[117]. A third metabolite which was identified in the urine is the monochloro adduct of TEPA[116].

Eight hours after HDCT, unchanged thiotepa can be found to a low extent (1.5% of the administered dose) in the urine[118]. After radioactive labelling, 64% of the radioactivity was found in the urine and 24% was due to active, identified metabolites suggesting other uniden-

tified active metabolites as the amount of identified metabolites did not correlate with the alkylating activity in the urine[119]. Regarding the clearance of thiotepa controversial findings exist with respect to its dose-dependency in conventional as well as HDCT regimens[120–122]. Whilst some authors suggested a capacity-limiting metabolism as the reason for a possible dose-dependency[120–122], others found no evidence of a saturable enzymatic elimination processes for high doses of thiotepa[112,123,124]. At conventional doses of 15 - 60 mg/m^2 BSA, the dose-limiting toxicity of thiotepa is myelotoxicity. In HDCT, thiotepa is mostly combined with carboplatin and cyclophosphamide and its dose can be increased by a factor of 30[51]. Pession et al.[125] and Chen et al.[126] reported a safe dosage of thiotepa up to 750 mg/m^2 BSA which was also administered in the study investigated in this thesis (section 2.2). Adverse events at this dose level are mucositis, toxicities concerning the central nervous system as well as lung impairment and hepatotoxicity.

1.4 Myelosuppression

1.4.1 Time course of myelosuppression

As previously described in section 1.3 and section1.3.3, myelosuppression is one of the most important dose-limiting adverse events in many anticancer regimens. Especially the highly proliferative stages in early haematopoesis are responsible for the sensitivity of the progenitor cells towards chemotherapeutics. Conversely, the slow cell cycle of stem cells protects them against the cytotoxic effects under normal conditions. The proliferative activity of the cells in the bone marrow can be stimulated by cytotoxic drugs which makes them even more sensitive during 3 - 5 days after the first drug administration[127]. Additionally, repeated administrations of cytotoxic drugs are not only more toxic but lead to a more pronounced rebound, illustrating the enormous capability of the haematopoietic system to react to stress[127]. A schematic time course of leukopenia following chemotherapy is shown in Figure 1.6. For the first few days, directly after drug administration, no drug effect, i.e. a decline in leukocyte concentrations, can be observed. This is due to the fact that the non-mitotic stages of cell maturation are more or less resistant to chemotherapy. As they make up a large part of the reservoir of the cells in the bone marrow the observable drug effect in the blood is delayed as only the early, highly proliferative cell stages are affected. Then, leukocyte concentrations decline rapidly until the nadir, i.e. the lowest observable cell concentration, is reached. After the drugs are eliminated from the body, the haematopoietic system recovers to physiological cell concentrations. In some cases a pronounced rebound can be observed as the system is highly

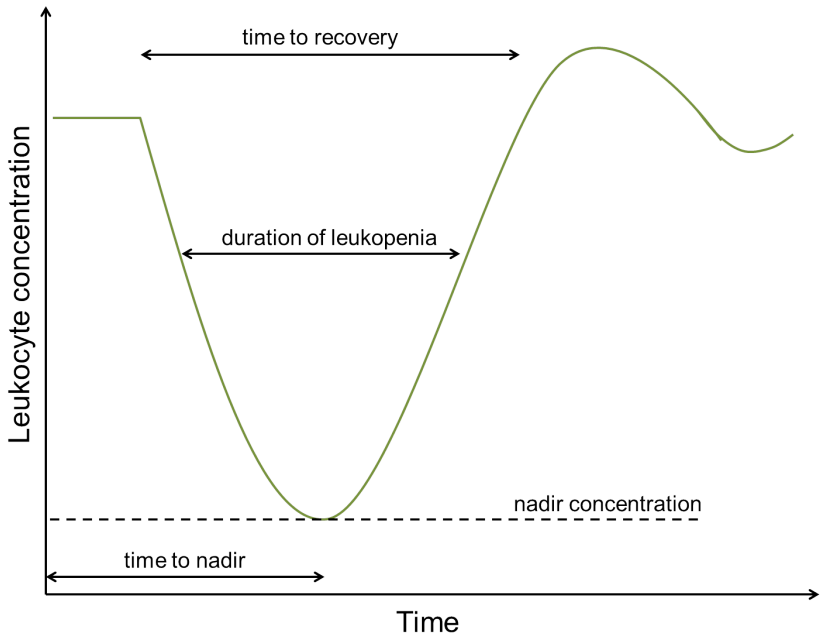

Figure 1.6 Schematic time course of leukopenia depicting the four characteristic parameters nadir, time to nadir, duration of leukopenia and time to recovery. Modified from Parchment et al.[128]

stimulated due to low cell concentrations and the supportive treatment, if applied. The time course can take different shapes depending on the cytotoxic drug and the sensitivity of the cells towards different regimens which is highly variable. For example, a more rapid decrease in cell concentrations can be observed for methotrexate and vinblastine whereas the recovery after melphalan administration is prolonged[20], probably due to impairment of the slowly cycling stem cells. Furthermore, patient specific factors, i.e. covariates such as sex, bilirubine and liver enzymes, were shown to have an influence the time course of myelosuppression[129]. According to the common criteria for adverse events[130] leukopenia and neutropenia can be classified into five categories (Table 1.1). A grade 3 neutropenia has been associated with a higher risk of developing serious infections that is increasing with lower cell concentrations. Furthermore, the longer the duration of the neutropenia or leukopenia, the higher this risk becomes[131]. Hence, not only the magnitude, but also the duration is of particular importance and it is necessary to characterise both to assess the risks associated with myelosuppression following chemotherapy. To describe the time course of myelosuppression, various PK/PD models have been developed during the past years (see next paragraph).

Table 1.1 Classification of haematotoxicity (leukopenia and neutropenia) according to the common criteria of adverse events version 4.03[130]

	Unit	Grade 1 Mild	Grade 2 Moderate	Grade 3 Severe	Grade 4 Life-threatening	Grade 5 Death
Leukopenia	10^9 cells/L	<LLN-3	3-2	2-1	<1	
Neutropenia	10^9 cells/L	<1.5	1.5-1	1-0.5	<0.5	

LLN: lower limit of normal

1.4.2 Pharmacometric models for myelosuppression

The simplest models for the assessment of myelosuppression link a measure of drug exposure, e.g. drug concentration or area under the curve (AUC), to a summary variable such as nadir concentrations or the relative/absolute change from baseline blood cell concentrations. These models characterise the decrease in cell counts by (log-)linear E_{max} or logistic regression models[132]. The most important disadvantage is that often samples for the determination of blood cell concentrations are taken only once or twice a week and therefore the models often overestimate the actual nadir. As empirical models provide a pure description of the data they are highly dependent on the quality of the data with respect to sampling frequency. In addition, the very important information about the actual duration of the myelosuppression is lost. Few empirical models take the duration into account: for example Rosner et al.[132] published a model consisting out of 3 mathematical functions describing the baseline, the decrease in blood cell concentrations and the recovery in dependency of the dose. However, this model neglected the PK of the drug which has been shown to be more predictive for myelosuppression than dose alone. Karlsson et al.[133,134] accounted for the PK in their model which described the myelosuppression by a cubic spline function. In contrast to empirical models which depend on the drug, the administered regimen and its schedule, mechanistic models are of higher predictive value as they describe the underlying physiological system in great detail. Although there do exist a few mechanistic models for the description of the effect of cyctotoxic drugs on granulopoiesis[20], they were not developed for estimations as they require information on parameters that are not available from clinical data. Therefore, semi-mechanistic models were developed, being simplified mechanistic models that are able to describe the whole time course of myelosuppression by estimation of a manageable number of parameters from clinical data. These models comprise enough physiologically and pharmacologically motivated features to be more reliable for extrapolations beyond the original

setting of the investigated regimen compared to empirical models[20].
Ideally, semi-mechanistic models are able to differentiate between drug- and system-specific parameters which allows for their application across different drugs and their use under various clinical setting whilst enabling the characterisation of the underlying physiological system. In their review, Friberg and Karlsson[20] compared five different semi-mechanistic models of myelosuppression[127,135–138] of which three were compared to the semi-mechanistic models by Panetta et al.[139] and Bulitta et al.[140] by Soto et al.[141] in a modelling and simulation study. All semi-mechanistic models consisted of two or more compartments, took the whole PK profile of the respective drugs into account and described the system of haematopoiesis by more or less complex elements. The production of the cells was either characterised by a zero-[135,136,140] or first-order process[138,139], imitating the self-renewal capacity, proliferative activity or differentiation of stem cells into more mature daughter cells. The drug inhibited the production rate constant[135,136] and[138,139]/or[127,140] stimulated a cell loss from the pool of cells in the bone marrow. All models took the delay in the drug effect into account and few[138,139] allowed for the integration of a physiological feedback mechanism. The model by Bulitta et al. was based on a model developed by Krzyzanski et al.[142] in 2002: They published a multiple pool cell lifespan model which comprised three stages the cells had to pass through: two precursor compartments, one being the mitotic compartment from which cells were lost due to treatment, the other one representing the maturation of cells in the bone marrow and one compartment for the cells in the circulation. One of the assumptions of this model were the lifespans of the cells in each compartment which were fixed to certain values and assumed to be the same for all cells. The model published by Friberg et al.[138] in 2002 (section 2.4.1) allowed for the maturation time of the cells in the bone marrow to vary for cells within each individual patient by modelling the delay of the drug effect by a chain of transit compartments. During the past years this model became the gold standard for the investigation of myelosuppression. This semi-mechanistic model allowed for the differentiation of drug- and system specific parameters which proved to be consistent across a variety of drugs in mono- and combinatorial regimens[129,143–147 138,148–153]. Moreover, it is able to characterise not only neutropenia but leukopenia and thrombocytopenia[138,154–158] and, among many other applications, was used to predict neutropenia in humans based on rat and *in vitro* data[159]. Therefore, this model was used to characterise leukopenia and the system of leukopoiesis in the special setting of HDCT in this thesis.

1.5 Characterisation of the cytotoxic potency of chemotherapeutic agents

1.5.1 Assessment of cytotoxic potency *in vitro*

Toxicology studies aim to identify potential adverse events of compounds. The prediction of haematotoxicity is of very important with respect to cytotoxic agents as they inhibit highly proliferative cells such as the progenitor cells in the bone marrow. Myelotoxicity is one of the major dose-limiting adverse events in anti-cancer therapy. Hence, it is of great interest to predict the maximum tolerated dose in early drug development to avoid the occurrence of severe adverse events when drugs are investigated in humans. *In vitro* assays can be used to bridge the gap between animal models and clinical investigations[160]. The most frequently used assays for the assessment of haematotoxicity *in vitro* are colony-forming unit (CFU) assays such as the CFU-GM (granulocytes macrophages), CFU-E (erythrocytes) and CFU-Mk (megacaryocytes) assay[161]. For a CFU assay cells are cultured in semi-solid medium in the presence of a growth factor cytokine cocktail which stimulates cell proliferation, differentiation and the formation of colonies which are manually enumerated after 14 days of incubation[160]. With these assays not only the maximum tolerated dose can be assessed, but the occurrence of grade 3 and 4 neutropenia can be predicted by the correlation of the clinical outcome to the inhibitory concentrations (IC) at 70% (IC_{70}) and 90% (IC_{90}) of the maximal cytotoxic effect (E_{max}) obtained *in vitro*[160]. Although the CFU assay offers many applications, the disadvantages of this method are the low throughput, the time-consuming protocol and the highly subjective manual counting of colonies. In the past, other assays based on liquid cell cultures were proposed. The inhibition of cell growth and cell death were quantified by an MTT (3-(4,5-Dimethylthiazol-2-yl)-2,5-diphenyltetrazolium bromide) assay[162] (section 2.6.1.1), flow cytometry[163], trypan blue staining[164] or a luminescence assay measuring intracellular adenosine trisphosphate. Recently, Haglund et al.[161] proposed a high-throughput fluorometric microculture cytotoxicity assay (FMCS) as a non-clonogenic alternative to the CFU-GM assay. Data from these assays are evaluated applying simple PD models to relate drug exposure to the assay signal. Among those models are linear models, the E_{max} model, the sigmoidal E_{max} model or the Richards' model (section 2.6.1.3). In comparison to the other models, the linear model was found to be inferior for the description of the drug effect on growing cells. The E_{max} model and its variants describe the drug effect in a more pharmacological way showing no or only little drug effect at low doses with a gradual change to a steeper dose-response relation which plateaus for high drug concentrations. To correct for

background noise or natural cell kill the assay signals are usually transformed before a model is fit to the data. They are often expressed in form of a survival index (% SI) or in percent of cell kill with the maximal effect being 1 for complete survival of the cells or total cell death, respectively[165].

The disadvantage of most *in vitro* assays is their static description of cytotoxicity as cells are incubated with the compound for a fixed period in time and at constant concentrations. Additionally, only the magnitude of the drug effect can be assessed without giving evidence about the time course which is very important regarding the risks associated with myelosuppression (section 1.4.2). The PK/PD models for myelosuppression presented in section 1.4.2, 2.4.1 and 3.3.8 offer the possibility to quantify, differentiate and rank the cytotoxic potency of chemotherapeutic agents. However, most of the models either describe the PD effect with respect to drug concentrations by a linear model, estimating a slope, or by an E_{max} model. Neither the linear nor the E_{max} model corresponds to the models used to predict toxicity from *in vitro* data as linear models are usually not applied for the analysis of *in vitro* data and the maximal effect of a drug is restricted to 1 in E_{max} models. In contrast to that, E_{max} models inhibiting the cell proliferation that are applied in PK/PD modelling predict a maximal effect which is beyond the maximal *in vitro* effect of 100% cell kill to obtain cell kill by mathematically forcing the proliferation rate to be negative as the drug effect becomes greater than 1 (section 2.6.2.1). This implementation of the drug effect also holds true for the linear models and allows the description of a cytostatic drug effect (inhibition of the proliferation rate) as well as a cytotoxic drug effect (negative proliferation rate, representing cell kill). Therefore the development of a model which combines a PD model based on *in vitro* data with a PK profile and cell concentration measurements *in vivo* is desirable to predict the entire time course of myelosuppression. Recently, population PK/PD modelling was shown to be of great value for the prediction of the clinical outcome for acute myeloid leukemia of individual patients from data obtained *in vitro*[166].

1.5.2 Comparing *in vitro* measures of cytotoxicity with estimates from a *in vivo* population PK/PD analysis

In this thesis, a model for the estimation of EC_{50} values from clinical data which are comparable to EC_{50} values obtained from *in vitro* assays was developed and applied to data from a clinical study in patients with different cancer types receiving docetaxel.

Docetaxel Docetaxel is generally recognized as possibly the most active chemotherapeutic in the current treatment of metastatic breast cancer. It is approved for the use of early and metastatic breast cancer, non-small cell lung cancer, prostate cancer, gastric adenocarcinoma and head and neck cancer[167]. Docetaxel belongs to the group of taxanes and is a semi-synthetic analogue of paclitaxel which is extracted from *Taxus brevifolia*. The cytotoxic activity is due to the stabilisation of the microtubular network as well as the inactivation of Bcl-2 (B-cell lymphoma 2), a protein which, in its active state, prevents apopotosis in cancer cells[167]. By binding to the tau side of the beta-tubulin subunit in the centrosome of the microtubular network, docetaxel inhibits its depolymerisation[168–170]. *In vitro* investigations showed that the stabilisation of the microtubulin network results in cell death as (de-)polymerisation processes are crucial for the vital processes of mitosis and interphase during cell replication[171]. The inactivation of Bcl-2 by phosphorylation induces apoptosis as the antiapoptotic activity of this regulatory protein is suppressed.
In the plasma, docetaxel is highly bound to α_1-acid glycoprotein (AAG), albumin (ALB) and lipoproteins (94%)[172]. Its elimination is dependent on BSA, AAG, age (AGE), ALB as well as the hepatic function. The reason for the latter is its oxidative metabolism of the *tert*-butyl ester group which is mediated by CYP3A4. 75% of radioactively labelled docetaxel is found in the bile and 6% in the urin. In contrast to its parent compound paclitaxel, a linear PK was reported for docetaxel[173]. Besides the dose-limiting adverse event of neutropenia, neuropathies, anemia, thrombocytopenia, liver dysfunction as well as alopezia and nausea were reported as the most common adverse events.

1.6 Glycation processes throughout the lifespan of erythrocytes

The estimation of lifespans of cells in different stages of their development cannot only be used to assess the duration of proliferation and/or maturation processes as it is often the case in the modelling of haematotoxicity, but also to characterise physiological processes related to cell ageing such as glycation of haemoglobin in erythrocytes. To be able to estimate any parameter of a system, changes in this system need to be observed to characterise the magnitude of the parameter value. Hence, to estimate the lifespan of a cell in the blood, a change in any parameter related to the system needs to take place. In the case of erythrocytes, changes in e.g. glycated haemoglobin (HbA_{1c}) can be used to describe the lifespan of the cells as the glycation process is irreversible and therefore persists throughout the whole lifespan of an erythrocyte. Vice versa if changes in HbA_{1c} are observed and the model takes the lifespan of red blood

cells into account, the description of this change enables the estimation of the lifespan of erythrocytes. In this thesis changes in HbA_{1c} values from a subgroup of patients enrolled in two studies in diabetes mellitus type 2 patients receiving lixisenatide were analysed with a semi-mechanistic PK/PD model which also allows for the estimation of the lifespan of erythrocytes.

Erythrocytes and their lifespan As any other blood cell, erythrocytes are produced in the bone marrow upon stimulation of their lineage specific precursor cells. The mean maturation time in the bone marrow is seven days and their differentiation is regulated by growth factors such as EPO (erythropoietin) as well as macrophages. About 10% to 30% of an erythrocyte's mass can be attributed to haemoglobin, a metalloprotein responsible for the transport of oxygen[174]. Virtue at al.[175] reported a lifespan of 123 d $\pm$ 23 d for an erythrocyte in healthy volunteers which was reduced to 112 d $\pm$ 25 d in patients with diabetes mellitus type 2. They postulated that the glycation alters the function of haemoglobin, increasing the oxygen affinity and adherence of erythrocyte to endothelial cells[176] and reducing the membrane fluidity, both resulting in a more rapid removal of the cells from the circulation[177]. In their study they found a decrease in the lifespan of 6.9 d for every 1% increase in HbA_{1c}. However, the alteration of the lifespan by glycation processes is discussed controversially. Cohen et al.[178] showed that the heterogenecity in red blood cell lifespans is enough to alter HbA_{1c} but they failed to prove a difference in lifespan between healthy volunteers and patients. Others found an increase in the erythrocyte survival in patients with higher HbA_{1c}[179].
The generated knowledge about the modelling of maturation processes of cells in the bone marrow was used to characterise the lifespan of erythrocytes in the circulation by modelling changes in HbA_{1c} in patients with diabetes mellitus type 2. Therefore, a model incorporating the lifespan of red blood cells for the description of HbA_{1c} was investigated and improved to characterise the process of glycation of haemoglobin in a more detailed way.

Models for the description of HbA_{1c} and glucose concentrations Several models for the description of altered glucose concentrations in patients with diabetes mellitus type 2 exist. The short-term effect of insulin on glucose concentrations was characterised by few models[180–182]. Ribbing et al.[183] developed a model which additionally took the beta cell mass into account. Other quite complex models account for the mid-term effect of fasting plasma glucose (FPG) and additionally incorporate the disease progression[184] as well as HbA_{1c} alteration[185]. DeWinter described the changes in HbA_{1c} by a zero-order production and first-order elimination from a single compartment with a stimulatory effect of FPG on the HbA_{1c} production rate constant[185]. In 2008, Hamrén et al.[186]published a model which explicitly took

the lifespan of erythrocytes into account (section 2.7.2.1). This model served as the basis for the investigations presented in this thesis.

1.6.1 Diabetes mellitus type 2

Diabetes mellitus type 2 is a metabolic disorder characterised by a progressive loss of glycaemic control, evident in rising plasma glucose concentrations beyond physiological ranges. In early stages the glucose-insulin homeostasis is disrupted due to a chronic loss of the insulin receptor sensitivity to insulin in liver, muscle and fat, finally resulting in the failure of beta cells which are compensating the decreasing sensitivity by a higher insulin secretion. The International Diabetes Federation termed diabetes mellitus as *the* epidemic of the 21st century. In 1980, 153 million patients were diagnosed with diabetes mellitus[187] increasing to 285 million patients in 2010[188]. An increase in the prevalence in Germany can be observed comparing the 5.9% in 1989 with the 8.9% in 2007. About 90% of these patients suffer from diabetes mellitus type 2. The disease pattern reaches from insulin resistance and a relative insulin deficiency to the absolute insulin deficiency in late stages. Hyperglycemia leads to long-term complications which can be differentiated into macro- and microvascular complications caused by glycation of proteins. Microvascular damages lead to retinopathy, nephropathy and neurophaties, whereas macrovasular complications include high blood pressure, coronary heart disease, heart attacks, ischemic stroke and the diabetic foot syndrome[189].

Diagnosis and therapy Diabetes mellitus is diagnosed by a concentration of FPG $\geq$ 7.0 mmol/L or postprandial glucose (PPG) concentrations $\geq$ 11.1 mmol/L two hours after the administration of 75 g glucose as an oral glucose tolerance test. Furthermore, glucose concentrations randomly sampled during the day should not exceed 11.1 mmol/L. If two of the mentioned conditions are met or if the glucose tolerance test is positive the diagnosis of diabetes mellitus is confirmed. PPG concentrations are highly variable but seldom higher than 7.8 mmol/L in healthy adults and decrease typically within 2 - 3 h after meal intake[190]. FPG on the other hand serves as a short-term marker in the surveillance of glycaemic control although being also highly variable and therefore not reliable to assess long-term effects. The primary surrogate marker for long-term glycaemic control is HbA_{1c} which is formed by a non-enzymatic, irreversible reaction. It is used to evaluate the overall glycaemic exposure during the past 4 - 8 weeks[191] as it is a result of fasting and postprandial glucose concentrations. Glycation of haemoglobin takes place during the entire lifetime of erythrocytes which is reflected by the fact that haemoglobin in older erythrocytes is glycated to a higher extent

compared to younger ones[192–194]. In healthy adults the proportion of glycated haemoglobin is 4% - 6%[1] (20.2 - 42.1 mmol/mol). The American Diabetes Association defines a value of $\leq$7.0% as the goal of diabetes mellitus therapy, whereas the American Association of Clinical Endocrinologists is in favour of values $\leq$ 6.5% as a stricter control is superior in prevention of macrovascular complications. The German Diabetes Association (Deutsche Diabetes Gesellschaft) defines the goal of diabetic therapy in dependency of the stage of the disease and aims for a value between $\leq$6.5% - 7.0%. To attain $HbA_{1c} \leq 7.0\%$ or 6.5%, studies suggest specific control and targeting of PPG concentrations[196]. To obtain these values in different stages of the disease, different therapy options exist. According to the guidelines the therapy consists mainly of physical training and weight reduction, during early stages of diabetes mellitus type 2. If no improvement is achieved a monotherapeutic regimen is started which comprises the treatment with metformin or glibenclamide or other options such as α-glucosidase inhibitors. Continuing resistance to therapy leads to the use of drug combinations, e.g. sulphonylurea in addition to metformin. The last treatment option for patients who do not benefit from oral drug combinations is the combination and ultimately the substitution with insulin.

1.6.2 Lixisenatide

Lixisenatide is a new, potent, short acting (half-life: 2 - 4 h) and selective glucagon-like peptide (GLP)-1 receptor agonist[197]. It is approved in the European Union for the "treatment of adults with type-2 diabetes mellitus to achieve glycaemic control in combination with oral glucose-lowering medicinal products and/or basal insulin when these, together with diet and exercise, do not provide adequate glycaemic control"[198]. Due to its rapid degradation by the enzyme dipeptidyl-peptidase-4 (exogenous) GLP-1 is showing a short half-life of 2 min[199] and is therefore not suitable as a therapeutic agent. Lixisenatide is a protein consisting out of 44 amino acids and a synthetic version of the hormone exendin-4 which is found in the saliva of *Heloderma suspectum* and displays similar biological properties to GLP-1. Stimulation of the GLP-1 receptor mediates an improvement of glycaemic control caused by meal-related and glucose-stimulated increase of insulin secretion, suppression of glucagon, delayed gastric emptying, weight loss and enhanced beta cell function[195,200]. In patients inadequately controlled on metformin lixisenatide significantly improved mean HbA_{1c}. A dose-dependent improvement in FPG, PPG and average glucose concentrations could be observed during a 13 week study including 542 patients[195].

[1] In this thesis % is used as unit for HbA_{1c} instead of the SI unit (mmol/mol) as HbA_{1c} was reported in % in the investigated study. Conversion from % HbA_{1c} to mmol/mol[195]: $(HbA_{1c}[\%] - 2.152) \cdot 10.929$

1.7 Objectives

Proliferation, maturation and ageing processes of blood cells can be regarded as different stages in which cells stay for a defined period of time, also referred to as a lifespan. In this thesis, the processes of proliferation and maturation were characterised for leukocytes and neutrophils whereas the process of ageing of a cell was investigated for mature erythrocytes in the circulation. For the characterisation of the system of leukopoiesis and the assessment of the lifespan of erythrocytes semi-mechanistic PK/PD models were developed based on different types of data. The semi-mechanistic models were able to differentiate between so called system-specific and drug-specific parameters. Estimation of system-specific parameters enabled the description of the underlying (patho-)physiological processes; here: the disturbed system of leukopoiesis due to HDCT and the formation of HbA_{1c}. Characterisation of the drug-specific parameters, i.e. the effect of the drugs on the systems enabled to gain further insights in the mode of action of the drugs, to investigate possible drug-drug interactions and to differentiate drug effects in terms of potency.

The first three projects were based on drug and leukocyte measurements from a clinical study in patients with testicular cancer which were treated with a HDCT regimen consisting of carboplatin, etoposide and thiotepa and an ASCR. In Project four the cytotoxic potency of carboplatin was further characterised by exploring different PD models for the description of data from a cellular cytotoxicity assay. Additionally, a model for the description of neutropenia following docetaxel treatment was reparametrised to resemble the characteristics of a model for the description of *in vitro* data to enable the comparison of EC_{50} values obtained from *in vitro* assays and clinical studies.

The last project, Project five, dealt with the description of HbA_{1c} values as a biomarker for the long-term evaluation of the anti-diabetic treatment in patients with diabetes mellitus type 2 who were treated with lixisenatide. For this purpose the generated knowledge on modelling of physiological cell maturation and differentiation processes was transferred to describe cell ageing and the lifespan of erythrocytes to enable the characterisation of glycation processes of red blood cells in the patient population. This was possible as the maturation processes of the leukocytes in the bone marrow as well as the lifespan of erythrocytes in the blood share a common element in modelling: a chain of transit compartments, characterising the delay in the occurrence of the drug effect due to maturation processes and the lifespan of the cells.

The objectives of the five projects are described in the following:

- Project 1: Characterisation of the PK of carboplatin, etoposide and thiotepa in the HDCT regimen, focusing on the description of the concentration-time profiles, considering the variability (and its sources) in the population to obtain individual PK parameter estimates for the subsequent PK/PD modelling of leukopenia.
- Project 2: Development of a semi-mechanistic PK/PD model for the description of leukopenia in the special setting of HDCT including ASCR with investigations regarding the myelosupportive treatment, i.e. the ASCR and G-CSF administration, as well as the analysis of other influential concomitant medication. The underlying system of leukopoiesis was characterised and the cytotoxic potency of each drug on the proliferative cells in the bone marrow was assessed.
- Project 3: Assessment of the optimal day to perform the ASCR with regard to nadir concentrations and the duration of (at least) grade 3 leukopenia by means of deterministic and stochastic simulations. Additionally, the influence of the amount of retransfused $CD34^+$ cells on the two parameters was investigated.
- Project 4: Investigation for the description of the cytotoxic potency of carboplatin based on *in vitro* data by different PD models. Moreover, a model for the estimation of EC_{50} values from clinical data with a reparametrised model for myelosuppression was developed. This model enabled the direct comparison of model-estimated EC_{50} values to those obtained from *in vitro* assays.
- Project 5: Description of the formation of a long-term biomarker in diabetes mellitus type 2 (HbA_{1c}), during clinical studies with the new GLP-1 receptor agonist lixisenatide. Simultaneously, the influence of lixisenatide on the contribution of fasting and postprandial plasma glucose to HbA_{1c} formation was characterised and the ageing process of erythrocytes and their lifespan was assessed.

2 Methods and Materials

2.1 Pharmacometric drug-disease modelling and simulation

In population pharmakokinetic/pharmakodynamic analysis the pharmacokinetics (PK) and pharmacodynamics (PD) of a drug in a population are investigated under consideration of different levels of variability (interindividual variability, interoccasion variability, residual variability). PK/PD modelling is applied to characterise the relation between given independent variables (design variables) and some dependent variable (e.g. drug concentration). In a population PK model the concentration (dependent variable) of a drug in the body is modelled in dependency of design variables such as the administered dose and the time and possibly other independent, individual-specific covariates such as weight and age[5]. The relation between the drug concentration and the PD effect is described with the population PD model. To describe the effect of a drug over time, the PK and the PD model are combined to the so called PK/PD model. All population PK and PK/PD analyses described in this thesis were performed applying the nonlinear mixed-effects (NLME) approach implemented in NONMEM®.

2.1.1 Nonlinear mixed-effects modelling

NLME modelling is a special kind of nonlinear regression analysis which describes observations (drug concentrations, PD markers) by a mathematical function (model) involving fixed-effects, i.e. design variables that can be quantified independent of the observation (e.g. time, dose, weight), and random-effects which enable the integration of unexplained inter-, intraindividual and residual variability into the model[201,202]. The function under consideration $f(\phi_i, X_{ij})$ depends on the model parameters ϕ_i in a nonlinear manner and as both fixed- and random-effects are accounted for in the model the term 'nonlinear mixed-effects' modelling is used[5]. The NLME modelling approach enables the analysis of data from different individuals at once by estimating so called typical (population) parameters such as the volume of distribution or a PD marker before the start of the therapy and their associated variability between individual patients. Hence, variability within the population can be quantified and then (partly) explained by the inclusion of covariates. One major advantage of this technique is that not each individual needs to provide data that sufficiently characterises its own PK or PK/PD profile. In fact, as data from all individuals is analysed at once whilst keeping

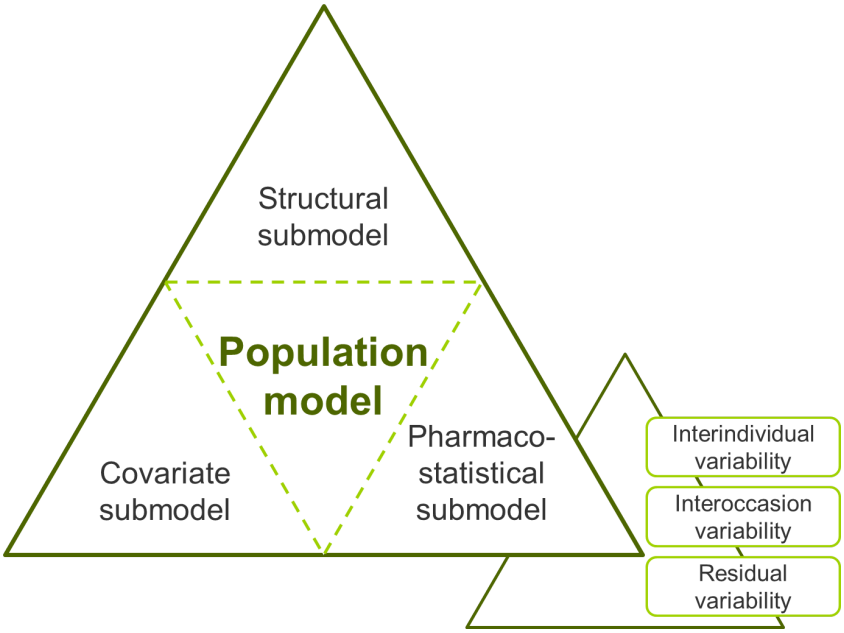

Figure 2.1 Schematic structure of a population model. Modified from Frank[205]

track of the information each individual provided, information can be "borrowed" between individuals to "fill the gaps", making it possible to analyse sparse data.

2.1.1.1 The population model

The NLME models discussed in this thesis are hierarchical models consisting of three components (Figure 2.1): the structural submodel (i) describing the PK or PD profile over time and a second stage model which explains interindividual variability (IIV) as a function of random effects (ii) and covariates (iii). In general, the model distinguishes between two levels of random effects: the interindividual variability and the residual variability[5,203,204]. Another level of variability, the interoccasion variability (IOV), might occur within a single individual whose PK or PD varies from one occasion (e.g. a cycle of chemotherapy) to another. Equation 2.1 and 2.2 describe the j-th observation of the i-th individual in a general NLME model assuming an additive residual variability

$$y_{ij} = f(\phi_i, X_{ij}) + \epsilon_{ij} \tag{2.1}$$

where y_{ij} is the j-th observation in the i-th individual, X_{ij} the design variables (fixed-effects covariates) for the j-th observation in the i-th individual. f is the nonlinear parametric function of X_{ij} and the parameter vector ϕ_i, which contains the model parameters of the i-th individ-

ual. The residual, unidentified, variability (section 2.1.2.2) of the j-th observation in the i-th individual is given by ϵ_{ij}[203]. A general form of the second stage model is defined in Equation 2.2 and allows for IIV and covariate influences

$$\phi_i = g(z_i, \theta) + \eta_i) \tag{2.2}$$

where g is a parametric function of the vectors z_i, θ and η_i which contain information on covariates for the i-th individual, fixed-effects parameters and individual random-effects parameters (section 2.1.2.2), respectively[206].

2.1.1.2 Estimation methods

The goal of NLME modelling is the estimation of a set of parameters for the model that describes the observed data in the best way. Therefore the principle of maximum likelihood is applied where a set of model parameters is selected which maximises the probability of a given set of observations to be derived from the model, i.e. the selected model parameters maximise the likelihood function[5]. Since the observations in a NLME model depend on the random effect parameters η_i and (possibly) ϵ_{ij} in a nonlinear way, the likelihood function has no closed-form solution. Hence, the likelihood function has to be found numerically which can be done by applying a Taylor series approximation. In mathematics Taylor series are used to describe the environment of a single point of a function through a power series. Therefore the infinite sum of terms that are calculated from the values of the functions derivatives at this point is formed[5]. Two general methods are used in NONMEM® to approximate the likelihood function by using a finite number of terms of a Taylor series: the first-order approximation (FO) and the more accurate first-order conditional estimation (FOCE) method[5]. Both methods approximate the solution of the model function through linearisation of the model into a first-order polynomial of the function itself and its first partial derivatives with respect to the random effects parameters η_i and ϵ_{ij}. The FO method approximates the linear solution of the model through a first-order Taylor series expansion around η_0=0, assuming the random effect parameters to be independently (multivariate) normally distributed with zero mean. The individual parameter (conditional) estimates are calculated *a posteriori* based on the individual's observations and the fixed- and random-effects using the maximum *a posteriori* Bayesian estimation method implemented in the NONMEM®s "post hoc" option[206]. During the iterative estimation process using the FOCE method the first-order Taylor series is expanded around the vector of the Bayesian (conditional) estimates of the η's, i.e. the η's are computed conditionally on the variance-covariance matrix Ω (see also section 2.1.2.2) during each iteration

step. The use of the interaction option is a further refinement of the estimation step allowing ϵ_{ij} to be dependent on η_i during maximisation of the likelihood function. Instead of maximising the likelihood, NONMEM® minimises the so called objective function value (OFV), which equals minus two times the logarithm of the likelihood (-2LL), by iteratively searching for the global minimum. The extended least square objective function (OF_{ELS}) given in Equation 2.3 provides the approximation of -2LL applying the FO approximation method to a model with an additive residual variability model[201]

$$OF_{ELS} = \sum_{i=1}^{n} \left[\frac{(y_i - E(y_i))^2}{var(y_i)} + ln\,|var(y_i)| \right] \tag{2.3}$$

where y_i is the vector for the observations and $E(y_i)$ the vector for the expectations of y_i for the i-th individual after linearisation and $var(y_i)$ denotes the variance-covariance matrix of y_i containing all variability parameters of the model. The squared residual error $(y_i - E(y_i))^2$ is weighted by $var(y_i)^{-1}$. This weighting could drive the minimisation into maximising the variance parameters by increasing them to infinity. To prevent this, the last term of Equation 2.3, $ln|var(y_i|)$, acts as an penalty of its own.
NONMEM® offers several other methods for parameter estimation[207] that are not described here as only the FOCE method with interaction (FOCE+I) was used, as was the FO method during certain steps of model development of the PK/PD model in Project 2 (section 2.4.2).

2.1.2 Model development

The development of a population PK or PK/PD model is a stepwise process either starting with the most complex model (full model) that is plausible with regard to prior knowledge or mechanistic understanding or with the simplest model, proceeded by multiple steps during which model parameters are added to or removed from the model. Here the word "complex" refers to the number of estimated parameters included in the model. The top down approach starts with the full model from which parameters are removed until the model contains only the relevant parameters which are supported by the data. It assumes the correlation of all structural model parameters and therefore all elements of the Ω matrix (section 2.1.2.2) are estimated. This process is computationally intense and problems may arise due to model stability. On the other hand, having included as many terms as possible the model is as close to the "real" model as possible. Another way is to start with the simplest model and expanding this model to a more complex one until no more terms can be justified (bottom up approach). At each step the intermediate models are evaluated based on statistical and graphical criteria (section 2.1.3) and it is decided whether a parameter is removed from or remains in the model.

During the first steps of model development random effects were generally considered for all structural parameters without taking correlation of the parameters into account. Depending on the information content in the data the model was then further reduced or, if suggested during model evaluation, expanded to take possible correlations into account.

2.1.2.1 Structural submodel

The first step in developing a population model is the identification of a structural model that best describes the central tendency of the observed data as a function of the model parameters. The structural model is given by Equation 2.4

$$f(\phi_i, X_{ij}) \tag{2.4}$$

where the function f relates the observations from the i-th individual with the independent design variable X_{ij} (e.g. time, dose) given a set of parameters ϕ_i for each individual. In this thesis different structural PK and PK/PD submodels were explored based on the respective data situation and *a priori* knowledge from literature. The PK/PD models in this thesis were developed following a sequential PK/PD modelling approach, i.e. PK models for the description of the concentration-time profiles of the respective drugs were developed, individual PK parameter were estimated with the models and then used as input in the PD model.

2.1.2.2 Pharmacostatistical submodel

The pharmacostatistical submodel describes the variability of a structural parameter θ_k (e.g. clearance, CL) in a population by accounting for the influence of random (non-measurable) effects. Thereby, the variability in a population can be quantified and an individual's empirical Bayes estimate (EBE) of a parameter (i.e. the value of CL for an individual i) can be determined. In general, there are two sources of variability: the interindividual variability (IIV) which describes the variance of a structural parameter across the population and the residual variability which covers the unexplainable variability, e.g. analytical error, after other sources of variability are being controlled for. Additional sources of variability may exist (IOV, interstudy variability, etc.) but are not explained here as they were not part of the analyses presented in this thesis.

Interindividual Variability In population models the IIV is often included on an exponential scale. This ensures that the parameter estimates are positive, avoiding non-physiological PK parameter estimates (e.g. negative CL or volume of distribution, V) and accounts for the

fact that distributions of parameters in a population are often right-skewed. The k-th model parameter for the i-th individual (P_{ki}) is then given by Equation 2.5

$$P_{ki} = \theta_k \cdot e^{\eta_{ki}} \tag{2.5}$$

where η_{ki} is the random-effects parameter accounting for the difference between the typical (population) parameter θ_k and P_{ki} and is assumed to be independent, symmetrically distributed with zero mean and constant variance ω_k^2. The variance ω_k^2 is the k-th diagonal element of the variance-covariance matrix Ω in a population model. A correlation between two random-effects parameters (ω_k^2 and ω_{k+1}^2) can be taken into account by estimating not only the digonal elements of Ω but the off-diagonal element $\omega_{k,k+1}$. The coefficient of correlation (ρ) is then calculated according to Equation 2.6.

$$\rho = \frac{\omega_{k,k+1}}{\sqrt{\omega_k^2 + \omega_{k+1}^2}} \tag{2.6}$$

Estimation of a full covariance matrix is mathematically complex and often leads to non-convergence or models which are very sensitive to the initial parameter values provided in the NONMEM® control file. Hence, correlation was only taken into account when graphically observed in a scatter plot matrix of EBEs, physiologically plausible and/or contributing to the overall model stability.

The variance ω_k^2 estimated on a log-scale can be expressed as the coefficient of variation (CV) on the original (linear) scale through Equation 2.7.

$$CV, \% = 100 \cdot \sqrt{e^{\omega_k^2} - 1} \tag{2.7}$$

For the FO estimation method Equation 2.7 can be approximated by Equation 2.8 which also holds true for conditional estimation methods[5].

$$CV, \% = 100 \cdot \sqrt{\omega_k^2} \tag{2.8}$$

Although it is physiologically and statistically plausible that all model parameters vary within a population, often the quality of the data (i.e. amount of data, sampling schedule, etc.) and the number of individuals that are investigated do not support the reliable quantification of this variability. Therefore during model development the decision about inclusion or removal of a variance component was based mainly on OFV, relevance of the estimated value and precision of the estimated CV. For example a value of 0.0001 for ω_k^2 was not considered relevant and therefore the variability component did not remain in the model.

Residual Variability The residual variance model describes the discrepancy between the observed and the model-predicted value in an individual at a certain time. The most common models for the description of residual variability are given in Equation 2.9-2.11.

- Additive model

$$y_{ij} = f(\phi_i, X_{ij}) + \epsilon_{add,ij} \tag{2.9}$$

- Proportional (coefficient of variation) model

$$y_{ij} = f(\phi_i, X_{ij}) \cdot (1 + \epsilon_{prop,ij}) \tag{2.10}$$

- Combined model

$$y_{ij} = f(\phi_i, X_{ij}) \cdot (1 + \epsilon_{prop,ij}) + \epsilon_{add,ij} \tag{2.11}$$

where y_{ij} is the observation in the i-th individual at time j, $f(\phi_i, X_{ij})$ denotes model prediction and $\epsilon_{add,ij}$ and $\epsilon_{prop,ij}$ are the additive and proportional random quantities which are assumed to be symmetrically distributed with mean zero and a constant variance σ^2. The variances σ^2 of the random quantities are estimated as the diagonal elements of the Σ matrix. The standard deviation of the residual variability is therefore given by $\sqrt{\sigma^2_{add}}$ and $100 \cdot \sqrt{\sigma^2_{prop}}$ represents its coefficient of variation (in %).
The implementation of an additive residual variability model is reasonable if a constant variance independent of the magnitude of the measurement can be assumed (homoscedasticity) which is often the case in PD where the range of observations is narrow (e.g. blood pressure). This assumption does not hold true, however, if the observations span multiple orders of magnitude and the residual variability increases with increasing values for the observations which is often the case in PK (drug concentrations). In PK the combined residual variability model (Equation 2.11) which combines the two models given in Equation 2.9 and 2.10 often is applied. In this model the proportional residual variability component dominates if large values for observations are present whereas the additive residual variability component has more influence on smaller values.

2.1.2.3 Covariate submodel

An important goal of many population analyses is the identification and quantification of relations between model parameters and covariates, i.e. variables specific to an individual which potentially influence the model parameters and partly explain the variability associated with the respective parameter[5,208]. Among other things, the identification of covariates can play

an important role for dose selection, safety with respect to toxic or sub-therapeutic drug concentrations as well as efficacy and can help to understand mechanisms of drug elimination or modes of action. Covariates can be variables describing the individuals' demographics (age, weight, sex), disease status (laboratory parameters, organ function, disease score) or extrinsic factors such as dose, smoking status or concomitant medication[5]. They can also be classified as categorical (dichotomous or ordered) covariates such as sex or severity categories of an adverse event or continuous covariates such as height or creatinine clearance. Depending on the former classifications covariates enter the model in different ways. Continuous covariate relations usually enter the model as a linear, exponential or power function, categorical covariates enter the model in either an additive, fractional or exponential way. In this thesis continuous covariates were included as a power function according to Equation 2.12

$$\theta_{k-Cov} = \theta_k \cdot (\frac{Cov}{Cov_{median}})^{\theta_{Cov_k}} \tag{2.12}$$

where θ_{k-Cov} denotes the parameter value for an individual given its associated covariate value Cov. For the median value of a covariate (Cov_{median}) in the population θ_k represents the typical population parameter estimate. As power models are linear on a logarithmic-logarithmic (ln-ln) scale (Equation 2.13) the exponent θ_{Cov_k} describes the change in $ln(\theta_k)$ per unit change in $ln(\frac{Cov}{Cov_{median}})$[5].

$$Ln(\theta_{k-Cov}) = Ln(\theta_k) + \theta_{Cov} \cdot Ln(\frac{Cov}{Cov_{median}}) \tag{2.13}$$

An example for the inclusion of a dichotomous categorical covariate is given in Equation 2.14 which represents a fractional function and was used during model development of the final PK/PD model presented in section 2.4.2.

$$\theta_{k-Cov} = \theta_k \cdot (1 + Cov \cdot \theta_{Cov_k}) \tag{2.14}$$

θ_k represents the typical population parameter of an individual when the covariate Cov is absent (coded as 0) and θ_{Cov_k} the fractional change in the respective θ_k when Cov is present (coded as 1).

The covariate submodel was developed in two steps: First, covariates that potentially had an influence on the model parameters were preselected based on plausibility, e.g. understanding of (patho-)physiological processes, life situation, influences from the study or concomitant medication, *a priori* knowledge from literature and graphical screening. The second step comprised a stepwise analysis of the preselected covariates in NONMEM®.

Graphical analysis The identification of possible covariate influences on population parameters can be guided by graphical screening. For this purpose a scatter plot depicting the EBE or the estimated IIV for each individual versus the continuous covariate under consideration was generated. The plot did not only reveal a potential influence but also provided information about the nature of the relation between the covariate and the parameter. A continuous increase or decrease indicated a linear model whereas a curvature in the data indicated an exponential or power function model. For categorical covariates Box-and-Whisker plots of the EBEs grouped for the categories were examined. If the graphic indicated a difference between the medians the categorical covariate entered the next step of the covariate screening. Drawbacks of this graphical approach are its subjectiveness, the fact that covariates that are highly influential are more likely to be identified and its dependency on possible η-shrinkage (section 2.1.3.1). Additionally, the covariates are evaluated independent of the model and relations are only contemplated in a univariate way[5]. Hence, this approach, although being useful to get a first impression on possible covariate relations, should be used cautiously.

Analysis in NONMEM® Different methods for the direct analysis of covariates in NONMEM® have been described[208–210] and currently there is no consensus on the most effective method. In the following the general procedure for a stepwise covariate model-building procedure (SCM)[209] is described (Figure 2.2).

Forward inclusion step: Starting from the base model (structural submodel + pharmacostochastical submodel) the preselected covariates were included in the model and tested in a univariate manner, i.e. one covariate was added to the model at a time. The resulting model was evaluated with respect to a decrease in the OFV (section 2.1.3.1) of 3.84 representing a statistically significant influence of the covariate on the respective model parameter (degrees of freedom, df=1, χ^2 distribution, p=0.05). Models including covariates that did not meet the selection criteria were excluded from further analysis. The model showing the highest decrease in the OFV (strongest model improvement) was retained and taken forward to the next step where the remaining covariates were tested. Covariates were added to the model until no more covariates met the inclusion criteria. The model comprising all statistically significant covariates was then referred to as the "full covariate model".

Backward deletion step: In the backward deletion step the covariates were removed from the full covariate model, one at a time. A stricter significance level was applied to test for the significance of the covariate influence. If the increase in the OFV was not greater than 10.83 points (p=0.001, df=1) the covariate was excluded from the model. The remaining covariate

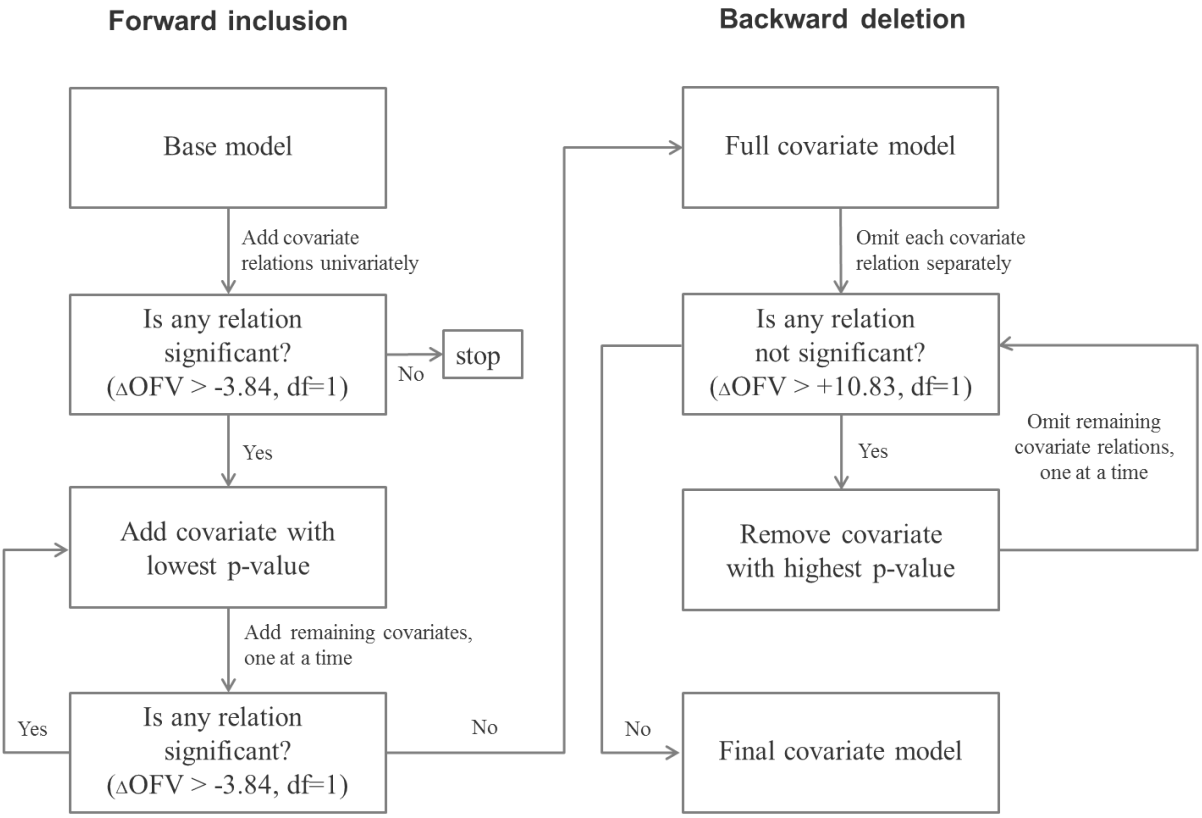

Figure 2.2 Flowchart for the stepwise covariate model-building procedure. OFV: objective function value, df: degrees of freedom. Modified from Uppsala pharmacometric summer school 2011 course material.

relations were tested until the removal of each remaining covariate did result in a significant increase in the OFV.

The SCM method is implemented in Pearl-speaks-NONMEM (PsN©, see 2.1.7) as a tool for automated covariate model-building and was used as such for the covariate analysis described in section 2.3.2.1. The model selection process during SCM is guided by the *statistically* significant influence of a covariate on a model parameter, only. Hence, the final model has to be evaluated with respect to the clinical relevance and biological plausibility of the covariate influence. For instance a covariate might show a statistically significant influence but its magnitude is not sufficient to be clinically relevant. An example for the biological plausibility is creatinine clearance (CLCR) as a predictor for CL of (almost) exclusively renally excreted drugs.

If highly correlated covariates are included in the model (e.g. CLCR and serum creatinine) the covariates will not have an unique effect on the model parameter any more as their effect is

dependent on the value of the correlated covariate[5]. In general, the most plausible covariate was included in the covariate analysis. If a significant influence was found the correlated covariate was evaluated starting from the full covariate model following the backward deletion step. Only the covariate leading to the stronger model improvement remained in the model. For the covariate analysis presented in this thesis the most plausible covariate was included in the SCM method implemented in PsN© if not stated otherwise in the respective sections.

2.1.3 Model selection and evaluation

The assessment of how well the data is described by a specific model is a key element in the model development process. Evaluation and comparison of different models during this process is guided by numerical, statistical and graphical methods. Some of the methods presented in the following section (2.1.3.1) are computationally intense and time-consuming (e.g. log-likelihood profiling and visual predictive check) and were therefore not applied to intermediate models but were used to evaluate key and final models.

2.1.3.1 Numerical and statistical methods

Objective function value and Akaike information criterion The objective function value (OFV) described in section 2.1.1.2 serves as a metric to evaluate model improvements or deteriorations due to additional model parameters in competing models. The likelihood ratio test which tests for the statistical significance of the added model parameters can be applied if the competing models are nested, i.e. the simpler model is a hierarchical simplification of the more complex one[5]. The difference in the -2LL of two nested models is asymptotically distributed as a χ^2 distribution with df representing the difference in the number of estimated model parameters. Thus, if the OFV decreases more than 3.84 points (df=1) the additional parameter significantly improves the model at p=0.05. One possibility for the comparison of non-nested models is the application of the Akaike Information Criterion (AIC) which includes a penalty term for the number of estimated model parameters P, thus, AIC being equal to $-2LL + 2 \cdot P$. As more parameters are added to the model the value of -2LL may decrease but eventually the penalty term ($2 \cdot P$) dominates the equation.

Relative standard error The relative standard error (RSE) is a metric for the assessment of the precision of the parameter estimates. In NONMEM® the absolute standard errors of the corresponding parameters are estimated as the square root of the diagonal elements of the variance-covariance matrix of estimates which is obtained from the NONMEM®s so called

covariance step. During this step the OFV at numerous parameter values close to the final parameter estimates is calculated, resulting in a matrix which includes the OFV for each pair of parameters[211]. This matrix is then inverted resulting in the covariance matrix. The RSE for fixed-effects parameters is then calculated as stated in Equation 2.15

$$RSE, \% = \frac{\text{absolute standard error}}{\text{parameter estimate}} \cdot 100 \tag{2.15}$$

whereas if the variance component is integrated into the model in an exponential way, the RSE for ω is calculated according to Equation 2.16 which results from application of the delta method[212] to transform the standard error from the variance to the CV scale .

$$RSE_{\omega;CV,\%} = \frac{\text{absolute standard error}(\omega^2)}{2 \cdot (\text{estimate } \omega^2)} \cdot 100 \tag{2.16}$$

Shrinkage The phenomenon of shrinkage is due to low information content in the data which might result from sparse and/or non-informative individual data. As the quantity of information at the individual level diminishes, the distribution of the EBEs shrinks towards zero, hence, the individual predictions towards the population mean and similarly the individual weighted residuals ($IWRES = (y_{ij} - y_{pred,ij})/\sigma$) shrink towards zero[213]. η- and ϵ-shrinkage are calculated as described in Equation 2.17 and 2.18, respectively.

$$\eta - shrinkage = 1 - \frac{SD(\eta)}{\sqrt{\omega^2}} \tag{2.17}$$

$$\epsilon - shrinkage = 1 - SD(IWRES) \tag{2.18}$$

where ω^2 is the variance of a population parameter, $SD(\eta)$ and $SD(IWRES)$ denote the standard deviation of ηs and $IWRES$, respectively. A shrinkage value close to 0 indicates a model with sufficient information on the individual level whereas a shrinkage of 1 implies that the data contains no information. The phenomenon of shrinkage is important when η- and ϵ-values are used to evaluate a model (section 2.1.3.2) and special caution should be paid to the corresponding diagnostic graphics (section 2.1.3.2) when η- and ϵ-shrinkage is high (>20% - 30%)[213].

Log-likelihood profiling The log-likelihood profiling (LLP) is a sensitivity analysis and can be used to assess the confidence interval of a parameter independent of any assumptions regarding its distribution. Generally, the model parameters are first estimated and then fixed, one at a time, to their estimate. Following this step the fixed parameter value is changed incrementally from the original estimate. If a confidence interval is to be assessed this is done until

the change in OFV exceeds a predefined value, e.g. 3.84 for the 95% confidence interval[5,214]. In this thesis a LLP was performed in case a parameter was fixed due to model stability to investigate whether or not fixing this parameter to a certain value influences the OFV and the estimates of the remaining parameters. This means that the question whether the parameter estimate resulted from a global minimum of the OFV, or not, was assessed. If the lowest OFV resulted from the originally estimated model parameter, the other model parameters remained unchanged and model stability improved, then the parameter was fixed to its estimated value.

2.1.3.2 Standard goodness of fit graphics

Graphical diagnostics are considered a powerful tool which is used for data visualisation, the assessment of model adequacy, evaluation of the predictive performance of a model as well as the communication of modelling results. They are used to asses the goodness of fit (GOF) of a model which means they detect model misspecifications and help to discriminate between competing models. The following goodness of fit plots were routinely investigated using the functions of the XPOSE package implemented in R:

- Measured observation versus individual (IPRED) and population predictions (PRED)
- Weighted residuals (WRES) versus TIME (or time after dose) and PRED
- Conditional WRES (CWRES) verus TIME (or time after dose) and PRED
- Individual WRES (IWRES) and (C)WRES versus individual identifier (ID)

WRES and IWRES are the weighted difference between the measured observation and the population prediction and the individual prediction, respectively. In contrast to WRES which are computed based on the FO approximation methods even when FOCE is chosen for parameter estimation, CWRES are calculated by linearisation at each individual's Bayesian estimate. Hooker et al.[215] recommend the use of CWRES even when using FOCE+I for parameter estimation although their usefulness for this has not been proven, yet[9,215]. An adequate fit of the model was assumed for figures showing a random, uniform and narrow spread of the data around the line of identity (measured observation vs. PRED and IPRED) or around the zero reference line (residual plots).

2.1.3.3 Visual predictive check

The visual predictive check (VPC) is a simulation-based diagnostic tool to asses the predictive performance of a model, i.e. how well do simulations based on the model resemble the ob-

servations the model under investigation was based on. This is of special importance when therapeutic decisions are made based on the model[216,217]. Furthermore, the VPC can be used during model development for model comparison and assessment of model appropriateness. To generate a VPC 1000 simulations were performed based on the model of interest under the original study design (i.e. dose, dosing interval, sampling times, etc.). The measured observations of the original dataset along with the median, 5^{th} and 95^{th} percentile of the observed and simulated measurements were plotted against the independent variable. If the model was capable of reproducing the central tendency, i.e. the structural model described the profile of a typical patient well, the median of the simulated measurements was, ideally, congruent with the one of the observed measurements. The variability was well captured by the model if approximately 10% of the data were outside of the 90% prediction interval or, in other words, the 5^{th} and 95^{th} percentile of the simulations did not deviate systematically from the ones of the observations.

Binning For data from clinical studies with sampling windows rather than distinct sampling points or when sampling did not take place at the planned time points the course of the simulated (and the observed) percentiles over time often includes spikes when data points are connected with lines for plotting purposes. This is due to the fact, that a reasonable amount of data for the calculation of the statistics is necessary. Additionally, if confidence intervals for the calculated statistics are to be included into the VPC they might be very large if the amount of data used to calculate them is too small, making their contribution useless for the interpretation of the VPC. Hence, in order to make VPCs easier to interpret it is desirable that the curve representing the median and the percentiles exhibits a smooth time course. This can be obtained by summarising certain observations and simulations into so called bins. By binning, clusters of observations, e.g. resulting from the same sampling windows, should not be split into different bins, the binning should be able to capture changes in the dependent variable and the bins should include similar amounts of data points. In this thesis two binning options implemented in PsN© were applied: Binning by a user-defined number of bins, i.e. a desired number of bins is defined and PsN© summarises the data to obtain comparable numbers of observations in each bin (final PK/PD model for leukopenia, section 3.3.9) and binning based on a user-defined time array where the bins are defined by time intervals (final PK models for carboplatin, etoposide and thiotepa, section 3.2.1.4, 3.2.2.4, 3.2.3.3 and the final PK/PD model for neutropenia, section 3.5.3.2). The number of bins as well as the user-defined time vectors are given in the respective result section.

2.1.4 Simulations

Simulations are a powerful tool to perform systematic investigations when resources are constrained and/or to answer questions which could otherwise only be investigated by performing an experiment or a study or when there are no means to answer the question experimentally. They are used to predict an outcome based on a given model together with defined input parameters. Among many other applications in population PK/PD simulations are conducted to design, optimise or simulate clinical trials, support decision making in the development process of a drug, answer questions regarding safety and efficacy, elucidate the impact of covariates on model PK and PD parameters, guide therapeutic decisions and assist in model selection and evaluation[5]. Two types of simulations were applied in this thesis and are introduced in the following paragraphs.

Deterministic simulations Deterministic simulations present the most simple form of simulations, allowing no variability on model parameters which instead are fixed to a deterministic value and therefore the range of the expected model output is neglected. Although being informative the predicted outcome should be treated with caution as in a nonlinear system the mean of the function does not equal the value of the function using the mean input[5]. Nevertheless deterministic simulations are a useful tool to investigate the underlying system without having random elements influencing the results[5]. Hence, they were applied to investigate the haematopoietic system in the setting of HDCT as described in section 2.5.

Stochastic simulations Stochastic simulations, often referred to as Monte Carlo simulations, take the variability of the model parameters into account. They thereby reflect the reality more accurately and give evidence about the range of the expected outcome. This is of importance and interest when questions regarding safety or efficacy should be answered. The variability is taken into account by randomly sampling different sets of model parameters from multivariate distributions which are defined by the parameter estimates that are typical for the population and their associated variability[5]. The expected outcome of the function describing the model is then calculated for each set of parameters and the range can be assessed from the model predictions. This kind of simulation was used to evaluate the predictive performance of the models (VPC, section 2.1.3.3) and to evaluate the optimal day for the performance of an ASCR based on the final PK/PD model presented in section 2.5.

2.1.5 Data management

Project 1-3: Characterisation of leukopenia following HDCT The raw data for the PK/PD analysis presented in section 2.3 and 2.4 was based on the clinical investigation presented in section 2.2. Leukocyte concentrations, demographic covariates, clinical chemistry parameters as well as blood samples for the determination of drug concentrations were collected during a clinical investigation at the Virchow Klinikum Berlin. Platinum and etoposide concentrations were determined at the Institute of Pharmacy at the Freie Universität Berlin and thiotepa concentrations were measured at the Institute of Pharmacy, Clinical Pharmacy at the Rheinische Friedrich-Wilhelms-Universität, Bonn. Determined concentrations were either available as a Microsoft Excel® spreadsheet (carboplatin, leukocytes) or on paper (etoposide, thiotepa); dosing and sampling history was available from the original study reports. For the calculation of the secondary covariate CLCR the information on serum creatinine (CREA) was taken from the Microsoft Excel® spreadsheet which comprised ultrafilterable platinum (Pt) measurements and demographic covariates[79].

Project 4: Characterisation of the cytotoxic potency of chemotherapeutics The *in vitro* data presented in section 2.6 was collected during the assay development of a cellular cytotoxicity assay as part of a diploma thesis[218] at the Institute of Pharmacy, Clinical Pharmacy, Martin-Luther-Universität Halle-Wittenberg. The data from a 96 well plate assay was provided in form of Microsoft Excel® spreadsheets. Data for the investigations on *in vitro-in vivo* comparability of measures for cytotoxicity were obtained from 24 open uncontrolled trials[219] and were provided by the Uppsala University in a NONMEM® readable format.

Project 5: Description of glycation processes throughout the lifespan of erythrocytes Data for the description of the PK of lixisenatide, FPG and HbA_{1c} measurements presented in section 2.7 were available for a subgroup of patients enrolled in two a clinical studies sponsored by Sanofi[220] and provided in a NONMEM® readable formate.

2.1.5.1 Dataset building

The general structure of a NONMEM® dataset is predefined by the software itself[206] and includes dependent variables (e.g. observed concentration measurements of a drug and/or a PD effect) and a number of independent variables such as time, dosing information and patient specific covariates such as age, weight or laboratory parameters. Additionally, NONMEM® specific variables such as EVID (event identifier) must be provided in the dataset. All datasets

were built in the R software package if not stated otherwise in the respective result section (sections 3.1.1, 3.5.1.1 and 3.6.1.1).

2.1.5.2 Derived covariates

Covariates derived from other individual-specific factors and included in the population analyses in this thesis comprised body surface area (BSA), creatinine clearance (CLCR) and predicted normal weight (PNWT). The BSA was calculated according to DuBois and DuBois[221] according to Equation 2.19.

$$\text{BSA}\,(\text{m}^2) = \text{weight}^{0.425} \cdot \text{height}^{0.725} \cdot 0.007184 \tag{2.19}$$

The CLCR was calculated according to the formula by Cockcroft and Gault[222] which is defined in Equation 2.20.

$$\text{CLCR}\,(\text{mL/min}) = \frac{(140 - \text{age}) \cdot \text{weight}}{72 \cdot \text{serum creatinine}\,[\text{mg/dL}]} \tag{2.20}$$

Calculation of the PNWT for males (and females) was based on the formula (Equation 2.21) developed by Duffull et al.[223]

$$\text{PNWT(kg)} = 1.57 \cdot \mathit{weight} - 0.0183(0.0242) \cdot \mathit{body\ mass\ index} \cdot \mathit{weight} - 10.5(12.6) \tag{2.21}$$

2.1.5.3 Data checkout

All datasets were subject to a data checkout before the modelling process was started. This procedure comprised a graphical analysis in the R package which was used for the plotting of the dependent variable versus time for the entire population and for each individual, as well as plotting of all independent variables before the start of the therapy versus the individual identifier (ID) of each patient to check for inconsistency, implausibility and completeness in the dataset. Additionally, the datasets were checked column by column in either Microsoft Excel® or R for implausible values in comparison to reference values. Moreover, a cross-column check was carried out to check for violations of NONMEM® predefined settings, e.g. for a dosing record EVID has to be set equal to 1.

2.1.5.4 Missing observations and covariates

Data missing completely at random, i.e. cases of missing data were indistinguishable from cases with complete data[5], were not included in the data analysis by any kind of substitution. Concentration measurements below the lower limit of quantification (LLOQ) were only

reported for concentration measurements of thiotepa and were treated according to the M5 method described by Beal[224]. According to this method the first value reported as below LLOQ was set to half the value of LLOQ and all preceding concentration measurements were omitted. Continuous covariates that were missing completely within one patient were replaced by the population median. A missing covariate within a time series of an individual was replaced by the last reported value of this covariate, which was carried forward until the next value for the covariate of the respective individual was reported. If present, missing data are described in the result section of the respective analysis.

2.1.5.5 Outliers

Outliers in the dependent variable, i.e. concentration of a drug (PK) or a measure of the drug effect (PD), were excluded from analysis. Measurements were declared outliers if one or multiple of the following conditions were met: (i) observations were conspicuous in diagnostic plots, (ii) model instabilities during the initiation or estimation process were reported for a specific observation, (iii) there was evidence for the observation to be suspiciously high or low (5 to 10-fold increased or decreased) compared to observations at the same time after the last dose administration (TALD) in the population. Final models were evaluated including and excluding the identified outliers and the results were carefully evaluated to judge the influence of the specific observation on the model parameters and the model performance. All excluded outliers and the reason for exclusion are documented and reported in the results section of the respective analysis (section 3.2.1.5, 3.2.2.5 and 3.2.3.4).

2.1.6 Descriptive statistics

For the descriptive analysis of the data and the results different metrics for the description of the central tendency (median, arithmetic or geometric mean) and the dispersion within the population (standard deviation, variance, coefficient of variation) were employed. Statistical analysis were performed in the R software package or Microsoft Excel®.

2.1.7 Software

All population modelling and simulation activities including simulations for the VPCs were performed using NONMEM® VI 2.0, NONMEM® 7.1 and 7.2 in combination with Pearl-speaks-NONMEM[225] (PsN©) version 2.5.3. - 3.5.3. All datasets were built using the R software package[226] (version 2.10.1-2.15.0) with only few final modifications done in Microsoft Excel®

2007/2010. Descriptive statistics were either performed in R or Microsoft Excel®. The data check out was performed in R as were the graphical analysis which were done in combination with the package Xpose[227] (version 4.1.0-4.3.5) and ggplot2[228] (version 0.9.0). For the estimation of EC_{50} values from *in vitro* data (section 2.6) the software package *drc*[229] (version 2.0-1) implemented in R was used.

2.2 CET Study

2.2.1 Study design

The clinical pharmaceutic investigation took place from November 1992 until October 1996 under the supervision of Prof. Dr. W. Siegert, Department of Haematology and Oncology at the Virchow-Klinikum of the medical faculty at the Humbolt-Universität, now part of the Charité, Berlin[79]. The investigation was approved by the ethics committee of the Virchow-Klinikum and comprised a HDCT regimen in patients with testicular cancer including an ASCR. All patients received a combination regimen consisting of carboplatin (C), etoposide (E) and thiotepa (T) which were administered consecutively as 1 h infusions via a double lumen, tunneled, central venous catheter on three (C, T) and four (E) consecutive days (Figure 2.3). The total amount of administered drug was 1500 mg/m^2, 2400 mg/m^2 and 750 mg/m^2 which was reduced in case of renal impairment by 20%, 25% and 40% for C, E and T, respectively. Instead of thiotepa two patients received ifosfamid as a 22 h infusion on 4 consecutive days at a total dose of 10000 mg/m^2. Among other concomitant medication the additional supportive treatment consisted of intravenous hydration, anti-emetic and anti-infective therapy, prophylaxis of hyperuricemia and transfusion of blood cell concentrates.

2.2.1.1 Patient recruitment

Eligibility criteria for HDCT with ASCR were an age $\geq$ 18 years, a histologically or tumour marker proven germ cell tumour, the insufficient response to one or multiple courses of cisplatin-based conventional chemotherapy, multiple relapse and/or refraction, a Karnofsky index[230] $\geq$ 60% and a written informed consent of the patient. Patients were excluded from the investigation if they met one of the following conditions: diffuse infection of the bone marrow with tumour, or impairment of one of the following organs:

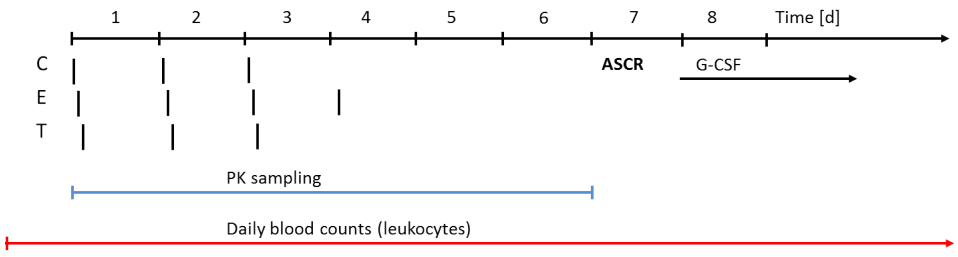

Figure 2.3 Study design: administration and sampling scheme. C: carboplatin, E: etoposide, T: thiotepa, ASCR: autologuous stem cell rescue, G-CSF: granulocyte colony-stimulating factor, PK: pharmakokinetic.

- Kidney: 1.3-fold of the reference value[1] or creatinine clearance < 70 mL/min
- Liver: bilirubin > 1.5-fold the reference value[1] or serum transaminases > 2-fold the reference value[1]
- Lung: diffusion capacity for carbon monoxide (DL_{CO}) < 60% of the reference value[1]
- Heart: clinically manifest heart insufficiency
- Bone marrow: peripheral leukocyte concentration < $0.3 \cdot 10^9$ cells/L or thrombocyte concentration < $5.0 \cdot 10^{10}$ cells/L

2.2.1.2 Sampling scheme

During HDCT plasma and ultrafiltrated plasma samples were taken to characterise the pharmacokinetic profiles of carboplatin, etoposide and thiotepa. Samples were taken prior to the first carboplatin infusion and 0, 1.5, 2.5, 4, 7, 11, 21, 23 h and 0, 23 h and 0, 1.5, 2.5, 4, 7, 11, 23, 35, 44, 56, 72, 96, 264 h relative to the end of the carboplatin infusion on the first, second and third day of HDCT, respectively. Haematological as well as clinical chemistry parameters such as CREA, liver enzymes, glucose, electrolytes were determined daily. An overview over the study protocol as well as the sampling scheme is depicted in Figure 2.3.

[1]Upper limit of normal: serum creatinine 1.0 mg/dL, bilirubin 1.0 mg/dL, AST (aspartate transaminase) 21 U/L, ALT (alanine transaminase) 23 U/L, GGT (gamma-glutamyltransferase) 28 U/L, DL_{CO} 100%

2.2.2 Carboplatin

Carboplatin (Carboplat 450©, Carboplatin Brystol-Myers Squibb, Munich) was dissolved in Glucose 5 Braun© (Glucosemonohydrate, Braun Melsungen, Melsungen) and administered with an Infusomaten® (Braun Melsungen, Melsungen).

2.2.2.1 Determination of carboplatin concentrations

Ultrafiltered plasma aliquots were obtained by separating blood from plasma via centrifugation and an additional centrifugation step of the plasma in either Centrisart™ (Sartorius, Goettingen, Germany) or in Centrifee™ tubes (Millipore, Eschborn, Germany). Aliquots were stored at -70° C until analysis. Pt concentrations in the ultrafiltrate were measured with a validated flameless atomic absorption spectrometry (FAAS) method[77]. Linearity of the calibration function was given from 0.021 to 32000 μg/mL with coefficients of variation of 1.2% - 7.3% (within-day precision) and 2.9% - 8.6% (between-day precision). The LLOQ for ultrafiltered measurements was 0.020 μg/mL[231].

2.2.3 Etoposide

Etoposide (Vepesid J®, Etoposid, Bristol-Myers Squibb, Munich) was administered undiluted with a Perfusor® (Braun Melsungen, Melsungen).

2.2.3.1 Determination of etoposide concentrations

Total etoposide concentrations were measured with a modified reversed-phase HPLC (high-performance liquid chromatography) method[97,232]. As stationary phase a Hypersil ODS RP-18 column (125x4 mm, particle size: 5 μm, integrated pre-column, Knauer, Berlin, Germany) was used. The mobile phase consisted of acetonitrile/methanol/0.01 M Na_2HPO_4 (3.5/ 35.0/ 60.5 v/v), adjusted to pH 5.3 with H_3PO_4 to avoid degradation of etoposide. Etoposide concentrations were determined on a HPLC system with electrochemical detection. For this method the LLOQ was 0.092 μg/mL and linearity of the calibration function was given up to 200 μg/mL. Within-day precision and between-day precision were determined to be 3.1% and 4.3%, respectively, and accuracy was -2.7% and -0.15% for the two days on which the between-day precision was investigated[232].

2.2.4 Thiotepa

Thiotepa "Lederle®" (Thiotepa, Lederle Arzneimittel, Münster) was administered without being diluted with a Perfusor® (Braun Melsungen, Melsungen).

2.2.4.1 Determination of thiotepa concentrations

Thiotepa samples were treated according to an optimised gas chromatography method[233] which was developed at the University of Essen[234]. In short, the solid phase extraction for the sample preparation was as follows: thiotepa was eluted into 100 μL of ethyl acetate from a Baker bond spe© C_{18}-column conditioned with 0.01 M methanol which was adjusted to pH 7 with phosphate buffer. The residue after evaporation was reconstituted in hexamethylphosphortriamid (2 μg/mL in ethylacetat). 1 μL of this solution was injected into the gas chromatograph (Hewlett Packard 5890, Palo Alto, USA). A HP-5MS column (30 m x 0.25 mm, phase film thickness: 0.25 μm, Palo Alto, USA) was used for analysis. Helium served as mobile phase at a flow rate of 1 mL/min (split: 1:20). The gas chromatograph was coupled to a mass spectrometer (Hewlett Packard GCD Plus G1800C, Palo Alto, USA) for detection and quantification of thiotepa by its two characteristic fragments of 115 and 147 m/z. For the optimised method[233] the LLOQ was 50 ng/mL and the calibration function was linear up to 10 μg/mL. Between-day precision on three days and was between 0.3% and 10.1% with an accuracy of 5.5% - 14.3%.

2.2.5 Investigation of the infusion duration

The infusion duration for all drugs was documented with two endpoints: the end of the infusion and the end of the washing period of the infusion tubes between the administration of the three drugs. Additionally, the usage of long infusion tubes motivated the investigation of the two infusion durations as, due to small infusion rates, drug still might have been present in the infusion tubes at the end of the infusion and, hence, might have been entering the circulation during the washing phase.

2.2.6 Leukocytes

Leukocyte concentrations were determined along with other routinely measured clinical chemistry parameters for the surveillance of the patients' vital functions. As suppression of the bone marrow function is one of the most important adverse events in HDCT blood counts were determined daily to strictly control for leukopenia and thrombocytopenia. Leukocyte

counts were determined using flow cytometry and/or by manual blood count using a counting chamber.

2.2.7 Supportive treatment

Of special interest for the investigations presented in this thesis were supportive treatments that were possibly influential on the system of leukopoiesis. The three most important ones being the autologuous stem cell rescue (ASCR), the administration of granulocyte colony-stimulating factor (G-CSF) and the antiemetic dexamethasone (DEXA).

Autologuous stem cell rescue To enable the immense dose escalation which is performed during HDCT the bone marrow function needs to be supported to achieve recovery of the haematopoietic system from severe myelosuppression in a clinical tolerable time frame. This can be done by an autologuous retransfusion of peripheral stem cells. The ASCR in the investigated study was performed three days after the last etoposide infusion, on day seven (D7) of HDCT. Stems cells were recruited on two to four days prior to HDCT by stimulation with G-CSF, collected from the peripheral blood via leukoapheresis before the start of HDCT, cryopreserved and tested for viability before retransfusion. For the ASCR an amount of $3 \cdot 10^6$ $CD34^+$ cells per kilogram body weight was being aimed for.

Granulocyte colony-stimulating factor In oncology G-CSF is used to accelerate the time to recovery from leukopenia after chemotherapy as patients are prone to severe infections and sepsis having low concentrations of leukocytes. G-CSF (Neupogen® 30 or 40) was administered as a 24 h infusion starting one day after the stem cell rescue was conducted, i.e. on day eight (D8) of HDCT. The supportive treatment was ceased after leukocyte concentrations were above 0.5 or $1.0 \cdot 10^9$ cells/L in 7 and 10 cases, respectively.

Dexamethasone The glucocorticoide dexamethasone was administered as part of the antiemetic treatment once or twice daily at 12 or 16 mg as a short infusion during the first 0 - 6 days of the therapy, as required. Glucocorticoides have shown to increase neutrophil concentrations by reversing margination to blood vessels and mobilising cells from the bone marrow by enhancing G-CSF levels[235]. Hence, the influence of DEXA on the system of leukopoiesis was of special interest during analysis.

2.3 Project 1: Pharmacokinetic analysis of high-dose carboplatin, etoposide and thiotepa

The objective of this analysis was the development of three population PK models that adequately described the concentration-time profile of carboplatin, etoposid and thiotepa. The empirical Bayes estimates derived from the estimated population parameters and their variances were then to be used as input in the population PK/PD model for the description of leukopenia following HDCT described in section 2.4.

2.3.1 Pharmacokinetic model for carboplatin

2.3.1.1 Model development

In 2010, Lindauer et al. published a model for the description of the PK of high-dose carboplatin based on data from five studies in children and adults[236]. Data of the population investigated in this thesis was part of one study used to develop the model by Lindauer et al. They defined a two compartment model with linear elimination from the central compartment and a combined model for the residual variability as the structural model.
Based on their structural model the base model for the description of ultrafilterable Pt concentrations presented in this thesis was developed. The next step of model development comprised the exploration of the stochastic submodel starting with a model comprising variance components for each parameter of the structural model without accounting for possible parameter correlation (section 2.1.2.2). For the covariate analyses the final covariate model by Lindauer et al. was defined the full covariate model and the included covariates were tested following the backward deletion step of the covariate analyses described in section 2.1.2.3. This was done based on the assumption all covariates identified by Lindauer et al. possibly have an effect on the PK parameters estimated during the analysis presented in this thesis, as the study population under investigation was part of the population Lindauer et al. investigated. However, as their PK analysis comprised five studies in children and adults the variability in the population investigated in this thesis was assumed to be lower compared to theirs, and therefore their final covariate model was further reduced. In a last step the final covariate model was refined re-evaluating the relevance of the variability components describing the IIV.

2.3.1.2 Model selection and evaluation

Model development was guided by plausibility and precision of parameter estimates, OFV and GOF plots as described in section 2.1.3. The predictive performance of the model was evaluated based on a VPC (section 2.1.3.3). The influence of observations excluded during model development on the parameter estimation and the model performance was evaluated based on the final model by inclusion of the respective outliers as described in section 2.1.5.5.

2.3.2 Pharmacokinetic model for etoposide

2.3.2.1 Model development

For the description of the central tendency in etoposide concentrations over time linear one, two, and three compartment models with first-order elimination from the central compartment were investigated as the structural submodel. Different pharmacostatistical submodels were explored starting with a model comprising variance components for each parameter of the structural model without accounting for possible parameter correlation (section 2.1.2.2). The residual variability was examined by testing an additive, proportional and a combined residual variability model. In a last step the automated SCM method implemented in PsN© was used for covariate analysis (section 2.1.2.3). The tested covariates included those identified during graphical covariate screening and covariates previously published in literature[237,238] which were available for the investigated study population and reasonable with regard to the population and the study design.

2.3.2.2 Model selection and evaluation

The evaluation of the investigated models was based on OFV, plausibility of parameter estimates and their precision as well as GOF plots (section 2.1.3.2). A VPC was performed to evaluate the predictive performance of the model (section 2.1.3.3). Since only data of 17 patients entered the final model and less data was available compared to carboplatin the 10^{th} and 90^{th} percentiles were chosen for this analysis as for smaller populations less extreme percentiles are more appropriate to asses the predictive performance of the variability of the model[239]. Outliers excluded during the process of model development were investigated after determination of the final model as described in section 2.1.5.5.

2.3.3 Pharmacokinetic model for thiotepa

2.3.3.1 Model development

For the determination of the structural submodel a linear, one and a two compartment model were investigated. The latter was previously published for a compartmental analysis conducted for a population including the patients of the CET-study[233] applying the standard two-stage approach. Despite the intravenous administration of thiotepa a delay in the observed maximal concentrations, C_{max}, was observed, probably due to the length of the infusion tubes and the slow infusion rate. Therefore two delay models including a lag time model and a transit model were investigated. The lag time method estimates a time that is added to the actual time of the drug administration, thus, assuming that the delay in the occurrence of drug concentrations in the plasma is due to a "lagged" dosing event[206]. The transit model describes the delay of C_{max} by a passage of the drug through a chain of transit compartments[240] with a single transition rate constant k_{tr}. Originally, this model was proposed for the estimation of a delay in the absorption process of an orally administered drug. One of the advantages of this model is that the number of transit compartments N can be estimated. The analytical solution for the estimation of the amount of drug a_N in the N-th compartment is given by Equation 2.22.

$$a_N(t) = F \cdot Dose \cdot \frac{(k_{tr} \cdot t)^N}{N!} \cdot e^{-k_{tr} \cdot t} \tag{2.22}$$

where F denotes the bioavailability which was set to 1 as thiotepa was administered intravenously and $N!$ is the N factorial function with the argument N (estimated number of transit compartments). The transition rate k_{tr} is derived from the mean transition time (TT) which was introduced as a model parameter to estimate the time it takes for the drug to reach the last transit compartment ($k_{tr} = n/TT$, with n being the number of transitions). For the approximation of $N!$ the Stirling's formula given by Equation 2.23 was used.

$$n! \approx \sqrt{2\pi} \cdot N^{N+0.5} \cdot e^{-1} \tag{2.23}$$

The passage from the last transit compartment to the central compartment of the model is usually described with the absorption rate constant k_a which was assumed to be equal to k_{tr} for the purpose of modelling the delay in plasma concentrations of an intravenously administered drug. For the application of the transit-delay model data was logarithmically transformed to prevent numerical difficulties in case of large N. The IIV was investigated following the bottom-up approach (section 2.1.2), residual variability was explored applying an additive and a combined residual variability model on the logarithmic scale. A covariate analysis for

the PK of thiotepa was not planned to be performed due to the sparse data situation (section 3.1.4.2).

2.3.3.2 Model selection and evaluation

The evaluation of intermediate models was based on OFV, plausibility and precision of parameter estimates as well as GOF plots (section 2.1.3.2). Key and final models were additionally assessed based on VPCs (section 2.1.3.3). Since only data of 17 patients entered the final model and less data was available compared to carboplatin the 10^{th} and 90^{th} percentiles were chosen for this analysis as for smaller populations less extreme percentiles are more appropriate to asses the predictive performance of the variability of the model[239]. During the model development process ten observations were removed from the dataset and their influence on model parameters as well as performance was evaluated based on the final model. Outliers are documented in detail in the respective result section (section 3.2.3.4).

2.3.4 Investigation of the infusion duration

For the investigation of the impact of the infusion duration on the PK profile of the drugs additional datasets were built containing either information about the short (carboplatin) or the long (etoposide) infusion duration. In the case of thiotepa the infusion duration was redundant as for the final model the infusion duration was not taken into account. The final PK models of carboplatin and etoposide were fit to the respective datasets and the precision of the parameter estimates and the prediction of C_{max} were investigated based on GOF plots (section 2.1.3.2) and plots of individual concentration-time profiles.

2.4 Project 2: Pharmacokinetic/pharmacodynamic modelling of leukopenia

In the following project the link between the PK profiles for high-dose carboplatin, etoposid and thiotepa and their PD effect on the leukopoietic system was to be established. Following a sequential modelling approach EBEs of the PK parameters of each drug were used as input in the population PK/PD model. Another objective of this analysis was the characterisation of the leukopoietic system with respect to the special setting of HDCT and the (myelo-)supportive treatment, i.e. the ASCR and the administration of G-CSF and DEXA as an antiemetic.

2.4.1 Model for myelosuppression

The analysis of the leukopenic-time course after HDCT was based on a semi-mechanistic population PK/PD model for myelosuppression published by Friberg et al.[138] in 2002 that meets the mentioned prerequisites of a semi-mechanistic model (section 1.4.2): it describes chemotherapy-induced myelosuppression and allows for the differentiation of drug-specific parameters and parameters which characterise the haematopoietic system (Figure 2.4, blue and red, respectively). In the model the compartment for the proliferating cells in the bone marrow is linked to the compartment of the cells in the circulation through a chain of transit compartments. The transit compartments account for the observed time delay in the decrease in leukocyte concentrations, mimicking the maturation process of the cells in the bone marrow which is estimated as the mean maturation time (MMT). A feedback mechanism, defined as the ratio of the number of circulating cells before the start of the HDCT (Circ(t_0)) and the observed circulating cells Circ(t) at time t, allows for the description of the rebound after nadir concentrations are reached and is introduced to the model as a power function (feedback exponent: γ). The drug exerts an inhibitory effect ($E_{drug}(t)$) on the proliferation rate constant k_{prol} of the cells in the bone marrow. In the original model $E_{drug}(t)$ was either described by a linear or an E_{max} model, linking the drug concentration to the PD effect. The drug-specific parameters slope (SL) or E_{max} (maximal effect) and EC_{50} (concentration at half maximal effect) are a measure for the sensitivity of the proliferating cells in the bone marrow towards the cytotoxic drug. Assuming steady state conditions before HDCT, i.e. no net change in cell concentrations in absence of a drug, k_{prol} and the elimination rate constant k_{el} are set equal to the transition rate constant k_{tr} which describes the transition of the cells from the bone mar-

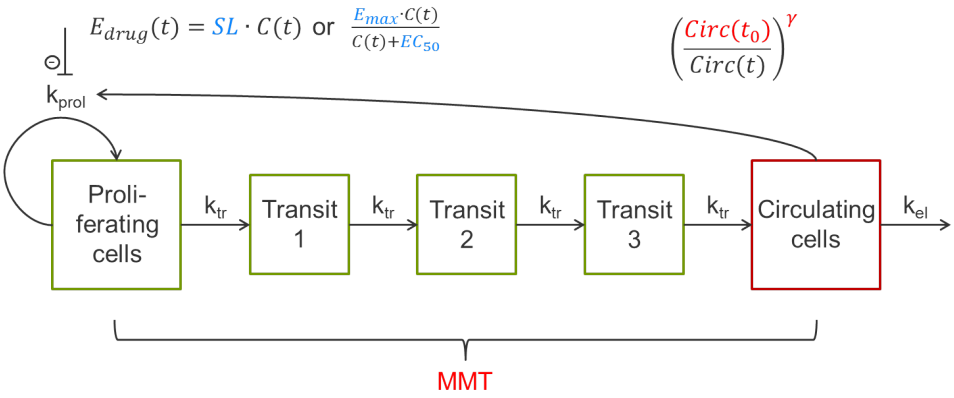

Figure 2.4 Structure of the PK/PD model for the description of myelosuppression. C(t): concentration of the drug at time t; k_{prol}, k_{tr}, k_{el}: proliferation, transition, elimination rate constant, respectively; Circ(t): leukocyte concentration in the circulation at time t; E_{drug}: drug effect. Drug-specific parameters: SL: slope, E_{max}: maximal effect and EC_{50}: drug concentration at half E_{max}. System-related parameters: $Circ(t_0)$: leukocyte concentration in the circulation before start of high-dose chemotherapy, MMT: mean maturation time and feedback exponent γ. Modified from Friberg et al.[138]

row to the circulation. This constant is defined as $k_{tr} = n/MMT$ with n being the number of transitions.

2.4.2 Model development

The model described in section 2.4.1 was modified to meet the special conditions of the HDCT study. The drug effect of the combinatorial regimen was investigated taking all three drugs into account (section 2.4.2.1). System-specific parameters were explored investigating the estimation of the baseline $Circ(t_0)$ and the number of transit compartments N (section 2.4.2.2 and 2.4.2.3). Furthermore, the influence of the myelosupportive as well as the concomitant treatment on the underlying physiological process of leukopoiesis was investigated (section 2.4.2.4 and 2.4.2.5). In a last step covariates were evaluated for their potential influence on model parameters (section 2.4.2.7).

2.4.2.1 Implementation of the drug effect

For incorporation of $E_{drug}(t)$ either a linear inhibitory model (Equation 2.24) or an inhibitory E_{max} model (Equation 2.25) were investigated for each drug. During model development the

effect of the three drugs of the combinatorial HDCT regimen was assumed to be additive and described by a linear inhibitory model (Equation 2.26).

$$E_{drug}(t) = SL \cdot C(t) \tag{2.24}$$

$$E_{drug}(t) = \frac{E_{max} \cdot C(t)}{C(t) + EC_{50}} \tag{2.25}$$

$$E_{drug}(t) = \sum_{i=1}^{N} SL_i \cdot C_i(t) \tag{2.26}$$

where SL_i and $C_i(t)$ denote the drug-specific parameter slope (SL) and the concentration C for the i-th drug at time t. E_{max} represents the maximal effect of the drug and EC_{50} the drug concentration at half maximal effect.

For the evaluation of a possible drug-drug interaction a response-surface model[141,241] for the interaction of carboplatin and etoposide was evaluated. This model enables the differentiation and quantification of a possible synergistic, antagonistic or additive drug-drug interaction by estimating the parameter α and was implemented as exemplarily described for a generic combination of two drugs (A and B) in Equation 2.27 and 2.28.

$$E_{A,B} = \frac{U_A + U_B}{E_{50}} \tag{2.27}$$

$$E_{50} = 1 - \alpha \cdot \frac{U_B}{U_A + U_B} + \alpha \cdot (\frac{U_B}{U_A + U_B})^2 \tag{2.28}$$

$E_{A,B}$ is the joint drug effect of drug A and B, U_A and U_B are equal to the concentration of drug A or B, respectively, times their respective SL, thus, expressing a transformed concentration taking the potency of each drug into account. E_{50} denotes the potency of the drug combination at a given combination of the drugs' concentrations.

Minto et al.[241] used fourth-order polynominal functions to obtain enough flexibility for the approximation of the functions describing the parameters at a given drug combination. However, for E_{50} they decided that the more simple quadratic form was sufficient to describe the curvature of the isobologram characterising the drug-drug interaction at a given drug concentration for A and B. After simplification of the fourth-order polynomal function the parameter α of this function remains. An additive effect is given if E_{50} equals one, a synergistic interaction is characterised by a value of E_{50} that is smaller than one whereas a value of E_{50} greater than one indicates an antagonistic interaction.

2.4.2.2 Baseline estimation methods

The estimation of the baseline value, i.e. the leukocyte concentration before start of the HDCT Circ(t_0) is particularly important, as this parameter not only defines Circ(t_0) but enters the model in the feedback and therefore influences the description of the leukopenia throughout the entire time course. Three baseline estimation methods[242] were investigated during model development (Equation 2.29, 2.30, 2.31).

- Baseline estimation method 1 (B1)

$$Circ(t_{0,i}) = \theta_{Circ(t_0)} \cdot e^{\eta_i} \tag{2.29}$$

- Baseline estimation method 2 (B2)

$$Circ(t_{0,i}) = Circ(t_{0,i,obs}) \cdot e^{\eta_{i,RV}} \tag{2.30}$$

- Baseline estimation method 3 (B3)

$$Circ(t_{0,i}) = (\theta_{Circ(t_0)} \cdot \frac{\sigma^2}{\omega^2 + \sigma^2} + Circ(t_{0,i,obs}) \cdot \frac{\omega^2}{\omega^2 + \sigma^2}) e^{\eta_{i,RV} \cdot \frac{\omega^2}{\omega^2 + \sigma^2}} \tag{2.31}$$

For the description of $Circ(t_{0,i})$ for each individual i, the B1 method (Equation 2.29) estimates a typical value for the baseline ($\theta_{Circ(t_0)}$) and its associated IIV (η_i). The underlying assumption of the B2 method given in Equation 2.30 is that the same residual variability (RV) that is applied to the rest of the data also applies to the baseline data. Hence, $Circ(t_{0,i})$ is allowed to deviate from the individual observed baseline ($Circ(t_{0,i,obs})$) by the random variable $\eta_{i,RV}$ which has a zero mean and is constrained to the same variance as the residual variability σ^2. Hence, the residual variability is allowed to vary between individuals but is the same within each individual[242]. The B3 method (Equation 2.31) combines the information in $\theta_{Circ(t_0)}$ and $Circ(t_{0,i,obs})$ and weights each source of information by its associated uncertainty. The interindividual variance ω^2 reflects the uncertainty with which $\theta_{Circ(t_0)}$ reproduces the actual observed individual baseline value ($Circ(t_{0,i,obs})$). Conversely, the uncertainty associated with $Circ(t_{0,i,obs})$ is reflected by the residual variability σ^2. The magnitude of the IIV and RV associated with the baseline data determines whether $\theta_{Circ(t_0)}$ or $Circ(t_{0,i,obs})$ dominate the estimation of the baseline. The three final key models were compared in terms of AIC, precision of parameter estimates, GOF plots and individual prediction of the leukopenic-time profile with special attention drawn to the first few days after start of HDCT.

2.4.2.3 Number of transit compartments

The observed delay in the effect of the cytotoxic treatment, i.e. the decrease in leukocyte concentrations, was described by a chain of transit compartments in the model. Since MMT defines the same transition rate constant (k_{tr}) for all compartments the number of transit compartments, N, can be increased without estimating additional parameters. Using a chain of transit compartment allows the maturation time to vary between cells within an individual[142]. Moreover, the number of transit compartments defines the shape of the effect curve, i.e. the decline in leukocyte concentrations, and the distribution of MMT[243]. The more transit compartments are added to the model the steeper the decrease in the predicted leukocyte concentrations and the lower the variability in MMT. Therefore, the model development process comprised the investigation of the number of transit compartments to determine the one that best described the leukopenic-time course in the population.

2.4.2.4 Initial increase in leukocyte concentrations

The time course of leukopenia in the special setting of HDCT revealed a pronounced increase in leukocyte concentrations during the first few days of the therapy. This increase has been described for other chemotherapeutic regimens and has been associated with the known effects of DEXA[148,151] which triggers the enhanced release of G-CSF[244]. No information for the DEXA administration was documented, besides the administered amount, the number of administered doses per day and, for few patients, a short infusion was reported as the route of administration. The exact dosing times were not available and therefore the first dosing was set to 9 a.m. as this time was reported for few patients. Multiple doses were spread evenly over the day (e.g. for two doses the second dose was set 12 h later to 9 p.m.). Several approaches for the integration of the effect associated with the anti-emetic treatment have been explored:

1. The initial increase was integrated as an additional compartment "INI_{DEXA}" that was linked to the compartment of circulating cells (Figure 3.23). INI_{DEXA} was initiated with an estimated amount of cells (C_{INI}) at the time associated with the first administration of DEXA for each patient. The mean elapsed time until the additional cells appeared in the circulation (MT_{INI}) was estimated and the transition rate constant k_{ini} was calculated as the reciprocal of MT_{INI}.

2. In contrast to 1., INI_{DEXA} was initiated with another estimated amount of C_{INI} each time DEXA was administered.

3. The administration of DEXA coded as a dichotomous covariate as well as the amount of each dose and the total amount administered to each patient were subject to a covariate analysis (section 2.4.2.7).

In addition to the structural changes that were introduced to the model the variability of the new parameters C_{INI} and MT_{INI} was investigated.

2.4.2.5 Integration of the autologuous stem cell rescue

Different approaches for the integration of the ASCR were explored based on a model proposed by Ramon-Lopez et al.[147] First, the ASCR was integrated as an additional compartment (compare INI_{DEXA} section 2.4.2.4). In contrast to the initialisation of INI_{DEXA}, the compartment for the autologuous stem cell rescue (SCR, Figure 3.23) was initiated with the reported, not estimated, amount of retransfused $CD34^+$ cells. The mean time it took for the retransfused cells to enter the system of leukopoiesis was estimated (MT_{SCR}) and the transition rate constant (k_{SCR}) was calculated as n/MT_{SCR}, with n being the number of transitions. In addition to the information about the amount of $CD34^+$ cells information on the content of colony-forming unit (CFU) cells was available for analysis. The implementation of the SCR was evaluated during two phases of the model development process:

- A) For a model comprising three transit compartments (T1 - T3) and
- B) For a model comprising the final number of transit compartments (T1 - T_N, section 2.4.2.3 and 3.3.3).

For the investigation of the ASCR the $CD34^+$ cells were divided into three groups:

- All $CD34^+$ cells (i)
- The CFU cell fraction alone (ii)
- $CD34^+$ cells excluding the CFU cell fraction (iii)

These subgroups were then allowed to enter

- The compartment of proliferating cells (Prol) and/or
- The transit compartments T1, T2,..., T_N

Retransfusion of the CFU cell fraction was only investigated for the compartment of proliferating cells. The rationale was that CFU cells are a subgroup of $CD34^+$ cells which is capable

of proliferation whereas $CD34^+$ cells contain both, cells with and without the ability to proliferate. Therefore in one approach the CFU cells (ii) were transferred into the compartment of proliferating cells (Prol) whereas the remaining $CD34^+$ cells (iii) were transferred into the different transit compartments (T1, T2,..., T_N). In a last step the homing process of the retransfused cells was further characterised by adding a transit compartment (Transit-CFU/-$CD34^+$) between SCR and the system of leukopoiesis.

2.4.2.6 Integration of an additional feedback

In the model for myelosuppression as proposed by Friberg et al.[138] the feedback mechanism is acting solely on k_{prol}, accounting for the stimulation of the proliferative activity of cells in the bone marrow if the haematopoietic system is under stress. However, cytokines responsible for the regulation of haematopoiesis also shorten the time of cell maturation. Therefore a second feedback mechanism (power exponent: β) acting on the transition rate constants k_{tr} was introduced to the model and its impact on the descriptive and predictive ability of the model was assessed.
A model containing two feedbacks was first proposed by Quartino et al.[153] who replaced the feedback, originally consisting of a power function including the fraction of the neutrophil concentrations before therapy and model-predicted concentrations during therapy, by predictions and baseline values of G-CSF concentrations. In contrast to using G-CSF concentrations, leukocyte concentration measurements were maintained for the present investigation as no G-CSF concentration measurements were available for data analysis.
In a first modelling approach the INI_{DEXA} compartment was excluded from analysis to resemble the model by Quartino et al. The motivation was that by adding the feedback the initial increase could possibly be described by a faster transit of the cells through the bone marrow due to a feedback acting on k_{tr}. During model development the additional feedback was allowed to act on either all (n) k_{tr} or on the last (n-1), (n-2), ..., 2 k_{tr} before cells are entering the circulation. In a second approach INI_{DEXA} was kept in the model and the model was evaluated containing the two feedback mechanisms.

2.4.2.7 Covariate analysis

The objective of the covariate analysis was to further characterise possible influences on the parameters describing the system of leukopoiesis in the setting of HDCT. A focus was laid on G-CSF and DEXA, as they were known to influence the time course of myelosuppression. Ad-

ditionally, other covariates were investigated which were identified during graphical analysis as potential predictors for the system-related parameters.

G-CSF The growth factor G-CSF is known to have a stimulating effect on the proliferation and maturation processes of granulocyte progenitors. This motivated the integration of G-CSF as a covariate for MMT, the exponent of the feedback mechanisms γ and the proliferation rate constant k_{prol}. G-CSF is, in parts, eliminated from the circulation via internalisation after binding to its receptor on the surface of neutrophils. Physiologically this means the more G-CSF in the circulation the less circulating leukocytes to eliminate G-CSF are present. Therefore G-CSF was also tested as covariate on k_{el}, "feigning" lower leukocyte concentrations during G-CSF administration, to activate the feedback mechanism. In this model k_{el} was estimated rather than set equal to k_{prol}. G-CSF entered the model as a dichotomous covariate (section 2.1.2.3) with the value 1 for the days on which it was administered until one day after the last administration and 0 for all other days.

Dexamethasone DEXA increases endogenous G-CSF concentrations and therefore the same covariate relations were investigated for DEXA (see also section 2.4.2.4). DEXA was coded as a dichotomous covariate being 1 from the first until the last administration. The influence of DEXA as a covariate on MMT and k_{prol} was assessed in a model that did not include the description of the initial increase by initialisation of INI_{DEXA} in order to assess the ability of DEXA to describe the initial increase by changing MMT and k_{prol}. Another covariate relation that was investigated for DEXA was the single (0, 12 and 16 mg) and the total amount of administered DEXA on C_{INI} for the multiple initiation of INI_{DEXA} and for the single initiation of INI_{DEXA}, respectively.

Remaining covariates Covariates which were selected during graphical analysis comprised HT as a predictor for $Circ(t_0)$ and AGE, albumin (ALB), CLCG and gamma-glutamyltransferase (GGT) for MT_{SCR}. All covariates were included as an exponential function (Equation 2.12).

2.4.3 Model selection and evaluation

Model selection was based on OFV, plausibility and precision of parameter estimates as well as GOF plots. Key and final models were additionally evaluated based on VPCs (section 2.1.3.2 and 2.1.3.3). Since only data from 17 patients was available for analysis the 10^{th} and 90^{th}

percentiles were chosen for this analysis as for smaller populations less extreme percentiles are more appropriate to asses the predictive performance of the variability of the model[239].

2.5 Project 3: Assessing the optimal day for the autologuos stem cell rescue

Simulations were performed based on the final population PK/PD model for the description of leukopenia following HDCT and comprised the investigation of the day on which the ASCR was performed and the amount of retransfused cells with respect to leukocyte nadir concentrations and the duration of at least grade 3 leukopenia (from here on referred to as duration of grade 3 leukopenia). The objective was the exploration of the best day to perform the ASCR under consideration of the retransfused amount of $CD34^+$ cells.

2.5.1 Deterministic simulations

For the investigation of the optimal day for the ASCR, first, deterministic simulations were performed to gain information about the underlying system. Nadir concentrations and the duration of grade 3 leukopenia were evaluated for different days on which the ASCR was performed starting from day 5, i.e. one day after the last etoposide administration, up to day 11. Additionally, the amount of retransfused $CD34^+$ cells was subject to analysis and its impact on the day for ASCR with raged to nadir concentrations and the time below grade 3 leukopenia was investigated. The minimal ($0.072 \cdot 10^9$), median($0.2329 \cdot 10^9$) and maximal ($0.5698 \cdot 10^9$) amount of retransfused $CD34^+$ cells from the investigated study population were evaluated during simulations.

2.5.2 Stochastic simulations

In a second step stochastic simulations were carried out to determine whether the differences in nadir concentrations and duration of grade 3 observed during the deterministic investigations hold true when variability within the population was allowed. Simulations were performed for a retransfused amount of cells of 0.072, 0.1, 0.15, 0.2, 0.2329, 0.3, 0.4, 0.5 and 0.56 $\cdot 10^9$ $CD34^+$ cells with the ASCR taking place on day 6, 7, 8, 9, or 10 (D6 - D10) of HDCT. The best day proposed with the help of the simulations was then compared to the day of the original study setting (D7) applying the Mann-Whitney-Wilcoxon test (next paragraph). All simulations were based on parameter estimates of the final population PK/PD model for the

description of leukopenia. The IIV for the MT_{SCR} was taken from a model which was evaluated without patient number 19. For this patient twice the amount of retransfused $CD34^+$ cells compared to the rest of the population was reported and the original laboratory report was missing. Exclusion of this patient resulted in a parameter distribution for the IIV of the MT_{SCR} that was much closer to a normal distribution than for a model including this patient. As all other model parameters were not affected by the exclusion of this patient the variance component for MT_{SCR} from the model excluding this patient was used during simulations. The leukopenic time course was simulated for a typical patient who received median doses of 449.2, 1100 and 330 mg of C, E and T, respectively, for each application of the drug and various amounts of retransfused $CD34^+$ cells. INI_{DEXA} was initiated with C_{INI} on the first day of HDCT, also allowing variability for this parameter.

Mann-Whitney-Wilcoxon test The Mann-Whitney-Wilcoxon test (or Wilcoxon rank sum test) is a non-parametric hypothesis test for assessing whether two independent sample distributions belong to the same statistical population[245]. It was performed to compare nadir concentrations and the durations of grade 3 leukopenia resulting from n=1000 simulations based on the final PK/PD model for the description of leukopenia applying a level of statistical significance of 0.05 (section 3.4.2). The null hypothesis was that there was no difference between between nadir concentrations or the duration of grade 3 leukopenia for an ASCR performed on the original day of the study (day 7) compared to any other day the ASCR was performed during the simulations.

2.6 Project 4: Characterisation of the cytotoxic potency of chemotherapeutics

One goal of the description of the leukopenic-time course by a semi-mechanistic model is the quantification and differentiation of the sensitivity of the proliferative cells in the bone marrow towards the cytotoxic drugs. The separation of drug- from system-specific parameters by the semi-mechanistic model enables the characterisation of the drug effect independent from the underlying leukopoietic system. This provoked the investigation of drug-specific parameters obtained from other systems such as cell-based assays which describe the cytotoxic potency of drugs in terms of an E_{max} model.
Project 4 was subdivided in two parts: First, different PD models for the description of the effect of different carboplatin concentrations on the survival of cells ("response") in a cell-based

assay were investigated and compared. For this purpose the parameters characterising the concentration-response relation (e.g. E_{max} and EC_{50}) were estimated in NONMEM® and with the R software package.
The second part then focused on the proposal of an enhanced semi-mechanistic PK/PD model for myelosuppression which was suitable for the evaluation of clinical data and estimated drug-specific parameters which were comparable to EC_{50} values obtained from *in vitro* data. The objective was to explore the possible use of *in vitro* data for the prediction of the myelosuppresive time course following chemotherapy.

2.6.1 Assessing the cytotoxic potency from *in vitro* data

The comparison of different PD models for the description of the PD effect of cytotoxic drugs on the survival of cells was based on data collected during the assay development of a cellular cytotoxicity assay with peripheral blood mononuclear cells (PBMC) which was subject of a (supervised) diploma thesis[218]. The PD models were implemented in NONMEM® to determine the one that best described the data. Then, parameter estimates from a corresponding model implemented in the *drc* package in R were compared to the ones obtained during analysis of the data in NONMEM® to have a simpler and more cost-effective analysis tool at hand.

2.6.1.1 MTT assay

The MTT assay is a colorimetric assay which is used to asses the cytotoxic effects, i.e. the inhibition of cell growth and cell death by certain concentrations of compounds. MTT (3-(4,5-Dimethylthiazol-2-yl)-2,5-diphenyltetrazolium bromide) is a yellow tetrazole which is reduced via an enzymatic reaction in viable cells to the purple formazan. The formazan crystals were dissolved in dimethylsulfoxide (DMSO) and the absorbance of the resulting solution was measured at the wavelength of 570 nm. For the current investigation data from an MTT assay that was developed to asses the cytotoxic potential of carboplatin on PBMCs was used[218]. The PBMCs for the assay were isolated from buffy coats via centrifuging, resuspended and seeded on a 96 well plate. For this purpose 100 μL of the PMBC suspension were transferred to each well resulting in a cell density of 150,000 cells/well. 10 μL of a serial dilution of carboplatin was added to each column of the plate resulting in an assay concentration of 0, 1.8, 5.5, 18, 55, 109, 182, 364, 727 and 1818 μmol/L for each column (8 replicates, 1 in each row of the plate). The plate was incubated for 72 h before MTT was added to the plates. The plates were then incubated for additional 2 h before formazan crystals were dissolved and the absorption was

measured. A column with DMSO treated cells served as positive control and a column containing untreated cells represented the negative control. To control for background staining a column containing neither cells nor drug was also stained with MTT.

2.6.1.2 Data processing

The raw data from the absorption measurement of three plates was subjected to analysis. The data was processed prior to modelling to represent the survival index (SI, %) of the cells. In the first step outliers, i.e. wells with unusual high or low absorption values, were identified applying the Grubbs test for one outlier in R and removed from the dataset.The Grubbs test compares the potentially outlying data point with the average and the standard deviation of measurements from the same drug concentration[246]. After comparison with a tabulated criterion (Grubbs statatistic G=0.2032, n=8 measurements/concentration, p=0.05), the data point was discarded from the dataset if the calculated value for G exceeded the tabulated value, i.e. the observation was a outlier.
In the next step the geometric mean of each column of the plate, i.e. wells containing the same carboplatin concentration was calculated. The mean absorption of the wells containing DMSO was subtracted from the absorption means of each of the other columns as DMSO was assumed to represent 100% cell kill. Hence, the absorption values were corrected for background staining resulting from living, non-proliferative cells. In the last step the mean absorption of the untreated wells was set to 1 representing a cell survival of 100 % and the survival index for the other concentrations was calculated.

2.6.1.3 Analysis in NONMEM®

The analysis of the data in NONMEM® was divided in two parts: (i) a population analysis for the three plates and (ii) the individual analysis for each plate. During the first part different PD models were evaluated with respect to their descriptive ability. The second part was based on the final model from (i) and was conducted in order to obtain parameter estimates for each plate for the direct comparison of the estimated parameters with those from the analysis in R. The following inhibitory PD models were investigated: a simple E_{max} model (Equation 2.32, with h=1), a sigmoidal E_{max} model (Equation 2.32) and the Richards' model[247] (Equation 2.33) which estimates an additional factor for asymmetry ($ASSY$). For $ASSY$ equal to 1 the

Richards' model collapses to the sigmoidal E_{max} model which is equal to the simple E_{max} model if the hill factor h is equal to 1[248].

$$E = 1 - \frac{E_{max} \cdot C^h}{C^h + EC_{50}^h} \tag{2.32}$$

$$E = 1 - \frac{E_{max}}{(1 + ASSY \cdot e^{SLOPE \cdot ln \frac{ED_i}{C}})^{\frac{1}{ASSY}}} \tag{2.33}$$

$$E = 1 - E_0 + \frac{(E_{max} - E_0) \cdot C^h}{C^h + EC_{50}^h} \tag{2.34}$$

Besides the estimation of the maximum effect E_{max}, the sigmoidal E_{max} model implemented in the *drc* package took an effect size for the cells that were unaffected by the drug (E_0) into account (Equation 2.34). The hill factor h and the $SLOPE$ factor are measures for the steepness of the effect-concentration curve. For ASSY equal to 1, SLOPE corresponds to h and ED_i, the concentration at the point of inflection, corresponds to EC_{50} which denotes the concentrations C at the half maximal effect of the drug[248,249] (see appendix section 8.3).

2.6.1.4 Analysis in R

For the analysis in R the *drc* package was used. Within this package the LL4() function reflected the parametrisation of the sigmoidal E_{max} model including a basline effect for unaffected, surviving, cells (Equation 2.34) which was used to analyse % SI of the cells. In a first step data from all three plates was analysed simultaneously followed by the estimation of a parameter set for each plate individually.

2.6.1.5 Comparision of the data analysis in NONMEM® and R

The parameters estimated from the population analysis in NONMEM® and the simultaneous fit of all plates in R were compared. To be able to directly compare parameter estimates, the sigmoidal E_{max} implemented in NONMEM® was recoded to resemble the one implemented in the *drc* package (Equation 2.34). This means a parameter estimating the remaining percentage of surviving cells was introduced to the model (E_0). Additionally, the parameter estimates resulting from the individual analysis of the three plates in NONMEM® and R were compared and evaluated with respect to their precision.

2.6.2 Comparing *in vitro* measures of cytotoxicity with estimates from an population PK/PD analysis of clinical data

The goal of this project was to propose a model for the description of myelosuppression that enabled the estimation and prediction of EC_{50} values from clinical data which were comparable to EC_{50} values from cytotoxicity assays reported in literature. Therefore the model for myelosuppression[138] was modified to reflect conditions under which EC_{50} values are determined *in vitro*. The following section describes the development of such a model and exemplifies the estimation and comparison of EC_{50} values obtained from a population PK/PD analysis of clinical data with EC_{50} values from an *in vitro* CFU-GM assay. The CFU-GM assay is the most frequently used haematotoxicity assay and measures the acute effect of compounds on bone marrow progenitor cells[250].

2.6.2.1 Model development

In the original model by Friberg et al.[138] the sensitivity of the cells in the bone marrow towards the drugs was expressed as a linear inhibition model ($E_{drug}(t) = SL \cdot C(t)$) with the slope ($SL$) being the measure for the sensitivity and C the concentration of the drug at a given time t. The drug exerted an inhibitory effect $E_{drug}(t)$ on the proliferation rate constant k_{prol} of the cells in the bone marrow and was implemented as $E(t) = k_{prol} \cdot (1 - E_{drug}(t))$. Hence, for $E_{drug}(t)$ <1, k_{prol} was inhibited (cytostatic effect) whereas for $E_{drug}(t)$ >1 the whole expression became negative, reflecting a net cell loss from the compartment of proliferating cells (cytotoxic effect). The same applies for an E_{max} model which can be used to describe the cytotoxic drug effect and where E_{max} is estimated and can become greater than 1. However, if % SI data from an *in vitro* assay is analysed with an E_{max} model the maximal effect that can be achieved is a cell kill of 100%. This means that the value of E_{max} is bound to be between 0 (no cell kill) and 1 (100% cell kill). Hypothetically this means that if the "*in vitro* E_{max} model" is implemented directly into the model for myelosuppression the maximal effect that can be achieved would "only" be the complete inhibition of k_{prol} (cytostatic effect) without taking the cell kill (cytotoxic effect) into account. Therefore the model was reparametrised to take the special conditions applying for E_{max} of the "*in vitro* E_{max} model" into account. A new rate constant k_{kill} which allowed for cell loss from the compartment of proliferating cells was introduced (Figure 2.5). The drug effect was then implemented as an E_{max} model with inhibitory effect on k_{prol} and stimulatory effect on k_{kill}.

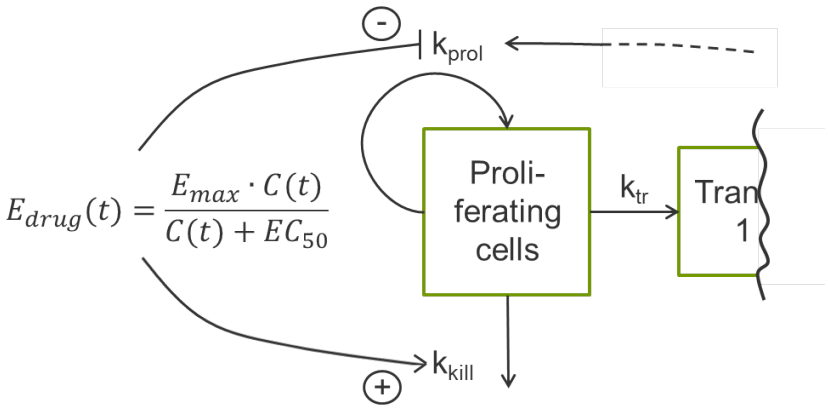

Figure 2.5 Image detail from the schematic structural model of the re-parameterised model for myelosuppression. $E_{drug}(t)$: drug effect at time t; E_{max}: maximal drug effect (fixed to 1); EC_{50}: concentration at half maximal effect; C(t): drug concentration at timt t; k_{prol}, k_{tr}, k_{kill}: proliferation, transition, cell kill rate constant, respectively

2.6.2.2 Docetaxel study

For the evaluation of the proposed reparametrised model and for the comparison of the estimated EC_{50} value a previously published study for the analysis of neutropenia following treatment with docetaxel was chosen[129,138,219]. In contrast to the CET study, the study comprised a monotherapeutic chemotherapy regimen which was of importance to easily separate the drug-specific from the sytem-specific parameters and to omit a potential drug-drug interaction. The study comprised 637 patients suffering from carcinoma, melanoma or sarcoma who were included in 24 open, uncontrolled trials at over 50 study sites. Docetaxel was administered at a dose of 75 or 100 mg as a 1 h infusion every 3 weeks. Neutrophil concentrations from the first cycle were subject to analysis, representing a total of 3,549 neutrophil counts (1 - 26 per patient). The individual predicted concentrations from a previously published population PK model[219] were used as input for the PK/PD model following a sequential modelling approach. A summary of the estimated model parameters that were obtained when reanalysing the data with the model by Kloft et al.[129] is presented in Table 3.13. For the purpose of this analysis the model was reparametrised as described in section 2.6.2.1 and was fit to the docetaxel data. All covariate effects but AAG as a covariate for the drug effect were implemented as in the original model. The reason was that when analysing drug potencies *in vitro* no such covariate relations are considered and the parameter estimate for EC_{50} from the reparametrised model was supposed to be directly comparable to the one obtained *in vitro*.

2.6.2.3 Model evaluation

The parameter estimates of the reparametrised model were compared to those resulting from the analysis with a model that was previously published by Kloft et al.[129] and evaluated with respect to precision of the parameter estimates. The estimated EC_{50} value from the population analysis was then compared to a EC_{50} for docetaxel previously published by de Graaff et al.[251] which was obtained from an CFU-GM assay for the assessment of haematotoxicity.

2.7 Project 5: Investigation of glycation processes throughout the lifespan of erythrocytes

Cell lifespan models have become a common way for the investigation of haematological drug effects. The objective of the project described in the next section was to transfer the generated knowledge about transit compartment modelling as described in section 2.3.3.1 and 2.4.2.3 to another model that is used for the description of changes in HbA_{1c} in patients with diabetes mellitus type 2 undergoing therapy. As a long-term biomarker for the evaluation of antidiabetic treatment HbA_{1c} can be used for the characterisation of the ageing process of erythrocytes as glycation of haemoglobin increases with increasing age of the cells. For the description of changes in HbA_{1c} in patients with diabetes mellitus type 2 treated with lixisenatide a previously published lifespan model[186] was investigated and a new, extended version of the lifespan model[220] was developed. The third objective was to gain a more mechanistic understanding of the formation of HbA_{1c} under lixisenatide treatment and the characterisation of the lifespan of erythrocytes in this population.

2.7.1 Study characteristics

The investigation of the lifespan model and the extended version of the model was based on HbA_{1c} measurements from 162 patients constituting a subgroup of patients enrolled in two clinical studies sponsored by Sanofi one of which was published in 2010 by Ratner et al.[195] The randomised, double blind, placebo-controlled, parallel-group studies were conducted in diabetes mellitus type 2 patients inadequately controlled ($HbA_{1c} \geq 7\%$) on metformin (> 1000 mg/d) to evaluate the dose-response relationship of lixisenatide. The characteristics of the study population are summarised in Table 2.1. Overall, the investigated study population reflected the expected characteristics of patients with diabetes mellitus type 2 with a median age of 61 (range: 43 - 74) years and a median weight of 81 (51 - 118) kg. Creatinine clearance,

predicted normal weight (PNWT), race and fasting plasma glucose (FPG) before the start of the therapy reflect covariates that were included in the population PK model for lixisenatide (see 2.7.1.3) and the population PK/PD model for the description of FPG (see 2.7.1.4) which were previously published[252] and used as input for the present analysis.

Table 2.1 Characteristics of study population: Distribution of continuous and categorical covariates[220].

Parameter	Unit	Median	2.5^{th} percentile	97.5^{th} percentile
Age	[year]	61	43	74
Weight	[kg]	81	51	118
Height	[cm]	167	149	187
PNWT	[kg]	72	49	106
CLCR	[L/h]	5.9	3.7	10.4
FPG before study	[mM]	8.7	7.0	12.9
Race	[caucasian/black/asian/other]		104/3/45/10	
Sex	[male/female]		106/56	

PNWT: predicted normal weight[223], CLCR: creatinine clearance[221], FPG: fasting plasma glucose

2.7.1.1 Lixisenatide

Lixisenatide was administered subcutaneously (s.c.) at doses of 5, 10, 20 or 30 μg once or twice daily for 13 weeks. The studies included an intraindividual dose escalation which took place during the first 2 - 4 weeks starting at 5 μg for week one with the addition of 5 μg/week until target doses of 20 or 30 μg/week were reached.

2.7.1.2 Observations and data acquisition of HbA_{1c} values

The PK and PK/PD analyses of lixisenatide (Frank[253]) and FPG (Rüppel et al.[252]), respectively, were performed prior to the analysis of the HbA_{1c} data and were not part of the PK/PD modelling activities presented in this thesis. Therefore details on data acquisition are only given for HbA_{1c}. Samples for the determination of HbA_{1c} values were taken once before the start of the treatment period, once directly before or on the day of the first lixisenatide administration and on four occasions during the observation period of the study. Glycated haemoglobin values were determined with a high-performance liquid chromatography method and were given as NGSP (National Glycohemoglobin Standardization Program) standardised values[195].

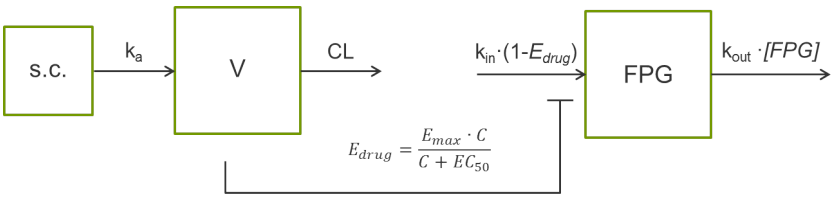

Figure 2.6 Structural model for the PK of lixisenatide (left) and the PD of FPG (right). s.c.: sub cutaneous; k_a: absorption rate constant; $E_{drug}(t)$: drug effect over time; E_{max}: maximal effect; EC_{50}: concentration at half maximal effect; C(t): concentration at time t; k_{in}: production rate constant for fasting plasma glucose (FPG); k_{out}: elimination rate constant of FPG

2.7.1.3 Pharmacokinetic model for lixisenatide

EBEs from a population PK model for the description of lixisenatide concentrations[253] were used as input for the population PK/PD models for the description of FPG and HbA_{1c}. PK profiles were described by a one compartment model (Figure 2.6, left) which was parametrised in terms of volume of distribution (V) and clearance (CL), the latter describing the elimination of lixisenatide from the circulation by a first-order process. The first-order absorption rate constant k_a determined the drug absorption process from the subcutaneous compartment. PNWT and CLCR (section 2.1.5.2) were identified as influential covariates on CL, V was best predicted after inclusion of PNWT as a covariate and the study site, race (Asian) and PNWT were influential covariates for k_a. The distributions of EBEs from the analysis by Rüppel et al.[252] are described in the upper part of Table 2.2 by means of the respective median, 2.5^{th} and 97.5^{th} percentile.

2.7.1.4 PK/PD model for fasting plasma glucose

Prior to the analysis of HbA_{1c} values, the PD effect of lixisenatide on fasting plasma glucose (FPG) has been described with an indirect response model[252]. In general, indirect response models control the response by factors describing its production and elimination. The drug exerts an indirect effect on the response by either stimulating or inhibiting its production or elimination, respectively[254]. For the description of FPG over time (the response) under lixisenatide treatment a zero-order rate constant k_{in} characterised the production of FPG and the elimination followed a first-order process described by the elimination rate constant k_{out} (Figure 2.6, right). FPG concentrations before therapy were used to characterise the initial conditions in the compartment for FPG in each patient. Lixisenatide concentrations served as input for an E_{max} model with an inhibitory effect on k_{in}.

Table 2.2 Distribution of the empirical Bayes estimates of the PK model for lixisenatide and of the PK/PD model estimates for fasting plasma glucose[220].

Parameter	Unit	Median	2.5th percentile	97.5th percentile
PK Parameter (lixisenatide)[253]				
CL/F	[L/h]	33.4	18.1	61.2
V/F	[L]	40.2	20.2	82.4
k_a	[1/h]	0.37	0.27	0.45
PD Parameter (FPG)[252]				
k_{in}	[mmol/(L·h)]	0.29	0.23	0.43
k_{out}	[1/h]	0.03	-	-
EC_{50}	[ng/L]	12.3	0.31	115
E_{max}		0.44	-	-

CL: clearance; V: volume of distribution; k_a: absorption rate constant

k_{in}, k_{out} : production and elimination rate constants for fasting plasma glucose, respectively

EC_{50}: concentration at half-maximal effect; E_{max}: maximal effect

2.7.2 Development of the HbA_{1c} model

In a first step the lifespan model by Hamrén et al.[186] was applied to the data to describe the change in the observed HbA_{1c} values in the patient population. To improve the fit and gain further insights in the mode of action of lixisenatide, the lifespan model was extended. The rationale behind the extension were the different modes of actions of lixisenatide and tesaglitazar, a $PPAR_{\alpha,\gamma}$-agonist for which Hamrén et al. originally developed the model. In contrast to tesaglitazar, which is acting as a insulin sensitiser, lixisenatide is able to influence postprandial glucose (PPG) concentrations by enhancing insulin secretion and delaying gastric emptying. These effect were indirectly taken into account by the extended model (section 2.7.2.2).

2.7.2.1 Lifespan model

One of the advantages of the lifespan model proposed by Hamrén et al.[186] is that the description of the process of HbA_{1c} formation does not depend on the presence of data on haemoglobin or erythrocytes. The semi-mechanistic population PK/PD model (Figure 2.7) describes and quantifies the underlying physiology of haemoglobin turnover and glycation based ob HbA_{1c} data only and establishes the link between FPG and HbA_{1c}. It enables the

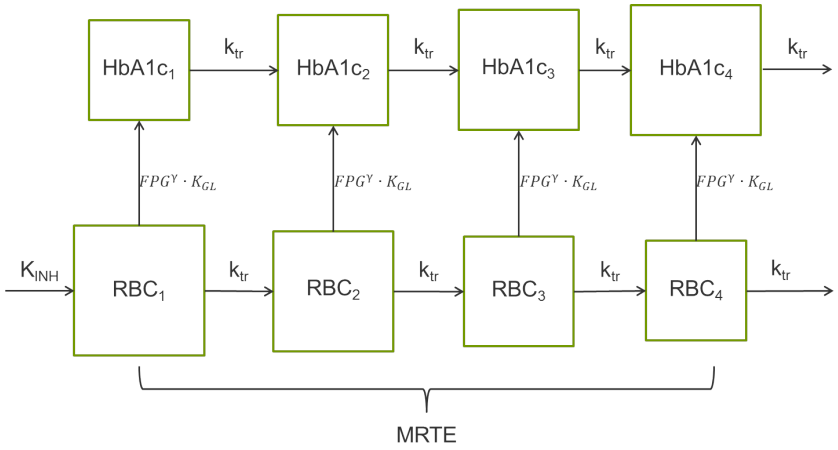

Figure 2.7 Schematic structure of the lifespan model for the description of HbA_{1c} values[255]. MRTE: mean residence time erythrocytes; HbA_{1c}: glycated haemoglobin; γ exponent of glycation process defined by fasting plasma glucose (FPG) and the glycation rate constant (KGL); k_{tr}: transition rate constant; K_{INH}: release rate of red blood cells (RBC) from the bone marrow.

differentiation between parameters describing the system of erythrocyte cell aging/their lifespan (release rate of erythrocytes from the bone marrow and their mean residence time) and the glycation process of haemoglobin (glycation rate constant linked to FPG by the exponent γ) on the one hand and drug-related parameters characterising the drug effect ($E_{drug}(t)$, Figure 2.6) on FPG concentrations on the other hand. The following assumptions were made during model development[255]:

- Haemoglobin is released from the bone marrow into the circulation by a zero-order rate constant (K_{INH}) and is not glycated
- Glycation of haemoglobin is a function of FPG and linked to the glycation rate constant K_{GL} by the exponent γ ($FPG^{\gamma} \cdot K_{GL}$)
- The proportion of gylcated haemoglobin increases continuously with age of erythrocytes, i.e. glycation takes place during the entire lifespan of an erythrocyte (characterised by the mean residence time, MRTE)

The model describes the lifespan of erythrocytes in the circulation by a chain of transit compartments. The compartments are linked by transition rate constants k_{tr} which are calculated as the reciprocal of the mean residence time of the erythrocytes (MRTE) multiplied by the number of transitions n. The MRTE estimates the lifespan of the erythrocytes in the blood.

K_{INH} resembles a zero-order rate constant with which erythrocytes are released from the bone marrow into the circulation. At each state during the lifespan of an erythrocyte haemoglobin is glycated as a function of FPG. This process is described by the glycation rate K_{GL} which reflects the rate at which FPG glycates haemoglobin to HbA_{1c}. The exponent γ describes the curvature of the nonlinear relation between FPG and HbA_{1c} which is given by a power function. The HbA_{1c} value (in %) is calculated as the ratio between the sum of all compartments containing glycated haemoglobin and the sum of all compartments times 100. During the model development process the variability in the structural model parameters and the ability of the model to describe the change in HbA_{1c} values was assessed.

2.7.2.2 Extended lifespan model

For the description of the change in HbA_{1c} values due to lixisenatide treatment the lifespan model was extended to better describe the data. In contrast to tesaglitazar, a $PPAR_{\alpha,\gamma}$-agonist for which the model was developed at first lixisenatide, among other modes of action, enhances insulin secretion and delays gastric emptying. Hence, not only is FPG reduced by a more effective uptake of glucose but PPG peaks are reduced due to insulin secretion and a delay in gastric emptying leading to a delay in absorption of glucose in the intestine[200]. This lead to the implementation of a second glycation pathway, which was described by another glycation rate constant K_{GL2}. This glycation rate constant was inhibited by an E_{max} model which was directly linked to lixisenatide concentrations and possibly described the glycation due to PPG. Linking the effect directly to lixisenatide concentration-time profiles also enabled to take an effect on a much shorter time scale (hours) into account without actually incorporating measurements of PPG lowering in the model. The resulting extended lifespan model is shown in Figure 3.38 and includes an additional system-related parameter (K_{GL2}) as well as new drug-related parameters characterising the E_{max} model.
The implementation of the E_{max} model, the number of transit CMTs and correlations observed during parameter estimation were investigated. Regarding the number of transit compartments, N=4, 6, ..., 12 transit compartments were investigated for the extended lifespan model. Less than four transit compartments were not investigated, as Kalicki et al.[256] reported a decrease in OFV for increasing numbers of transit compartments. Additionally, variance components for the model parameters and the contribution of the two glycation pathways to the HbA_{1c} formation was assessed.

2.7.3 Model evaluation and comparison

Final and intermediate models of the original and the extended model were evaluated and compared with respect to precision and plausibility of parameter estimates, η-shrinkage, goodness of fit and OFV. Investigations regarding the predictive performance of the final models by means of a VPC were not planned.

3 Results

3.1 CET study

3.1.1 Population characteristics

A total of 19 patients that were enrolled in the CET study were subject to analysis. The most important demographic covariates and clinical chemistry parameters before the start of HDCT of the study population are summarised in Table 3.1. Table 3.2 summarises the concomitant medication with potential influence on the time course of leukopenia. Statistical parameters for the covariates and clinical chemistry parameters were calculated at time=0 h, reflecting the start of the study. The distribution of the covariates and their correlations are depicted in Figure 3.1. No unexpected correlations between the covariates were observed. In general, the expected distribution patterns were reflected by the histograms. For leukocyte concentrations all measurements before start of HDCT were used for calculation of the statistics, i.e. two concentration measurements for each patient but one, for whom only one was documented. Leukocyte concentrations before the start of the therapy revealed that 30% of the patients suffered from a leukopenia of at least grade 2. Although each patient received the ASCR one patient (ID 7) did not receive G-CSF treatment. Two patients did not receive DEXA as part of the anti-emetic therapy. The liver enzymes ALT (alanine transaminase) and AST (aspartate transaminase) showed a slight increase in few patients before start of the therapy. During therapy changes in covariates over time were mainly observed for liver enzymes (AST, ALT) which were increased and protein concentrations, especially albumin concentrations (lowest value: 2.5 U/L), which were decreasing during therapy. These changes in clinical chemistry parameters were transient and back to reference values at the end of the observed time period.

3.1.2 Carboplatin

3.1.2.1 Dataset

Information on determined platinum concentrations, demographic covariates and serum creatinine (CREA) were obtained from a dataset from a previous analysis[79], transformed into a NONMEM® readable format and merged with information on the actual dosing and sampling time points from the study report. For the evaluation of the infusion durations the information

Table 3.1 Summary of the populations' characteristics (n=19): Distribution of the relevant continuous covariates

Covariate	Unit	Median	Mean	Range	5^{th} - 95^{th} percentile
Age	[y]	33.3	34.2	20.7-54.2	22.2-45.7
Weight	[kg]	80.0	81.1	58.0-105	62.5-101
Height	[cm]	177	178	160-190	169-190
Body surface area	[m^2]	2.00	1.98	1.70-2.30	1.70-2.21
Leukocytes	[10^9cells/L]	3.97	4.31	1.75-14.5	2.01-7.26
Serum creatinine	[μmol/L]	0.95	1.01	0.80-1.30	0.80-1.30
Creatinine clearance	[mL/min]	115	121	72.6-188	88.1-171
Protein	[g/dL]	6.50	6.66	5.70-7.90	5.97-7.81
Albumin	[g/dL]	4.30	4.25	3.30-5.50	3.30-5.14
ALT	[U/L]	12.0	13.0	5.00-32.0	5.00-31.1
AST	[U/L]	9.00	9.11	6.00-17.0	6.90-12.5
Bilirubine	[mg/dL]	0.50	0.51	0.30-1.10	0.30-0.92

ALT: alanine transaminase, AST: aspartate transaminase

Table 3.2 Summary of concomitant medication influencing the time course of leukopenia (n=17)

Covariate		Number of patients	%
ASCR	yes	17	100
DEXA	yes	15	88.2
	no	2	11.8
G-CSF	yes	16	94.1
	no	1	5.88

ASCR: autologuous stem cell rescue; DEXA: dexamethasone

G-CSF: granulocyte colony-stimulating factor

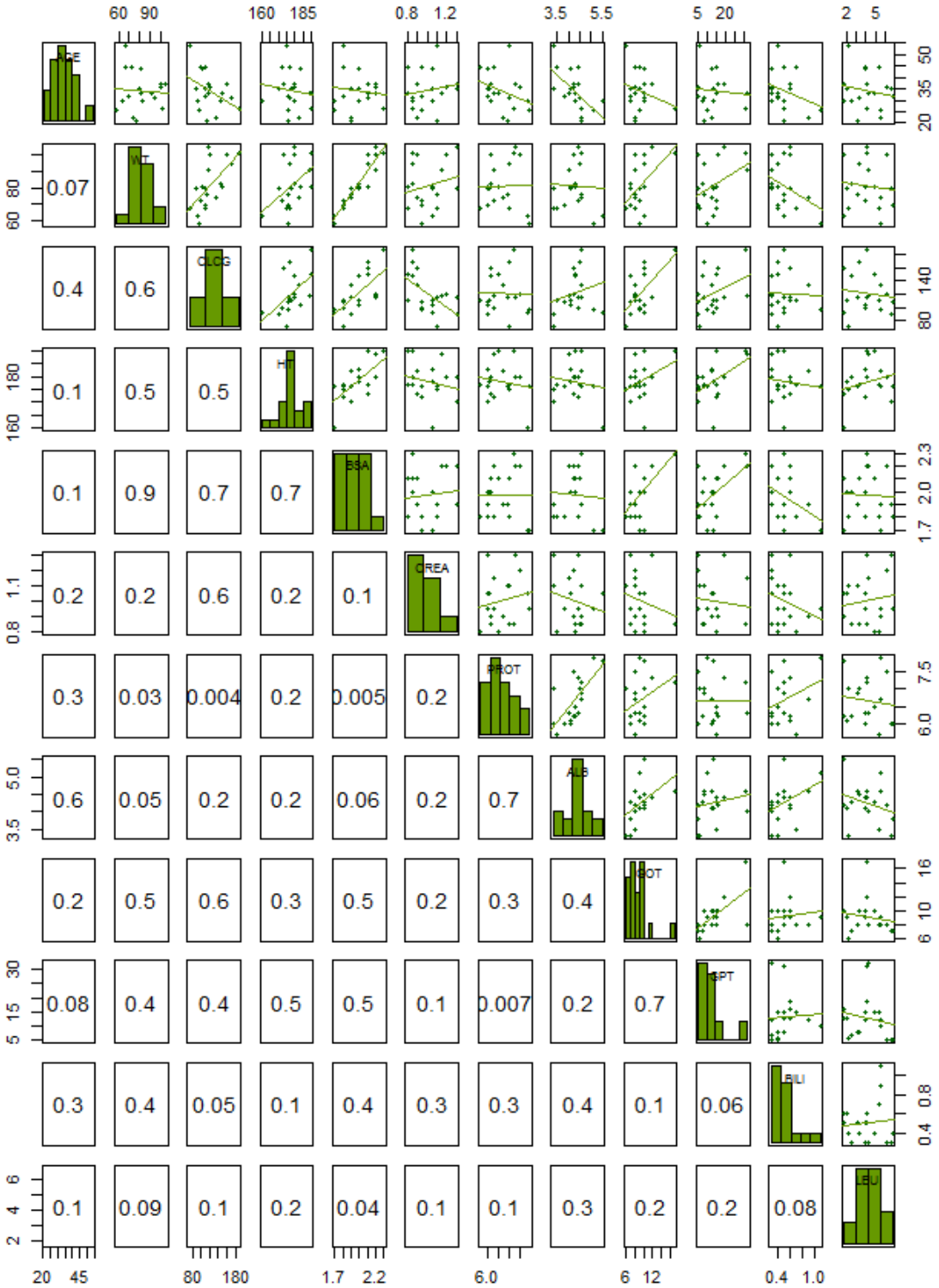

Figure 3.1 Scatter plot matrix and parameter distributions of the continuous covariates age (AGE) in years, weight (WT) in kg, creatinine clearance (CLCR) in mL/min, height (HT) in cm, body surface area (BSA) in m^2, serum creatinine (CREA) in μmol/L, protein (PROT) in g/dL, albumin (ALB) in g/dL, aspartate transaminase (AST) in U/L, alanine transaminase (ALT) in U/L,bilirubin (BILI) in mg/dL, leukocytes (LEU) in 10^9 cells/L. Numerical values express parameter correlation.

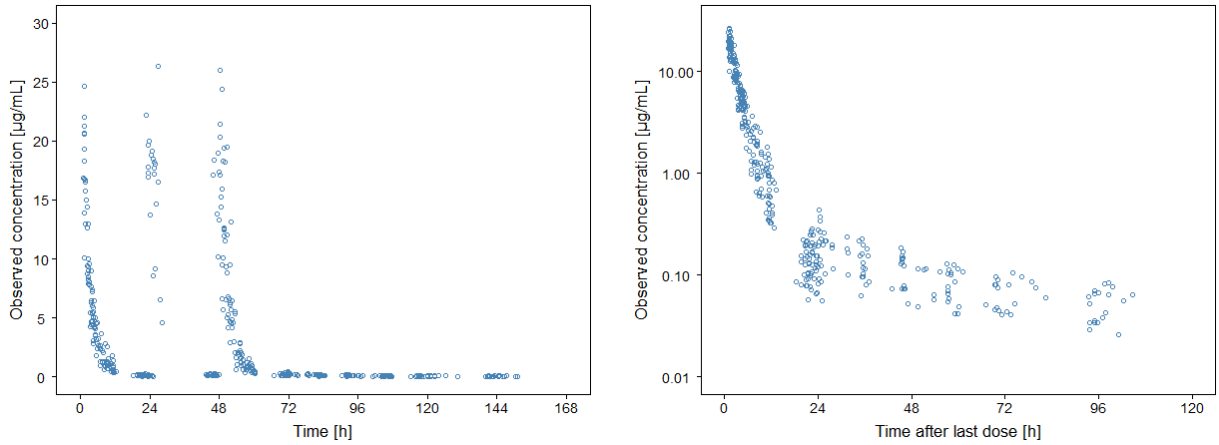

Figure 3.2 Ultrafilterable platinum plasma concentrations versus time (original, linear scale, left) and time after last dose (semi-logarithmically scale, right).

about the duration of the infusion was collected from the original study reports and merged with the dataset.

3.1.2.2 Observations

In total data from 19 patients were available for PK analysis. The sampling resulted in a rich data situation with a mean of 7.1, 2.2 and 11.2 samples per patient after the 1^{st}, 2^{nd} and 3^{rd} infusion, respectively. No missing data or concentration measurements below LLOQ were reported. The concentrations for ultrafilterable platinum (Pt) covered a wide range from 0.026 - 30.07 μg/mL. Figure 3.2 shows the Pt concentrations versus time and time after last dose (TALD) for all individuals on the original, linear (left) and a semi-logarithmic (right) scale, respectively. The latter reveals a distinct biphasic profile suggesting a two compartment model for the description of the concentration-time course of ultrafilterable Pt in the plasma.

3.1.3 Etoposide

3.1.3.1 Dataset

Etoposide concentration measurements were digitalised and merged with information on the administration time points and infusion durations from the original study reports. Demographic covariates and clinical chemistry parameters (Table 3.1) were taken from the carboplatin dataset as they were already available in a NONMEM® readable formate.

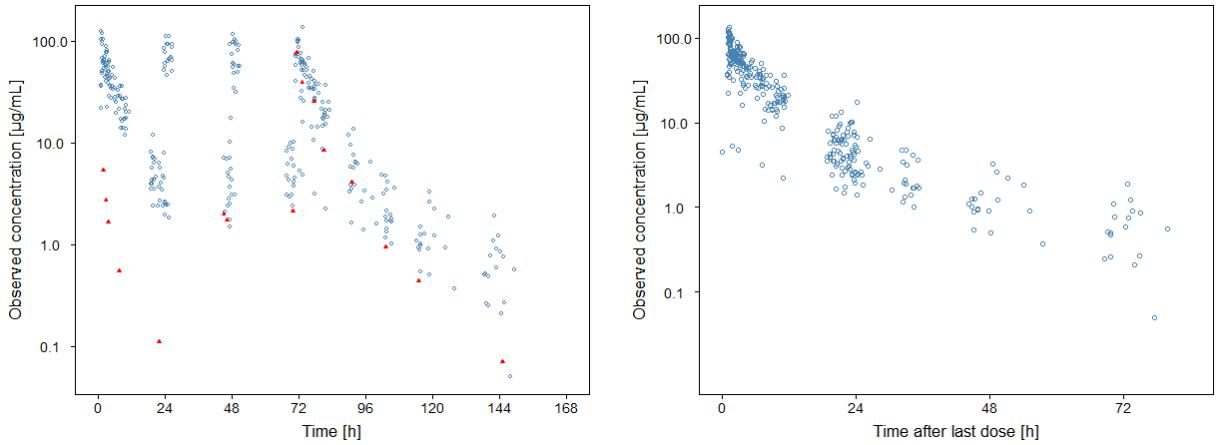

Figure 3.3 Etoposid plasma concentrations versus time (left) and time after last dose (right) on a semi-logarithmic scale. Red triangles: plasma concentrations of patient (ID) 4; excluded in plot on the right hand side.

3.1.3.2 Observations

Etoposide concentrations measurements from 19 patients were available for PK analysis. Plasma concentrations from one patient (ID 4, Figure 3.3 (left), red triangles) were excluded prior to analysis during the data checkout procedure due to implausibility (section 3.2.2.5). Overall, sampling after the 1^{st}, 2^{nd}, 3^{rd} and 4^{th} infusion resulted in a mean of 6.2, 2.0, 2.0 and 7.8 samples per patient, respectively. Neither missing concentration measurements nor values below the LLOQ were reported. Etoposide concentrations in the final dataset covered a range from 0.05 - 168.6 μg/mL. The semi-logarithmically scaled concentration-time profiles are illustrated in Figure 3.3 and indicate a two compartment model by a biphasic shape of the profiles.

3.1.4 Thiotepa

3.1.4.1 Dataset

Concentration measurements were obtained from a diploma thesis[233], digitalised and merged with information on the infusion duration and administration time points for thiotepa from the original study reports. Covariates and clinical chemistry parameters (Table 3.1) were taken from the already NONMEM® readable dataset for carboplatin. Values below the LLOQ (< 50 ng/mL) were treated according to the M5 method for values below the quantification limit[224], setting the first value reported as LLOQ to $LLOQ/2$ and discarding all succeeding measurements below LLOQ. Two datasets were built for the purpose of the current analysis: one for

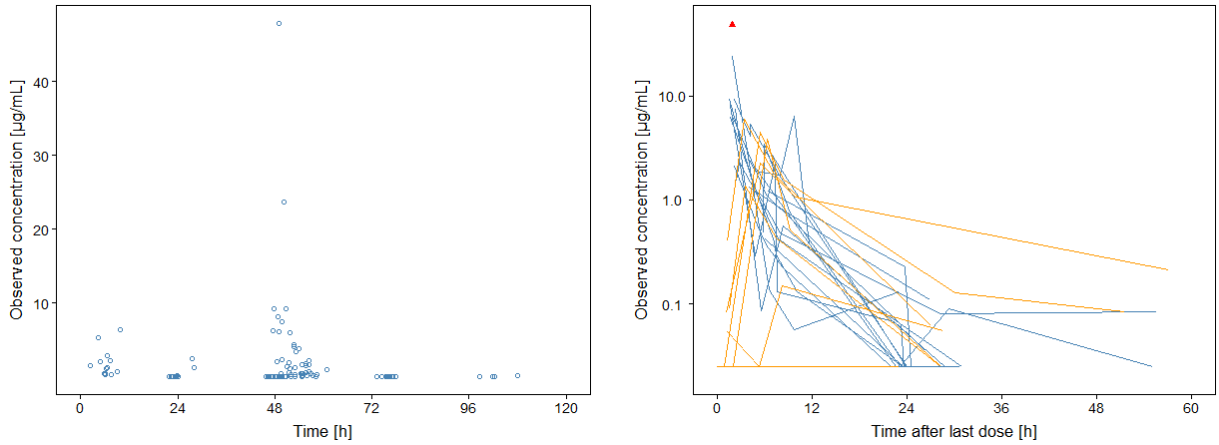

Figure 3.4 Thiotepa plasma concentrations versus time (original, linear scale, left) and time after last dose (semi-logarithmic scale, right). Right panel: red triangle: excluded plasma concentration measurements, yellow lines: patients exhibiting a delay in C_{max} after the end of infusion.

the transit compartment model having logarithmically transformed concentration measurements and one with concentration measurements on the original scale. The dataset for the transit compartment model was extended by additional time points 0.1 h prior to each dosing but the first one of each individual to enable the analysis of the data with the transit compartment model. These so-called "dummy" observations were required for the implementation of mutiple dosing into the transit delay model.

3.1.4.2 Observations

A total of 17 patients were subject to PK analysis. For thiotepa the sampling times that were originally planned to characterise the PK of carboplatin in the patient population were inopportune and resulted in a sparse data situation with a mean of 1.2, 0.8 and 5.0 samples per patient after the 1^{st}, 2^{nd} and 3^{rd} infusion, respectively. The concentration of one sample was not determined and therefore missing and 12.7% of the reported data was below the LLOQ. Figure 3.4 depicts the concentration-time profiles for the determined thiotepa concentrations on a linear (left) and a semi-logarithmic (right) scale, which indicated a two compartment model showing a biphasic shape for some of the profiles. Although thiotepa was administered as an i.v. infusion a delay in the occurrence of C_{max} was observed with concentration measurements close to or below the LLOQ at the end of the infusion which was the case for 12% of the administrations (Figure 3.4, right, yellow lines). For the other patients the delay

was not observed as their first samples were taken later relatively to the end of the infusion (> 1.9 h TALD). One concentration measurement of 47.9 μg/mL was excluded prior to analysis due to an implausible high value which was more than 5 times higher compared to C_{max} for the rest of the population. In the final dataset, excluding this data point, thiotepa concentrations varied from 0.025 (1/2 lower LLOQ) to 23.8 μg/mL.

3.1.5 Investigation of infusion duration

3.1.5.1 Datasets

For carboplatin the two different endpoints (end of the infusion, end of the washing period) were well documented and an additional dataset containing the 'short' infusion duration, i.e. the duration from the start of the infusion to the actual end was built. The additional dataset for etoposide, on the other hand, comprised the 'long' infusion duration which was computed based on information on the end of the washing of the infusion tubes. In contrast to the well documented carboplatin infusions the quality of information on the end of the washing period for etoposid varied and the washing times were reported between 3 - 45 min. Although the infusion tubes were long and it is possible that at the end of the infusion a certain amount of drug was still present in the tubes, the range of washing times might be problematic as the longer the washing time the less the probability of the drug still being in the tube. Hence, the infusion duration for long washing periods might be biased. For one patient (ID 16) the median infusion duration of the population was assumed as the end of the washing was not documented. Three patients (ID 17 - 19) had very short infusion durations (20 - 30 min) with regard to the end of the infusion, but when the end of the washing period was taken as the endpoint the duration resembled the duration reported for the rest of the population. Building of an additional dataset for thiotepa was not necessary as in the transit compartment model the dose was administered as an i.v. bolus into the first transit compartment. Hence, there was no need for an investigation of the influence of the infusion duration of thiotepa on the description of the data.

3.1.6 Leukocytes

3.1.6.1 Dataset

A flow chart depicting the most important steps for the dataset building for the sequential PK/PD analysis is depicted in the appendix (8.1). In short, leukocyte measurements and clinical chemistry parameters were merged with information on the amounts of retransfused

cells, DEXA and G-CSF treatment as well as the dosing history of carboplatin, etoposide and thiotepa. Retransfusion of the stem cells, administration of G-CSF and leukocyte sampling times were set to 8 a.m. as no information on the actual time points was available. Leukocyte measurements one day prior to the start of HDCT were available for all patients. Additional measurements prior to that day were set to two days before the start of HDCT. Dosing time points for DEXA were either included as reported, or treated as described in section 2.4.2.4.
In a next step the EBEs for the PK parameters of all drugs and covariates describing the patients demographics were included in the dataset. Based on each patients' weight the total amount of retransfused cells for the ASCR was calculated. Patient 1 and 2 who received ifosphamid instead of thiotepa were removed from the dataset as no information on the PK of ifosphamid was available. The NONMEM® specific variable EVID was created based on leukocyte measurements, dosing events for the 3 drugs and initialisation of SCR and INI_{DEXA} and the numbers for the compartments were assigned based on the respective information (e.g. PK or PD measurement). In the case of missing individual PK parameters due to exclusion of a patient from PK analysis, the (typical) population parameters for the respective drug were assigned for this patient. Covariates that were missing for specific time points within a patient were replaced according to the last observation carried forward method described in section 2.1.5.4. Information on urea concentrations for one patient was missing and was replaced by the median of the population.
Following this step the secondary covariates were calculated according to the equations given in section 2.1.5.2. For the analysis of the baseline estimation methods B2 and B3[242] the first leukocyte measurement available for each patient was added as a covariate into an additional column. In the last step different datasets were created depending on multiple or single initialisation of INI_{DEXA}.
The coding of the G-CSF and DEXA treatment according to section 2.4.2.7 for the covariate analysis was done in Microsoft Excel®, as was the removal of lines from the dataset containing information on the multiple initialisations of INI_{DEXA} for the investigation of single initialisation of that compartment. For the investigation of the covariate influence of DEXA on C_{INI} a column containing the total amount of DEXA doses (0, 36 - 108 mg) and a column with the information on the amount of the single doses (0, 12, 16 mg) was added to the dataset.

3.1.6.2 Observations

In total, data from 17 patients were available for PK/PD analysis. The sampling resulted in a rich data situation with a median of 24 (range: 19 - 46) leukocyte measurements per pa-

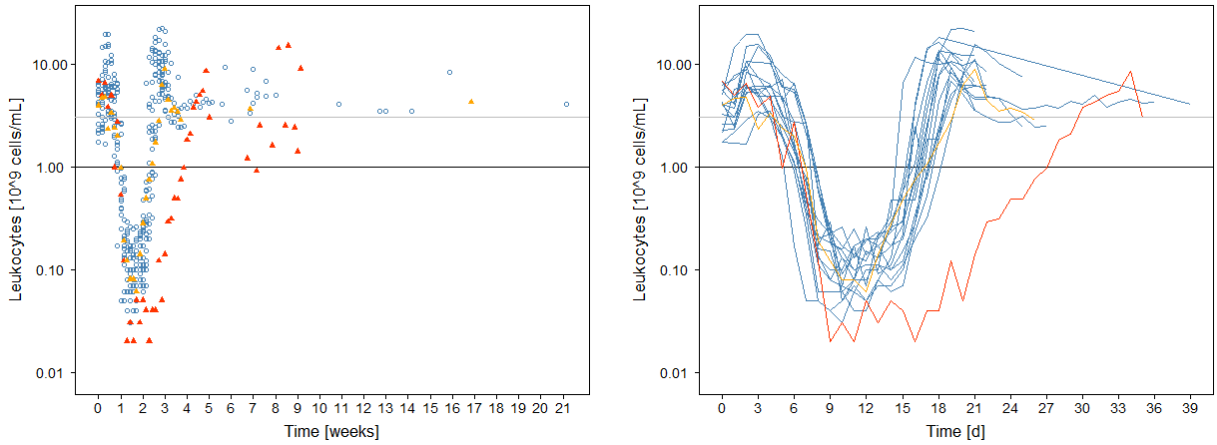

Figure 3.5 Leukocyte concentrations in the circulation versus time on a semi-logarithmic scale. Left panel: entire observation period. Right panel: first 39 days. Red triangles/line: leukocyte concentrations of the patient not receiving granulocyte colony-stimulating factor and dexamethasone (ID 7); yellow triangles/line: leukocyte concentrations of a patient not receiving dexamethasone (ID 6); grey/black horizontal line: lower limit of grade 1/3 leukopenia.

tient. Leukocyte concentrations covered a wide range from 0.02 - 22.3 $\cdot$ 10^9 cells/L and were therefore logarithmically transformed for analysis. Figure 3.5 shows the leukocyte concentrations versus time on a semi-logarithmic scale. One patient (ID 7, red) showed a deviating time course which might be due to the missing G-CSF administration for this patients. Two patients (6 and 7) did not receive any DEXA as part of the anti-emetic treatment and are depicted in red (ID 7) and yellow (ID 6). The time course revealed an initial increase in leukocyte concentrations (except for patient 6 and 7) followed by a steep and pronounced decrease. Nadir concentrations showed that all patients suffered from a grade 4 leukopenia, i.e. leukocyte concentrations below 1 $\cdot$ 10^9 cells/L (corresponding to the lower boundary of grade 3 leukopenia depicted as a black horizontal line). After nadir concentrations were reached all patients but patient 7 showed a fast recovery with a pronounced overshoot in leukocyte concentrations above baseline values before returning to reference concentrations.

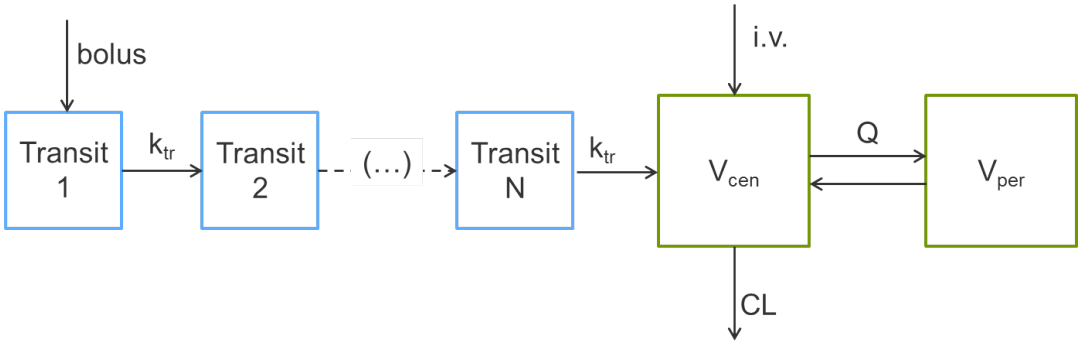

Figure 3.6 Schematic structural PK model for the plasma concentrations of carboplatin, etoposide (both in green) and thiotepa (additional transit delay model in blue). $V_{cen/per}$: central/peripheral volume of distribution; CL: clearance; Q: intercompartmental CL; k_{tr}: transition rate constant; i.v. intravenous administration route of carboplatin and etoposide; Transit N: N-th transit compartment.

3.2 Project 1: Pharmacokinetic analysis of high-dose carboplatin, etoposide and thiotepa

Pharmacokinetic models for carboplatin, etoposide and thiotepa were developed for the prediction of individual pharmacokinetic parameters which were used as input for the PD model to describe the time course of leukopenia in the study population of patients undergoing HDCT.

3.2.1 Carboplatin

3.2.1.1 Base model

The model was developed based on the model for high-dose carboplatin in children and adults by Lindauer et al.[236] as described in section 2.3.1. It comprised two disposition compartments with a first-order elimination from the central compartment (Figure 3.6, green). In line with the previously proposed model by Lindauer et al. the residual variability in the PK model for carboplatin was described by a combined residual variability model with an additive and a proportional component. The data supported the estimation of two variance components: an interindividual variability (IIV) for the central volume of distribution (V_{cen}) and one for the clearance (CL). Inclusion of further variability parameters did not improve the model. A summary of the key models from the model development process is given in Table 8.1 (Appendix).

3.2.1.2 Covariate model

The covariate analysis for the population PK model for ultrafilterable Pt concentrations was based on the investigations by Lindauer et al[236]. Their final model severed as the full covariate model in the covariate analysis presented in this thesis. The reason for this was the hypothesis that the study population investigated in this thesis was part of their analysis but was smaller and much more homogeneous compared to the one investigated by Lindauer et al. and therefore no additional covariates were likely to be statistically significant. The full covariate model included CLCR and height (HT) as a covariate for CL. AGE and HT were included as predictors for the intercompartmental clearance (Q), and body weight (WT) was identified as a covariate for V_{cen}. Following the backward deletion step (section 2.1.2.3) the covariates were excluded, one at a time, until a statistically significant increase in the OFV was observed. Two covariates remained in the final covariate model: CLCR was found to have a statistically significant influence on CL and WT on V_{cen}. Both covariates were included into the model as a power function (section 2.1.2.3).

3.2.1.3 Final model

In a last step the pharmacostatistical submodel was reevaluated. Due to the inclusion of WT as a covariate for V_{cen} the IIV related with V_{cen} which was already low in the base model (10.3% CV) was further reduced to 5.6% CV. Exclusion of this IIV did not result in a statistically poorer model fit and was therefore not retained in the model.
The PK of ultrafilteralbe Pt concentrations after a 1 h infusion was described by a two compartment model with linear first-order elimination from V_{cen}. The coefficient of variation for the IIV on CL was estimated to be 13.2%. Inclusion of IIV on other model parameters did not significantly improve the model. The proportional component of the combined residual variability model was estimated to be 18.8% CV and the additive component was small with 0.013 μg/mL.
Two covariates were included in the final model as a power function: CLCR as a predictor for platinum CL and WT for V_{cen}. Parameter estimates for the base and the final model are summarised in Table 3.3. The OFV of the final model was reduced by 39.1 points compared to the base model with only one additional parameter to be estimated. Inclusion of CLCR as a covariate reduced the coefficient of variation of CL from 19.9% to 13.2%. To investigate the covariate influence in the population the deviation of the 5^{th} and 95^{th} percentile of the covariate value within the population from the median of the respective covariate was investigated. The clearance was reduced by 16% for the 5^{th} percentile of CLCR and increased by 25% for the

Table 3.3 Population PK parameter estimates from the base (left) and the final (right) model for carboplatin (ultrafilterable Pt) concentrations

		Base model		Final model	
Parameter	Unit	Estimate	RSE,%	Estimate	RSE,%
OFV		-856.22		-895.35	
Fixed effects					
CL	[L/h]	7.23	5.4	6.81	3.2
V_{cen}	[L]	22.0	3.9	21.2	2.7
Q	[L/h]	0.763	5.3	0.707	5.5
V_{per}	[L]	30.7	6.4	29.0	6.7
θCL_CLCR				0.606	17
θV_{cen}_WT				0.362	39
Interindividual variability					
ωCL	% CV	19.9	11	13.2	17
ωV_{cen}	% CV	10.3	34		
Residual variability					
σ proportional	% CV	19.5	9.4	18.8	6.5
σ additive	[μg/mL]	0.0138	15	0.0125	16

OFV: objective function value; CL: clearance; Q: intercompartmental CL

V_{cen} and V_{per}: central and peripheral volume of distribution

θCL_CLCR: covariate influence of creatinine CL on CL

95th percentile compared to the median CLCR. The 5th and 95th percentile of the WT reduced and increased V_{cen} by 7% and 9%, respectively.

The estimated CL of 6.81 L/h (113.5 mL/min) resembled the glomerular filtration rate and resulted in a median half-life for ultrafilterable Pt of 1.95 (range: 1.49 - 2.60) h and 31.7 (30.7 - 33.2) h for the initial and terminal elimination phase, respectively. Hence, on the day of ASCR the Pt concentration in V_{cen} and the peripheral volume of distribution (V_{per}) was 0.02 and 0.2 μg/mL, respectively.

Overall, the model performed well in terms of precision of parameter estimates with relative standard errors ranging from 2.7% to 17%, except for the RSE of the covariate influence of WT on V_{cen} which was estimated to be 39%.

3.2.1.4 Evaluation

The goodness of fit plots shown in Figure 3.7 demonstrated a good description of the data by the model and revealed no model misspecification. The data points of observed versus predicted concentrations as well as the CWRES spread randomly and uniformly around the line of identity and the zero reference line, respectively. Only high concentrations around the maximal concentration (C_{max}) were slightly underpredicted by the model which can be seen in the plot showing measured concentrations versus predicted concentrations (Figure 3.7, top panel). The predictive performance of the model was evaluated by performing a visual predictive check (VPC). For binning of the observations a user-defined time array was applied which was given by the following time points relative to the end of the infusions: 0, 2, 3.3, 6, 15, 30, 40, 65, 90, 110 h. The time intervals were chosen based on observed clusters in the data and to obtain bins with comparable numbers of data points. The VPC depicted in Figure 3.8 shows the appropriateness of the prediction of the structural model by the central tendency (median of the observed and simulated concentrations, solid red and black line, respectively) and a good prediction of the variability within the population (5^{th} and 95^{th} percentile of the observed and simulated concentrations, dashed red and black lines, respectively).

3.2.1.5 Outliers

One concentration (ID 12, TIME=10.983) of the ultrafilterable Pt measurement was ignored during analysis and in the final model. The influence of the excluded measurement was assessed by fitting the model to the data including the observation. The resulting parameter estimates were comparable showing that the exclusion had no influence on the final model for the description of Pt concentrations.

3.2.2 Etoposide

3.2.2.1 Base model

As described in the model development section (section 2.3.2.1) a one, two and three compartment model with first-order elimination from the central compartment were investigated as the structural model. A summary of the investigated key models is given in Table 8.2 in the Appendix. In comparison to the one compartment model the two and three compartment model were superior with a difference in the OFV of more than 530 points. The three compartment model was inferior in terms of OFV (ΔOFV 8.1, df=1), GOF and individual plots. Therefore the two compartment model was chosen as the structural model (Figure 3.6, green).

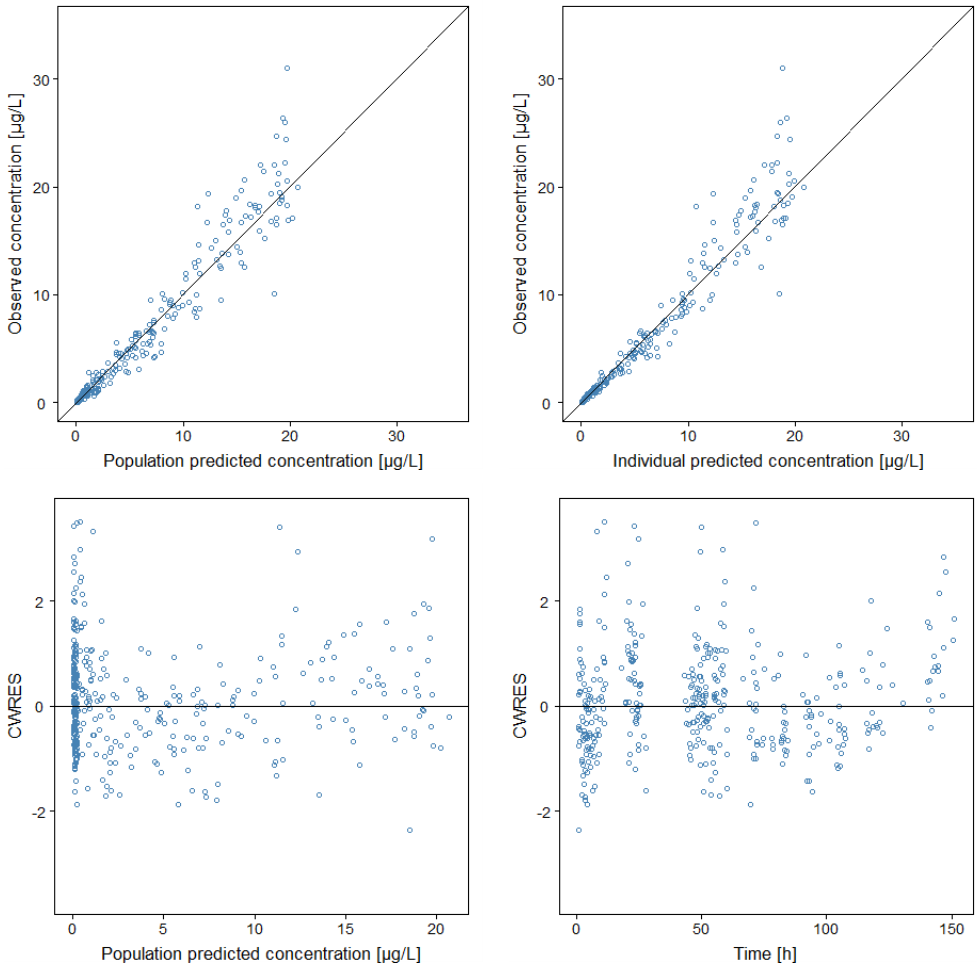

Figure 3.7 Goodness of fit plots for the final PK model for ultrafilterable platinum (Pt) plasma concentrations: observed versus population predicted C concentrations (top, left), observed versus individual predicted Pt concentrations (top, right), conditional weighted residuals (CWRES) versus population predicted Pt concentrations (bottom, left), CWRES versus time (bottom,right).

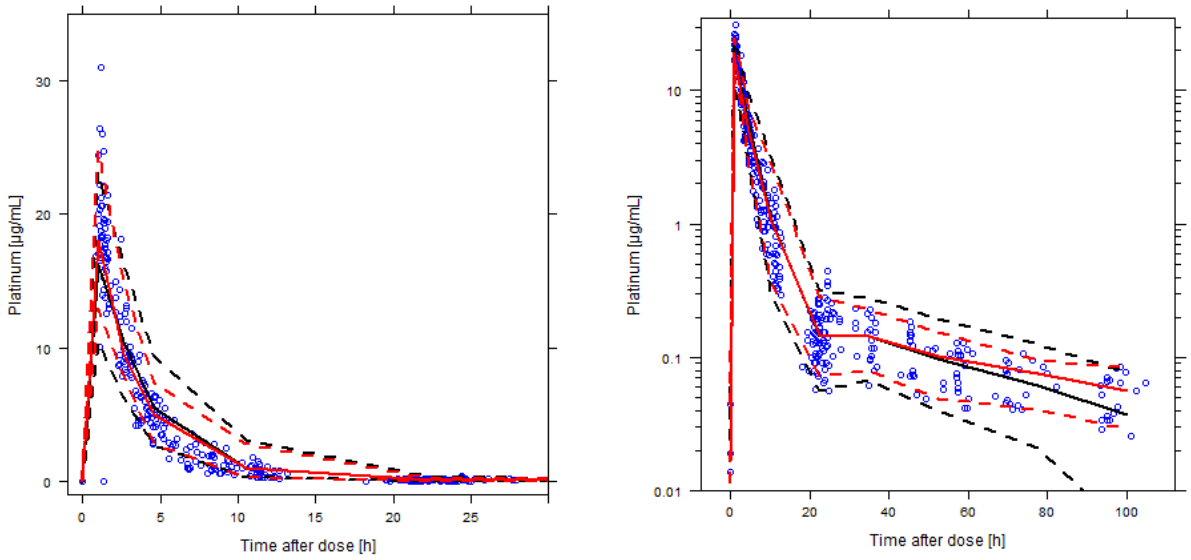

Figure 3.8 Visual predictive check for the final PK model of ultrafilterable platinum. Blue circles represent the measured ultrafilterable platinum concentrations. Solid and dashed lines represent the median, 5^{th} and 95^{th} percentile of the measured ultrafilterable platinum concentrations (red) and the simulations (black).

The residual variability was best described by a combined model. Interindividual variability was explored starting from a model including variance components for all structural parameters. Inclusion of an IIV for CL and V_{cen} was supported by the data. A correlation of those two parameters was identified and taken into account by estimating the off-diagonal element of the variance-covariance (Ω) matrix (section 2.1.2.2).

3.2.2.2 Covariate model

The covariate analysis for the PK model for etoposide was performed applying the stepwise covariate modelling (SCM) procedure implemented PsN©. The covariates tested for were either previously described in literature[237,238,257], and investigated if applicable and available, or identified during graphical analysis. AGE, body surface area (BSA), CREA, CLCR, protein (PRO), albumin (ALB) and the liver enzymes AST and ALT were tested for their influence on CL. As potential descriptors for the variability in V_{cen} AGE, WT, BSA, CREA, CLCR, bilirubin (BILI) and the administered dose (DOSE) were identified and tested. As CREA and CLCR and AST and ALT were correlated only one covariate of each pair (CLCR and AST) was included into the forward inclusion step. CLCR did not have a statistically significant influence on CL and therefore CREA was not tested. AST on the other hand was included into the full covariate model but was eliminated during the backward deletion step as the OFV only increased 5.4 points upon exclusion. Including ALT into the full covariate model and eliminating it in the backward deletion step did also result lead to exclusion of this covariate relation as the OFV increased only 5.3 points.

3.2.2.3 Final model

The final (=base) model was a two compartment model with a first-order elimination from the central compartment. Parameter estimates of the final population PK model are presented in Table 3.4. The variability of CL and V_{cen} was moderate with a CV of 23.9% and 20.3%, respectively. Taking the correlation between V_{cen} and CL into account led to a drop in the OFV of 12.6 points and the correlation was estimated to be 74.6%. The half-lives of the initial and terminal elimination phase were determined to be 5.51 h and 20.5 h, respectively, resulting in total etoposid concentrations of 0.25 μg/mL in the central and 1.70 μg/mL in peripheral volume of distribution on the day of ASCR. Precision of the fixed-effects parameters was high (< 10% RSE) and the overall precision of the parameter estimates was good being $\leq$ 30.4%. The residual variability was best described by a combined model with a proportional and additive component of 19.6% CV and 0.182 μg/mL, respectively. For the final model none of

Table 3.4 Population PK parameter estimates from the final PK model for etoposide concentrations

Parameter	Unit	Estimate	RSE,%
OFV		1007.0	
Fixed effects			
CL	[L/h]	1.86	5.8
V_{cen}	[L]	12.9	5.5
Q	[L/h]	0.248	9.6
V_{per}	[L]	6.23	7.4
Interindividual variability			
ωCL	[% CV]	23.9	11
ωV_{cen}	[% CV]	20.3	12
Parameter correlation			
$\rho_{CL,V_{cen}}$		0.0362	30*
Residual variability			
σ proportional	[% CV]	19.6	7.1
σ additive	[μg/mL]	0.182	20

*relative standard error of ρ on the corresponding variance scale

OFV: objective function value; CL: clearance; Q: intercompartmental CL

V_{cen} and V_{per}: central and peripheral volume of distribution

$\rho_{CL,V_{cen}}$: correlation of CL and V_{cen}

the investigated covariates showed a statistically significant influence on the model parameters although during the SCM the liver enzymes AST and ALT showed an influence on the clearance of etoposide.

3.2.2.4 Evaluation

The good description of the data by the model was reflected in the observed versus predicted concentration plots which showed a random and uniform distribution of the data points around the line of identity. Additionally, no trend of the CWRES over time or over predicted etoposide concentrations was observed (Figure 3.9). The VPC depicted in Figure 3.10 illustrates the good predictive performance of the model. For binning of the observations a user-defined time array was applied which was given by the following time points relative to the end of the infusions: 0, 3, 7, 15, 24, 28, 46, 52, 70, 74, 77, 85, 110, 160 h. The time intervals were

chosen based on observed clusters in the data and to obtain bins with comparable amount of data points. The median of the simulations (black solid line) did not show any deviation from the median of the observations (red solid line), reflecting a good prediction of the central tendency of the data, whereas the variability was slightly overpredicted which was illustrated by the wider 80% prediction interval of the simulations (black dashed lines) compared to the 10^{th} and 90^{th} percentile of the observations (red dashed lines).

3.2.2.5 Outliers

As stated in section 3.1.3.2 concentration measurements from one patient (ID 4) were excluded prior to data analysis. The concentration measurements at the end of the first and second infusion deviated from the ones observed in the rest of the patient population, being 22 times smaller and 5 times higher, respectively. In addition, three samples were not taken as they were either planned to be too late at night or not analysed due to a too small plasma volume. The model was reevaluated including ID 4 which resulted in an increase in the proportional residual variability from 19.6% to 27.4% CV and higher imprecision for the parameter estimates for the IIVs. Overall, resulting parameter estimates were comparable which showed that the exclusion had no influence on parameter estimation. Hence, and due to the increase in the residual variability, ID 4 was excluded in the final model.
Patient 9 was excluded during model development as concentration measurements after the first application peaked 1 h after the end of the infusion and concentration measurements after the second, third and forth application were at least 2-fold lower compared to the rest of the population. Inclusion of ID 9 into the final model resulted in an increase in the proportional residual variability from 19.6% to 23.4% and higher imprecision for the estimate of this parameter. Overall, the exclusion of this patient did not influence the parameter estimation since parameter estimates were comparable with the estimates from the final model and therefore ID 9 was excluded in the final model.
The infusion tube leaked during the last administration of etoposide for ID 10. Therefore only an estimated amount of 8.32 mg was administered. First, this accounted for in the dataset but deviation for the individual predicted concentrations from the observed concentrations was intolerable high. Hence, all measurements from the last application of ID 10 were ignored in the final model.
Additionally three concentration measurements were excluded during model development (ID 3: TIME=1.32, ID 17: TIME=47.55, ID 13: TIME=142.43) as they were up to 6 times higher in comparison to concentration measurements observed in the rest of the population. Re-

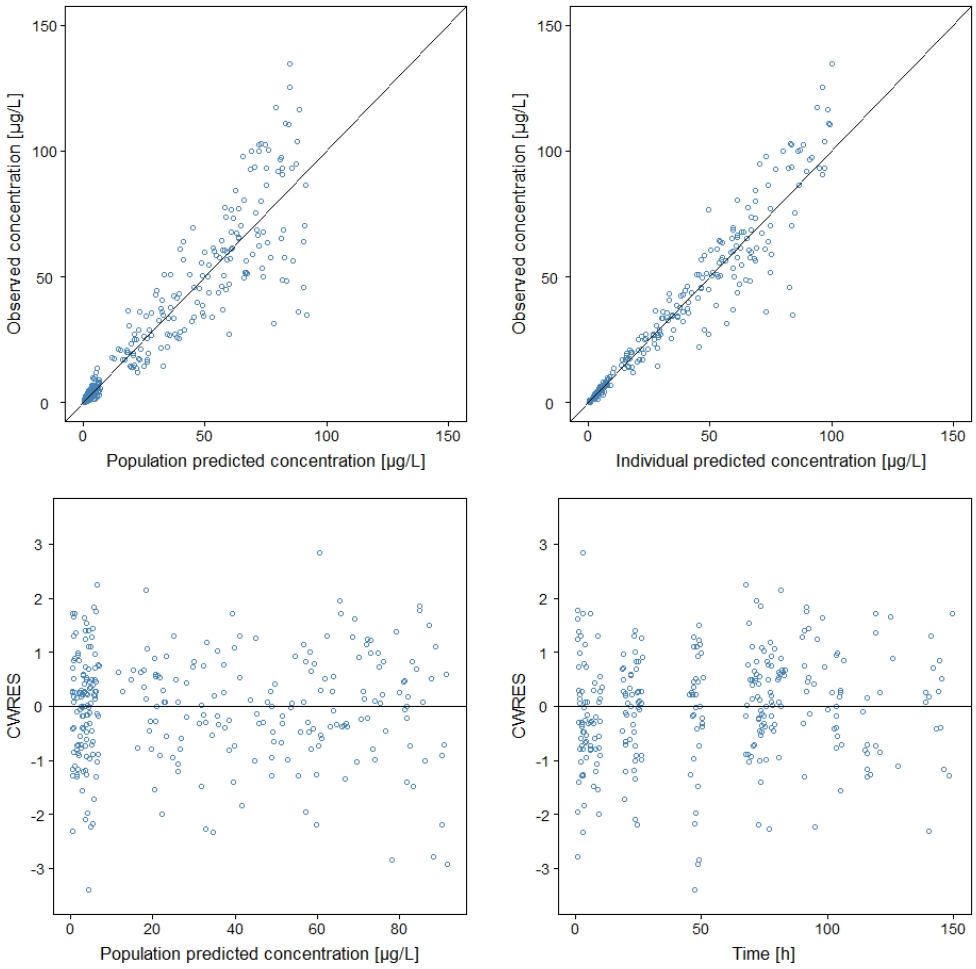

Figure 3.9 Goodness of fit plots for the final PK model for etoposide (E) plasma concentrations: observed versus population predicted E concentrations (top, left), observed versus individual predicted E concentrations (top,right), conditional weighted residuals (CWRES) versus population predicted E concentrations (bottom, left), CWRES versus time (bottom,right).

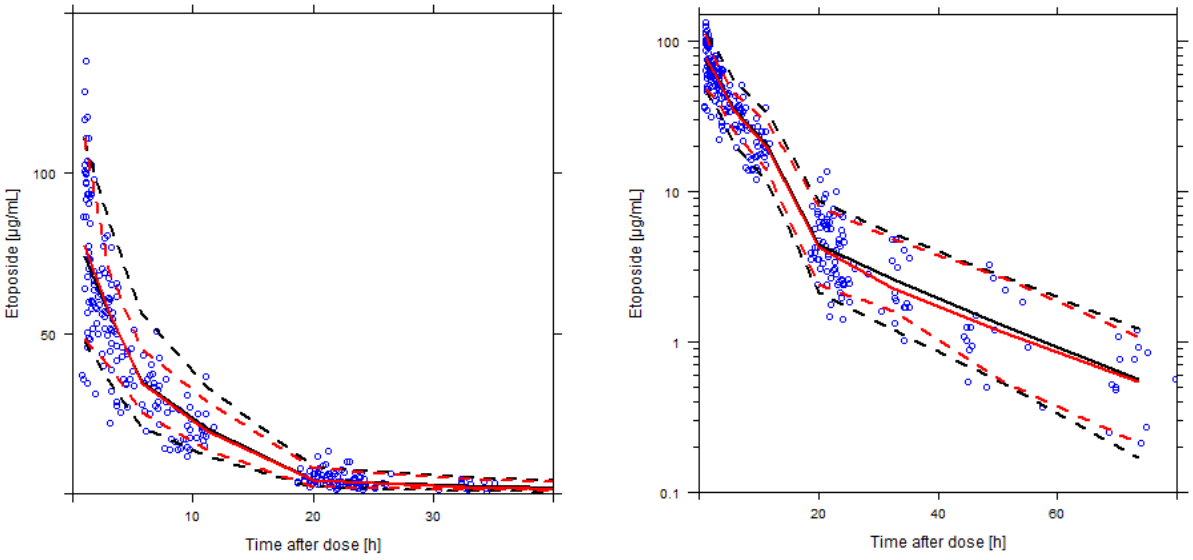

Figure 3.10 Visual predictive check for the final PK model of etoposide. Blue circles represent the measured etoposide concentrations. Solid and dashed lines represent the median, 5th and 95th percentile of the measured etoposide concentrations (red) and the simulations (black).

inclusion of the observed concentration of ID 17 led to an increase in RSE for all parameters which was most pronounced for Q with an increase from 9.9% to 18.9%. Inclusion of the other two data points resulted in an increase in the proportional residual variability from 19.6% to 22.7% and slightly poorer precision of parameter estimates. The outliers were most probably due to measurement errors or mistakes in the recording of sampling times. All three observations were excluded in the final model.

3.2.3 Thiotepa

3.2.3.1 Base model

For the structural model a one and a two compartment model were investigated (run summary of key and final models see appendix Table 8.3). The two compartment model was superior compared to the one compartment model with regard to OFV (ΔOFV: -90.1). Additionally, plots of population predicted concentrations versus observations did suggest a model misspecification for the one compartment model (appendix Figure 8.2). Nevertheless, the GOF plots and the individual plots of the two compartment model revealed an immense overprediction of observed concentration measurements at the end of the infusion which were close

to LLOQ. These overpredicted concentrations corresponded to the ones belonging to patients showing a delay in the concentration-time profiles as described in section 3.1.4.2. To take the observed delay in time into account a LAG time model and a transit model were applied. Although the implementation of a lag time resulted in a statistically significant improvement of the model (ΔOFV: -28.1), the observed low concentrations were still not adequately predicted as they occurred after the estimated lag time (LAG) of 1.15 h. It was not possible to estimate an IIV for LAG, even when the HYBRID option was used, i.e. all parameters were estimated with the FOCE+I algorithm whereas the IIV for LAG was estimated with FO. Hence, a transit model was investigated which enabled a better description of the delay in occurrence of C_{max} in the plasma. The data supported the estimation of an IIV for V_{cen} and the mean transition time TT. For the description of the residual variability an additive model for the log-transformed data, used for the transit model, was chosen which corresponds approximately to a proportional residual variability model on a normal scale. A combined residual variability model for log-transformed data was investigated, but the additional variability component was estimated to be close to 0 and therefore the model for the residual variability resembled the additive one.

3.2.3.2 Final model

The final structural model for thiotepa was given by a two compartment model with first-order elimination from the central compartment. The delay in the occurance of C_{max} in the plasma which was observed after six of the drug administrations was taken into account by a transit model (Figure 3.6, blue). Table 3.5 summarises the PK parameter estimates for the final model. TT was estimated to be 1.47 h and was of a comparable magnitude to the observed time delay in Figure 3.4. Due to model instability N was fixed to the estimated value of 125. The interindividual variability was moderate with 39.9% CV for V_{cen} and 28.4% CV for TT. Precision of parameter estimates was acceptable with respect to the given data situation which was reflected by RSE for the structural parameters ranging from 8.0% for TT to 29.5% for Q. For the description of the residual variability an additive model for the log-transformed data was chosen. CL of thiotepa was 19.1 L/h (318 mL/min) resulting in a median half-life of 1.6 h and 11.9 h for the initial and terminal elimination phase, respectively. On the day of ASCR the concentration of total thiotepa for a typical patient receiving a median dose of thiotepa was $1.4 \cdot 10^{-4}$ and $1.5 \cdot 10^{-3}$ μg/L in the central and the peripheral compartment, respectively.

Table 3.5 PK parameter estimates from the final PK model for thiotepa concentrations

Parameter	Unit	Estimate	RSE,%
OFV		1007.0	
Fixed effects			
CL	[L/h]	19.1	12
V_{cen}	[L]	46.8	20
Q	[L/h]	1.76	30
V_{per}	[L]	27.2 FIX	
TT	[h]	1.47	8.0
N		125 FIX	
Interindividual variability			
ωV_{cen}	[% CV]	39.9	43
ωTT	[% CV]	28.4	33
Residual variability			
σ proportional	[% CV]	77.5	11

OFV: objective function value; CL: clearance

V_{cen} and V_{per}: central and peripheral volume of distribution

Q: intercompartmental CL; TT: mean transit time; N: number of transit compartments

3.2.3.3 Evaluation

The goodness of fit plots depicted in Figure 3.11 showed a good description of the data by the model. The observed and predicted thiotepa concentrations spread uniformely and randomly around the line of identity and the CWRES versus TIME and predicted concentration plots revealed no trend in the data. The line of data points at 0.025 μg/mL for the plot depicting observed versus individual and population predicted concentrations is due to the values below LLOQ which were set to 1/2 LLOQ. The VPC for the final model showed that the variability, given by the 10^{th} and 90^{th} percentile of the observed and simulated concentrations was well predicted (Figure 3.12, dashed lines). The central tendency for time points >5 h was predicted well by the model (solid lines). Only the prediction of C_{max} was not adequately but still acceptable given the data situation. For binning of the observations a user-defined time array was applied which was given by the following time points relative to the end of the infusions: 0, 1.5, 3.7, 5.6, 6.8, 15, 25, 40 h. The time intervals were chosen based on observed clusters in the data and to obtain bins with comparable amount of data points.

3.2.3.4 Outliers

During the model development process seven concentration measurements were excluded from the analysis due to model instability or due to implausibility, i.e. concentrations measurements which were 5 to 10-fold higher compared to the rest of the population at the same time after the last dosing. One concentration below LLOQ which was set to 0.025 μg/mL had to be excluded as the iteration process did not start when it was kept in the dataset. Exclusion of another two concentration measurements (0.227 μg/mL (ID 17: TIME=23.8 h) and 1.73 μg/mL (ID 3: TIME=54.6 h)) which were more than 10 times higher than concentration measurements at the same time for the rest of the population enabled a successful convergence of the model although it still was not possible to obtain standard errors during these analyses. For the other four excluded concentrations (6.36 μg/mL (ID 3: TIME=9.7 h), 47.95 μg/mL (ID 6: TIME=49.0 h), 23.77 μg/mL (ID 4: TIME=50.2 h) and 0.025 μg/mL (ID 7: TIME=47.0 h)) the RSE of the structural model parameters showed a, at least, two fold increase and were greater than 90% and 100% for the concentrations of 6.36 and 0.025 μg/mL, respectively. Exclusion of the two highest concentration measurements was also supported by the fact that the linearity for the calibration curve for the analysis of thiotepa concentrations was only given up to 10 μg/mL. All seven mentioned outliers were excluded from the final model.

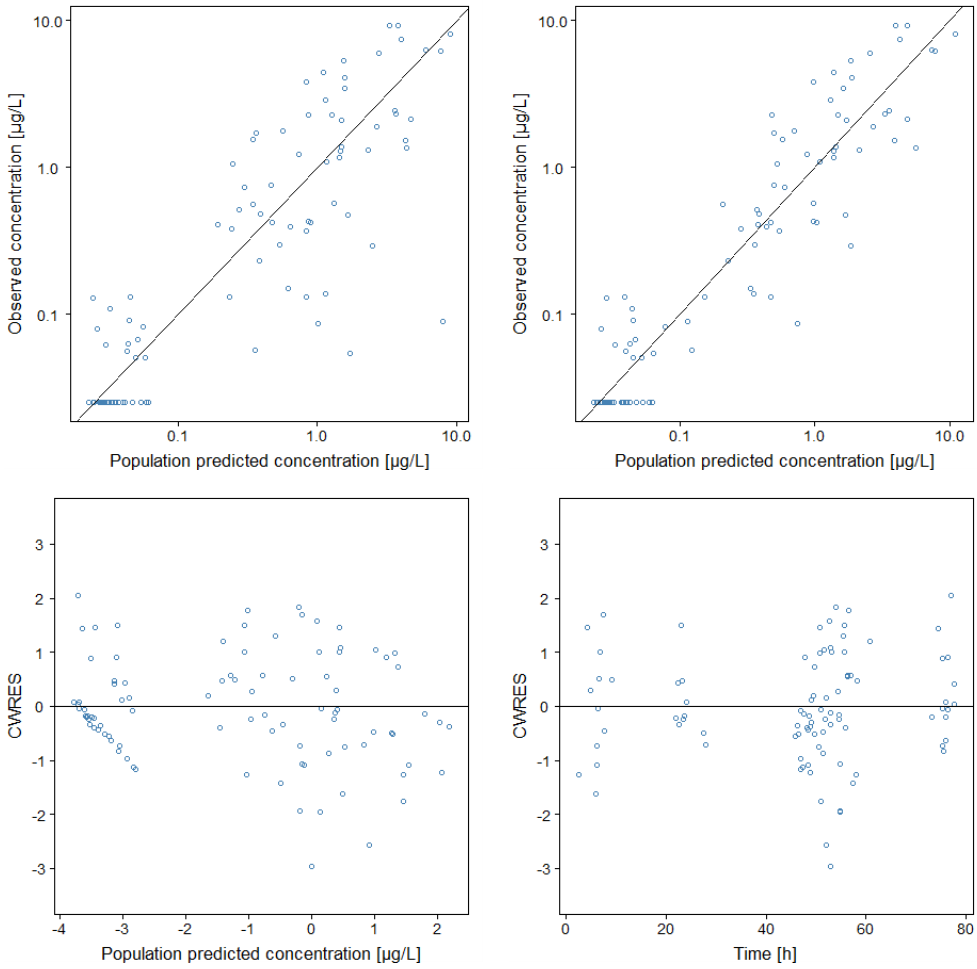

Figure 3.11 Goodness of fit plots for the final PK model for tiotepa (T) plasma concentrations: observed versus population predicted T concentrations (top, left), observed versus individual predicted T concentrations (top,right), conditional weighted residuals (CWRES) versus log-transformed population predicted T concentrations (bottom, left), CWRES versus time (bottom,right).

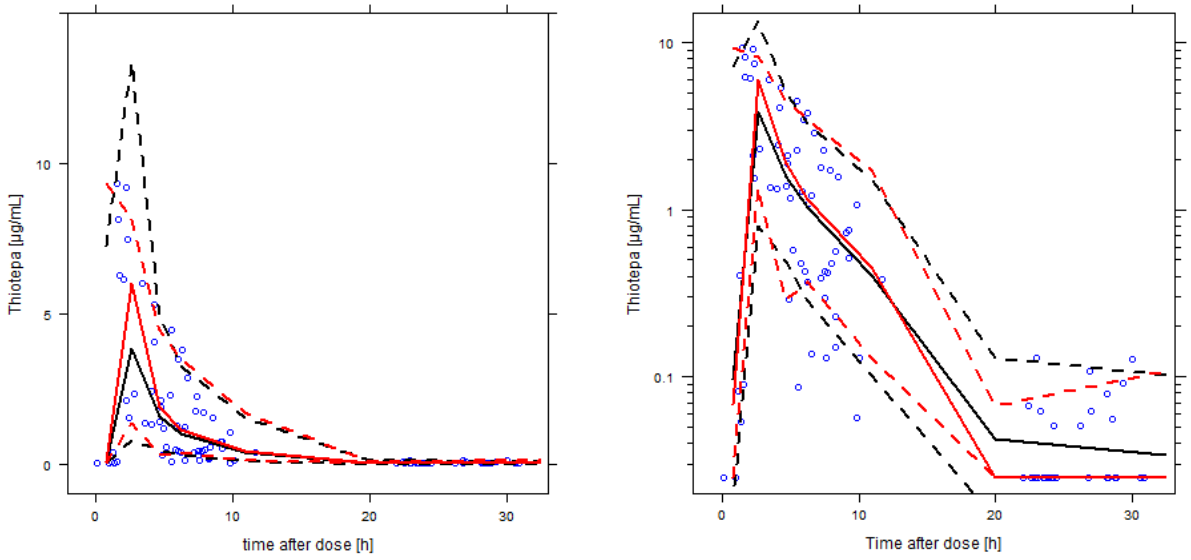

Figure 3.12 Visual predictive check for the final PK model of thiotepa. Blue circles represent the measured thiotepa concentrations. Solid and dashed lines represent the median, 5th and 95th percentile of the measured thiotepa concentrations (red) and the simulations (black).

3.2.4 Investigation of the infusion duration

Parameter estimates and their precision were comparable for both infusion durations for carboplatin and etoposide. The OFVs of the models describing carboplatin and etoposide concentrations based on the dataset including the shorter infusion times were lower (ΔOFV: -7.2 (carboplatin), -5.0 (etoposide)) compared to the ones based on the long infusion duration. C_{max} concentrations for both drugs were slightly better described for the datasets containing the short infusion duration (appendix, Figure 8.3). For the three patients with the very short infusion times for etoposide the model based on the dataset with the short infusion times showed a minimal better prediction of the C_{max} concentrations. Due to these findings and the fact that the end of the washing period was not very well documented in the case of etoposide the datasets containing the short infusion duration, i.e. from the start until the end of the infusion, were used for parameter estimation. As the final model for thiotepa was a model with transit compartments describing the process of infusion the infusion duration did not influence the parameter estimation, as for the transit model an i.v. bolus into the first transit compartment is assumed (Figure 3.6).

3.3 Project 2: Pharmacokinetic/pharmacodynamic modelling of leukopenia

In total, leukocyte concentrations and covariates from 17 patients were available for PK/PD analysis. The EBEs from the population PK analysis (section 3.2) were used as model input for the population PK/PD model, following a sequential modelling approach. Model development was conducted according to the steps described in section 2.4.2 and aimed for the adjustment of a semi-mechanistic model for myelosuppression[138] (section 2.4.1) to the special setting of HDCT. As the model distinguished between drug- and system-specific parameters it enabled the investigation of the implementation of the drugs' effects on the one hand (section 3.3.1) and, on the other hand, the evaluation of possible model extensions to describe the system of leukopoiesis during HDCT. Model development regarding the system of leukopoiesis comprised the investigation of the baseline estimation method (section 3.3.2), the number of transit compartments describing cell maturation (section 3.3.3), the administration of DEXA (section 3.3.4), the implementation of the supportive treatment influencing leukopoiesis, i.e. the ASCR (section 3.3.5) and G-CSF, the feedback mechanism (section 3.3.6), and the investigation of possible covariate effects (section 3.3.7).

3.3.1 Implementation of the drug effect

For the implementation of the drug effect of carboplatin, etoposide and thiotepa linear inhibitory and inhibitory E_{max} models were investigated. The E_{max} model was not statistically superior in comparison to the simpler linear model for etoposide and thiotepa and therefore a linear relation, defined by the slope SL, between the drug effect and the drugs' concentrations was chosen. Applying the E_{max} model for carboplatin resulted in a statistically significant drop in the OFV of 16.5 points. However, the precision of the parameter estimates for C_{INI} and the IIV of MMT were lower with RSE being 45.8% and 69.0%, respectively, compared to RSEs of 40.2% and 38.3% for a linear inhibitory model. As the GOF plots (appendix, Figure 8.4) and individual predictions of the leukopenic time course were not improved when the E_{max} model was implemented, the simpler linear inhibitory model was also chosen for carboplatin.

During model development an additive effect for all drugs was assumed (Equation 2.26). For the final model a possible interaction of the drugs was investigated applying the response surface model described in section 2.4.2.1. Convergence for a model allowing a drug interaction between all three drugs could not be achieved, as it was not possible to start the iteration pro-

cess. As SLs for carboplatin and etoposide were the highest, suggesting a high sensitivity of the cells in the bone marrow towards those two drugs, an interaction for the two compounds was investigated. For the investiation thiotepa was included as before, assuming an additive, linear inhibitory effect on the proliferation rate constant of the cells in the bone marrow. The OFV decreased 4.5 points for the model including the drug-drug interaction in comparison to the model with an additive drug effect for all drugs. The estimated SL for thiotepa did not change, although the RSE increased from 5.1% to over 900%. In contrast to the model with an additive drug effect the SL for carboplatin was smaller with 0.35 (RSE: 8.9%) than SL of etoposide which was estimated to be 0.85 (RSE: 12%). All other parameter estimates were comparable to the model with an additive drug effect.
The response surface analysis assumes an additive effect for the drugs for E_{50} equal to one whereas a synergistic drug interaction is given for E_{50} smaller than one. Directly after the end of the infusion, when drug concentrations were the highest, the median of E_{50} was 0.9 (5^{th} and 95^{th} percentile: 0.7 - 1.0) which supports the implementation of an additive drug effect. Hence, as no major improvement in the OFV and the GOF plots (appendix, Figure 8.5) could be observed, the precision of the parameter estimate of SL for thiotepa decreased and an additive effect for the two drugs was supported by the estimate of E_{50}, the implementation of an additive drug effect for all drugs was kept in the final model.

3.3.2 Baseline estimation methods

Different baseline estimation methods[242] (section 2.4.2.2) were evaluated during various steps of the model development process with regard to OFV, AIC, GOF plots and precision of parameter estimates. The parameter estimates obtained during model development for the three baseline estimation methods are given in Table 3.6. Implementation of the B2 method required for two parameters less compared to the B1 and the B3 method. The B1 method was superior compared to the B2 method in terms of AIC with an increase of 15.3 points for the B2 method. Neither the B1 nor the B3 method were statistically superior with regard to the AIC as the AIC of the B3 method was only 1.2 points smaller compared to the B1 method. Precision of parameter estimates for all methods was comparable with the exception of the RSE for SLT with 18.6%, 85.0%, and 146.8% for the B1, B2 and B3 method, respectively. Additionally, the RSE for C_{INI} for the B2 method was higher being 45.3% compared to 37.2% (B1) and 35.4% (B3) RSE. GOF plots of the predicted versus observed leukocyte concentrations revealed a slightly wider distribution of the concentrations around the line of identity (Figure 3.13) for the B2 method. For the final model the B1 baseline estimation method, i.e. the estimation of

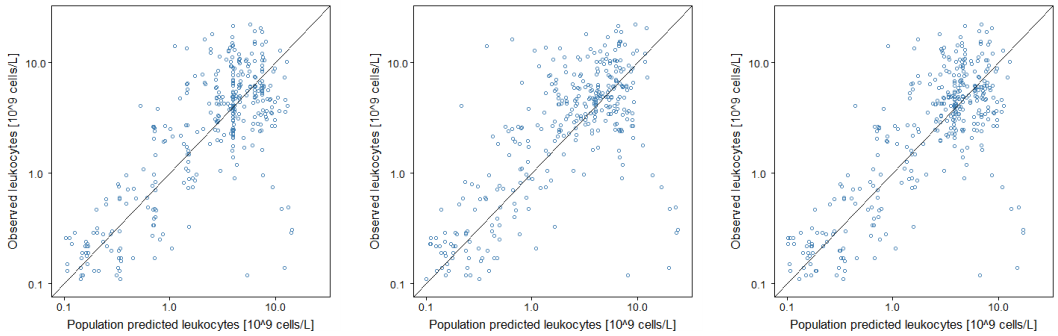

Figure 3.13 Goodness of fit plots depicting observed versus predicted leukocyte concentrations for the B1 (left), B2 (middle) and B3 (right) method[242] on a logarithmic scale.

the baseline and the respective interindividual variability, was chosen as it was superior (B2) or comparable (B3) in terms of OFV, the precision of parameter estimates was higher and the B1 method showed a slightly better distribution of measured leukocyte concentrations in the GOF plots compared to the B2 method (Figure 3.13).

3.3.3 Number of transit compartments

For the description of leukocyte concentrations following HDCT different numbers of transit compartments (N) were implemented. All models converged successfully, but since not for all models RSE were available the OFV served as the selection criterion. The OFV of the models could be compared directly as the MMT defined the transition rate constants k_{tr} and therefore N could be increased without adding parameters to the model. Figure 3.14 depicts the OFV in dependency of the number of transit compartments. The minimum in the OFV was given for N=6 transit compartments which therefore was chosen for the final model.

3.3.4 Description of the initial increase in leukocyte concentrations

The increase in leukocyte concentrations following chemotherapy has been associated with the known effects of glucocorticoides[148,151]. Hence, during model development the initial increase was evaluated considering the administration of DEXA. In a first approach an additional compartment (INI_{DEXA}) was introduced to the model which was initiated once with an estimated amount of cells (C_{INI}) the first time DEXA was administered (see 1., section 2.4.2.4). A second approach comprised multiple initialisations of INI_{DEXA} every time DEXA was administered to the patient (see 2., section 2.4.2.4). The model with the single initialisation of

Table 3.6 Population PK/PD parameter estimates from the PK/PD models including the three baseline estimation methods[242] B1, B2 and B3

Parameter	Unit	B1 method Estimate (RSE, %)	B2 method Estimate (RSE, %)	B3 method Estimate (RSE, %)
AIC		72.6	87.9	71.4
Fixed-effects parameters				
$Circ(t_0)$	[10^9 cells/L]	3.97 (7.50)		3.84 (6.70)
MMT	[h]	93.2 (4.80)	93.7 (3.30)	93.0 (6.70)
γ		0.115 (7.00)	0.112 (7.50)	0.115 (7.00)
SLC	[L/μmol]	2.83 (22.7)	2.86 (23.4)	2.82 (22.2)
SLE	[L/μmol]	0.696 (24.9)	0.73 (24.1)	0.70 (24.3)
SLT	[L/μmol]	0.010 (18.6)	0.011 (85.0)	0.011 (146.8)
C_{INI}	[10^9 cells/L]	19.2 (37.2)	12.1 (45.3)	20.2 (35.4)
MT_{INI}	[h]	43.7 (10.4)	49.1 (11.3)	43.4 (9.70)
MT_{SCR}	[h]	4.37 (56.3)	4.86 (50.8)	4.31 (55.9)
Interindividual variability				
$\omega Circ(t_0)$	[% CV]	22.1 (40.2)	1 FIX	30.8 (30.9)
ωMTT	[% CV]	14.3 (37.5)	11.6 (33.7)	14.4 (37.4)
$\omega\gamma$	[% CV]	28.1 (31.2)	28.0 (31.0)	28.7 (31.5)
ωC_{INI}	[% CV]	97.3 (30.9)	88.6 (29.9)	96.5 (30.2)
ωMT_{SCR}	[% CV]	172.6 (36.4)	152.6 (29.6)	174.4 (35.5)
ωIBASE	[% CV]			1 FIX
Residual variability				
σ proportional	[%]	53.1 (6.90)	53.3 (7.20)	53.1 (6.90)

$Circ_0$: leukocyte concentration before start of therapy; MMT: Mean maturation time

γ: exponent of the feedback; MT_{SCR}: stem cell rescue time; C_{INI}: concentration of cells describing the initial increase; MT_{INI}: mean time describing the initial increase

SLC, SLE, SLT: slope factor of ultrafilterable platinum, total etoposide and total thiotepa

ωIBASE: interindividual variability for the estimation of the population baseline response

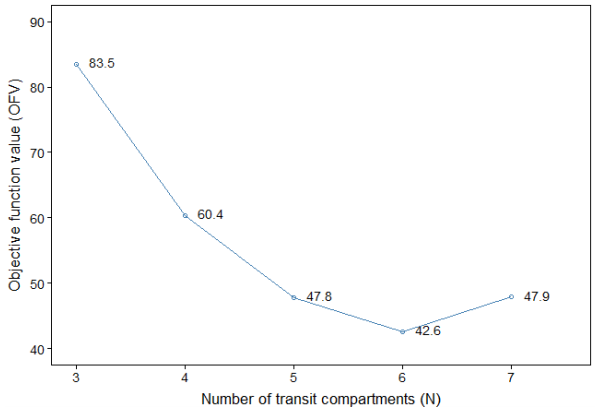

Figure 3.14 Objective function value versus number of transit compartments (N) of the PK/PD model including N = 3 - 7 transit compartments.

INI_{DEXA} was superior compared to the one with the multiple initialisations with regard to OFV (ΔOFV: 21.5) and, more importantly, with regard to the ability to describe the initial increase in each patient. Figure 3.15 clearly illustrates that the single initialisation approach better described the initial increase in leukocyte concentrations. Overall, the inclusion of INI_{DEXA} in the model led to a drop in the OFV of 61.7 points. For the graphical evaluation of this improvement a GOF plot depicting the observed versus the population predicted leukocyte concentrations of the first 150 h after the start of HDCT is depicted in Figure 3.16. A model missfit for the model without INI_{DEXA} (Figure 3.16, right) is indicated by an unequal distribution of the leukocyte concentrations around the line of identity. In addition to the structural model the IIV for C_{INI} and MT_{INI} was investigated. The IIV for C_{INI} was high with 94.8% CV and was estimated with sufficient precision (RSE: 40.1%). Inclusion of a variance component for MT_{INI} did not further improve the model.

3.3.5 Integration of the autologuous stem cell rescue

The integration of the ASCR was evaluated twice during the model development process, first (A) based on a model comprising three transit compartments and later (B) based on a model with 6 transit compartments as described in section 3.3.3. Results from scenario A which was investigated early during the model development process can be regarded as results from a pre-investigation and were used to decide which scenarios should be investigated for the model comprising the final number of transit compartments. For the investigation the retransfused $CD34^+$ cells were subdivided into 3 groups as follows: (i) all $CD34^+$ cells including CFU

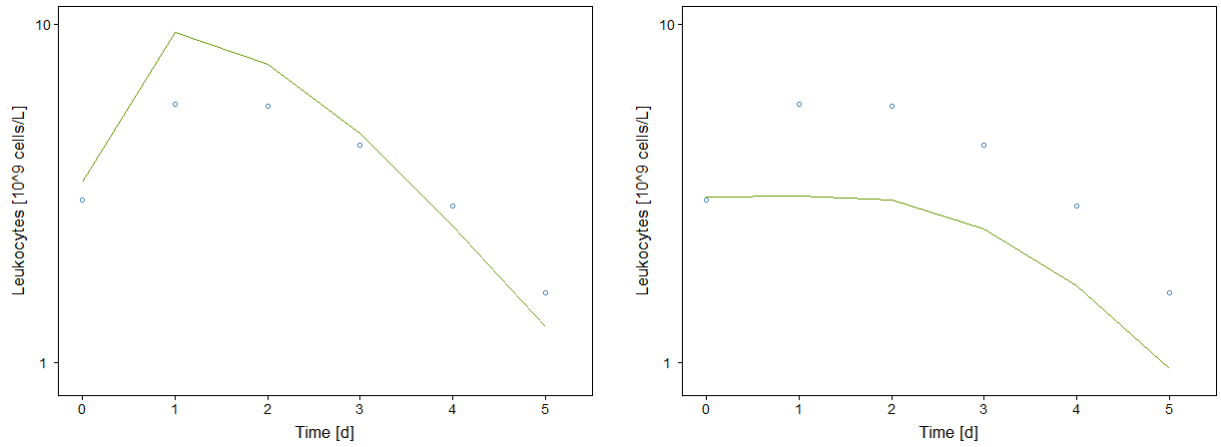

Figure 3.15 Model prediction of the observed initial increase in leukocyte concentration for one patient (ID 4) for a model with single initialisation of the INI_{DEXA} compartment (left) and multiple initialisations (right). Blue circles represent observed leukocyte concentrations, green lines the individual's model prediction.

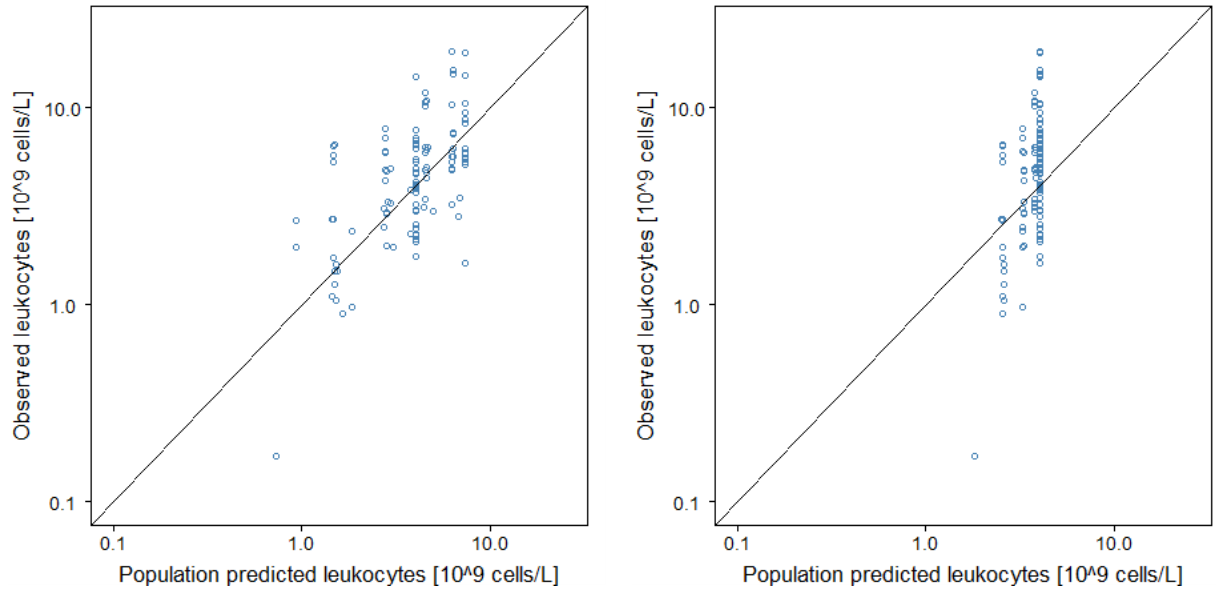

Figure 3.16 Goodness of fit plots depicting observed versus model-predicted leukocyte concentrations for a PK/PD model including the INI_{DEXA} compartment (left) and without the INI_{DEXA} compartment (right) for the description of the initial increase in leukocyte concentrations.

cells, (ii) CFU cells only and (iii) $CD34^+$ cells excluding CFU cells. The different subgroups were then allowed to enter the compartment of proliferating cells (Prol) and/or the different transit compartments (T1, T2, ...,T_N). Figure 3.17 and 3.19 summarise the investigated structural models. For the pre-investigation based on a model with three transit compartments the following structural models were evaluated:

A1) All $CD34^+$ cells (i) entering either the compartment of proliferating cells (Prol) or the first (T1), second (T2) or third (T3) transit compartment (A-i-Prol or A-i-T1/T2/T3, Figure 3.17 top left)

A2) CFU cells only (ii) entering Prol via one transit compartment (A-ii-Prol , Figure 3.17 top right)

A3) CFU cells (ii) entering Prol via a transit compartment (Transit CFU) and the remaining $CD34^+$ cells (iii) entered T1 (A-ii-Prol + A-iii-T1, Figure 3.17 bottom left)

Scenario A1 Within scenario A1 the model in which all $CD34^+$ cells entered Prol (A-i-Prol) was superior in terms of OFV compared to A-i-T2 and A-i-T3 which had OFVs $\geq$ 956 points higher than A-i-Prol. The residual variabilities for those two models were high, being > 192% CV compared to a residual error of 59% CV for model A-i-Prol. Additionally, the parameter estimates for MMT and C_{INI} were not plausible being much shorter (MMT< 52.8 h, half of the previously reported value) and 10 times higher ($C_{INI} > 97.4 \cdot 10^9$ cells/L) than previously reported by others[138,148,151]. The exponent of the feedback for model A-i-T3 was implausibly high with 0.74 compared to the usual estimate[138] of around 0.1. Thus, the two models in which all $CD34^+$ cells entered the second and third transit compartment were discarded. Only model A-i-T1 had a lower OFV (ΔOFV -12.6 points) compared to A-i-Prol and showed a similar residual variability (57% CV) but parameter precision for this model was worse. Especially with regard to C_{INI}, SL of carboplatin and MT_{INI} were the RSE was 146%, 138% and 185%, respectively, compared to 36.3%, 61.6% and 10.9% for model A-i-Prol. Figure 3.18 depicts plots of predicted versus observed leukocyte concentrations of model A-i-Prol and A-i-T1/T2/T3 and illustrates the model misspecification for A-i-T1/T2/T3 by an uneven spread of the data around the line of identity.

Scenario A2 Based on the findings of A1 and due to the fact that the amount of CFU cells was available for analyses scenario A2 was investigated. However, the model was rejected due to the predicted versus observed leukocyte concentration plot (Figure 3.18, bottom left)

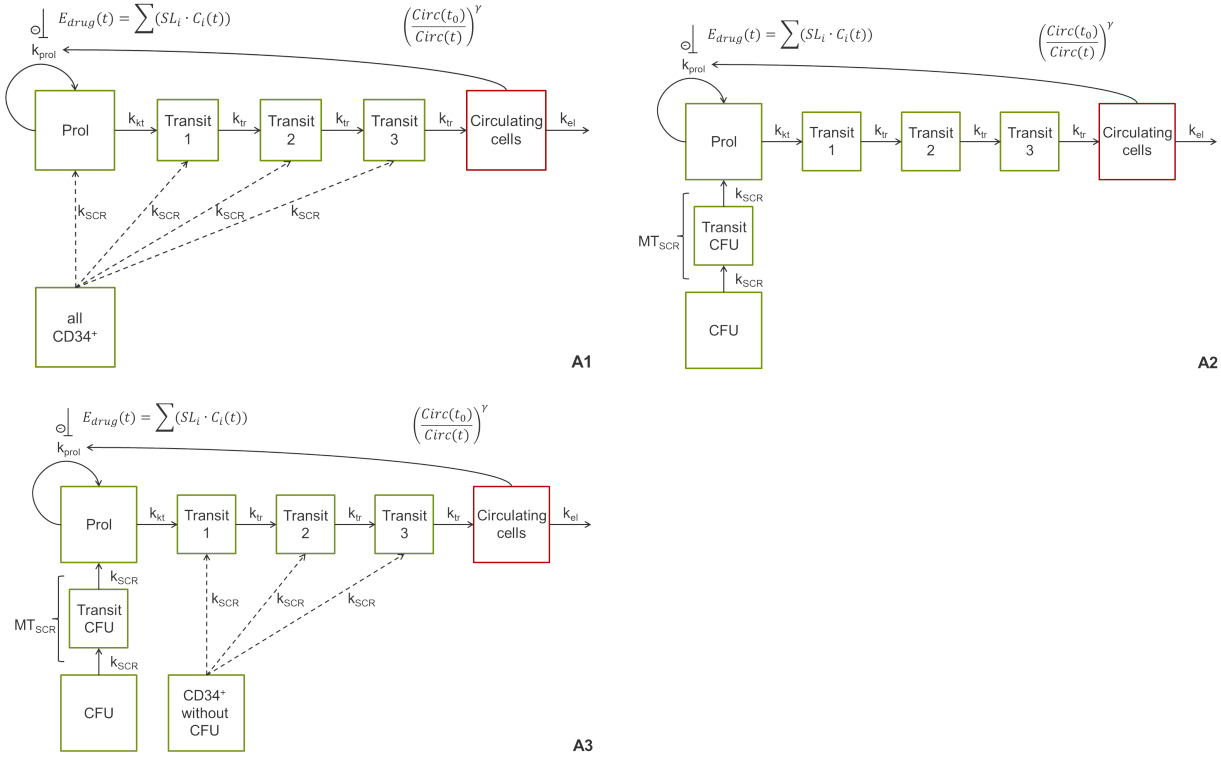

Figure 3.17 Schematic key structural models for the investigation concerning the implementation of the ASCR. A1: all $CD34^+$ cells enter either the compartment of proliferating cells (Prol), or the first, second or third transit compartment (top left, A-i-Prol/T1/T2/T3). A2: the CFU cells only enter Prol via one transit (Transit CFU) compartment (top right, A-ii-Prol). A3: CFU cells enter Prol via Transit CFU and the remaining $CD34^+$ cells enter either the first, second or third transit compartment (bottom left, A-ii-Prol + A-iii-T1/T2/T3). Circ(t_0): leukocyte concentrations before start of high-dose chemotherapy; Circ(t): leukocyte concentration at time t; γ: feedback exponent of the original feedback acting on the proliferation rate constant k_{prol}; k_{tr}: transition rate constant; k_{SCR}: transition rate constant of the ASCR; MT_{SCR}: mean time of the ASCR; $E_{drug}(t)$: drug effect at time t; SL_i and $C_i(t)$: slope and concentration of drug *i*.

which showed a model misspecification and based on implausible high parameter estimates for MT_{INI} and C_{INI} with $171 \cdot 10^9$ cells/L and 51700 h, respectively.

Scenario A3 The third scenario comprised the separation of the CFU cells, which entered Prol, from the remaining $CD34^+$ cells which were transferred to the first transit compartment. The goodness of fit plots for this model showed a good description of the data. Only the precision for the estimate of the SLE was poor (RSE: 384%). To allow for more variability and a possibly better precision for the parameter estimate an IIV on the rate constant (k_{in}), describing the transition from the $CD34^+$ cells to T1, was included but did not significantly improve the model (ΔOFV -1.11). Since the parameter imprecision for SLE increased (RSE, 1505%) the IIV was removed for further model development.
Due to these findings model A-i-Prol and A-ii-Prol + A-iii-T1 were re-investigated for the model comprising the final number of six transit compartments (B). The following models were investigated:

B1) CFU cells (ii) entering Prol via one transit compartment (Transit CFU) and the remaining $CD34^+$ cells (iii) entering either T1, T2,..., T6 (B-ii-Prol + B-iii-T1/T2/.../T6, Figure 3.19 left)

B2) All $CD34^+$-cells (i) entering Prol via one transit compartment (B-i-Prol, Figure 3.19 right)

Scenario B1 All investigated models (B-ii-Prol + B-iii-T1/T2/.../T6) converged but it was not possible to estimate SL of etoposide which either became negligibly small when the parameter was constrained to be > 0 or negative with a RSE of 462% when the constrain was removed.

Scenario B2 This model in which all $CD34^+$ cells entered the compartment of proliferating cells did enable the estimation of a SL for etoposide with acceptable precision (RSE =83.5%). Inclusion of an IIV for MT_{SCR} further reduced the RSE of SL for etoposide to 24.6%. The observed and predicted leukocyte concentrations spread uniformly and randomly around the line of identity showing the adequate description of the data (Figure 3.20) and indicating a plausible integration of the ASCR.
In the final model the ASCR was described by a model of the structure B-i-Prol, i.e. a model comprising 6 transit compartments with all $CD34^+$ cells including the CFU cells entering the compartment of the proliferative cells in the bone marrow via one transit compartment.

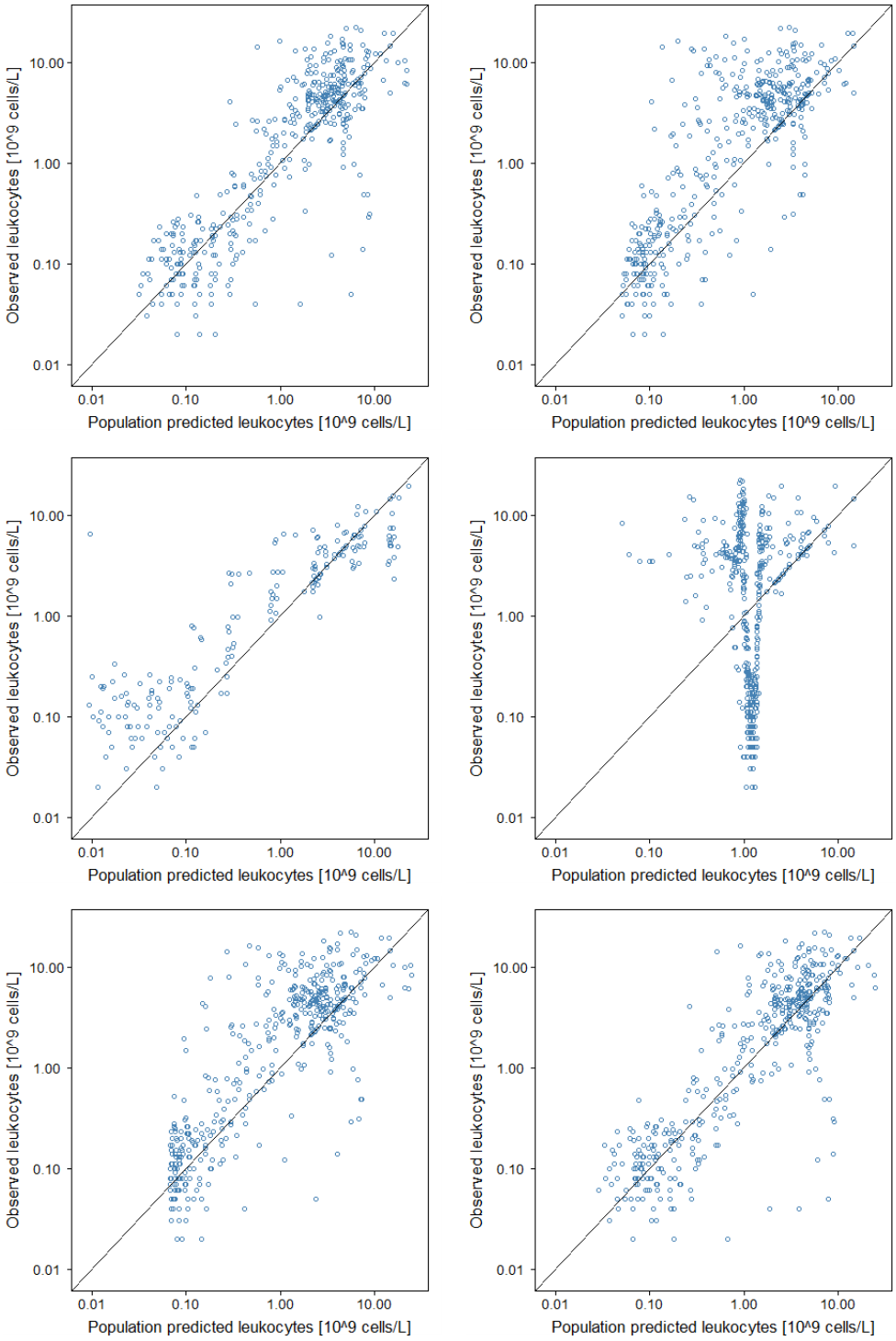

Figure 3.18 Goodness of fit plots depicting observed versus poulation predicted leukocyte concentrations for the models A-i-Prol, A-i-T1 (top left and right), A-i-T2, A-i-T3 (middle left and right), A-ii-Prol (bottom left) and A-ii-Prol + A-iii-T1 (bottom right)

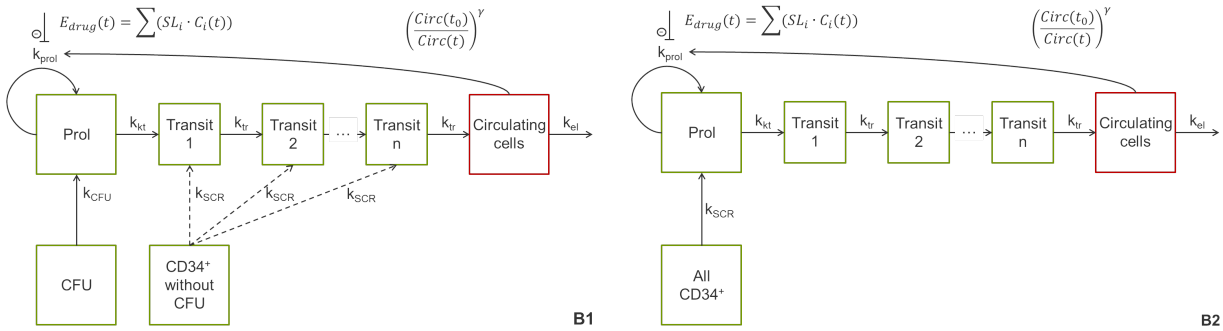

Figure 3.19 Schematic key structural models for the investigation concerning the implementation of the ASCR. B1: CFU cells enter the compartment of proliferating cells (Prol) via Transit CFU and the remaining $CD34^+$ cells enter either the first, second or third transit compartment (left, B-ii-Prol + B-iii-T1/T2/.../T6). B2: all $CD34^+$ cells enter Prol (right, B-i-Prol) via one transit compartment (right, B-i-Prol via transit). $Circ(t_0)$: leukocyte concentrations before start of high-dose chemotherapy; Circ(t): leukocyte concentration at time t; γ: feedback exponent of the original feedback acting on the proliferation rate constant k_{prol}; k_{tr}: transition rate constant; k_{CFU}: transition rate constant of the CFU cells; k_{SCR}: transition rate constant of the ASCR; MT_{SCR}: mean time of the ASCR; $E_{drug}(t)$: drug effect at time t; SL_i and $C_i(t)$: slope and concentration of drug *i*.

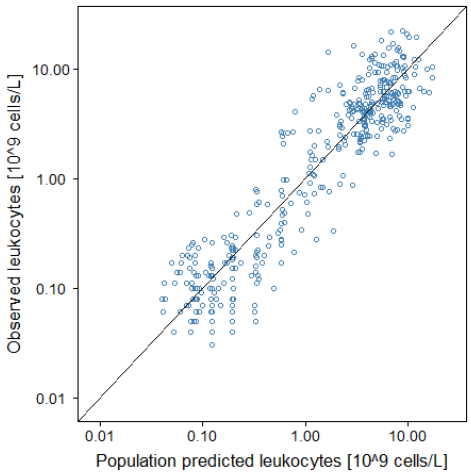

Figure 3.20 Goodness of fit plots depicting observed versus poulation predicted leukocyte concentrations for the B-i-Prol model (scenario B2)

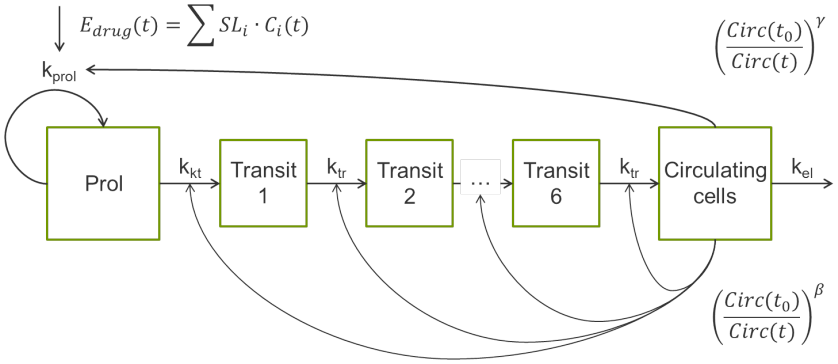

Figure 3.21 Schematic structural PK/PD model for myelosuppression including a second feedback mechanism (exponent β) acting on the transition rate constants k_{tr}. Prol: compartment of proliferating cells; Circ(t_0): leukocyte concentrations before start of high-dose chemotherapy; Circ(t): leukocyte concentration at time t; γ: feedback exponent of the original feedback acting on the proliferation rate constant k_{prol}; E_{drug}(t): drug effect at time t; SL_i and C_i(t): slope and concentration at time t of drug *i*.

3.3.6 Integration of an additional feedback

For the implementation of the regulatory mechanisms of leukopoiesis the introduction of a second feedback mechanism acting on the transition rate constants (k_{tr}) as proposed by Quartino et al.[258] was investigated. The exponent β of this feedback mechanism was introduced as an additional parameter to the model (Figure 3.21).

For the model without INI_{DEXA} (section 2.4.2.6) it was not possible to obtain a reasonable estimate for β which was estimated to be close to zero (< 0.0001). The implementation of the second feedback mechanism on all 6 k_{tr} or on the last 5, 4, ..., 2 k_{tr} before the cells were entering the circulation was investigated. Letting it act only on a reduced number of k_{tr} did not enable the estimation of β and, additionally, it was not possible to estimate MT_{SCR} anymore.

Implementation of the second feedback in addition to INI_{DEXA} enabled the estimation of β which was 0.006 with a RSE of 387%. Compared to the model without the second feedback the OFV was not significantly improved (ΔOFV: -0.2). Hence, the final model included only one feedback mechanism as originally proposed by Friberg et al.[138] Nonetheless, the model including INI_{DEXA} and the additional feedback was reevaluated during the covariate analysis (section 3.3.7) to investigate a possible covariate influence and stabilisation of the estimation of β by inclusion of a covariate.

3.3.7 Covariate analysis

First, the influence of G-CSF and DEXA on the system of leukopoiesis following HDCT was assessed. Both covariates were coded as dichotomous covariates and were included as a fractional function given by Equation 2.14.

G-CSF G-CSF was tested for its influence on MMT, k_{prol}, k_{el}, MT_{SCR} and γ. No statistically significant covariate influence was found for all parameters, although inclusion of G-CSF on the parameters describing leukopoieses except for MT_{SCR} resulted in a drop of the OFV. A reduction of MMT under G-CSF treatment of 9.75% (RSE: 95.1%, ΔOFV: 3.1) was estimated, suggesting a faster maturation of the cells in the bone marrow. Despite the fact that G-CSF is supposed to increase the proliferation rate of the cells in the bone marrow k_{prol} was found to be reduced by 8.6% (RSE: 49.4%, ΔOFV: 7.6). The elimination rate constant k_{el} and MT_{SCR} were not affected by the inclusion of G-CSF which was reflected in an estimate close to zero for both covariate relations and no change in the OFV. The exponent γ of the feedback was increased by 144% under G-CSF treatment (RSE: 26.2). The decrease in the OFV was 10.84 compared to the base model which was technically a statistically significant drop for p=0.001 (ΔOFV > 10.83). However, the difference in OFV was driven by only one patient who did not receive the G-CSF treatment (ID 7) and did show a deviating leukopenic time profile. GOF plots depicting observed versus population predicted leukocyte concentrations did not change for all tested covariate relations, except for inclusion of G-SCF as a covariate on k_{prol}, in which case a deterioration was observed and on γ where the respective GOF plot revealed an improvement of the model fit regarding the better prediction of leukocyte concentrations for ID 7 (see Figure 3.22).
This finding motivated the reinvestigation of the predictive performance and model stability of the model including a second feedback (section 3.3.6) with regard to parameter estimation of β. A decrease in the OFV of 9.6 and 9.8 points was observed for the model with G-CSF influence on (i) γ and (ii) β compared to the model including two feedback mechanisms without covariate influence, respectively. Inclusion of G-CSF enabled the estimation of β which was 0.016 for (i) and 0.056 for (ii). The estimate for γ was halved (0.12 versus 0.07) after inclusion of G-CSF on γ, but did not change when G-CSF was included as a covariate on β. Model (i) was very unstable and it was not possible to obtain a covariance step for this model. Model (ii) converged successfully but resulted in a poor precision for SL of thiotepa with RSE being 94.7%. The GOF plots for model (i) and (ii) were comparable to those from the model including one feedback and G-CSF as a covariate for γ (plots not shown) but inclusion of G-CSF in

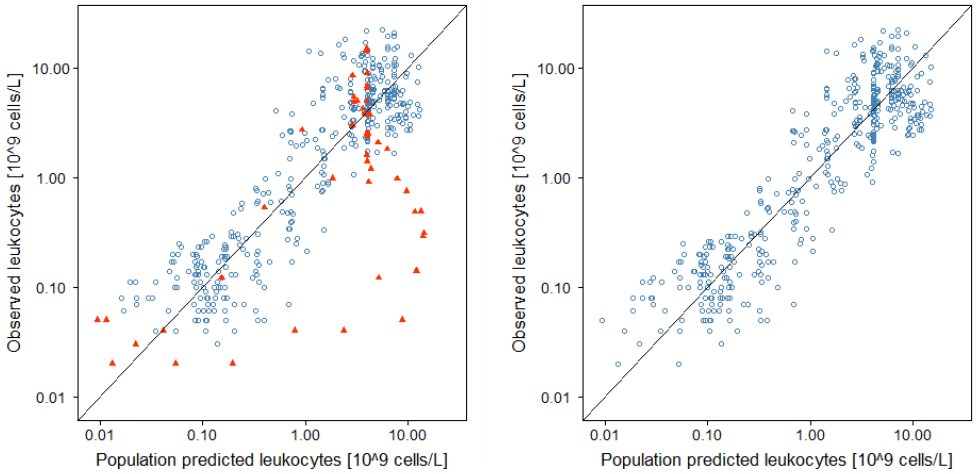

Figure 3.22 Goodness of fit plot depicting observed versus model-predicted leukocyte concentrations for the final PK/PD model (left) and the model including G-CSF as a covariate on the feedback exponent γ (right). Red triangles: leukocyte concentrations of the patient not receiving granulocyte colony-stimulating factor (ID 7).

the model with two feedback mechanisms did not result in a statistically significant improved fit (ΔOFV: 2.2).
In summary, none of the covariate relations were statistically significant, although tendencies were found and the estimation of β was supported. Therefore G-CSF was not included as a covariate in the final model.

Dexamethasone The amount of administered DEXA was evaluated as a predictor for the estimated amount of cells (C_{INI}) that was used to initiate INI_{DEXA}, as a dose dependent increase of circulating neutrophils, and therefore total leukocytes, can be associated with the administration of DEXA[70]. The total amount of DEXA was analysed with the model including the single initialisation approach of the INI_{DEXA}. Inclusion did not lead to a change in the OFV (ΔOFV: -0.1) and the influence of the total administered amount of DEXA on C_{INI} was negligible being 0.3% (RSE: 593%). For the model including multiple initialisations of INI_{DEXA} the influence of the single dose administration of DEXA was investigated but the model was rather instable and did not converge with standard errors. Additionally, the estimate of the covariate influence proposed decreasing number of cells with increasing dosages of DEXA which is physiologically implausible.
The implementation of a covariate influence of DEXA on k_{el} did not lead to a change in the

OFV and was estimated to be close to zero (0.1%). Inclusion of DEXA as a covariate influencing MMT and k_{prol} to assess its predictive potential for the description of the initial increase resulted in a reduction of MMT by 24.1% under DEXA treatment and k_{prol} was increased by 496%. Despite the magnitude of the covariate influence ΔOFV was only -6.7 points and the initial increase could not be described apart from a very small and short increase of leukocytes directly after start of therapy. Therefore inclusion of DEXA as a covariate on MMT and k_{prol} was not considered in the final model nor was a covariate influence of DEXA on any other model parameter.

Other covariate relations The last step comprised the analysis of potential covariates that were identified during graphical analysis. The following covariate relations were included as a power function (Equation 2.12): HT as a predictor for Circ(t_0) and AGE, ALB, CLCR and GGT were tested for their influence on MT_{SCR}. None of the relations was found to be statistically significant with the highest decrease in the OFV of 1.4 points for the influence of AGE on the MT_{SCR}. Hence, no covariate was included in the final model.

3.3.8 Final model

Implementation of the drug effect The drug effect of the three drugs was assumed to be additive and was implemented as a linear inhibitory model (Equation 2.26) for each drug. It was possible to estimate a slope factor for each drug. Assuming that only the fraction of the drug molecules that is not bound to plasma proteins exhibits an effect on cell proliferation and survival the slopes estimated for total etoposide and thiotepa had to be transformed, taking the plasma protein binding into account. For etoposide and thiotepa a plasma protein binding of 79% to 96% (see section 1.3.4) and 10% to 30% (see section 1.3.4), respectively, was used for calculations. Etoposid then showed the highest cytotoxic potency with SLE of 3.32 L/μmol assuming a fraction unbound (f_u) of 21% (SLE: 0.698 L/μmol for total etoposide), followed by carboplatin with SLC being 2.85 L/μmol. The higher f_u for etoposide was considered more likely as it was reported for cancer patients receiving high-dose (35 - 60 mg/kg) etoposide[95] and was therefore used for calculation and comparison of the SL for unbound etoposide. Thiotepa was the drug with the least influence on cell proliferation and survival with a slope of 0.014 L/μmol for unbound (f_u: 20%) and 0.011 L/μmol for total drug concentrations.

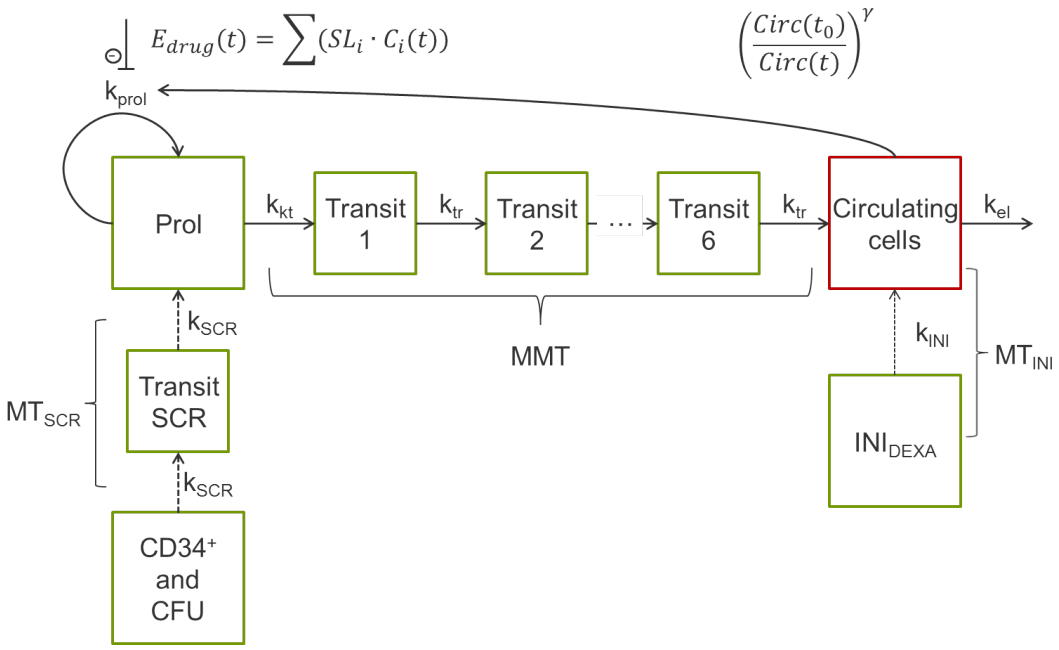

Figure 3.23 Schematic structural model for the final PK/PD model for the description of leukopenia in a high-dose chemotherapy regimen. Prol: Compartment of proliferating cells; Circ(t_0): leukocyte concentrations before start of high-dose chemotherapy; Circ(t): leukocyte concentration at time t; γ: exponent of the feedback acting on the proliferation rate constant k_{prol}; k_{tr}: transition rate constant; k_{el}: elimination rate constant; MMT: Mean maturation time; MT_{SCR}: mean stem cell rescue time; INI_{DEXA}: compartment for the description of the initial increase in leukocyte concentrations; MT_{INI}: mean time for the initial increase; $E_{drug}(t)$: drug effect; SL_i and $C_i(t)$: slope and concentration of drug *i*.

System-specific parameters describing leukopoiesis/leukopenia following HDCT The final model for the description of leukopenia in the setting of the HDCT regimen including an ASCR as well as the administration of DEXA is depicted in Figure 3.23. The baseline, i.e. the leukocyte concentration before the start of the therapy was estimated with the B1 method described in section 2.4.2.2. Its estimate of $4.00 \cdot 10^9$ cells/L reflected the observed median of the population ($3.97 \cdot 10^9$ cells/L) and showed an interindividual variability of 26% CV. Directly after the first drug administration an increase in leukocyte concentrations was observed which is possibly related to the administration of DEXA and was best described by initiating an additional compartment 'INI_{DEXA}' once at the time of the first DEXA administration with an estimated amount of cells (C_{INI}). C_{INI} was $18.5 \cdot 10^9$ cells/L with an interindividual variability of 94.8% CV. The mean time it took for the cells to migrate from INI_{DEXA} to the compartment of circulating cells (MT_{INI}) was 44.3 h (almost 2 d).
The steep decrease in leukocyte concentrations caused by the administration of the cytotoxic drugs was best described by a chain of 6 transit compartments. The transition rates between those compartments, k_{tr}, was calculated from the estimated MMT which was 93.6 h (4 d) with a variability of 15% CV.
Integration of the ASCR performed on day 7 was realised as a retransfusion of all $CD34^+$ cells into the SCR compartment from where the cells entered the compartment of proliferating cells through a transit compartment, describing the migration of retransfused cells to the bone marrow. Again, the mean time it took the cells to pass through the transit compartment was estimated resulting in a MT_{SCR} of 8.83 h which was fixed in the final model to improve model stability. The interindividual variability for this parameter was substantial and estimated to be 175% CV. Transition rate constants of the ASCR (k_{SCR}) were calculated as $(n)/MT_{SCR}$ with n being the number of transitions of the ASCR.
Physiological regulation mechanisms of leukopoiesis were described by a single feedback acting on the proliferation rate constant k_{prol} of the cells in the bone marrow. The feedback exponent γ was 0.115 with an interindividual variability of 27.9% CV. Residual variability was implemented with an additive residual variability model for the ln-transformed data which corresponds approximately to a proportional residual variability model on the original scale. No significant covariate relation could be determined and therefore the final model was equal to the base model. Table 3.7 summarises the PD parameter estimates of the final PK/PD model for the description of leukopenia following HDCT.

Table 3.7 Population PK/PD parameter estimates for the final PK/PD model for the description of leukopenia in a high-dose chemotherapy setting

Parameter	Unit	Estimate	RSE, %
Fixed-effects parameters			
$Circ(t_0)$	[10^9 cells/L]	4.00	9.10
MMT	[h]	93.6	4.80
γ		0.115	7.10
SLC	[L/μmol]	2.85	19.3
SLE	[L/μmol]	0.698	24.6
SLE (unbound)	[L/μmol]	3.32-17.5	(f_u: 21%-4%)
SLT	[L/μmol]	0.011 (0.014)	28.8
SLT (unbound)	[L/μmol]	0.012-0.016	(f_u: 90%-10%)
C_{INI}	[10^9 cells/L]	18.5	40.1
MT_{INI}	[h]	44.3	11.5
MT_{SCR}	[h]	8.83 FIX	
Interindividual variability			
$\omega Circ(t_0)$	[% CV]	26.0	38.0
ωMMT	[% CV]	15.1	38.1
$\omega\gamma$	[% CV]	27.9	31.7
ωC_{INI}	[% CV]	94.8	29.9
ωMT_{SCR}	[% CV]	174	30.3
Residual variability			
σ proportional	[%]	53.1	7.00

$Circ(t_0)$: leukocyte concentration before start of therapy

MMT: mean maturation time; γ: exponent of the feedback; f_u: fraction unbound

SLC, SLE, SLT: slope factor of carboplatin, etoposide and thiotepa, respectively

C_{INI}: amount of cells describing initial increase; MT_{INI}: mean time decribing the initial increase

MT_{SCR}: mean stem cell rescue time..

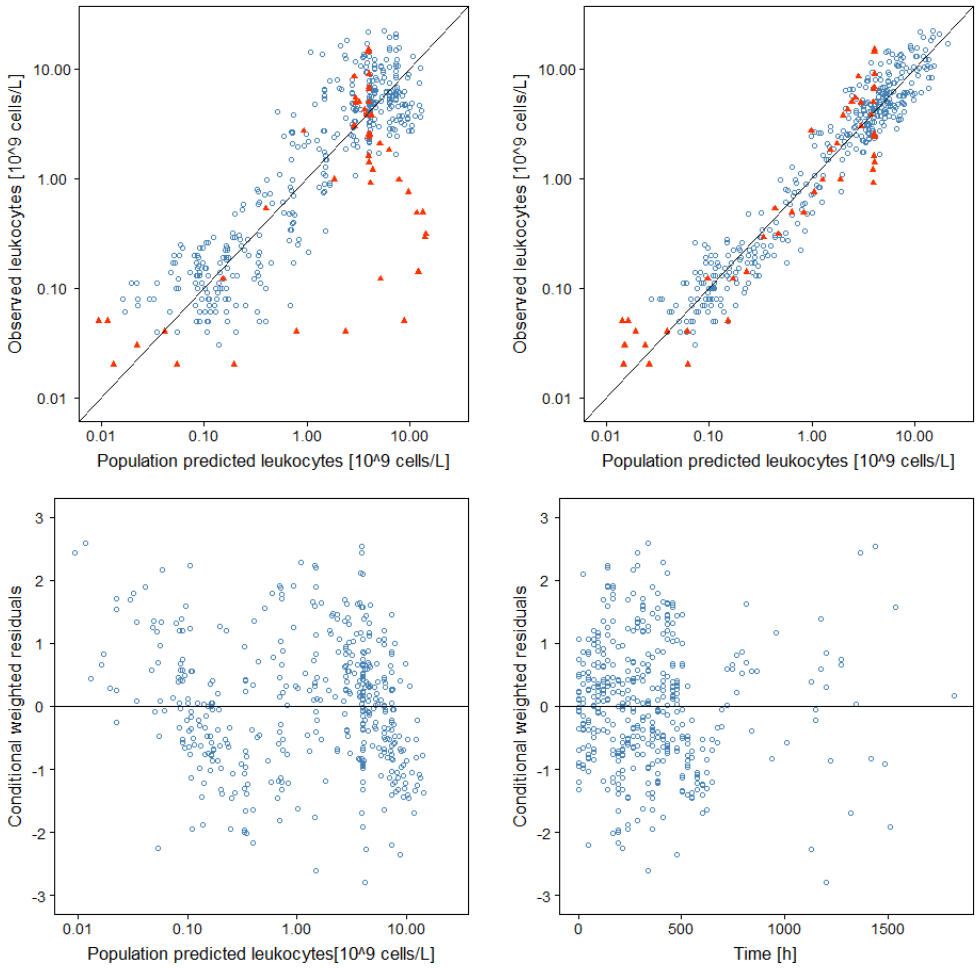

Figure 3.24 Goodness of fit plots for the final PK/PD model for the description of leukopenia following high-dose chemotherapy: observed versus population predicted leukocyte concentrations (top, left), observed versus individual predicted leukocyte concentrations (top, right), conditional weighted residuals versus predicted leukocyte concentrations (bottom, left) and versus time (bottom, right).

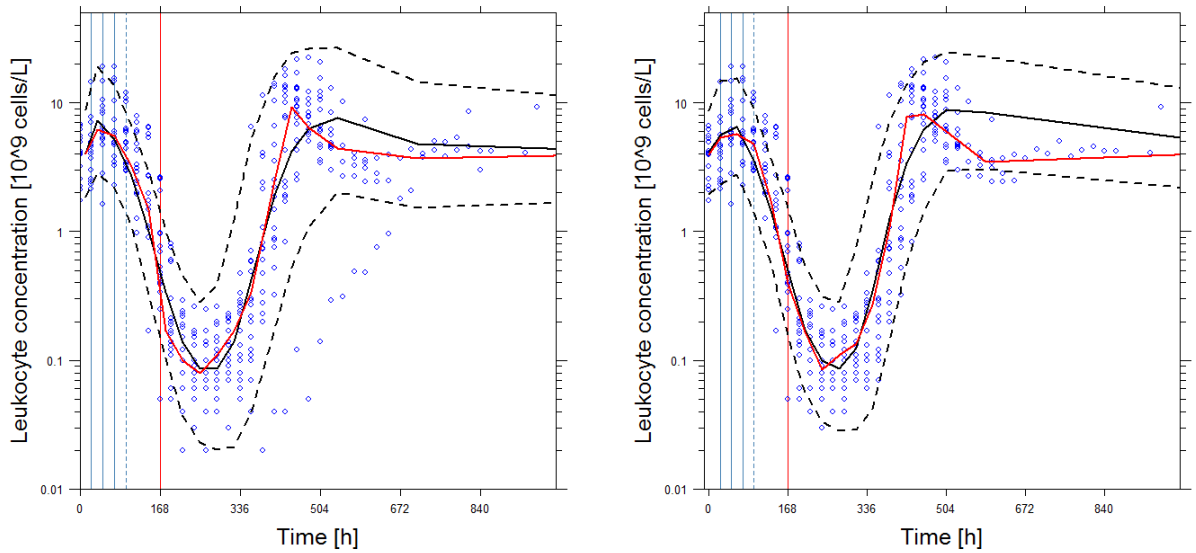

Figure 3.25 Visual predictive check for the final PK/PD model for the description of leukopenia following high-dose chemotherapy (left) and for a model excluding the one patient not receiving granulocyte colony-stimulating factor (ID 7) in the dataset. Blue circles represent the measured leukocyte concentrations. Solid and dashed lines represent the median, 10^{th} and 90^{th} percentile of the measured leukocyte concentrations (red) and the simulations (black). Vertical solid blue lines: days of drug administration (D1, D2, D3), vertical dashed blue line: etoposide administration on D4, vertical red line: day of the ASCR (D7)

3.3.9 Evaluation

The goodness of fit plots (Figure 3.24) showed a good description of the data by the final PK/PD model and reveal no model misspecification. Only the population predictions for the patient with a deviating leukocyte-time course who did not receive G-CSF (ID 7, red triangles) showed an overprediction of small concentrations which was corrected after inclusion of variability components, demonstrated by the plot depicting individual predicted versus observed leukocyte concentrations. The observed leukocyte concentrations spread randomly and uniformly around the line of identity and the zero reference line in the observed versus (individual) predicted concentration plots and the CWRES plots, respectively. The predictive performance of the model was assessed by a VPC (Figure 3.25, left) which demonstrated the appropriateness of the prediction of the central tendency throughout the whole time course by revealing only minor deviations of the simulated (black) from the observed (red) median of leukocyte concentrations. Small deviations of the simulated median from the median of the

observed leukocyte concentrations were observable for the high concentrations at late time points, i.e. the rebound described by the implemented feedback mechanism, which were slightly underpredicted. However, from a therapeutic point of few concentrations at time of the rebound are not as relevant as the adequate description of the decline in, nadir and recovery of leukocyte concentrations. The variability in the observed data was very well predicted before the nadir was reached, illustrated by the 90% prediction interval of the simulations. After nadir concentrations a slight overprediction of the variability by the model could be observed. For binning of the observations a user user-defined number of 17 bins was selected, although a median of 24 samples were available for each patient. This was chosen in order to obtain bins with comparable amount of included data points as especially during later observation time points less data was available.

3.3.10 Outlier

One patient (ID 7) showed a deviation in the leukocyte-time profile in comparison to the rest of the population (Figure 3.5, red triangles). Exclusion of this patient did not lead to a considerable change in parameter estimates and their precision. Only the IIV on γ was influenced by the exclusion and was estimated lower with 14.2% compared to 27.9% in the final model as well as the residual error which was 49.7% (RSE: 5.0%) instead of 53.1% (RSE: 7.0%). Comparison of a VPC from the model excluding the patient with the VPC of the final model showed that parts of the overprediction of the variability after the nadir was reached can be attributed to the IIV in γ as the 80% prediction interval was narrower for the VPC excluding the patient (Figure 3.25, right). As it was possible to describe the leukopenic time course for this patient without influencing the estimation of the model parameters in general the patient was not excluded from the final model.
For another patient (ID 19) twice the amount of $CD34^+$ cells, compared to the highest amount of retransfused cells reported for the rest of the investigated population, was retransfused ($1.1 \cdot 10^9$ versus $0.6 \cdot 10^9$ cells) and compared to the highest amount of $CD34^+$ cells reported to be retransfused in other studies[53,57]. Exclusion of this patient resulted in a reduction of the IIV for MT_{SCR} from 175% CV to 125% CV. All other parameters were not affected by the exclusion of this patient except for C_{INI} which was estimated to be $12.1 \cdot 10^9$ cells/L (RSE: 52.1%, range: 2.09-45.8 $\cdot 10^9$ cells/L) instead of $18.5 \cdot 10^9$ cells/L (RSE: 40.2%, range: 2.93-60.8 $\cdot 10^9$ cells/L) in the final model. With respect to the range of C_{INI} the exclusion of patient 19 was not considered influential for this parameter. No obvious mistake in the documentation for

the retransfused cells could be found and as neither the parameter values nor their precision was affected by exclusion of patient 19 the data remained in the dataset.

3.4 Project 3: Assessing the optimal day for an autologuos stem cell rescue

The influence of the ACSR on the time course of leukopenia during HDCT was investigated by means of simulations. First, the influence of the day of the ASCR was assessed by deterministic simulations (section 2.5.2). Then, the amount of retransfused cells was taken into account. In order to propose the optimal day for the ASCR the IIV and the residual error were included to evaluate the findings from the deterministic simulations with regard to the variability in the population (stochastic simulations, section 3.4.2).

3.4.1 Deterministic simulations

Deterministic simulations for a typical patient receiving median doses of carboplatin, etoposide and thiotepa and the median amount ($0.2329 \cdot 10^9$) of retransfused $CD34^+$ cells were conducted to illustrate the influence of the day (D5 - D11) on which the ASCR was performed (Figure 3.26). The drugs were administered on three (carboplatin, thiotepa) and four (etoposide) consecutive days starting on day one, as described in the original study protocol. For the first administration of dexamethasone, and hence the initialisation of INI_{DEXA} with C_{INI}, day one of the HDCT was assumed for the simulations.
The simulations revealed increasing nadir concentrations for the performance of an ASCR on D5 of HDCT ($0.007 \cdot 10^9$ cells/L) to D7 ($0.093 \cdot 10^9$ cells/L) which were then decreasing for an ASCR performed on D8 ($0.075 \cdot 10^9$ cells/L) to D11 ($0.019 \cdot 10^9$ cells/L). Duration of grade 3 leukopenia was shortened for an ASCR from D5 (12.1 d) to D9 (8.14 d) and then was prolonged again for an ASCR on D10 (8.44 d) and D11 (9.02 d). A summary of the resulting nadir concentrations, time to nadir and the duration of grade 3 leukopenia for the deterministic simulations is given in Table 3.8.
The next step comprised the investigation of the influence of the amount of retransfused cells (minimal, median and maximal amount of cells transfused in the population) and the day of the ASCR (D6 - D10) on nadir concentrations and the duration of grade 3 leukopenia (Figure 3.27). For the amount of $0.072 \cdot 10^9$ cells (minimum amount) nadir concentrations for the ASCR on D8 were the highest compared to the performance of the ASCR on all other days. In contrast, for the median and maximal amount of retransfused cells ($0.2329 \cdot 10^9$ and 0.5698

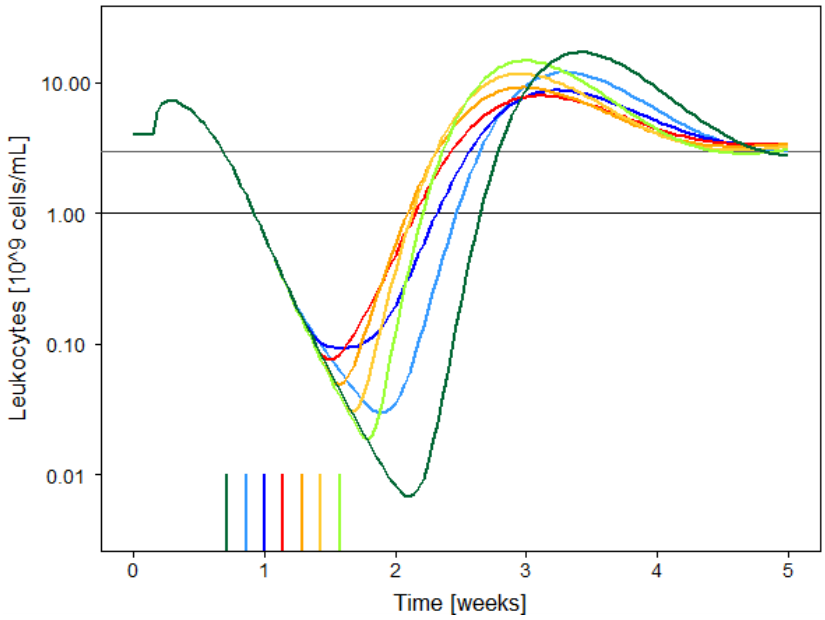

Figure 3.26 Impact of the day on which the autologuous stem cell rescue (ASCR) was performed on the time course of leukopenia for a typical patient receiving the median amounts of carboplatin, etoposide and thiotepa and the retransfusion of populations' median of $0.2327 \cdot 10^9$ $CD34^+$ cells. INI_{DEXA} was initialised with the typical amount of C_{INI} on the first day of HDCT. Deterministic simulations included an ASCR performed on day 5 (darkgreen), 6 (lightblue), 7 (darkblue), 8 (red), 9 (orange), 10 (yellow) and 11 (lightgreen). Vertical lines represent respective day of ASCR. Grey and black horizontal line: lower limit of leukopenia grade 1 and 3.

Table 3.8 Summary of the resulting nadir concentrations, time of nadir and the duration of grade 3 leukopenia from the deterministic simulation of a typical patient receiving the median amount of carboplatin, etoposide and thiotepa and an amount of $0.2329 \cdot 10^9$ $CD34^+$ cells on day 5 - 11. INI_{DEXA} was initialised with the typical amount of C_{INI} on the first day of HDCT

Day of ASCR	Nadir [10^9 cells/L]	Time of nadir [h (d)] ([d])	Duration of grade 3 leukopenia [h (d)]
5	0.007	353.7 (14.7)	290.0 (12.1)
6	0.030	318.3 (13.3)	259.5 (10.8)
7	0.093	264.9 (11.0)	233.6 (9.73)
8	0.075	251.7 (10.5)	206.5 (8.60)
9	0.049	264.1 (11.0)	195.4 (8.14)
10	0.030	281.0 (11.7)	202.5 (8.44)
11	0.019	300.2 (12.5)	216.4 (9.02)

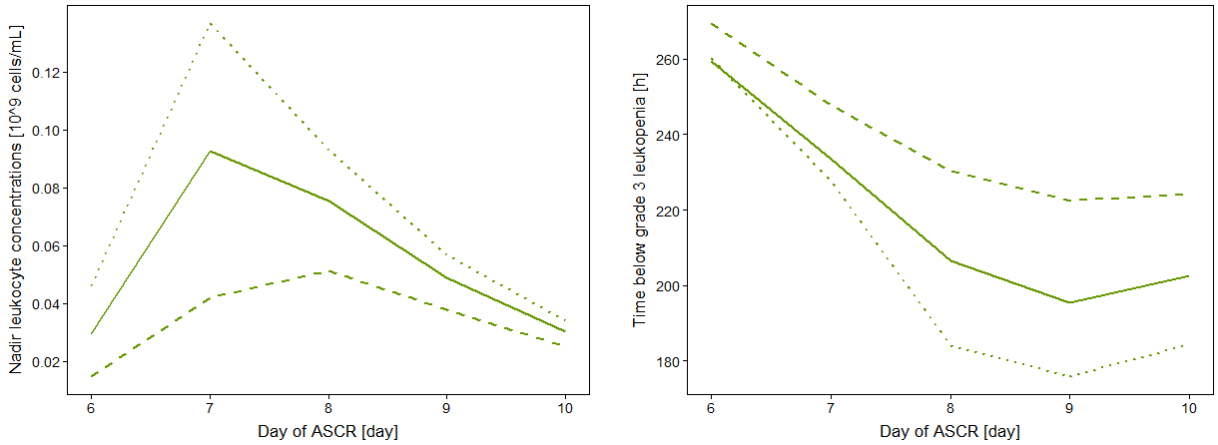

Figure 3.27 Impact of the day (day 6 - day 10) for the performance of an autologuous stem cell rescue (ASCR) on nadir concentrations (left) and the duration of grade 3 leukopenia (right). Simulations were performed for a typical patient receiving the median amount of carboplatin, etoposide and thiotepa and the populations' median of $0.2329 \cdot 10^9$ $CD34^+$ cells. INI_{DEXA} was initialised with the typical amount of C_{INI} on the first day of HDCT. Dashed, solid and doted green lines: minimal, median and maximum amount of retransfused $CD34^4$ cells, respectively.

$\cdot 10^9$ cells), the ASCR on D7 resulted in the highest nadir concentrations. With regard to the duration of grade 3 leukopenia the optimal day for the ASCR was D9, showing the shortest duration of grade 3 leukopenia. Regarding nadir concentrations and duration of grade 3 leukopenia further simulations were conducted to assess to assess the optimal day for the performance on the ASCR and the amount of cells for which no difference for the performance of the ASCR on D7 and D8 could be observed (section 3.4.2).

3.4.2 Stochastic simulations

To gain a more detailed understanding for the influence of the amount of retransfused $CD34^+$ cells on the time course of leukopenia simulations were carried out for a retransfused amount of cells of 0.072, 0.1, 0.15, 0.2, 0.2329, 0.3, 0.4, 0.5, $0.5698 \cdot 10^9$ $CD34^+$ cells and the ASCR taking place on D6 - D10 of HDCT. The nadir concentrations (Figure 3.28) and the duration of grade 3 leukopenia (Figure 3.29) were evaluated in dependency on the amount of retransfused cells and the day on which the ASCR was performed. Box-and-Whisker plots illustrate the immense variability in nadir concentrations and the durations of grade 3 leukopenia for n=1000 simulations which is also shown by the rather large 80% prediction interval given by the 10^{th} and 90^{th} percentile of the observations in Table 3.9 and 3.10. The lower and upper whisker are

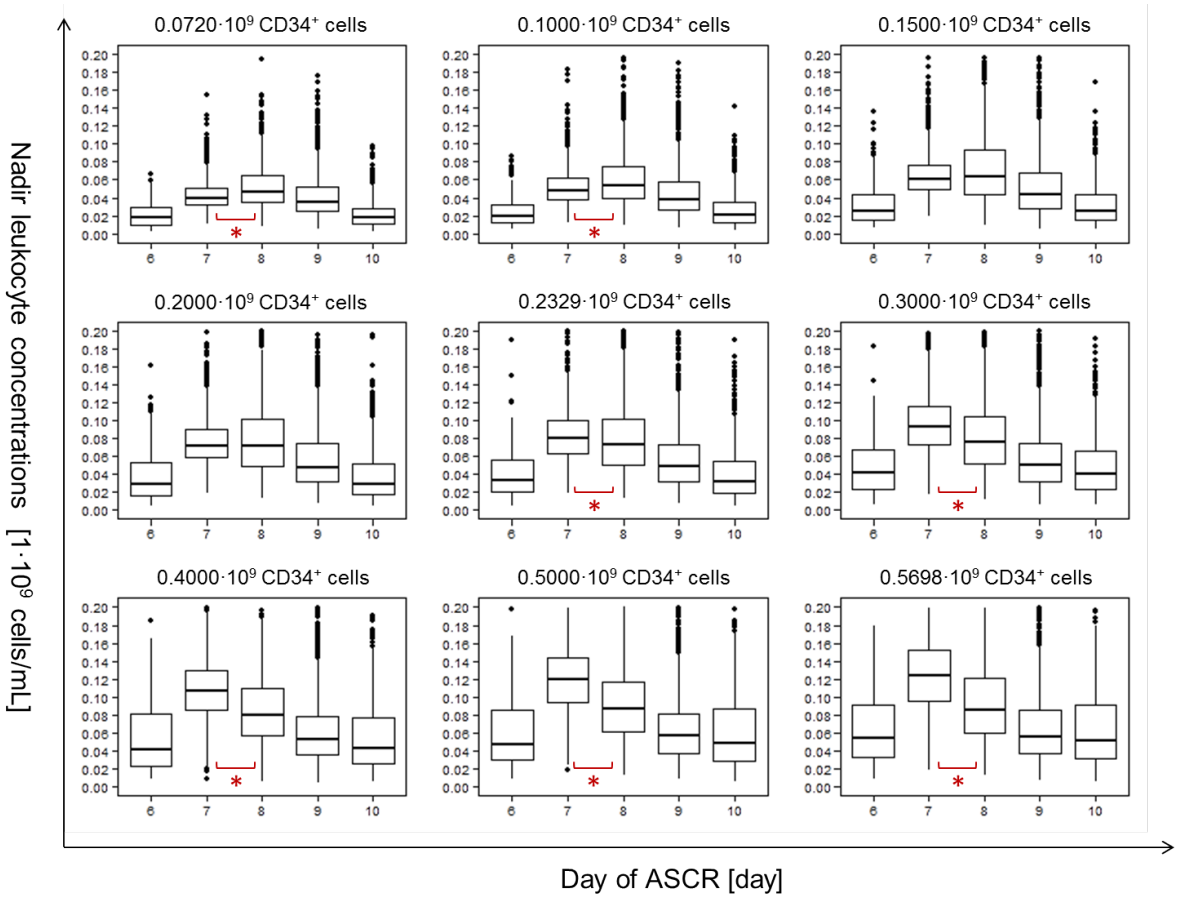

Figure 3.28 Stochastic simulation for a typical patient receiving median doses of carboplatin, etoposide and thiotepa. INI_{DEXA} was initialised with the typical amount of C_{INI} on the first day of HDCT. Box-and-whisker plots depict median (solid line), 50% prediction interval (box) and $\pm$ 1.5 times the interquartile range (whiskers) of the simulated nadir concentrations for the retransfused amount of $CD34^+$ cells versus the day on which the ASCR was performed (D6 - D10). Black circles indicate simulated data points outside $\pm$ 1.5 times the interquartile range. "*" indicates statistically significant difference in mean cell concentrations between D7 and D8.

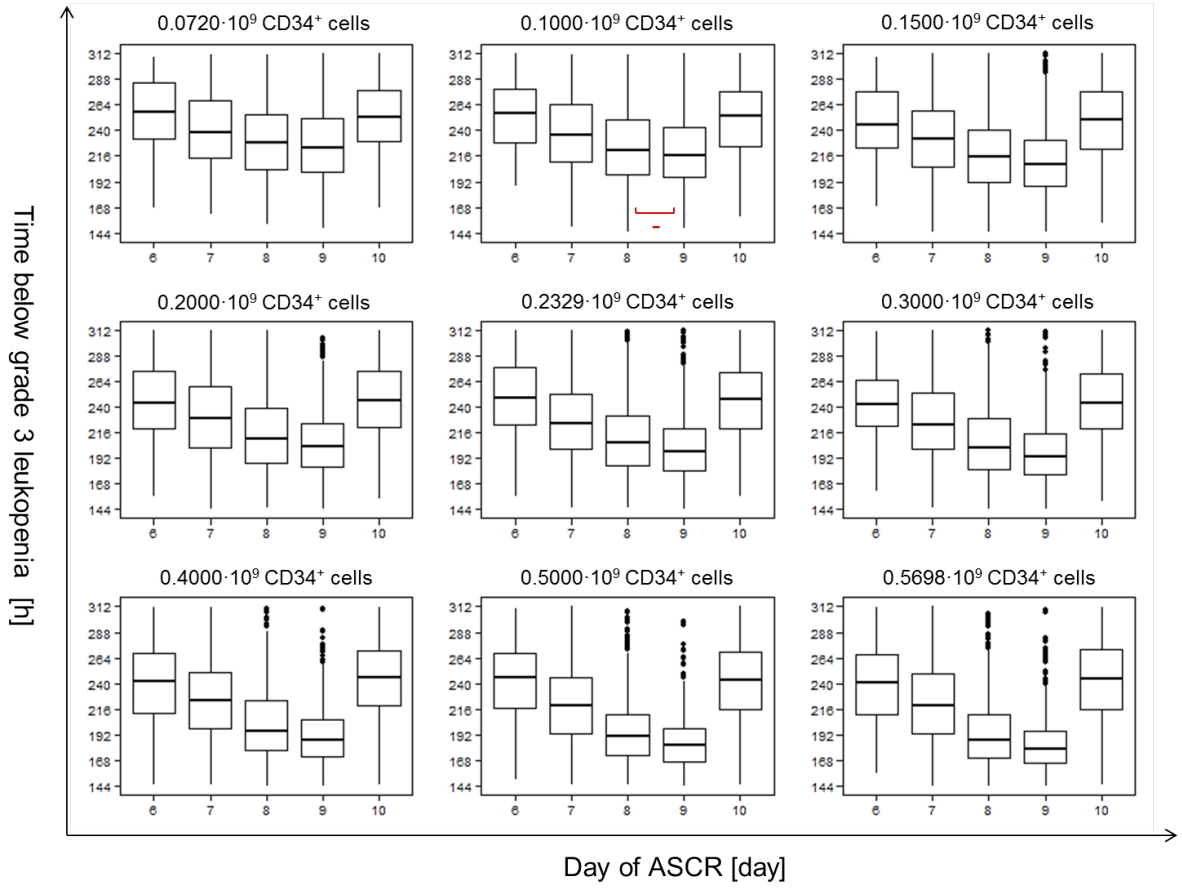

Figure 3.29 Stochastic simulation for a typical patient receiving median doses of carboplatin, etoposide and thiotepa. INI_{DEXA} was initialised with the typical amount of C_{INI} on the first day of HDCT. Box-and-whisker plots depict median (solid line), 50% prediction interval (box) and $\pm$ 1.5 times the interquartile range (whiskers) of the simulated time below grade 3 leukopenia for the retransfused amount of $CD34^+$ cells versus the day on which the ASCR was performed (D6 - D10). Black circles indicate simulated data points outside $\pm$ 1.5 times times the interquartile range. "-" indicates a difference in time below grade 3 leukopenia that is not statistically significant.

Table 3.9 Distribution of relevant nadir concentrations in dependency of the amount of retransfused $CD34^+$ cells and the day of the performance of the autologuous stem cell rescue (ASCR) resulting from stochastic simulations

Number of retransfused cells	Day of ASCR	Nadir concentrations		
		10^{th} percentile	Median	90^{th} percentile
$[10^9]$		$[10^9$ cells/L]		
0.072	7	0.026	0.039	0.064
	8	0.025	0.047	0.089
0.10	7	0.032	0.048	0.078
	8	0.028	0.054	0.104
0.20	7	0.050	0.072	0.116
	8	0.036	0.072	0.142
0.2329	7	0.051	0.081	0.125
	8	0.034	0.075	0.157
0.5698	7	0.072	0.130	0.197
	8	0.043	0.094	0.198

$\pm$ 1.5 times the interquartile range, the lower and upper hinge the 25^{th} and 75^{th} percentile of the simulations and the median is depicted as the vertical black line. Black circles illustrate the simulated data outside $\pm$ 1.5 times the interquartile range. A Mann-Whitney-Wilcoxon test (p=0.05, section 2.5.2) was performed to determine whether the difference in nadir concentrations and the duration of grade 3 leukopenia were statistically significant between the original day on which the ASCR was performed (D7) compared to the best day resulting from the simulations.

Nadir Table 3.9 summarises the results for the 1000 simulations that were performed for each scenario. ASCR on D7 resulted in higher nadir concentrations than ASCR on D8 for more than $0.2329 \cdot 10^9$ $CD34^+$ retransfused cells whereas for less than $0.2329 \cdot 10^9$ $CD34^+$ cells an ASCR performed on D8 resulted in highest nadir concentrations compared to all other days. Nadir concentrations for an ASCR on D6, D9 and D10 were below the ones reported for an ASCR on D7 (day from original study protocol) and D8 for all amounts of retransfused $CD34^+$ cells and were therefore not considered during the analysis for the duration of grade 3 leukopenia (see next paragraph "Duration of grade 3 leukopenia"). The difference between the means of nadir concentration for an ASCR on D8 and D7 was statistically significant (p=0.05) for $\leq 0.1 \cdot$

Table 3.10 Distribution of the relevant durations of grade 3 leukopenia in dependency of the amount of retransfused $CD34^+$ cells and the day of the performance of the autologuous stem cell rescue (ASCR) resulting from stochastic simulations

Number cells $[10^9]$	Day of ASCR	10^{th} percentile	Median [h]	90^{th} percentile
0.072	7	199.7	249.9	348.1
	8	188.3	234.0	322.0
0.2329	7	182.9	229.9	315.0
	8	168.2	208.6	282.4
0.5698	7	172.1	221.0	290.3
	8	152.9	186.2	242.4

10^9 retransfused $CD34^+$ cells with nadir concentrations on D8 being higher than on D7 (median D8: $0.054 \cdot 10^9$/L, median D7: $0.048 \cdot 10^9$/L). For retransfused amounts of $CD34^+$ cells from 0.15 - 0.2 $\cdot 10^9$ there was no statistically significant difference in nadir concentrations. Although nadir concentrations for an ASCR on D7 were statistically significant higher compared to ASCR on D8 for an amount of retransfused $CD34^+$ cells $\geq 0.2329 \cdot 10^9$ the difference was negligible when taking the range into account. When 0.2327 and $0.5698 \cdot 10^9$ $CD34^+$ cells were retransfused median nadir concentrations ranged between 0.08 (0.05-0.11) - 0.13 (0.07-0.20) for an ASCR on D7 compared to 0.08 (0.03-0.16) - 0.09 (0.04-0.20) on D8. Overall, D8 was the best day for the performance of an ASCR when no difference in the amount of retransfused cells was made.

Duration of grade 3 leukopenia The higher the amount of retransfused $CD34^+$ cells the shorter was the duration of grade 3 leukopenia (Table 3.10). An ASCR performed on D9 resulted in the shortest duration of grade 3 leukopnia for all investigated amounts of retransfused cells (Figure 3.29). For an ASCR on D9 the duration of grade 3 leukopenia was shortened by 15.9 (range: 11.4 - 26.1) h for retransfusion of $0.072 \cdot 10^9$ $CD34^+$ cells up to a shortening of 34.8 (19.2 - 47.9) h for $0.5698 \cdot 10^9$ cells compared to an ASCR on D7. However, as nadir concentrations were below the ones of the original day for the performance of the ASCR (D7) D9 was not considered superior to D7 and D8.

In summary, for an amount of $CD34^+$ retransfused cells below $0.2329 \cdot 10^9$, D8 for the ASCR performs best with regard to nadir concentrations. Additionally the duration grade 3 leukope-

nia was shortened by 15.9 (11.4-26.1) h - 21.1 (12.5-30.4) h for 0.072 - 0.02 $\cdot$ 10^9 $CD34^+$ cells, respectively. For an amount of retransfused $CD34^+$ cells $\geq$ 0.2329 nadir concentrations for an ASCR on D7 were statistically significant higher compared to an ASCR performed on D8, but with regard to the range of nadir concentrations on both days, the difference was negligible. Comparing the median duration of grade 3 of leukopenia from D7 and D8, it was shortened on D8 by 21.3 (14.7-32.6) h - 34.8 (19.2-49.9) h for 0.2329 - 0.5698 $\cdot$ 10^9 retransfused $CD34^+$ cells, respectively. Hence, for the investigated regimen D8 of HDCT shows the overall best performance as the day for the ASCR with regard to nadir concentrations and duration of grade 3 leukopenia.

3.5 Project 4: Characterisation of the cytotoxic potency of chemotherapeutics

Semi-mechanistic models are able to characterise the underlying physiological processes of a system and to distinguish drug-specific parameters from those specific to the system. In the next section the drug-specific parameter which characterises the sensitivity of the proliferating cells in the bone marrow towards the cytotoxic compounds is more closely investigated. The first part of the following section deals with different PD modelling approaches for the estimation of EC_{50} values from *in vitro* cytotoxicity assays (section 1.5.2 and 2.6.1). In the second part a model is proposed which allows (i) the prediction of EC_{50} values from clinical data by a population PK/PD model and (ii) the exploration of the possible use of *in vitro* EC_{50} values for the prediction of the myelosuppresive time course following chemotherapy, by comparing the model predicted to *in vitro* EC_{50} values from literature.

3.5.1 Assessing the cytotoxic potency from *in vitro* data

In a first step different PD models were implemented in NONMEM® and compared with respect to their ability to describe the *in vitro* data, as described in section 2.6.1.3. A corresponding model from the *drc* package in R was chosen and the resulting parameter estimates were compared with those obtained during the NONMEM® analysis.

3.5.1.1 Data

The measured absorption values for each plate were transformed in R into % survival index (SI) as described in section 2.6.1.2. Figure 3.30 depicts a plot of the geometric means of the %

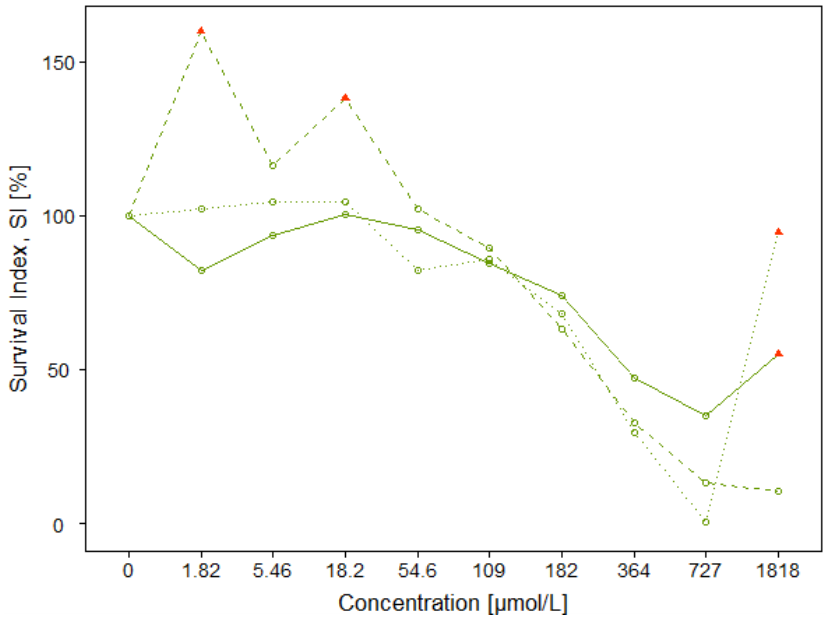

Figure 3.30 Percent survival index (geometric mean of n=8) of the peripheral blood mononuclear cells versus drug concentration for the three plates: plate 1 (solid line), plate 2 (dashed line) and plate 3 (dotted line).

SI after exclusion of the outliers for all plates. Additionally, data points marked in red were excluded from analysis during the modelling process (section 3.5.1.5).

3.5.1.2 Analysis in NONMEM®

The analysis was subdivided in two parts: (i) a population analysis of the three plates during which the PD model with the best description of the data was determined and (ii) the analysis of each plate individually based on the chosen PD model for the comparison with the analysis in R. The % SI was best described fitting the sigmoidal inhibitory E_{max} model (OFV: 135.4, Equation 2.32), followed by the Richards' model (OFV: 155.4, Equation 2.33) and the inhibitory E_{max} model (OFV: 166.4, Equation 2.25). Parameter estimates for the sigmoidal E_{max} model and the Richards' model (section 2.6.1.3) were comparable but the precision of parameter estimates was higher for the sigmoidal E_{max} model. The asymmetry factor (ASSY) of the Richards model was 1.2 with a high RSE of 108.3%. For ASSY close to 1 the Richards' model converts to a sigmoidal E_{max} model which was the case in the present analysis. Hence, the sigmoidal E_{max} model was chosen as the final model. During the population analysis of the

three plates it was not possible to estimate an IIV (or in this case an interplate variability) for any of the parameters.

3.5.1.3 Analysis in R

Within the *drc* package, the LL.4 function (Equation 2.34) describes a sigmoidal E_{max} model. First, data from all plates was analysed with the model simultaneously. In a second step, the model was fit to each plate individually to assess differences in the parameter estimates between the plates. For the simultaneous analysis the precision of parameter estimates was high except for the precision of EC_{50} which was estimated to be 248.3 μmol/L with a RSE of 34.6%. The maximal effect E_{max} was 99.8% SI which reflects survival of all cells at low drug concentrations as observed in the data. The Hill factor, h, which was estimated with 2.08 (RSE: 0.5%) indicated a concentration-effect relation which was steeper than for a simple E_{max} model. E_0 was 7.85 % SI (RSE: 7.9%) and characterised the remaining cell survival. Overall, the model showed a good fit of the data with a residual error of 8.91% SI. Resulting parameter estimates from the fit of the model to the individual plates showed similar estimates for E_{max} and h varying from 97.96% to 101.78 % SI and 1.46 - 2.18, respectively. For plate 1 and 2 E_0 was 28.8% SI and 9.0% SI and the E_{50} values were 232.6 and 204.8 μmol/L, respectively. For plate 3 the E_0 resulted in negative values of -37.8% SI and a higher E_{50} value (366.8 μmol/L). This was due to the geometric mean for the highest drug concentration included in the analysis for this plate which was very low (0.53% SI) but still in the linear part of the concentration-response curve. Therefore the lower "plateau" of the effect-concentration curve, reflecting E_0, was below zero. Compared to the overall precision of parameter estimation for the analysis in R both parameters were estimated with (very) high RSE of 42.6% and 178%. The overall fit for each plate was good with the additive residual variability ranging between 3.1% and 6.4 % SI.

3.5.1.4 Comparison of the data analysis in R and NONMEM®

For the comparison of the parameter estimates obtained in R and NONMEM® the sigmoidal E_{max} model implemented in NONMEM® was recoded to resemble the LL.4 model of the *drc* package (Equation 2.34). This means the parameter E_0 which estimates the effect size for cells not affected by drug disposition, i.e. the remaining cell survival at high drug concentrations, was introduced to the model. The parameter estimates for the simultaneous analysis of the plates in R and NONMEM® were comparable (Table 3.11). Precision of parameter estimates was higher for the analysis in R, especially for E_0 with an RSE of 7.9% compared

Table 3.11 Parameter estimates from the simultaneous fit of the three plates in R and NONMEM® applying a sigmoidal E_{max} model with correction for remaining surviving cells

		R	NONMEM®
Parameter	Unit	Estimate (RSE,%)	Estimate (RSE,%)
E_{max}		99.8 (2.7)	99.8 (2.7)
E_0		7.85 (7.9)	7.79 (72)
E_{50}	[μmol/L]	248.25 (35)	248 (8.5)
Hill factor		2.08 (0.5)	2.08 (3.9)
Residual variability	[μmol/L]	8.91 (NA)	8.3 (7.9)

RSE: relative standard error; E_{max}: maximal effect

E_0: effect size for cells not affected by drug disposition

EC_{50}: concentration at half maximal effect.

to an RSE of 71.9% in NONMEM®. The EC_{50} value on the other hand was estimated with higher precision in NONMEM® (RSE: 8.5% versus 34.6% in R). Parameter estimates from the individual fit of each plate for both approaches were comparable. Figure 3.31 depicts the resulting concentration-effect profiles from the individual fits in NONMEM® showing the good description of the data especially for drug concentrations higher than 55 μM. RSEs for the analysis in NONMEM® were estimated to be $< 1 \cdot 10^{-3}$ and are therefore not reported in Table 3.12 which summarises the parameter estimates for the individual analysis of all plates for both approaches. The low RSEs were most probably due to the fact, that during the individual analysis of each plate the uncertainty of the parameter estimates were attributed to the residual variability.

3.5.1.5 Outlier

Although outliers in the raw data were identified with the Grubbs test (section 2.6.1.2) and removed prior to data processing four of the calculated geometric means were excluded during analysis (Figure 3.30, red dots). The two geometric means (54.8% SI and 94.5% SI) related to the highest drug concentration (1818 μmol/L) were excluded due to implausibility as they were more than two times higher as the % SI of the next lower drug concentration (727 μmol/L). The other two excluded values reflected a SI of 138% and 160% at concentrations of 18.2μmol/L and 1.81μmol/L, respectively, which were very high in comparison to the other % SI for the same drug concentration (around 100% SI) and indicated a (implausible) cell

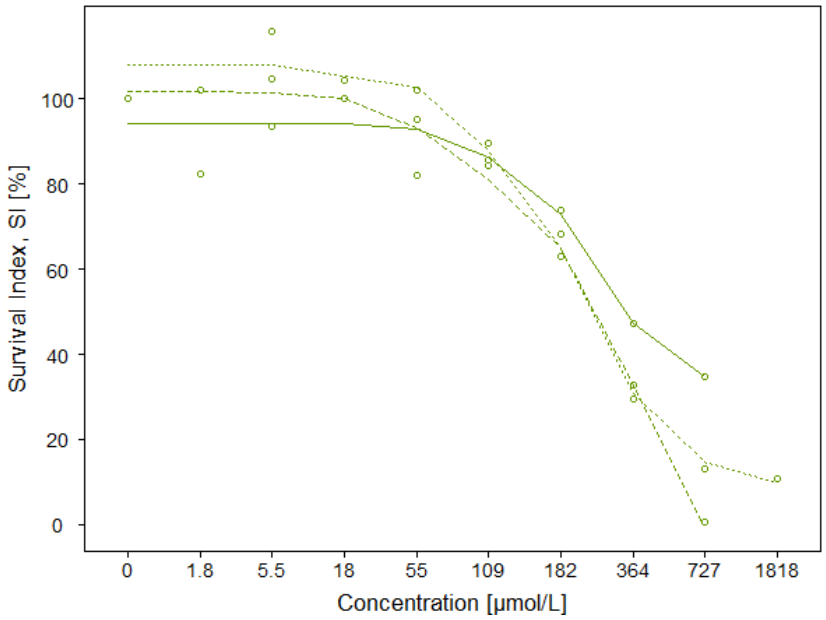

Figure 3.31 Resulting % survival index versus concentration profiles for the individual fit of each plate in NONMEM®. Dots: percent survival index (geometric mean of n=8) of the peripheral blood mononuclear cells. Plate 1 (solid line), plate 2 (dashed line) and plate 3 (dotted line).

Table 3.12 Parameter estimates from the individual fits for each of the three plates in R and NONMEM® using a sigmoidal E_{max} model with correction for remaining surviving cells

		Plate 1		Plate 2		Plate 3	
		Estimate (RSE,%)		Estimate (RSE,%)		Estimate (RSE,%)	
Parameter	Unit	R	NM	R	NM	R	NM
E_{max}		98.0 (1.7)	94.4	108 (3.9)	108	102 (3.6)	102
E_0		28.8 (6.3)	31.1	9.01 (5.7)	9.01	-37.8 (42.6)	-43.1 (0.1)
E_{50}	[μmol/L]	233 (30.6)	238	205 (24.1)	205	367 (178)	389
Hill factor		2.11 (0.4)	2.5	2.18 (0.5)	2.18	1.46 (0.5)	1.4
Residual variability	[μmol/L]	3.08 (NA)	4.98	5.96 (NA)	4.22	6.39 (NA)	4.76

RSE: relative standard error; E_{max}: maximal effect; E_0: effect size for cells not affected by drug disposition

EC_{50}: concentration at half maximal effect; NM: NONMEM®; NA: not available.

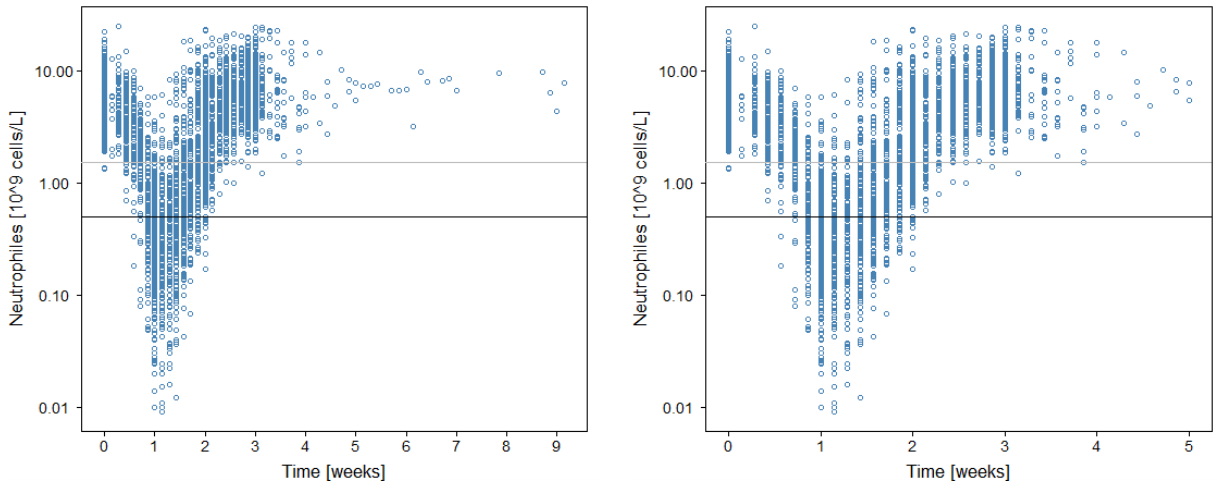

Figure 3.32 Neutrophil concentrations[129,138,219] in the circulation versus time on a semi-logarithmic scale. Left panel: complete observation period. Right panel: first five weeks. Grey and black horizontal line: lower limit of grade 1 and 3 neutropenia, respectively.

growth. Inclusion of these points resulted in a residual error of 21.5% SI compared to 8.91% SI during analysis in R. EC_{50} and E_0 were most influenced by the exclusion and were estimated with 159.4 μmol/L and 33.5% SI. This was comprehensible as especially the two outliers at the highest drug concentration influence the estimation of these parameters.

3.5.2 Comparing *in vitro* measures of cytotoxicity with estimates from a population PK/PD analysis of clinical data

The following section focuses on the proposal of a model for the estimation of EC_{50} values from clinical data with a reparametrised model for myelosuppression that are comparable to EC_{50} values obtained from analysis of *in vitro* assays.

3.5.3 Data

To assess the predictive performance of the proposed, reparametrised model the model was fit to the docetaxel dataset described in section 2.6.2.2. This study was chosen to easily separate the drug- from the system-specific parameters of the semi-mechanistic model, as docetaxel was administered as monotherapy and, hence, a possibly confounding drug-drug interaction was excluded. Figure 3.32 depicts neutrophil concentration-time courses in cancer patients following docetaxel administration. Overall, the variability of the extent of neutropenia was

high with nadir concentrations reflecting all grades of neutropenia (grade 1-4)[130]. Neutrophil concentrations covered a wide range from 0.005 to $34.00 \cdot 10^9$ cells/L and were ln-transformed for analysis to support model stability. In total, 637 patients were subject to analysis and n=3.55 (range: 1 - 26) neutrophil measurements were available per patient[129]. Individual, model-predicted concentrations for docetaxel from a previous population PK analysis[219] were included in the dataset following a sequential modelling approach.

3.5.3.1 Model development

For the estimation of an EC_{50} value describing the sensitivity of the cells in the bone marrow towards cytotoxic drugs which was comparable with an EC_{50} value from *in vitro* assays, the model for myelosuppression was modified (see section 2.6.2.1). For this purpose the model was reparametrised to take the conditions of an "*in vitro* E_{max} model" into account, i.e. a maximal drug effect of 100%. This enabled the comparison of the model estimated EC_{50} value from clinical data to the *in vitro* assay signal which reflects reduction in % survival index. A new rate constant, k_{kill}, which allowed for cell loss from the compartment of proliferating cells was introduced (Figure 2.5). The drug effect was then implemented as an E_{max} model (E_{max}=1, equal to a maximal drug effect of 100%) with an inhibitory effect on k_{prol} (cytostatic drug effect) and a stimulatory effect on k_{kill} (cytotoxic drug effect). The ordinary differential equation implemented for the compartment of proliferating cells (Prol) is given by Equation 3.1

$$\frac{dProl}{dt} = k_{prol} \cdot Prol \cdot (1 - E_{drug}(t)) \cdot FB - (k_{tr} + k_{kill} \cdot (1 + E_{drug}(t))) \cdot Prol \qquad (3.1)$$

where k_{prol} is the proliferation rate constant of the cells in the bone marrow, $E_{drug}(t)$ is the drug effect of docetaxel ($E_{drug}(t) = (E_{max} \cdot C(t))/(C(t) + EC50)$ with $E_{max} = 1$, EC_{50} is the concentration C at half maximal effect, FB is the feedback mechanism and k_{tr} is the transition rate constant. k_{kill}, the rate constant responsible for the cell loss from Prol, was defined by the initial conditions for the system of ordinary differential equations before start of the therapy, where the system is in equilibrium and no change in Prol is observed, hence, $k_{kill} = k_{prol} - k_{tr}$. Parameter estimates of the new, reparametrised model and parameter estimates from a fit to the original model by Kloft et al.[129] are given in Table 3.13. Comparing the two models all parameter estimates, including covariate effects on Circ(t_0) and the estimated IIV, were similar and of same precision, except for the MMT which was slightly shorter for the reparametrised model with 79.3 h instead of 84.1 h. The covariate effect of AAG (α_1-acid glycoproteine) on SL in the original model was not implemented in the E_{max} model. This was decided due to the desired comparability with *in vitro* data where covariates like protein content in the assay

medium are usually not taken into account. The exponent γ of the feedback acting on k_{prol} was half the size as in the original model, but as k_{prol} was estimated differently in both models the estimates cannot be compared directly. In the original model k_{prol} was set equal to k_{tr} whereas in the reparameterised model k_{prol} was estimated and had to be higher by definition as a cell loss from the same compartment was implemented by introduction of k_{kill}. The high IIV of EC_{50} of 113.6% CV reflects the high variation in the extent of neutropenia in the population which was originally explained, in parts, by AAG as a covariate for SL. The proportional residual variability was of equal magnitude for both models.

3.5.3.2 Model evaluation

The GOF plots for both models were comparable and demonstrated a good description of the data by the two models. The observed neutrophil concentrations spread randomly and uniformly around the line of identity and the zero reference line for the observed versus (individual) predicted neutrophil concentrations and the CWRES versus time plots, respectively (Figure 3.33). For some observed neutrophil concentrations (top left corner) the plots depicting the observed versus predicted concentrations revealed concentrations that were underpredicted by the model. However, in comparison to the total number of concentration measurements those few concentrations are negligible.

The VPCs for both models showed a good predictive performance of the models as there was no major deviation of the median of observed and simulated neutrophil concentrations (red and black solid line) and the variability was well predicted by the 90% prediction interval of the simulated profiles (black dashed lines) which contained about 90% of the observed neutrophil concentration measurements (Figure 3.34). Only the 5^{th} percentile of the VPC for the reparametrised model showed a slight overprediction of the nadir concentrations in comparison to the VPC from the original model. This might be due to the fact, that the covariate influence which was implemented for the SL of docetaxel was not taken into account in the reparametrised model. For binning, a user-defined time array was provided which was given by the following time intervals: 0, 48, 71, 96, 120, 144, 168, 192, 216, 240, 264, 288, 312, 336, 360, 384, 408, 432, 456, 480, 504, 528, 1536 h. The array was selected to obtain a rather smooth time profile for the observed and simulated percentiles whilst providing a comparable amount of data in each bin.

The EC_{50} value predicted by the reparametrised model was 11.14 nM $\pm$ 2.7 nM (RSE: 24.1%) compared to the *in vitro* EC_{50} value of 12.4 nM $\pm$ 1.8 nM which was published by deGraaff et al.[251] in 1999. This exemplarily demonstrates that the new, reparametrised proposed model

Table 3.13 Population PD parameter estimates for the original (left) and the reparametrised (right) model for the description of neutropenia following docetaxel treatment

Parameter	Unit	Original model Estimate (RSE, %)	Reparametrised model Estimate (RSE, %)
Fixed-effects parameters			
Circ(t_0)	[10^9 cells/L]	5.33 (5.9)	5.16 (4.0)
for AAG $\leq$ 1.34		0.176 (73)	0.189 (45)
for AAG $>$ 1.34		0.495 (19)	0.594 (15)
SEX		-0.121 (-25)	-0.126 (25)
Performance status		0.131 (31)	0.116 (28)
Previous Chemotherapy		-0.148 (-19)	-0.142 (20)
MMT	[h]	84.1 (1.1)	79.3 (0.9)
γ		0.145 (1.6)	0.079 (6.0)
SL / EC_{50}	[L/μmol]/[nM]	15.6 (2.0)	11.1 (24)
AAG		-0.344 (-5.3)	
k_{prol}	[1/h]	0.048*	0.097 (6.3)
Random-effects parameters			
$\omega$$Circ_0$	[% CV]	25.2 (5.7)	23.3 (7.1)
ωMMT	[% CV]	14.0 (4.0)	16.2 (5.6)
$\omega\gamma$	[% CV]	14.8 (9.4)	20.7 (6.2)
ωSL / EC_{50}	[% CV]	35.9 (4.5)	113.6 (6.3)
Residual variability			
σproportional	[%]	42.4 (3.5)	42.3 (4.0)

*calculated as 4/MMT. RSE: relative standard error; Circ(t_0): neutrophil concentration before start of therapy

AAG: α_1-acid glycoproteine; MMT: mean maturation time; SL: slope

EC_{50}: concentration at half maximal effect; k_{prol}: proliferation rate constant.

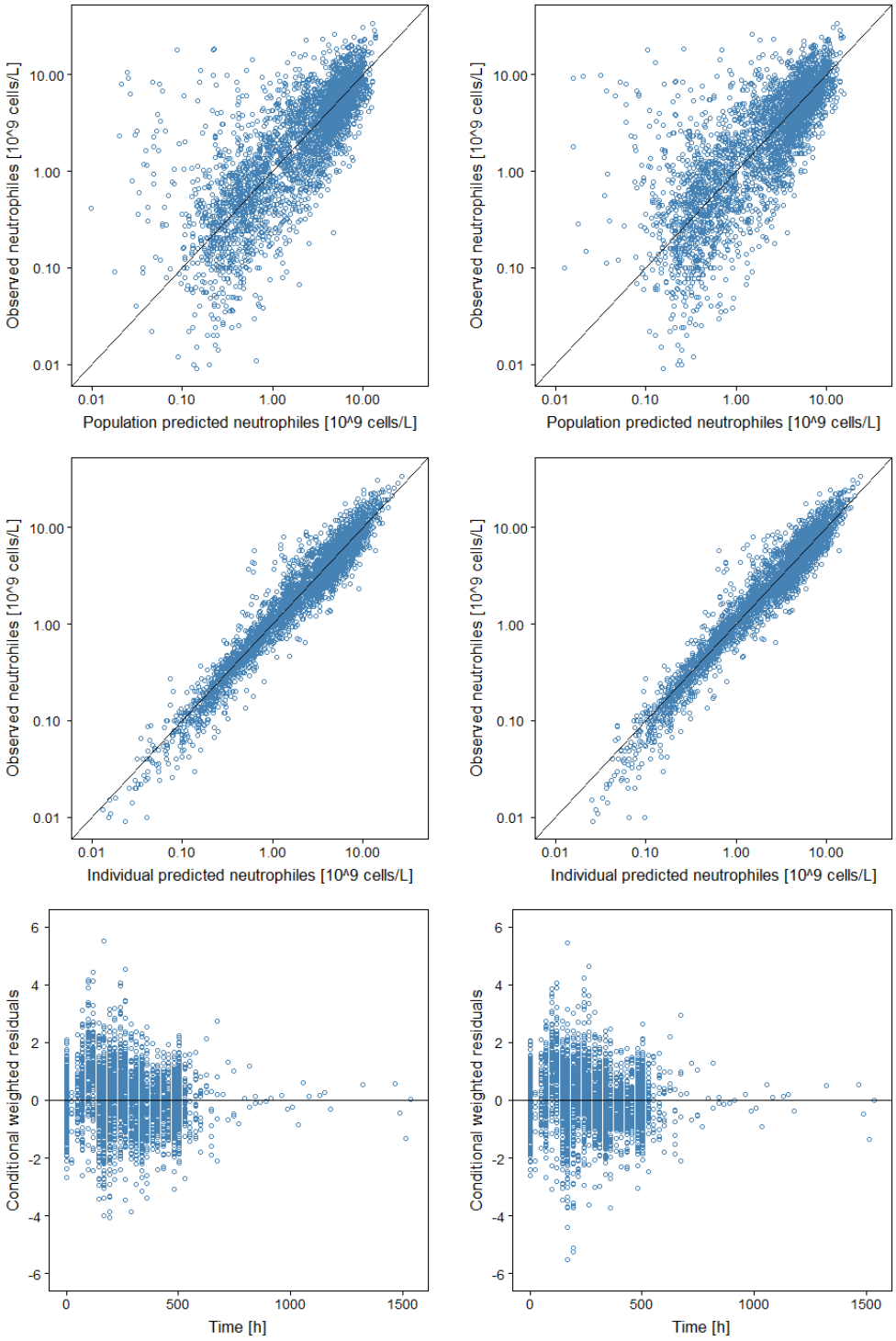

Figure 3.33 Goodness of fit plots for the original (left) and the reparametrised (right) PK/PD model for myelosuppression: observed versus population predicted (top) and versus individual predicted (middle) neutrophil concentrations, respectively, conditional weighted residuals versus time (bottom).

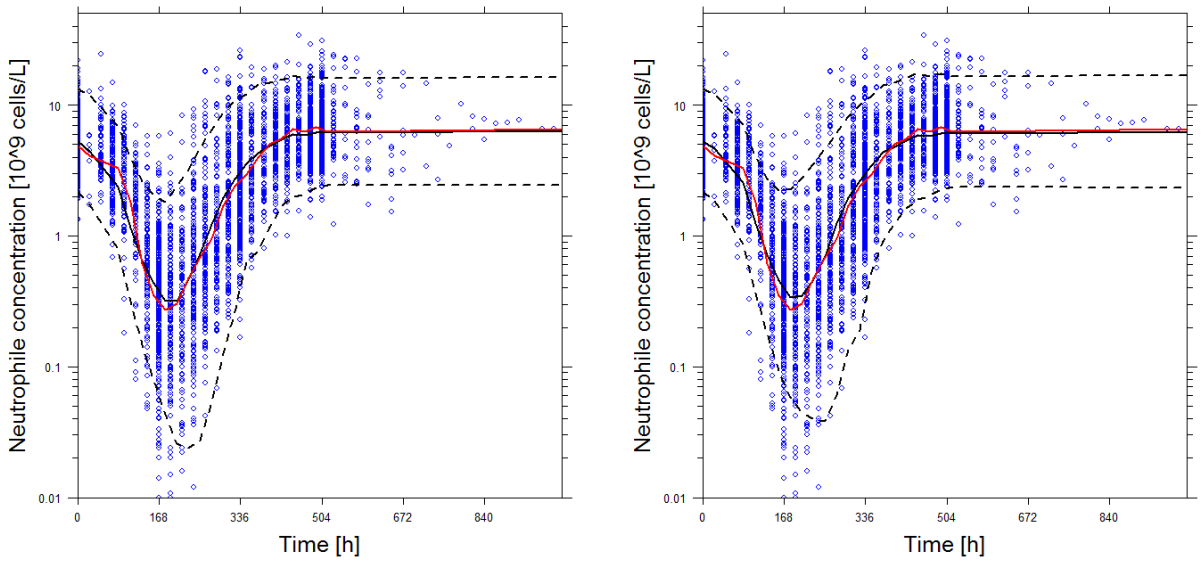

Figure 3.34 Visual predictive check for the original (left) and re-parametrised (right) PK/PD model for neutropenia. Blue circles represent the measured neutrophil concentrations. Black solid, dashed lines represent the median, 5^{th} and 95^{th} percentile of the simulated and the solid red line the median of the observed neutrophil concentrations.

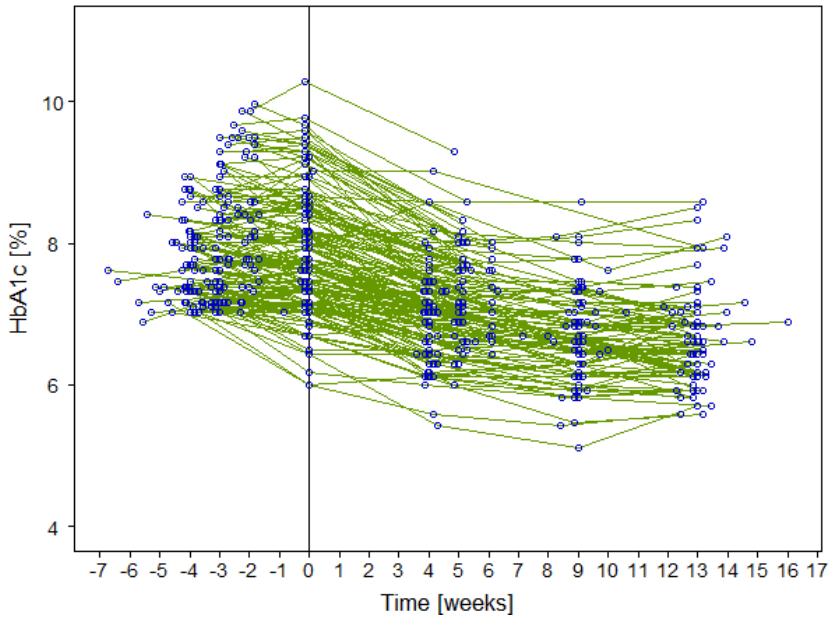

Figure 3.35 HbA_{1c} measurements (blue points) versus time. Vertical line: start of therapy. Green solid lines: HbA_{1c} values over time for the individual patients.

was able to predict EC_{50} values from clinical data which were comparable to those obtained from *in vitro* assays, such as the CFU-GM assay.

3.6 Project 5: Investigation of glycation processes throughout the lifespan of erythrocytes

3.6.1 Study characteristics

From the two studies 162 patients were included in the analysis. The study characteristics and covariates that were included in the PK analysis of lixisenatide are shown in Table 2.1. Figure 3.35 shows the course of HbA_{1c} values during the observation period of the study. Before the start of therapy the median HbA_{1c} was 7.77% (5^{th} - 95^{th} percentile: 6.97% - 9.23%), reflecting the inclusion criteria of the study ($HbA_{1c} \geq 7\%$).

3.6.1.1 Dataset

The dataset was built in R by merging information on individual lixisenatide PK parameter estimates, individual PD parameter estimates for the description of FPG and information on

HbA_{1c} measurements. Individual parameter estimates for the PK of lixisenatide[253] and the PD of FPG[252] were obtained from previous analysis. The dosing history of lixisenatide was taken from the dataset the PD model for FPG was based on.

3.6.1.2 Model development

In accordance with the model development procedure described in section 2.7.2 the HbA_{1c} data was first analysed with the model developed by Hamrén et al.[186] which describes the reduction of HbA_{1c} in dependency of FPG. In a next step, the model was extended to additionally take the influence of lixisenatide on postprandial glucose (PPG) concentrations into account.

3.6.1.3 Lifespan model

Implementation of IIV for the model parameters was investigated starting with a model including IIV for all parameters. The variance ω^2 for MRTE and K_{GL} was excluded as it was estimated $< 1 \cdot 10^{-5}$ and exclusion of the two parameters did not result in significant change in OFV. The interindividual variability for K_{INH} could not be estimated, i.e. the estimated parameter value never differed from the initial value provided in the NONMEM® control file. The OFV and the parameter estimates for the other parameters did not change whether the initial value for ω^2 of K_{INH} was varied or when ω^2 for K_{INH} was excluded. Hence, only the IIV of γ was kept in the final model. Table 3.14 summarises the parameter estimates for the lifespan model and the extended lifespan model presented in section 3.6.2.1. K_{INH} was fixed to its estimated value of 1.16 g/L/d due to model stability and to obtain a successful covariance step. Estimation for MRTE was not possible as the estimate either did not change from the provided initial estimate or was implausibly high (250 d) or low (30 d). Therefore, and to enable a direct parameter comparison of this model with the extended lifespan model (section 3.6.2.1), MRTE was fixed to 101 d which was estimated with the extended lifespan model. K_{GL} was estimated with high precision (RSE: 0.67%) and was $3.01 \cdot 10^{-4}$ 1/(d·mM). The exponent γ linking FPG to K_{GL} was 0.67 (RSE: 9.66%) with a high interindividual variability of 100% CV.

3.6.2 Model evaluation

Goodness of fit plots indicated an overall sufficient description of the data by the model (Figure 3.36, left). The plot of the observed HbA_{1c} values versus the model-predicted values

Table 3.14 Population PD parameter estimates for the lifespan model and the extended lifespan model for the description of HbA_{1c} values

		Lifspan model		Extended lifespan model	
Parameter	Unit	Estimate	RSE,%	Estimate	RSE,%
Fixed-effects parameters					
K_{INH}	[g/L/d]	1.16 FIX		1.10	2.98
MRTE	[d]	101 FIX		101 FIX	
K_{GL}	[1/(d·mM)]	$3.01 \cdot 10^{-4}$	0.67	$1.22 \cdot 10^{-4}$	0.25
γ		0.67	9.66	0.75 FIX	
K_{GL2}	[1/d]			$6.74 \cdot 10^{-4}$	0.30
EC_{50}	[ng/L]			62.8	3.07
Random-effects parameters					
$\omega\gamma$	[% CV]	100	15.2*	33.0	15.6*
ωEC_{50}	[% CV]			108	21.5*
Residual variability					
σproportional	[% CV]	105	5.04*	4.09	1.95*

*relative standard error of ω on the corresponding variance scale.

RSE: relative standard error; K_{INH}: release rate of erythrocytes from the bone marrow

MRTE: mean residence time erythrocytes; $K_{GL/GL2}$: glycation rate constants

γ: exponent of the fasting plasma glucose dependent glycation pathway

EC_{50}: concentration of the half maximal effect for the inhibition of the second glycation pathway

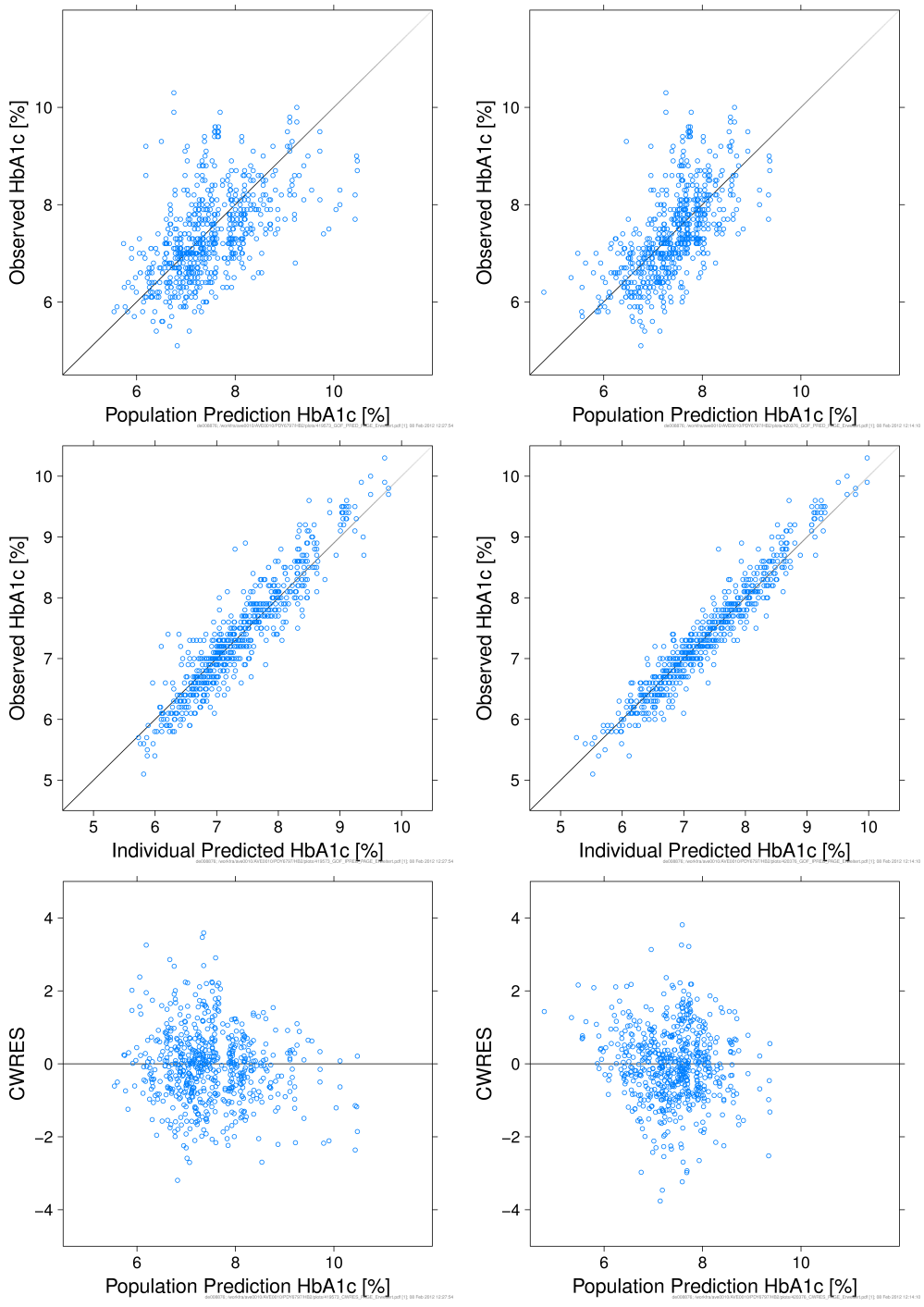

Figure 3.36 Goodness of fit plots for the lifespan (left) and the extended lifespan (right) model. Observed versus population predicted HbA_{1c} values (top), observed versus individual predicted HbA_{1c} values (middle), conditional weighted residuals (CWRES) versus population predictions (bottom).

showed a random and uniform distribution of the values around the line of identity without revealing a trend. CWRES versus population predicted HbA_{1c} values demonstrated a uniform spread around the zero reference line with a slight trend for high HbA_{1c} values being overpredicted by the model. The high residual variability of 105 % CV cannot be explained as all parameters were estimated with high precision, ranging from 0.67% (K_{GL}) to 9.66% (γ) and GOF plots suggest an overall sufficient description of the data. The general trend of a decrease in HbA_{1c} during the observed study period was predicted by the model, but it failed to describe the extent of the decrease in some patients. The top panel of Figure 3.37 depicts (individual) predictions and the measured HbA_{1c} values for two patients (7605u0004 and 1205u005), demonstrating the insufficient description of the decline in HbA_{1c} values under therapy by the lifespan model.

3.6.2.1 Extended lifespan model

In contrast to tesaglitazar, a $PPAR_{\alpha,\gamma}$ agonist the lifespan model was originally developed for, lixisenatide not only decreases FPG but also shows short-term effects such as the reduction of PPG concentrations due to increased insulin secretion and delaying of gastric emptying. To account for this additional mode of action the lifespan model was extended by a glycation pathway describing Hb glycation possibly related to PPG. The glycation process of the additional pathway was characterised by another gylcation rate constant, K_{GL2}, which was linked directly to lixisenatide concentrations. This enabled the estimation of the effect of lixisenatide on the inhibition of the additional glycation process that was taking place and was most probably due to PPG without the need for data describing the of decline in PPG. The extended lifespan model is depicted in Figure 3.38 including the new glycation pathway (blue).
Lixisenatide concentrations were directly linked to K_{GL2} by an inhibitory E_{max} model. When E_{max} was allowed to take any value the OFV decreased by 26.4 points and E_{max} was 7.54, exceeding 1. Due to the implementation of the drug effect ($K_{GL2} \cdot (1 - E_{drug}(t))$, with $E_{drug}(t) = E_{max} \cdot C(t)/(C(t) + EC_{50})$), K_{GL2} became negative. To describe the overall decline in HbA_{1c} K_{GL} then was estimated to be higher than previously estimated with the lifespan model to compensate for the purportedly reduction in HbA_{1c} formation. The deglycation of Hb especially by the glycation rate constant that describes glycation due to PPG is physiologically implausible. Therefore E_{max} was fixed to 1 in the final model as the glycation can either take place (E_{max}=0) or be completely inhibited (E_{max}=1).
The final number of implemented transit compartments was four, as no significant change in the OFV with increasing/decreasing numbers of transit compartments was observed. Four

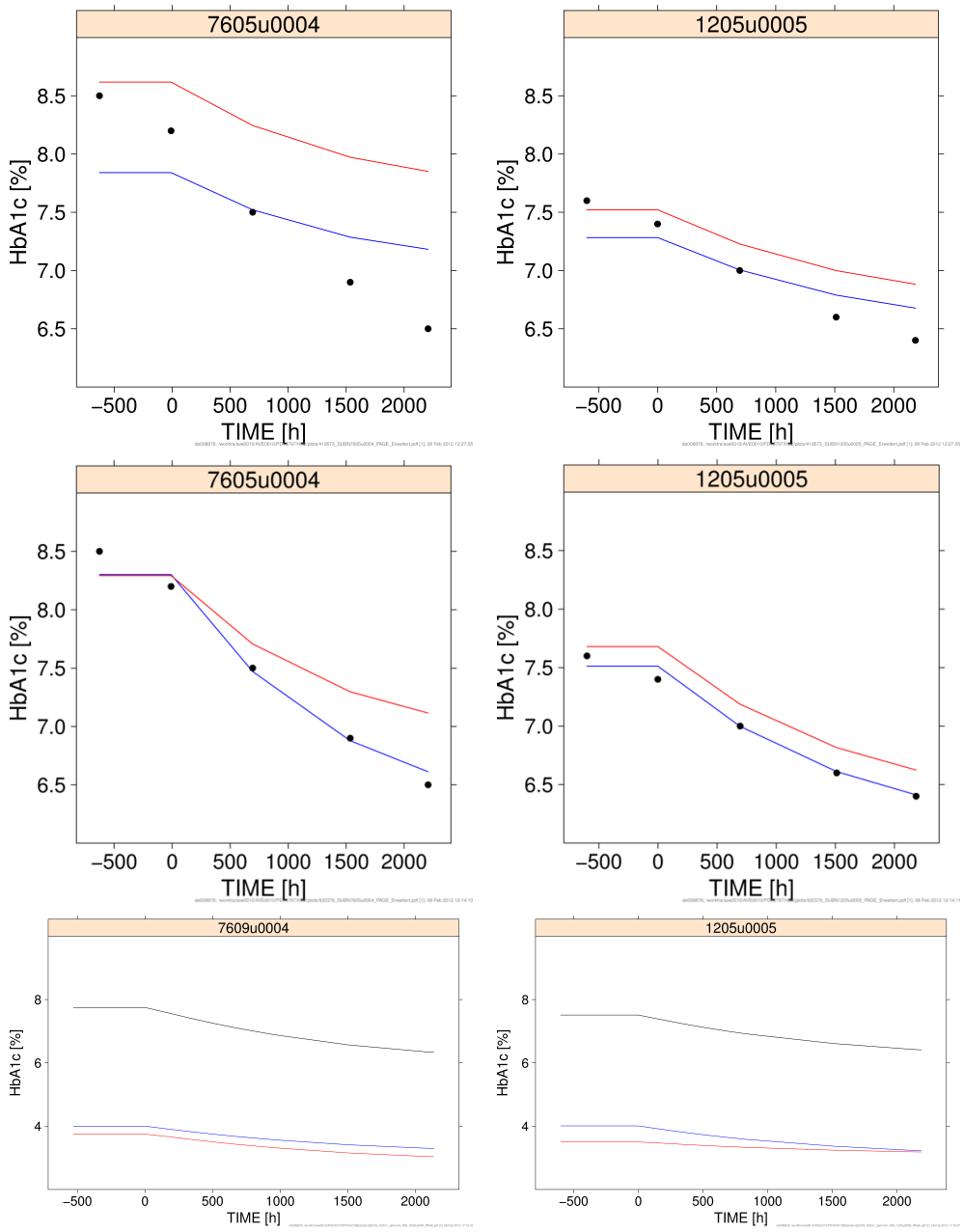

Figure 3.37 HbA_{1c} values versus time profiles of two individuals for the lifespan model (top) and the extended lifespan model (middle). Red line: population predictions, blue line: individual predicted time course, black dots: observed HbA_{1c} values. Bottom: contribution of fasting plasma glucose (blue line) and postprandial plasma glucose (red line) to the formation of total HbA_{1c} for the extended lifespan model.

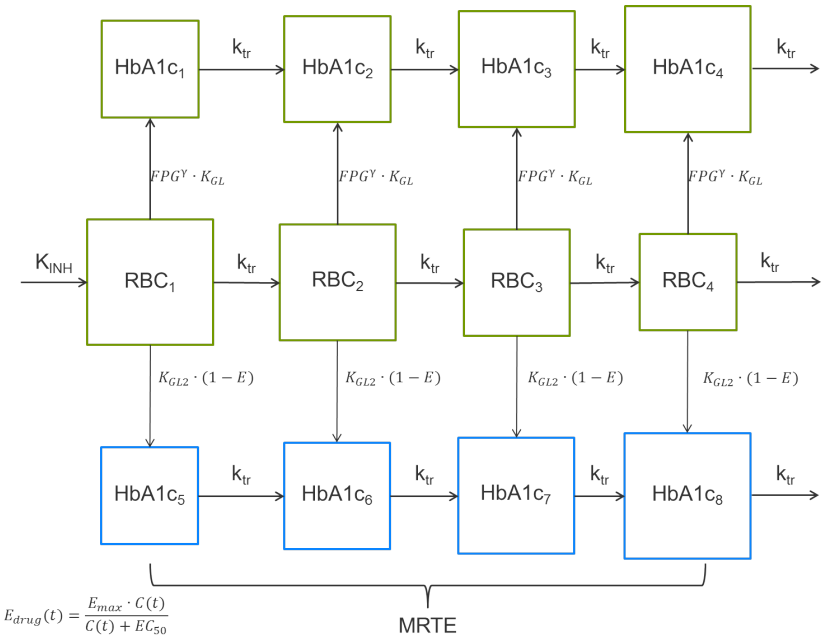

Figure 3.38 Schematic structure of the extended model for the description of HbA_{1c} (glycated haemoglobin) values. γ exponent of glycation process defined by fasting plasma glucose (FPG) and the glycation rate constant (K_{GL}); k_{tr}: transition rate constant; K_{INH}: release rate of red blood cells (RBC) from the bone marrow; $E_{drug}(t)$: drug effect on the second glycation process (blue) which is defined by K_{GL2} (glycation rate constant); C(t):drug concentration at time t; E_{max}: maximal effect; EC_{50}: concentration at half maximal effect.

compartments also corresponded to the number of transit compartments in the lifespan model in this thesis and the model published by Hamrén et al.[186] which simplified model comparison. It needs to be noted that it was not possible to investigate more than twelve transit compartments for the extended lifespan model due to the predefined maximal number of compartments in NONMEM® which was exceeded when 13 transit compartments were coded for. The data supported the estimation of two variance components: the IIV for γ and the EC_{50} value related to the second glycation pathway.
Parameter estimates for the final model are summarised in Table 3.14 (right). Due to model stability and to obtain a successful covariate step the MRTE was fixed to its estimated value of 101 d. A correlation between K_{GL} and γ was observed, but the estimation of the off-diagonal element of the Ω matrix was not supported by the data. Therefore it was decided to fix γ to its estimate of 0.75 as the estimation of K_{GL} was of special interest with regard to the evaluation of the impact of the two glycation pathways on HbA_{1c} formation. K_{INH} of the extended model was comparable to the one of the lifespan model being 1.10 g/L/d (RSE: 2.98%). The glycation rate constants K_{GL} and K_{GL2} characterising the glycation of Hb in dependency of FPG and possibly the glycation related to PPG were $1.22 \cdot 10^{-4}$ 1/(d·mM) and $6.74 \cdot 10^{-4}$ 1/d, respectively. The EC_{50} characterising K_{GL2} was 62.8 ng/L (RSE: 3.07%) and was highly variable with an IIV of 108% CV (RSE: 21.5%). Overall, the second glycation pathway which is possibly attributed to PPG, explained 50% (95% confidence interval: 43% - 59%) in the reduction of HbA_{1c} formation (Figure 3.37, bottom).

3.6.3 Model evaluation

The GOF plots depicted on the right hand side of Figure 3.36 showed a good description of the observed HbA_{1c} values by the model. No trend in either of the plots was observable and the measured HbA_{1c} values spread uniformly and randomly around the line of identity and the zero reference line for observed versus (individual) model-predicted HbA_{1c} values and CWRES versus model-predicted HbA_{1c} values, respectively. Precision of parameter estimates was high with the highest RSE being 10.8% for the IIV of EC_{50}. In addition to the GOF plots and precision of parameter estimates special attention was drawn to the shrinkage for the selection of the final extended lifespan model. It was decided to do so due to the observation that the more influence the FPG dependent glycation pathway was estimated to have the lower the OFV for the respective models was. Whereas in contrast to that the more influence was attributed to this pathway the higher the imprecision of parameter estimates was and, especially, the higher the shrinkage. Therefore the model was chosen as the final model which

showed a shrinkage below 30%[213] and reasonable precision of parameter estimates (RSE < 50%). Introduction of the second glycation pathway enabled the description of the time course of HbA_{1c} for all patients including the ones that had not been adequately described by the lifespan model (Figure 3.37, middle).

3.6.4 Model comparison

The extended lifespan model was superior compared to the lifespan model with regard to AIC (-2911.3 versus 2762.2), prediction of individual HbA_{1c} profiles and GOF plots which showed a narrower distribution around the line of identity for the observed versus model-predicted HbA_{1c} values. The residual variability was smaller for the extended lifespan model (4.09% CV compared to 105% CV for the lifespan model) and the value itself was much more plausible taking visual model evaluation tools (GOF plots and individual plots) into account. Additionally, it enabled the differentiation and the estimation of the contribution of the FPG dependent and possibly PPG dependent glycation of Hb. Hence, the extended model was chosen as the final model.

4 Discussion

The population PK/PD analyses presented in this thesis provided new insights into the system of leukopoiesis in the special setting of HDCT. The optimal day to perform an ASCR was investigated and compared to the day on which it had been performed in the original setting of the study. Furthermore, the PK of high-dose carboplatin, etoposide and thiotepa was characterised, their influence on the proliferation of the cells in the bone marrow was investigated and a model for the prediction of EC_{50} values from *in vitro* data was established. A reparametrised model for myelosuppression for the prediction of EC_{50} values from clinical data was established and the comparability to *in vitro* EC_{50} values was exemplified. In Project 5 the generated knowledge on the modelling of cell maturation was transferred to the therapeutic area of diabetes mellitus type 2 to describe the lifespan/cell ageing of erythrocytes and characterise the change of a long-term biomarker for the diabetic control (HbA_{1c}) during treatment with a new GLP-1 receptor agonist. In the following the results from each project will be discussed.

4.1 Project 1: Pharmacokinetic analysis of high-dose carboplatin, etoposide and thiotepa

The PK for the three drugs of the CET study regimen, carboplatin, etoposide and thiotepa, was successfully characterised and the predictive performance of the models was evaluated. This was of special importance as the individual PK parameters were used as input in the population PK/PD model for the description of leukopenia following HDCT. For the dose escalation in HDCT the performance of an ASCR and, potentially, G-CSF treatment is mandatory and therefore other, non-haematological, adverse events become dose-limiting as myelosuppression is modulated by the myelosupportive treatment. These toxicities as well as dosing recommendations are discussed elsewhere[79,257,259,260] and will not be discussed here as the focus of the present work was the characterisation of the haematopoietic system, its impairment and the impact of the myelosupportive treatment on the time course of myelosuppression. The concentrations of the individual drugs on the day of the ASCR as well as the cytotoxic potential of the compounds will be discussed in this and the following section (section 4.2).

4.1.1 Carboplatin

The final two compartment PK model was able to adequately characterise and predict the concentration-time profiles of ultrafilterable platinum. Only few concentration measurements above 20 mg/mL were underpredicted which can possibly be attributed to a rapid initial distribution phase that can be described by a three compartment model and was not adequately captured by the two compartment model. This is in line with previous findings from an individual analysis where a three compartment model was superior for few of the patients[79]. However, the three compartment model did not result in a statistically significant better description of the data and with regard to the principle of parsimony the two compartment model was selected as the final model for the description of ultrafilterable Pt concentrations. Other population PK analyses also described the concentration-time profiles of carboplatin and ultrafilterable Pt by a 2 compartment model[144,236,261–263]. The testicular cancer population of the CET study was previously investigated in a population PK analysis by Kloft[77] and was part of the dataset for the investigations of Lindauer et al.[236] Parameters and covariate influences resulting from these two analyses are referred to as estimates from the "CET study population" in the following. The analysis presented in this thesis comprised the development of a population model for the subgroup of patients from the CET study for whom leukocyte concentration measurements were available.

Fixed-effects and derived PK parameters Table 4.1 summarises the parameter estimates of studies analysing ultrafilterable Pt after carboplatin administration. Platinum CL was estimated to be 113.5 mL/min for a typical patient resembling the renal function which was characterised by the median CLCR of 114.5 mL/min for the population analysed in this thesis. This is in accordance with Woloschuk et al.[264] who published a high correlation for the renal CL of unbound Pt with CLCR. The magnitude of CL for ultrafilterable Pt was comparable to previously described values of 110.5 mL/min[79] and 109.8 mL/min[236] for the CET study population and the 101 mL/min[261], 123 mL/min[144] and 113.3 mL/min[262] for other populations. The central volume of distribution V_{cen} was 21.2 L and in line with the 19.9 L and 20.4 L reported for the CET study population. In comparison to estimates from other population analyses, V_{cen} was slightly higher as it was previously estimated with 15.5 L[261], 11.9 L[144] and 14.8 L[262]. V_{per} (29.0 L) was in accordance with the parameter estimate published by Lindauer et al. (32.3 L) and higher than V_{per} reported by Shen et al.[261] (7.07 L), Joerger et al.[144] (8.23 L) and Duffull et al.[262] (6.80 L). With an estimate of 0.7 L/h Q was in the same range of the

Table 4.1 Comparison of PK parameter estimates for carboplatin (platinum) from selected studies and the CET study investigated in this thesis

Study	Sampling [d]	CL [mL/min]	V_{cen} [L]	Q [L/h]	V_{per} [L]	Half-life [h]
Thesis (CET Study)	6	113.5	21.2	0.7	29.0	31.7**
Kloft[79]	6	110.5	19.9	0.8*	36.3*	35.4 $\pm$ 6.5
Lindauer et al.[236]	$\leq$ 6	109.8	20.4	0.8	32.3	31.6**
Shen et al.[261]	1	101.0	15.5	0.8	7.07	7.20**
Joerger et al.[144]	0.4	123.0	11.9	5.4	8.23	2.47**
Duffull et al.[262]	1	113.3	14.8	4.4	6.80	1.70-17.0
Elferink et al.[265]	1					2.0 $\pm$ 0.0
Mulder et al.[266]	1					6.3 $\pm$ 2.6

CL: clearance; $V_{cen/per}$: central/peripheral volume of distribution; Q: intercompartmental CL

* calculated from V_{cen} and micro-constants k_{12} and k_{21}

** calculated from population estimates for a typical patient [1]

estimates by Shen et al. and Lindauer et al. (both 0.8 L/h), on the other hand the value for Q reported by Duffull et al. and Joerger et al. and were about 6.2 - 7.7 times higher with 5.4 L/h and 4.4 L/h, respectively. This difference also holds true for the distribution from the central to the peripheral volume of distribution and vice versa, as the micro-constants (k_{12} and k_{21}) describing these processes were approximately 10 times higher compared to the ones estimated in this thesis. The half-life for the terminal phase was 31.7 h and is in accordance with the 35.4 $\pm$ 6.5 h previously reported for the CET study population[79]. Others reported a terminal half-life for ultrafilterable Pt of 2.0 $\pm$ 0.0 h[265] and 6.3 $\pm$ 2.6 h[266] for an observed time period of 24 h. The duration of the observation period might explain the difference as for the investigated population samples were taken for a period of 5 d, resulting in a more accurate determination of low concentrations which are highly influential for the determination of the half-life. Duffull et al.[262] described a wide range for the terminal half-life of carboplatin which varied from 1.70 - 17.0 h and was largely dependent on the renal function.

Interindividual variability and covariates Compared to the variability in the parameter estimates from the investigation by Lindauer et al. the variability in the base model was much lower for the present investigation. As stated previously (section 2.3.1.1 and 3.2.1.1) the population under investigation was only one part of the study population Lindauer et al. investi-

gated. Their population was much more heterogeneous comprising five studies, one of them having been conducted in children. In contrast to their findings the final model in this thesis comprised only one IIV (for CL) instead of the three IIVs (CL, V_{cen}, Q) included in their model which was due to the more homogeneous study population on which the present analysis was based. Upon inclusion of CLCR as a covariate the IIV for CL in the final model was reduced by 33.7% to 13.2% CV. The covariate relation was included as a power function and described a 1.5-fold increase in CL of ultrafilterable Pt for a 2-fold increase in CLCR. This corresponds to the findings of Lindauer et al. who described a 2-fold increase in CL for a 3-fold increase in CLCR. In addition to the influence of the renal function on CL a covariate relation for body size descriptors on CL such as WT, lean body weight and/or HT was described for other investigated populations[79,236,261,262,267]. Moreover, Lindauer et al. took the infusion duration into account and Chatelut et al.[267] added AGE and SEX to the predictive variables for CL. As the final model of Lindauer et al.[236] served as the full covariate model (section 3.2.1.2) the body size descriptors WT and HT were tested for their influence on CL as well, but only CLCR was found to be statistically significant. Kloft et al.[77] used the CLCR determined from 24 h collective urine to characterise the influence of the renal function on the clearance of Pt in the CET study population. Nevertheless, CLCR calculated according to Cockcroft and Gault[222] (section 2.1.5.2) was used in the final model presented in this thesis. This was done in accordance with the final model presented by Lindauer et al. and due to its wide use in clinical practice, knowing that the Cockcroft Gault equation has been criticised in particular when used as a substitute for the GFR in the Calvert equation, as it overestimates GFR in patients with normal renal function[268].

The variability in V_{cen} of ultrafilterable platinum was explained by adding WT as a covariate to the model. Inclusion of an IIV for this parameter became unnecessary as the estimated CV was only 5.6% and did not significantly improve the model fit (p=0.05). Kloft explained 63% of the variability in V_{cen} by including WT as a covariate which is slightly more than the 54.4% that could be explained in the present investigation. A possible explanation for that might be the additional 10 patients that were not available for the present investigation but were included in the analysis presented in the dissertation by Kloft[79]. Increasing the WT by a factor of 1.5 led to a 1.2-fold larger volume of distribution which corresponds to the findings of Shen et al.[261] and Lindauer et al.[236] who found a 1.3 and 1.4-fold increase in V_{cen}, respectively. Duffull et al.[262] found a factor of 0.26 per kg but their findings are not directly comparable as they used LBW in a linear relation to predict V_{cen}. The *a priori* inclusion of WT as a covariate with the exponent of 1 and 0.75 for V_{cen} and CL, respectively, as proposed by Anderson and

Holford[269] is a common approach in PK modelling. This so called allometric scaling apporach was investigated by Lindauer et al.[236] based on the final model and was presented as an alternative for their final model. However, they found that allometric scaling of the base model did not result in successful convergence of the model and therefore the covariate analysis, on which the covariate analysis presented in this thesis is based, was conducted without prior inclusion of any covariate. Therefore, the allometric scaling approach was not investigated during the model development in the presented work.

Toxicity The focus of the present analysis was the cytotoxic potential of carboplatin with respect to leukopenia and its potential impact on the retransfused $CD34^+$ cells from the ASCR. Ultrafilterable Pt, and therefore carboplatin was the drug showing the second highest cytotoxic potential towards the proliferative cells in the bone marrow and was around 0.86 times (14%) less toxic compared to etoposide (assuming a f_u of 21% for high-dose etoposide) and 200 times more potent than thiotepa (Table 3.7). The myelotoxic potency of the 3 drugs will be discussed in more detail in the PK/PD section of this chapter (section 4.2.2). On the day of the ASCR the concentrations of ultrafilterable Pt were 0.02 and 0.2 μg/mL in the central and the peripheral volume of distribution. Assuming unbound platinum to be the pharmacologically active agent and regarding the *in vitro* EC_{50} value of 1.7 μg/mL for carboplatin ($\hat{=}$ 0.89 μg/mL platinum) from a CFU assay[270] the concentration of Pt on the day of ASCR was at least 4.5-fold below the *in vitro* EC_{50}. Hence, although showing a high cytotoxic potency, carboplatin concentrations on the day of ASCR can be assumed to be of minor importance in terms of cytotoxicity towards the proliferative cells in the bone marrow and the retransfused $CD34^+$ cells.

4.1.2 Etoposide

Etoposide concentration-time profiles are most often described by a two compartment model with linear elimination from the central compartment[232,238,271–273]. A three compartment model was described for some studies[109,110,274,275]. The final population PK model for the description of etoposide concentrations in this thesis was a two compartment model. The GOF plot showing observed versus individual predictions revealed an underprediction of concentrations greater than 90 μg/mL, indicating a rapid initial distribution phase which theoretically could be described by a three compartment model. As the two compartment model was superior in terms of OFV (ΔOFV: 8.1), no difference in the GOF and individual plots was observed and following the principle of parsimony the two compartment model was chosen as the final

structural model. Hence, the results will be discussed with regard to analyses performed with two compartment models, only.

Fixed-effects and derived PK parameters Table 4.2 summarises PK parameter estimates from models for etoposide described in literature[94,232,237,238,257,271,272,276]. Overall, the parameter estimates from the present analysis were in line with those previously described for HDCT and conventional dosing. Values for etoposide CL were reported to be between 1.81 L/h[237] and 3.34 L/h[272]. The estimate of 1.86 L/h (31.0 mL/min) was in this range and resembles a renal CL for etoposide of 27% with respect to the median CLCR of the population. This corresponds to the lower end of the previously published 30% to 40% renal clearance for etoposide[91,277].
With 12.9 L, V_{cen} was in the range described in literature which was between 6.38 L[272] and 16.3 L[232]. V_{per} was 6.23 L and is comparable to the parameter estimate published by Nguyen et al.[237] which was 7.8 L. If available, V_{per} was calculated based on the micro-constants k_{12} and k_{21} and resulted in a value of 4.08 L and 6.65 L for constants published by Reif in her thesis[257] and You et al.[238] The same applies for Q which was calculated to be 0.95 L/h (Reif) and 2.59 L/h (You et al.) and was therefore higher than the estimated 0.25 L/h in the present analysis.
The terminal half-life of 20.5 h was longer than the previously reported 4-8 h[273] but in line with findings of Stremetzne[97] who reported a terminal half-life of 20.0 h and Reif et al.[232] who found a prolonged half-life of 12.3 h in a HDCT setting. The patient population analysed in this thesis was a subpopulation of the one analysed by Reif et al.[232] which might explain the longer half-lives in both investigations. This prolonged half-life was probably due to the addition of polysorbate 80 to increase etoposide solubility to the formulation of VEPESID J® which was administered in the CET study[278]. Polysorbat 80 is known to influence the distribution of etoposide as it increases the uptake of etoposide into cells by affecting biological membranes[279,280]. This might also explain the slightly higher volumes of distribution found in this thesis and reported by Reif et al. A longer sampling period (6 d compared to 1 d in other studies[94,237,238,271,272,276]) in combination with a more sensitive method for determination of etoposide concentrations might also contribute to the deviating half-life[232] as low concentrations are crucial for the determination of the elimination of a compound.

IIV and covariates Interindividual variability for V_{cen} and CL was moderate (20.3% and 23.9% CV) and a correlation of 74.6% between the two parameters was identified reflecting the interdependence of CL and V_{cen}. This interdependency can either be caused by an unidenti-

fied variability that was not taken into account by the model or due to too little information in the data for the adequate estimation of both parameters. Possible predictors for the variability of CL and V_{cen} were investigated during the covariate analysis but none of the tested covariate relations was statistically significant. Previously, renal function, hepatic metabolism and protein binding were described as the most important factors involved in etoposide elimination[281]. Other covariates that were identified to influence etoposide CL were concomitant medication influencing the hepatic function (e.g. induction of CYP405 by ifosfamide[238,282]), the renal function characterised by CREA or CRCL[238,257], protein and albumin concentrations, WT and the presence of metastasis[237]. During the covariate analysis of the present investigation AST was identified to have an influence on CL but was not statistically significant any more during the backward deletion process. You et al.[238] identified the liver enzymes AST and ALT as predictors of CL in their full covariate model but in line with the results presented in this thesis both enzymes were not included in the final model. In contrast to the findings by Reif et al.[232], Nguyen et al.[237] and You et al.[238] the renal function was not identified to have an influence on the elimination process. This was probably due to the fact, that patients with renal impairment were not enrolled in the study and, if a mild renal impairment was observed, the dose was reduced (section 2.2.1.1). This dose adjustment is recommended in literature[94,237,277,281] and is due to the fact that etoposide CL is strongly influenced by the renal function[238]. CREA and therefore CLCR were probably not impaired enough in the CET study population to prove influential, reflecting the strict inclusion criteria and the homogeneous study population. As nephrotoxicity is the most important adverse event of carboplatin if myelotoxicity is controlled for by the myelosupportive treatment carboplatin might influence CL of etoposide. However, only few patients suffered from a mild nephrotoxicity during the study[79]. This is in accordance with the results of You et al.[238] who reported that patients receiving platinum compounds in addition to etoposide revealed no change in PK. As long as the renal function is not strongly impaired, liver impairment does not influence etoposide elimination[94]. This underlines the finding that the liver enzymes, although being elevated during therapy and for some patients before the start of therapy, did not statistically influence CL. Stewart et al.[281] identified albumin as the 2nd strongest predictor of etoposide CL, reflecting the high plasma protein binding which varies from 84.4 - 98.1%[94] in cancer patients receiving *conventional* chemotherapy. Although PRO and ALB were reduced during the observed time period they were not identified as potential covariates. However, in contrast to the distinct hypoalbuminaemia reported for the study population investigated by Stewart et al.[281] the variation in ALB concentration was only moderate (5th - 95th percentile: 3.3 - 5.5

Table 4.2 Comparison of PK parameter estimates for etoposide from selected studies and the CET study investigated in this thesis

Study	Sampling [d]	V_{cen} [L]	CL [L/h]
CET	6	12.9	1.86
Reif Dissertation[257]	1-6	10.5	2.32
Reif et al.[232]	1.8	16.3	2.54
You et al.[238]	1	6.83	2.75
Ngyen et al.[237]	1	9.60	1.81
Aita et al.[94]	1		1.1 m^{-2}
Freyer et al.[272]	1	6.38	3.34
Ciccolini et al.[271]	1		1.92
Tranchand et al.[276]	1	8.37	2.43

CL: clearance; V_{cen}: central volume of distribution

g/dL). Covariates described in literature which showed an influence on the volume of distribution were BSA[237] and, in addition to that, the administered dose of etoposide and ALB concentrations[257]. The fact that BSA and the dose were not influential might be due to the dose adjustment which was based on BSA and therefore these covariates were taken into account from the beginning. Thus, the fact that no covariate was identified for this patient population was due to the inclusion criteria with respect to organ function (renal clearance and liver function), the homogeneous study population with regard to e.g. demographic covariates and the absence of influential concomitant medication as well as a distinct hypoalbuminemia.

Toxicity Etoposide was identified to have the highest myelosuppressive influence of the drugs in the CET study on the proliferation of the cells in the bone marrow (see section 4.2.2), which was of comparable magnitude with the SL of carboplatin, assuming a f_u of 21% which was reported for cancer patients after administration of *high-dose* etoposide[95]. If a smaller fraction unbound is used for the calculation of the SL(unbound), higher values are achieved, reaching up to a SL of 17.2 L/μmol for a f_u of 4%. However, the assumption of the higher unbound fraction is reasonable as the investigated study population received high-dose etoposide and the albumin concentration was decreased during therapy (section 3.1.1). The finding of a higher slope for etoposide compared to carboplatin might also be explained by the fact that etoposide-catchol, a cytotoxic metabolite of etoposide, was not taken into account but its myelosuppressive effect might have been attributed to etoposide as half-lives and therefore

presence in the plasma are comparable between the two[283]. Hence, taking the active metabolite of etoposide into account might improve discrimination of the SL for the drugs in future analyses. Regarding the day of ASCR etoposide was the drug with the highest concentration. This is due to the fact that etoposide showed the lowest CL of the three drugs (1.86 L/h versus 7.23 L/h and 19.1 L/h for C and T) and was administered on four consecutive days compared to three for carboplatin and thiotepa. The total concentration in the central and the peripheral volume of distribution on the day of the ASCR was 0.25 and 1.70 μg/mL, respectively. Compared to the *in vitro* EC_{50} value of 0.97 μg/mL[284] the concentration was rather high and retransfused $CD34^+$ cells might still have been harmed by etoposide.

4.1.3 Thiotepa

The PK of thiotepa was best described by a two compartment structural model which is supported by models described in literature[119,285–287]. Previously, Geisler analysed thiotepa concentration measurements from the CET study with a two compartment model by means of a compartmental analysis based on a two-stage approach[233]. In contrast to the model by Geisler the model proposed in this thesis took the delay in the occurrence of thiotepa in the blood into account. In the final model this was realised by implementing a transit compartment model[240] which delays the occurrence of the drug in the circulation by a passage of the compound through a chain of transit compartments. Compared to a simpler lag time model this modelling approach offers various advantages: for one, the transit model avoids the modelling of a change point which makes a model more stable as it describes the concentration-time profile by a continuous function. Additionally, the lag time model assumes an abrupt increase of drug concentration from a value of zero, reflecting a non-physiological approach. The transit model on the other hand describes the delay by a gradually increasing continuous function and is therefore more stable which was confirmed during the PK model development. Also, the continuously increasing concentrations resemble the physiological concentration-time profile during a continuous infusion. A possible reason for the delayed appearance of thiotepa in the plasma was the combination of long infusion tubes with a slower infusion rate for thiotepa due to the smaller volume of drug solution in comparison to carboplatin and etoposide. The median infusion rate for thiotepa was 330 mg/h whereas for carboplatin and etoposide it was 898 and 1063 mg/h, respectively. Due to the higher infusion rates the delay was not observed for carboplatin and etoposide, although the slight underprediction of C_{max} for both drugs might not only result from the two compartment model which was used for

data analysis, but also from a delay in appearance of the drugs in the plasma which was not accounted for.

Fixed-effects and derived PK parameters The number of the transit compartments (N) used to describe the delay of the appearance of thiotepa in the plasma was 125 and was fixed in the final model due to model stability. N resulted from a fit without covariance step and was confirmed in a LLP (section 2.1.3.1) of this parameter. For an infinite number of transit compartments the transit model collapses into a lag time model, showing a steep increase in drug concentration which is comparable to an i.v. bolus injection. Savic et al.[240] estimated an N between 8.15 and 22.9 transit compartments for orally administered drugs which underlines that N=125 transit compartments are reasonable for an i.v. infusion as this number of transit compartments indicates a steeper increase in drug concentration due to the fast accumulation of the drug in the plasma. The TT was estimated with 1.47 h which was comparable to the 1.5 h observed visually during data inspection and plausible, as the infusion duration was planned with 1 h in the original study protocol. In comparison to the V_{cen} reported by Geisler[233] (27.7 L) the estimated V_{cen} of 46.8 L obtained from the population analysis was rather high. With regard to parameter estimates from other analyses (45.5 - 47.4 L) the 46.8 L compares very well (Table 4.3) which underlines the need for taking the delay into account in order to obtain more plausible parameter estimates. Only the 20.0 L reported by Cohen et al.[119] are close to the 27.7 L of Geisler but Cohen et al. report V in L/kg and unfortunately the actual WT of the patients was not given in the publication.
CL was estimated to be 19.1 L/h which corresponds well to the CL estimated by Geisler (15.9 L/h), Cohen et al.[119] (22.3 L/h) and DeJonge et al.[286] (17.0 L/h). The parameter estimate of CL reported by Huitema et al.[285] and Przepiorka et al.[287] are higher with 34.5 and 36.2 L/h. In both therapy regimens cyclophosphamide was administered in addition to thiotepa. Renal elimination of thiotepa is of secondary importance as the hepatic metabolism to its metabolite TEPA plays the mayor role with regard to the elimination process[259]. Cyclophosphamide enhances the metabolism of thiotepa to its metabolite TEPA by induction of CYP enzymes[288] and therefore the overall CL is higher. This was taken into account by DeJonge et al.[286] who estimated an additional, inducible clearance of 12.4 L/h. Considering this, the CLs estimated by Huitema et al. and Prezpiorka et al. also resemble the magnitude of the estimate from the present analysis.
V_{per} was fixed due to model instability to the 27.2 L which were previously reported by Huitema et al.[285]. It was not fixed to the 23.3 L estimated by Geisler for the CET study popu-

Table 4.3 Comparison of PK parameter estimates for thiotepa from selected studies and the CET study investigated in this thesis

Study	Sampling [d]	V_{cen} [L]	CL [L/h]	V_{per} [L]	Q [L/h]
CET	4.5	46.8	19.1	27.2 FIX	1.76
Geisler[233]	4.5	27.7	15.9	23.3	N.R.
Huitema[285]	0.9	45.8	34.5	27.2*	12.5*
Jonge[286]	0.9	44.5	17.0	28.34*	14.0*
Przepiorka[287]	1.0	47.4	36.2**	NR	NR
Cohen[119]	0.17	20.0***	22.3**	36.8	NR

*Calculated from micro-constants k12 and k21, **for BSA=2 m^2 and ***WT=80 kg; N.R.: not reported

lation as, due to differing estimates in V_{cen} and the omission of taking the delay into account, the confidence in the population parameter estimate reported by Huitema et al. was higher. Overall V_{per} was comparable with those from other analysis (Table 4.3), with exception of a V_{per} of36.8 L reported by Cohen et al.[119], but the volume had to be calculated for the median weight of the CET-study population due to lack of information about the weight of the original study population.

The intercompartmental clearance Q was 1.76 L/h and much lower compared to the one published by DeJonge et al.[286] and Huitema et al.[285] with 12.5 and 14.0 L/h, respectively. A possible explanation for the deviation is the sparse data situation especially during the distribution phase of thiotepa.

The half-life of the terminal phase was 11.9 h which was higher than the usual 1.4 -4 h[112,119,285,287] and might be attributed to the longer observation period (4.5 d versus 1 d, Table 4.3) which enables a more accurate description of the low concentrations and therefore influences the calculation of the terminal half-life.

Interindividual variability and covariates The data supported the estimation of IIV for V_{cen} and TT which were moderate with 39.9% CV and 28.4% CV, respectively. DeJonge et al.[286] reported an IIV for V_{cen} of 24.6% CV. The higher IIV found during PK analysis might result from the fixation of V_{per} and N during parameter estimation. As N was fixed to 125 it is likely that IIV actually attributed to this parameter was found in the IIV of TT. Interindividual variability for TT cannot be compared to the IIV found for p.o. administered drugs as the IIV for the latter results from the absorption process of the drug.

A covariate analysis was not planned due to the sparse data situation, absence of trends dur-

ing the visual inspection of covariate plots and the rather homogeneous study population. In her diploma thesis Geisler described an influence of BSA on the volume of distribution at steady state, but it is not clear whether this influence was found for the CET study population alone, or during a joint analysis with data from a female study population which might explain why BSA was not identified during graphical covariate analysis in the present investigation. Jonge et al. found an increased CL of thiotepa due to coadministration of cyclophosphamide and accounted for that in the structural model by adding an additional compartment representing an enzyme pool which induces cyclophosphamide metabolism. Alkaline phosphatase and ALB were identified to influence CL by Huitema et al.[285] who also found an influence of PROT and WT on V_{cen} of distribution. The inclusion of these two covariates into their model explains the small, remaining IIV (7.4% CV) reported for V_{cen}.

Toxicity In comparison to carboplatin and etoposide, thiotepa revealed the least myelotoxic potency towards proliferating cells in the bone marrow (see also section 4.2.2). Due to the high clearance of thiotepa from the plasma the concentration of thiotepa on the day of the ASCR was negligible with 0.14 and $1.5 \cdot 10^{-3}$ μg/mL for the central and the peripheral volume of distribution although the *in vitro* EC_{50} from a CFU-GM assay is also low with 0.08 μg/mL[287]. In the present PK/PD analysis a potential myelosuppressive effect of TEPA, the active metabolite of thiotepa, was not taken into account. Hagen et al.[122] found no correlation between myelosuppression, the AUC, C_{max} or the elimination half-life of TEPA although substantial exposure to TEPA in terms of AUC was found, which is due to the longer half-life (factor 2-7[289]) of TEPA in comparison to its mother compound. Nevertheless, integration of TEPA into the model for myelosuppression might supply further insights into the myelosuppressive potency of the metabolite. Also, the threshold concentration for which myelosuppression might be observed might not have been reached in the study analysed by Hagen et al. as thiotepa was dosed with 60 - 80 mg for the first and the second cycle of chemotherapy.

4.2 Project 2: Pharmacokinetic/Pharmakodynamic Modelling of leukopenia

4.2.1 Models for myelosuppression

Various models for the description of myelosuppression have been published over the years (section 1.4.2). Empirical models enable the description of the time course of myelosuppression but no information about the underlying system can be gained. Therefore simulations

and extrapolations to new settings need to be treated cautiously, if done at all. Mechanistic models on the other hand require the implementation of many parameters and only few have been parametrised to take chemotherapy-induced myelosuppression into account[20]. Due to the rather complex character of mechanistic models, they require a lot of data and therefore semi-mechanistic model are preferred for analysis of clinical studies, in which sampling is limited and some parameters of the mechanistic models cannot be characterised without additional sampling of e.g. bone marrow aspirates. Soto et al.[141] investigated five different models for the description of neutropenia and recommended the use of the model proposed by Friberg et al.[138] together with a model from Panetta et al.[139] and the lifespan model by Bulitta et al[140]. The latter requires 17 ordinary differential equations and parameter estimation is therefore very time consuming especially in combination with complex PK models or drug combinations. During the past years, the model for myelosuppression by Friberg et al. has become the gold standard for analysis of neutropenia following chemotherapy and was also applied for the description of leukopenia[138,156,157] as well as thrombocytopenia[150,155,158]. Due to its wide use parameter consistency for the system-specific parameters such as MMT and γ was proven, reflecting the successful differentiation of system-specific and drug-specific parameters. Hence, the model by Friberg et al. was chosen for the characterisation of the system of leukopoiesis under HDCT to investigate its applicability for this special setting and to be able to compare system- and drug-specific parameters. Additionally, the model comprises a feedback mechanism allowing the description of the recovery after nadir and the pronounced rebound in leukocyte concentrations which were observed in the raw data. The pronounced rebound results from a highly active physiological feedback due to low leukocyte concentrations and therefore high G-CSF levels and was found to be even more pronounced after multiple injections of cytotoxic drugs[127]. Even when this rebound was not observed, a feedback mechanism proved to better describe nadir concentrations and recovery to physiological neutrophil values[141].

4.2.2 Final model for myelosuppression

4.2.2.1 Implementation of drug-specific parameters

Implementation of the drug effect In the past, implementation of the drug effect as a linear, E_{max} and a sigmoidal E_{max} model was investigated but most of the studies implemented it in a linear manner[129,151,152,154,155,290] despite the fact that an E_{max} model describes the effect of a drug in a more pharmacological way. The superiority of the linear model for the description of the drug effect suggests that the cytotoxic effect for most of the investigated drugs was still

in the linear part of the concentration-effect curve. Only recently, Quartino et al.[153] reported a substantial improvement in OFV compared to only a small improvement for the implementation of a sigmoidal E_{max} model instead of the simpler E_{max} model. However, a sigmoidal E_{max} model requests the estimation of two additional parameters for each drug implemented and was not investigated in this thesis due to the high number of parameter estimates with regard to the rather small study population. For larger populations, however, a sigmoidal E_{max} model should be explored for carboplatin as already a simple E_{max} model was slightly superior to the linear one in terms of OFV. Friberg et al.[138] reported a significantly better description of the data for the application of an E_{max} model with only minor changes in the system-specific parameters. However, they reported relatively high relative standard errors (> 17% and > 50%) for the parameter estimates of E_{max} and therefore they decided to implement the linear model. The same was found during model development when an E_{max} model for carboplatin was implemented. Imprecision of the system-specific parameter estimates increased whereas a small improvement in OFV (ΔOFV -16.5 points) was observed. This decrease in OFV was statistically significant but with regard to parameter precision and no observable improvement in GOF and individual plots it was decided to implement the linear model. Zandvliet et al.[291] reported a linear PD model for carboplatin as well. However, they stated that their data did not contain sufficient information for the evaluation of an E_{max} model. For etoposide and thiotepa, the linear model was found to be statistically superior which was also previously described in literature for etoposide[129,138]. A regimen containing thiotepa has been analysed with the model for myelosuppression by Ramon-Lopez et al.[147] but as no information on the PK of the drugs was available they applied the K/PD modelling approach[292] which allows the analysis of PD data in absence of PK. Hence, the implementation of a linear model for the drug effect of thiotepa cannot be compared to other analysis.

Drug-drug interaction in the setting of HDCT In the final model the drugs were assumed to exercise an additive effect on the proliferation rate constant of the cells in the bone marrow. The assumption of an additive effect in an combinatorial regimen has been described for other studies[19,144,156,157,290]. A possible drug interaction with regard to the myelosupressive potency of carboplatin and etoposide was explored for the final model applying the response-surface analysis (section 2.4.2.1). This was first done by Soto et al.[151] for the model of myelosuppression. They described an additive drug effect based on an insignificant change in OFV but unfortunately did not report the value for E_{50} which provides the information on the type of interaction. During analysis of the data presented in this thesis E_{50} was estimated to be 0.9

(5^{th} and 95^{th} percentile: 0.7 - 1.0) directly after the end of the infusions on each day of drug administration. Kano et al.[293] described an additive drug effect for carboplatin and etoposide on leukemia cell lines *in vitro*, whereas a synergistic anti-tumour effect of etoposide and alkylating agents including platinum compounds has been demonstrated *in vivo*[294]. Based on the estimate of E_{50} and due to high imprecision of the parameter estimate for the SL of thiotepa and a decrease in OFV of only 4 points an additive drug effect was implemented in the final model. However, the lower value of the range for E_{50} (0.7) indicates a slight synergism. Further investigation of this possibly schedule-dependent synergism in a larger population or by inclusion of data from other studies, ideally with different dosing schedules to differentiate between the drug effects more efficiently might provide a better insight for a possible interaction of carboplatin and etoposide. Another option for the investigation of drug-drug interactions constitute *in vitro* studies in which different combinations of drug concentrations and a possible schedule-dependency can be investigated.

4.2.2.2 System-specific parameters describing leukopoiesis/leukopenia following HDCT

Baseline estimation methods The correct estimation of the leukocyte concentration before start of HDCT is crucial, as the estimate $Circ(t_0)$ enters the feedback mechanism, influencing the estimation of all other parameters, the description of nadir concentrations as well as the recovery to physiological values. Although no investigation regarding the baseline estimation method for the model of myelosuppression was previously reported, the three baseline estimation methods[242] B1, B2 and B3 (section 2.4.2.2) were investigated. In the original model by Friberg et al.[138] the B1 method was applied which was used for most of the analyses conducted with the model for myelosuppresion. Only few did not estimate $Circ(t_0)$ assuming the measurement before start of the therapy to be determined without any associated residual variability[144,148,152]. The model performed best applying the B1 method regarding the OFV and the description of individual profiles, especially with regard to differences in the description of the initial increase in leukocyte concentrations. Superiority of the B1 method for the description of a PD baseline was demonstrated in a simulation study by Dansirikul et al.[242], although they report a similar performance for the methods with slightly decreasing performance in the order B1, B2, B3. They indicated that the B2 method might be superior in a setting with few data or when the distribution of the baseline effect is not easy to assess, which was not the case for the data this analysis was based on.

Number of transit compartments in HDCT The original model as proposed by Friberg et al.[138] comprised three transit compartments. Friberg et al. reported only little improvement in the OFV for increasing or decreasing the number of compartments for the four drugs they investigated. Investigations regarding the number of transit compartments were also undertaken by Soto et al.[151] and Troconiz et al.[154] who both found that changing the number did not result in a better description of the data. In 2012, Quartino et al.[153] published a model for the simultaneous description of leukocyte and neutrophil concentrations following docetaxel treatment. Neutrophil concentrations were best described using six transit compartments whereas for leukocytes one transit compartment resulted in the best fit. The higher number of transit compartments which was also used in the final model presented in this thesis enables the description of a sharper profile with a rapid decrease in cell concentrations and a pronounced rebound after a prolonged time delay. All patients enrolled in the CET study suffered from a grade 4 leukopenia followed by a pronounced rebound. Additionally, nadir concentrations for a typical patient receiving median doses of carboplatin, etoposide and thiotepa were reached after a median of 276 h (11.5 d) after start of HDCT reflecting the fast decrease in leukocyte concentrations which was well captured by the six transit compartments. Quartino et al. justified a single transit compartment describing leukocyte concentrations by the large variety of cells belonging to the group of leukocytes which underlie different maturations processes. One transit compartment allows for a wider distribution of maturation times for individual cells within one patient. However, the analysis by Quartino et al. was based on a conventional chemotherapy regimen without ASCR which might result in varying MMTs for different cell lines due to different sensitivity towards docetaxel treatment. In contrast, during HDCT a higher degree of leukopenia was observed (median nadir according to Quartino: approximately $2 \cdot 10^9$ leukocytes/L; CET study: $0.08 \cdot 10^9$ leukocytes/L), hence, the system of leukopoiesis is under much more stress and massively activated due to physiological regulation processes. Therefore, the difference in sensitivity of the different cell lines towards the cytotoxic drugs might not have been as substantial any more because the drugs reached such high concentrations that maturation of all cell lines was impaired to the same extent and due to the stimulation by the feedback mechanisms maturations times were more similar. This finding suggests, that the number of transit compartments is dependent on the sensitivity of the cells and the degree of the impact of the cytotoxic treatment, with HDCT showing such an immense effect that no difference in the maturation processes of the different cell lines can be observed any longer.

4.2.2.3 Implementation of dexamethasone an the myelosupportive treatment

Description of the initial increase The leukopenic time course revealed an increase in the early phase, directly after start of HDCT. This increase was best described by an additional compartment (INI_{DEXA}) which was initiated once with an estimated concentration of cells (C_{INI}). The cells entered the circulation over an estimated period of time making it possible to predict the temporary increase in leukocytes. In line with other investigations[148,151] INI_{DEXA} was activated once when the first DEXA administration took place, linking the observed initial increase to the known effects of glucocorticoides. On the one hand DEXA increases leukocyte concentrations in the circulation by causing demargination of cells from the vessels[70] and on the other hand by increasing G-CSF levels[235]. G-CSF itself increases the proliferation of the haematopoietic progenitor cells in the bone marrow, shortens cell maturation processes and mobilises cells that are marginated around the vessels[63,64]. The increase in numbers of leukocytes following DEXA administration can be observed in two phases. A first increase was previously described 4 - 6 h, and a second one 24 h after administration, reflecting the different mechanisms of action and the complex reaction of the leukocyte concentrations in the blood to concomitant DEXA administration[70]. In the present study only little information, i.e. doses and for some patients dosing times of DEXA, were available. A more sophisticated model e.g. with multiple initialisations of INI_{DEXA} linked to each dosing event of DEXA was not supported by the data. One reason might be the multi-level response of the leukopoietic system including the pool of marginated cells upon DEXA administration. The empirical integration of the effect of DEXA administration neglects the complexity in the treatment response which was reflected in the high non-differentiating IIV that was estimated for C_{INI} (94.8%). Moreover, the patients received 0 to 9 administrations of DEXA in two different doses on up to six consecutive days of treatment which was not taken into account either. The assumptions that were made during dataset building (section 2.4.2.4) which were due to lack of more detailed information possibly added to the high but precisely estimated variability in C_{INI}.

Implementation of an additional feedback In 2011, Quartino et al.[295] introduced a model for myelosuppression which was linked to a model for endogenous G-CSF. The models were linked at three points: the absolute neutrophil concentration in the blood enhanced G-CSF clearance in a linear way and the ratio between G-CSF before and during chemotherapy replaced the feedback mechanism of the original model. A new feedback did not only act on the proliferation rate of the cells in the bone marrow (feedback exponent γ) but on k_{tr} (feedback exponent β), imitating a decrease in MMT due to higher G-CSF concentrations. G-CSF

was modelled by an indirect response model with the option to increase G-CSF levels due to administration of glucocorticoides by a first-order input process[258]. An increased production of G-CSF due to concomitant glucocorticoid administration was reported but it was not possible to describe the observed increase in neutrophil concentrations after administration of the cytotoxic agents. This supports the finding that DEXA showed an influence on MTT and k_{prol} (section 3.3.7) but a sole decrease and increase of the two parameters did not sufficiently describe the observed increase in leukocytes. Nevertheless, the model by Quartino et al. offers the possibility to integrate endogenous concentrations of G-CSF which, together with G-CSF measurements during e.g. HDCT, enables the integration of G-CSF treatment in a more mechanistic and physiologically motivated way. This was also done by Pastor et al.[296] who used a variation of the model to describe neutropenia following carboplatin treatment. They implemented the feedback mechanism as a function of unbound circulating G-CSF concentrations (endogeneous and exogeneous) that stimulated cell proliferation of the haematopoietic progenitor cells as well as cell maturation of the non-proliferative cells in the bone marrow. Unfortunately, no parameter estimates were published which makes it impossible to compare their results with the results from this thesis. Integration of G-CSF treatment based on the model and parameter estimates published by Quartino et al. was not done in the present analysis as, compared to the CET study, their study population comprised female breast cancer patients and excluded those receiving additional G-CSF treatment. As G-CSF depends on a circadian rhythm and additionally varies between males and females and not a single measurement of G-CSF was available for the CET study population nor was information on the exact dosing, it was decided that the assumptions that would have been made by fixing the parameters to parameter estimates of Quartino et al. would have been too strong. Moreover, the estimate for G-CSF prior to therapy in their study showed a large variability even in the study population of breast cancer patients (% CV: 68) which makes it difficult to transfer the parameter estimates to the CET study without making too decisive assumptions. However, with more information on G-CSF administration and additional determination of G-CSF concentrations before and maybe during therapy, the models by Quartino et al. and Pastor et al. might be of great value to gain further insight and understanding of G-CSF treatment in the setting of HDCT.

Implementation of an additional feedback mechanism in analogy to the model by Quartino et al.[258] was investigated in various ways during model development, none of them improving the model. In their joint model for leukopenia and neutropenia[153] Quartino et al. found, that introducing a second feedback on the transition rate constants for the leukocyte progenitors

in the bone marrow did not improve the model. In contrast to the feedback implemented by Quartino et al., the second feedback investigated in this thesis was not based on G-CSF concentrations as no information was available. Additionally, the second feedback in the model by Quartino et al. was also dependent on neutrophil concentrations as they contributed to G-CSF clearance. Because of these differences in the implementation of the additional feedback the findings in this thesis were not directly comparable to their results. As mentioned in the previous paragraph, additional information on G-CSF concentrations prior to and during therapy would be desirable for a more mechanistic investigation of the activation of physiological feedback mechanisms during HDCT.

Stem cell rescue For the ASCR an additional compartment (SCR) was introduced to the model. All $CD34^+$ cells were dosed into this compartment on the day of the ASCR. From there they entered the model in the compartment of proliferating cells via one transit compartment, mimicking the physiological process of migration of the progenitor cells back into the bone marrow, also known as homing[297]. $CD34^+$ haematopoietic progenitor cell comprise highly proliferative lineage-specific precursor cells, capable of forming colonies, as well as more mature haematopoietic progenitor cells which both contribute to the reconstitution of the bone marrow. During model development it was tried to integrate the CFU cells separately, letting them enter the compartment of proliferating cells whilst the rest of the $CD34^+$ cells entered the first transit compartment which resembles the early stages in cell maturation. For the model comprising six transit compartments it was not possible to estimate SL of etoposide whilst separating the two cell fractions. On the other hand this was possible with the preliminary model comprising three transit compartments for the description of cell maturation, however, it needs to be stated that this model was evaluated using the less precise FO algorithm. Nevertheless, if new data on HDCT regimens with different dosing regimes becomes available this model should be revised as a better discrimination of the drugs' effects might enable the implementation of this model.

The $CD34^+$ cells in the model published by Ramon-Lopez et al.[147] entered the first transit compartment assuming that the retransfused $CD34^+$ cells were not capable of proliferation any more which is rather unlikely. In contrast to the final PK/PD model presented in this thesis the cells in their model entered the first transit compartment following a zero-order process which resulted in a statistically significant drop in the OFV in comparison to a first-order process. This was not considered during model development and might help to further improve the model. However, the assumption of a first-order process is reasonable as the migration of

the cells into the bone marrow is comparable to the first-order process with which C_{INI} entered the compartment of circulating cells for the description of the initial increase in leukocyte concentrations after DEXA administration[148,151]. Overall investigations based on a larger study population or less complex therapy regimens with regard to the number of combined drugs might help to gain further insights into the role and meaningfulness of ASCR during HDCT.

4.2.2.4 Covariates

In the final model no covariate was identified to have a statistically significant influence on the model parameters. This is probably due to the homogeneous, small study population and the restrictive inclusion criteria. Neither G-CSF nor DEXA proved influential for leukocyte progenitor proliferation or maturation processes and the administered amount of DEXA showed no influence on C_{INI}, the number of cells that were estimated to describe the initial increase in leukocyte concentrations. A statistically significant influence of G-CSF on the feedback exponent γ was driven by one patient (ID 7) who did not receive G-CSF. When the base model and a model containing the covariate relation were applied excluding this patient no difference in the OFV was observed. Moreover, exclusion of this patient led to a reduction in IIV for γ from 27.9% CV to 14.2% CV. Hence, when including G-CSF as a categorical covariate a different value for γ for this one patient was estimated which explains the reduction in unexplained IIV and the statistical significance for the covariate influence which was dependent on this one patient. The influence of G-CSF on model parameters was investigated by Ramon-Lopez et al.[147] who estimated a reduction of MMT by 48% and an increase of k_{prol} of 120% when G-CSF was administered. An additional covariate influence of G-CSF on γ did not further improve their model. These covariate influences were also described by Sandström et al.[157] who reported a reduction in MMT and an increase in k_{prol} of 169%. In contrast to the CET study only 70% of the patients included in the study investigated by Sandström et al. received G-CSF treatment and the patients in the study analysed by Ramon-Lopez et al. were randomised in two groups, receiving different schedules regarding G-CSF treatment. All patients but one received G-CSF in the present study starting on the same day until a threshold concentration of leukocytes was reached, resulting in similar leukocyte-time profiles. This is most probably the reason why no covariate influence could be determined. However, a distinct deviation in the time course of ID 7 was observed, especially with regard to the duration of grade 3 leukopenia. Therefore further investigations should be conducted concerning the influence of G-CSF in a HDCT regimen as this explicit profile indicates a clear benefit for those patients treated with G-CSF. A clarification of whether this deviation was by chance, due to other influences

such as neutropenic fever or G-CSF administration would be desirable. Additionally, G-CSF concentration measurements would be important to implement the supportive treatment in a more mechanistic way (compare Roskos et al.[298] and Quartino et al.[153]) to gain further insights in its benefit for HDCT.
None of the previously reported covariates were identified during graphical analysis and therefore not tested for. Visual inspection of covariate plots led to the investigation of HT as a descriptor for Circ(t_0) and the influence of AGE, ALB, CLCG and GGT on MT_{SCR} were investigated but did not significantly improve the model. Among descriptive covariates for the model parameters that were reported in literature were AAG, ALB, BILI, SEX and previous chemo- and radiotherapy for the baseline of neutrophils and/or leukocytes. HT and liver enzymes were identified as predictors for the MMT, the latter together with BILI also influencing γ. The sensitivity of the cells in the bone marrow was reported to depend on AAG, ALB, BIL, concomitant cytotoxic agents if not specifically implemented as an additional drug, RACE, AGE and previous treatment[129,143–146 148–150,299]. An influence for ALB on the slope of etoposide might have been assumed as a decreased albumin concentrations in cancer patients during therapy influences protein binding[93] and, hence, the fraction unbound. However, as it was not possible to estimate an IIV for the slope of etoposide and the focus of the covariate analysis was laid on the system of leukopoiesis this covariate relation was unfortunately not being tested for and should be investigated in future analysis.

4.2.2.5 Final model for myelosuppression following HDCT

Final estimates for system-specific parameters The parameter estimates of the final population PK/PD model for leukopenia are summarised in Table 3.7. The leukocyte concentration before HDCT was $4.00 \cdot 10^9$ cells/L and lower compared to those previously estimated for leukocytes (6.74-8.10,[138]). Nevertheless, the estimate was in line with the median of the population which was $3.97 \cdot 10^9$ cells/L and most probably lower because of a bone marrow function impairment due to one or multiple cycles of previous chemotherapy with cisplatin.
MMT was 93.6 h and comparable to the range reported for leukocytes by Friberg et al.[138] in 2002 (90 - 135 h), with 90 h estimated for docetaxel. The docetaxel study was reevaluated with an extended model[153] in 2012 resulting in a MMT of 162 h. Comparing MMT estimates from 17 analyses[129,138,143–153] twelve were estimated to be higher than 100 h and five between 90 and 100 h. In comparison the estimate of 93.6 h is rather low, but can be explained by the administration of G-CSF as Ramon-Lopez et al.[147] reported a value of 92.3 h which was further reduced by 48% for patients treated with G-CSF. Sandström et al.[157] published a value of 58.4

h for MMT for patients receiving G-CSF. Moreover, as all patients were suffering from a grade 4 leukopenia physiological regulatory mechanisms are likely to have been highly active, contributing to faster maturation times by stimulation of maturation processes by the regulatory mechanisms. IIV of Circ(t_0) and MMT was comparable to those published in the 17 studies although most of them analysed neutrophils instead of leukocytes.
The estimated amount of cells which explained the initial increase in leukocyte concentrations was $18.5 \cdot 10^9$ cells/L and higher than the already published cell concentrations of $5.19 \cdot 10^9$ cells/L by Ozawa et al.[148] and $9.07 \cdot 10^9$ cells/L by Soto et al.[151]. In the study investigated by Soto et al. DEXA was administered p.o. twice on three consecutive days at a dose of 4 mg. Ozawa et al. only reported a single administration prior to docetaxel treatment which was administered once every three weeks. Hence, the higher estimate of C_{INI} can probably be explained by the higher dose and the (in most cases) longer supportive treatment with dexamethasone. A dose dependency of the increase in circulating neutrophils was previously reported by Jilma et al.[235] and Mishler et al.[70] who investigated different doses of 0.04 - 1.00 mg/kg and 4 - 8 mg/m^2, respectively.
The mean time it took for C_{INI} to enter the circulation was again higher compared to the ones previously published (44.3 h vs. 19.3 - 35.6 h) and can probably be explained by the longer treatment with DEXA. This assumption is supported by the finding that peak neutrophil concentrations were observed 24 h after a single administration in healthy volunteers[70,300] and therefore are observable after two up to seven days after start of HDCTn depending on the administration(s) of dexamethasone for each patient.

Implementation of ASCR Implementation of an ASCR into the model for myelosuppression was only published by Ramon-Lopez et al. in 2009[147]. The estimates for the time it took the CD34$^+$ cells to enter the compartment of proliferating cells cannot be compared to their model as they proposed a different structural model where the cells enter the first of three transit compartments. The migration of the cells to the bone marrow and therefore the fact that they are not present in the circulation after retransfusion was reflected by the still deceasing leukocyte concentrations after the day of ASCR until 1 - 2 days later when nadir concentrations were reached. MT_{SCR} was estimated with 8.83 h and was highly variable spanning from 1.21 h to 356 h. This high variability was also reflected in the IIV which was 175% CV and was most probably due to the fact that the number of retransfused cells was highly variable (0.072 - $0.5 \cdot 10^9$ cells) and the study had not been designed for explicitly evaluating the influence

of ASCR on the time course of myelosuppression. For example the actual time point of the administration was not reported and it is not clear when the cell number was determined (before retransfusion or before cryopreservation).

Final estimates for drug-specific parameters Sensitivity of the proliferative cells in the bone marrow was estimated by the SL parameter for each drug. At the first sight the model was able to distinguish between the drug effects in this regimen and rank the cytotoxic agents with respect to their myelotoxic potency. However, after transformation of the SL for etoposide and thiotepa taking plasma protein binding into account a higher cytotoxic potency of etoposide was observed. Comparing the slopes for unbound drug concentrations, etoposide revealed the highest cytotoxic effect followed by carboplatin and thiotepa with SLs of 3.32 (f_u=21%), 2.85 and 0.014 (f_u=20%) L/μmol, respectively. Precision for the parameter estimates was acceptable with 24.6%, 19.3% and 28.2% RSE for SL of etoposide, carboplatin and thiotepa, respectively. Comparing the cytotoxic potencies of etoposide and carboplatin with those previously published in literature a higher influence of carboplatin was expected as a 1.3 to 6.5-fold higher influence for carboplatin can be calculated from the respective publications[129,138,150,291].

A slope for thiotepa has not been published until now and therefore no comparison can be made. The fact that the dose of thiotepa can be escalated by a factor of 30 compared to a factor of 5 and 4 - 7 for carboplatin and etoposide, respectively, in comparison to conventional chemotherapy[51] underlines how much lower the cytotoxic potency of thiotepa in comparison to the other two compounds is. This was confirmed with the present analysis reflected by the very low estimated for the slope in comparison to the slopes of etoposide and carboplatin.

The higher estimate for SLE (between 3.32 and 17.2 L/μmol, depending on protein binding) might reflect difficulties in the differentiation of the drug effects by the model. The reason for that most probably lies in the design of the study: etoposide was the only drug that was administered on day 4 of the HDCT regimen and, hence, concentrations of etoposide were the highest on that and the following days. Figure 3.5 shows that leukocyte concentrations start to decline on day 3 and 4 of HDCT. As the drug effect is implemented as the sum of the products of each drugs' concentrations times the respective slope the cytotoxic effect most probably was attributed to the drug with the highest concentration on those days. Therefore SLE might be overestimated to some extent simply due to the schedule for the administration of the drugs. However the overall drug effect, i.e. the sum of each drugs' effect was well predicted which was reflected by the correct description of the entire time course of leukopenia as well as nadir

concentrations (Figure 3.25). This is important with regard to Project 3 and the conclusion for the optimal day to perform the ASCR drawn from these simulations as the same study design as in the original study was used and therefore the overall drug effect was predictive for the time course.
With regard to the investigated study design and its possible influence on the estimation of the SLs a further analysis of a similar regimen with different dosing schedules of the drugs might be helpful to provide further insight in the magnitude of the slope estimates as well as a possible drug-drug interaction which might be schedule-dependent (see also section 4.2.2.1). As the drugs were administered one after another at a very high dose additional data from a study with a more spread out schedule might be of interest with regard to an easier and probably more precise estimation and differentiation of the drug effects.
Overall the parameter estimates for the slopes in the presented study are much higher compared to previously published ones. For carboplatin slopes of 0.46 and 0.22 L/μmol[150,291] were reported and for etoposide slopes of 0.16 and 0.07 L/μmol were estimated[129,138]. In contrast to the CET study all of the studies comprised a conventional chemotherapy regimen and the effect of DEXA was implemented in neither of these models. As the concentration of circulating leukocytes was increased during the first few days of the study compared to Circ(t_0) the SLs had to be estimated higher in order to achieve nadir concentrations. Comparing the SL for docetaxel for a model taking the initial increase of neutrophils during DEXA treatment into account with a model that did not a 1.8 - 2.0-fold higher typical estimate for SL was found[138,148,149]. Additionally, for the model including DEXA treatment high variability for SL and C_{INI} was estimated (68.2 and 110% CV). Unfortunately, it was not reported whether patients showing a high increase in neutrophil concentrations also had high individual predictions for SL.
Another possible explanation for the higher estimates of the SLs might be due to the physiological effects of DEXA. As it increases G-CSF levels the proliferation of the cells in the bone marrow is enhanced making them more vulnerable to cytotoxic agents. Hence, the slope which is a measure for the sensitivity of the cells in the bone marrow should be higher in patients receiving DEXA. The higher estimates for etoposide and carboplatin are probably due to a combination of the two aspects: the increase in leukocytes in the blood and therefore a more pronounced decrease that can mathematically only be achieved by a higher estimate for SL and the physiological processes leading to this initial increase. As the data did not support the estimation of an IIV for the SLs of the three drugs this hypothesis requires further investigations.

4.3 Project 3: Assessing the optimal day for an autologuos stem cell rescue

The most important predictor for the risk of infection are the duration and the extent (nadir concentrations) of granulocytopenia. Bodey et al.[131] reported a 60% risk of developing a severe infection if granulocytopenia persists for three weeks. For very low levels of granulocytes ($< 0.1 \cdot 10^9$ cells/L, corresponding to 0.14 - 0.16 $\cdot 10^9$ leukocytes/L [2]) this risk increases to 100%. Neutrophil concentrations below at least grade 3 neutropenia ($0.5 \cdot 10^9$ cells/L, corresponding to 0.71 - 0.83 $\cdot 10^9$ leukocytes/L) increase the risk of an infection sharply. According to Crawford et al.[301] 10% of the patients in his study developed a serious infection for a neutropenia below grade 1 with a duration $\leq$1 week whereas 30% had an infection for the duration of $\leq$2 weeks. For even lower neutrophil concentrations ($0.1 \cdot 10^9$ cells/L, corresponding to 0.14 - 0.17 $\cdot 10^9$ leukocytes/L) 28% and 50% of the patients developed a serious infection, illustrating the influence of nadir concentrations and duration of neutropenia on the risk of infection.
To support the reconstitution of the bone marrow and to enable the dose escalation for a HDCT, generally, an ASCR with or without additional administration of growth factors is performed. A survey conducted in 2003 comprised 162 clinics performing ASCR in the framework of HDCT in patients with breast cancer[53]. Almost two thirds (64%) of the hospitals aimed for an amount of $CD34^+$ cells of $2 \cdot 10^6$ cells/kg, few (7%) used a value as low as $1 \cdot 10^6$ cells/kg, and all others reported a higher threshold for ASCR, usually within a range from 3 to $5 \cdot 10^6$ cells/kg. During the simulations the duration of grade 3 leukopenia as well as nadir concentrations were assessed with regard to the amount of retransfused cells. Moreover, the influence of the day on which the ASCR should be performed was investigated with regard to nadir concentrations as well as the duration of the leukopenia. The day on which the ASCR is performed is of particular interest as the $CD34^+$ cells should not be administered too early to protect them from the cytotoxic potential of the chemotherapeutic drugs and not too late as a fast recovery and "high" nadir concentrations are essential with regard to the risk of developing severe infections. The simulations comprised amounts of $CD34^+$ cells ranging from the minimum of $0.072 \cdot 10^9$ cells ($\triangleq 1 \cdot 10^6$ cells/kg for this patient), the median of the population 0.2329 ($\triangleq 2.9 \cdot 10^6$ cells/kg) to the maximum of 0.56 ($\triangleq 7.7 \cdot 10^6$ cells/kg) reflecting the administered amounts of retransfused cells from the survey.
The simulations showed that, altogether, the performance of the ASCR on day eight (D8) was superior in comparison to day seven (D7) on which the ASCR had originally been performed.

[2] Assuming the neutrophil fraction to constitute 60% to 70% of the total leukocyte count[20]

Also with regard to all other days investigated, D8 proved superior. Especially considering the duration of grade 3 leukopenia an ASCR performed on D8 turned out to perform better, as independent from the amount of retransfused cells the duration of grade 3 leukopenia was shortened. The higher the amount of retransfused cells the shorter was the duration of that time period: for a typical patient receiving dexamethasone on day one and the populations' median doses of carboplatin, etoposide and thiotepa the duration of grade 3 was shortened by 35 h (1.5 d) and 15 h to a total duration of 1.5 and 1.0 weeks for the minimal and maximal amount of retransfused cells, respectively. This illustrates how crucial the amount of retransfused cells is and underlines the importance of the day on which the ASCR is performed. With regard to the extremes of the simulations conducted, i.e. the 90^{th} percentile for a minimal amount of retransfused cells on D7 (longest duration) and the 10^{th} percentile for the maximal amount on D8 (shortest duration), the difference in the duration of this critical period in time was substantial, namely 1.2 weeks.
Moreover, the nadir concentrations were affected by the day on which the ASCR took place. Here, the amount of retransfused cells showed an impact on the day of the ASCR. For the minimal amount of retransfused cells up to $0.2 \cdot 10^9$ cells ($2.5 \cdot 10^6$ cells/kg for a patient with median body weight of 80 kg) an ASCR on D8 resulted in higher nadir concentrations. This was reversed for higher amounts of retransfused cells.
The results illustrate the need for further investigations based on, in the best case, varying dosing schedules for the determination of the SL and especially for the ASCR for the same regimen. Until now the recommendations of the guideline for ASCR in Germany are vague with regard to the PK of the administered drug stating that "it should be taken into account"[302]. Of the three drugs investigated in the HDCT regimen etoposide showed the highest concentration on the day ASCR was performed which additionally was still of relevant magnitude compared to the *in vitro* EC_{50} value for PBMC determined in a CFU-GM assay. The higher concentrations were due to the relatively long half-life described for etoposide in the HDCT and probably caused the finding that D8 was the favourable day for the ASCR.

Recommendations These findings underline the necessity of therapeutic drug monitoring which would enable to take the individual PK of each patient into account. Furthermore, the amount of cells that is available for retransfusion should be considered for the decision about the day of ASCR. Firstly, the simulations suggest that higher amounts are preferable, especially with regard to the duration a patient suffers from grade 3 leukopenia and, hence, the

increased risk of a severe infection. Secondly, if it is not possible to obtain higher amounts of cells an ASCR performed on D8 is superior with regard to the duration of grade 3 leukopenia and nadir concentrations. For higher amounts of cells it needs to be decided whether nadir concentrations are of more importance or the duration of grade 3 leukopenia as the difference between nadir concentrations for an ASCR on D7 and D8 was $3.6 \cdot 10^7$ cells, being higher on D7 and the time difference was 34.8 h, being shorter for an ASCR on D8. Neglecting the amount of retransfused cells, overall, day 8 for the ASCR should be preferred over day 7 in the setting of the CET study regimen.

For the regimen investigated in this thesis this means concretely, that for an available amount of $CD34^+$ cells $\leq 0.1 \cdot 10^9$ D8 of HDCT is preferred for the performance of the ASCR as nadir concentrations are the highest. With regard to the time below grade 3 leukopenia for this amount of cells ASCR on D9 of HDCT performed best. However, comparing the duration of grade 3 leukopenia for $\leq 0.1 \cdot 10^9$ for an ASCR on D9 and D8 there is no statistically significant difference. Hence, for this low amount CD34+ cells the ASCR should be performed on D8 for this specific regimen.

For an available amount > 0.1 but < $0.2329 \cdot 10^9$ $CD34^+$ cells no statistically significant difference in nadir concentrations between an ASCR performed on D7 and D8 was observed. Regarding the duration of grade 3 leukopenia D8 is preferable and therefore D8 of HDCT should also be considered superior compared to D7 for all available amounts of < $0.2329 \cdot 10^9$ $CD34^+$ cells.

For all available amounts of $CD34^+$ cells ≥ 0.2329 the nadir concentrations needs to be weighted against the duration of grade 3 leukopenia and the physician in charge should decide on an individual basis. Taken to extremes of high amounts ($0.5698 \cdot 10^9$) of $CD34^+$ cells that might be available for retransfusion the difference in median nadir concentrations is $3.6 \cdot 10^7$ cells being lower for an ASCR on D8, compared to a approximately 2 d longer duration of grade three leukopenia for an ASCR on D7. The higher the amount of retransfused cells the higher the nadir concentrations on D7 and D8. Hence the physician in charge might decide in favour of duration of grade 3 leukopenia for available amounts of cells $\geq 0.2329 \cdot 10^9$ $CD34^+$ cells.

Limitations Regarding the recommendations, the following limitations should be considered: The investigated study population was rather small comprising only 17 patients and the study itself which was not designed to specifically investigate leukopenia or the optimal day for the ASCR. For example it was not reported, when the blood samples for the determination

of leukocyte concentrations had been taken which might influence some of the measurements as leukocyte concentrations underlie a circadian rhythm (5.5 - 7.5 $\cdot$ 10^9 cells/L[303]). It was not possible to integrate the G-CSF treatment into the model due to the homogeneous study population and the similar treatment of the patients. G-CSF influences the duration of leukopenia and therefore the time below grade 3 leukopenia.
With respect to the PK the active metabolite of thiotepa, TEPA was not taken into account. As stated in section 4.1.3 this might be of interest as TEPA is much longer present in the circulation compared to thiotepa although no myelotoxicity was, yet, associated with it[122]. Also, etoposide-catchol, an active metabolite of etoposide, was not considered as well. Lastly, the variability of the PK was not taken into account during simulations.
Nevertheless, the simulations enabled the quantification of the effect of the day of the ASCR and the amount of retransfused cells on nadir concentrations and the time below grade three leukopenia.

4.4 Project 4: Characterisation of the cytotoxic potency of chemotherapeutics

This project was divided in two parts. First a PD model was developed which enabled the estimation of EC_{50} values from *in vitro* data. In the second part an enhanced semi-mechanistic PK/PD model for myelosuppression was proposed which enabled the evaluation of clinical data and estimation of drug-specific parameters which were comparable to EC_{50} values obtained from analysis of *in vitro* data. The objective was to explore the possible use of *in vitro* data for the prediction of the myelosuppresive time course following chemotherapy.

4.4.1 Estimation of EC_{50} values from *in vitro* data

A sigmoidal E_{max} model best described the % SI data obtained from an MTT assay[218] which characterises the cytotoxic effect of compounds on viable cells. The data of all plates was first analysed simultaneously in NONMEM® which offers the advantage of estimating an inter-plate variability for each parameter implemented as an IIV. As only data from 3 plates were available for the present analysis, it was, unfortunately, not possible to estimate an IIV.
However, the use of NONMEM® for analysis of *in vitro* data in general offers some advantages: If absorption measurements need to be excluded, e.g. due to pipetting errors, unexplainable high measurements, impurities or other sources of random error, the plates can still be evaluated, as applying the population approach information from other plates can be

"borrowed". To characterise the parameters and their variances (interplate variability), first, a sufficient number of plates is necessary. Then, only few concentration-effect measurements are sufficient to describe the whole concentration-effect curve and estimate model parameters. This is of great interest if only limited volume of blood is available, e.g. if the cells are obtained from a single donor or patient. Analysing the sensitivity of cells from a single patient offers the possibility to determine the sensitivity of the cells for this specific patient in order to adjust the dose.

However, if only few plates are available and the variance of model parameters cannot be determined with sufficient precision evaluation of each plate individually is the better option in order to obtain valid and precise parameter estimates for each plate. The disadvantage is that plates for which many measurements need to be excluded cannot be evaluated any longer.

The prediction of a clinical outcome based on *in vitro* data by means of the population approach was investigated in 2007 by Quartino et al.[166] They predicted the clinical outcome for acute leukaemia based on few samples of tumour cells obtained from 179 patients. Due to the limited availability of tumour cells they applied the population approach for the estimation of EC_{50} values as it was only possible to obtain concentration effect measurements for one to few fixed concentrations. The work of Quartino et al. is a good example of how drug sensitivity of tumour cells towards chemotherapy can be predicted based on *in vitro* data resulting in drug and dose selection in clinical practice.

In the case of the MTT assay from which the data was obtained, buffy coats from different patients were pooled and enough cells were available for analysis. To support the evaluation of the assay a corresponding sigmoidal E_{max} model in the R software package *drc* was identified and the individual and simultaneous analysis in NONMEM® and R were compared. With the *drc* package in R a more easy to handle tool for the evaluation of the assay outcome was available and the parameter estimates from both programs were very similar. The resulting parameter estimate for EC_{50} of carboplatin for PBMCs was 248.0 μmol/L and 54 times higher compared to the 4.6 μmol/L (1.7 μg/mL) from a validated CFU-GM assay[270]. One reason might be the type of cells the assays were conducted with. For the MTT assay mononuclear cells from the peripheral blood were isolated which are more mature compared to the mononuclear cells from umbilical cord blood used in the CFU-GM assay. Hence, it is probable that the fraction of cells that shows a high proliferative activity and therefore is more sensitive towards the cytotoxic agent was smaller compared to the cells used in CFU-GM assay. Another explanation for this deviation probably lies in the isolation process of PBMCs. During the isolation the laboratory reported that the PBMC fraction contained a very high

amount of thrombocytes which could not be separated from the PBMCs. As thrombocytes are living cells they reduce MTT to formazan but are not proliferating and, hence, not as sensitive towards cytotoxic drugs. Due to a higher proportion of MTT being transformed to formazan the concentration effect curve is shifted to the right, resulting in higher EC_{50} values. Additionally, the MTT and the CFU-GM assay differ in the way cytotoxicity is assessed as the MTT assay measures cell death whereas the CFU assay only measures the inhibition of cell proliferation. However, the goal of this analysis was the establishment of a model to evaluate the % SI and to provide a tool which is less cost-intense and easier to handle compared to NONMEM®, which was successfully achieved. The disadvantage of the analysis in R is that interplate variability cannot be estimated and if samples from single patients need to be analysed the evaluation should preferably be done in NONMEM®, given a population model that was developed based on a sufficient amount of data and allowed for estimation of interplate variability.

4.4.2 Comparison of *in vitro* measures of cytotoxicity with estimates from an population analysis of clinical data

The model for myelosuppression was further enhanced as described in section 3.5.2. Comparable model structures describing a cell loss from the compartment of proliferating cells exist[127,137,296]. In 2000, Friberg et al.[127] published a model with cell loss from this compartment which was linked to the concentration of the drug via a linear model but the model did not consider cell proliferation nor its inhibition as cells were produced by a zero-order process. Pastor et al.[296] included the proliferation rate but the drug effect was incorporated into the model as a loss from the compartment of proliferating cells controlled by a linear function. The proposed model presented in section 3.5.2 included a proliferation rate constant k_{prol} and an additional cell kill rate. Both were linked to an E_{max} model which inhibited the proliferation and stimulated cell killing in the presence of a drug. To demonstrate the ability of the model to predict drug-specific parameters (EC_{50} values) from clinical investigations which are comparable to those obtained from *in vitro* assays the model was fit exemplarily to the data from a docetaxel study (section 3.5.3.1). The obtained value of 11.1 nM closely reflected the *in vitro* EC_{50} of 12.4 nM. Of course, the reparametrised model needs to be applied to a larger number of compounds. In case a correlation of the model-predicted and *in vitro* determined EC_{50} values can be established, *in vitro* EC_{50} could be used to predict neutropenia in reverse. Hence, assuming that myelosuppression is the dose-limiting adverse event of a

new compound dosing recommendations could be made based on *in vitro* EC_{50} values and system-specific parameters from the model for myelosuppression.

4.5 Project 5: Investigation of glycation processes throughout the lifespan of erythrocytes

The objective of the last project was to transfer the acquired knowledge on modelling of cell maturation processes to another application for cell lifespan investigations. Once physiological processes are understood and mathematically described they can be applied to other, physiologically similar, processes. In the case of the work presented in this thesis the same process which characterised the maturation of cells in the bone marrow can be used to describe the ageing of erythrocytes in the circulation. Knowledge generated during the modelling of an adverse event related to oncology can thus be transferred to a completely different therapeutic area, in this case diabetes mellitus type 2, in which similar physiological processes such as cell ageing and maturation characterise the underlying system.
HbA_{1c} is the proportion of glycated haemoglobin in the circulation and its formation depends on glucose concentrations in the blood. The process of glycation is non-enzymatic, irreversible under physiological conditions and, as such, a good surrogate marker for the surveillance of long-term glycaemic control in the blood. Hamrén et al.[186] proposed a model which mimics the ageing process of erythrocytes in the circulation once they are released from the bone marrow. The lifespan is described by a chain of transit compartments comparable to the ones applied in the model for myelosuppression (section 3.3) or the transit absorption model for the description of delay processes (section 3.2.3). In contrast to other lifespan models which assume an identical lifespan for all cells of one individual[142] the chain of transit compartments in the model by Hamrén et al. allows the lifespan of erythrocytes to vary within one individual patient. Moreover, it accounts for the fact that the fraction of glycated haemoglobin increases with increasing age of erythrocytes[304] by allowing for the glycation process taking place at each cell age, i.e. in each transit compartment. Other PK/PD models[184,185] have been proposed for the description of drug exposure and biomarkers in diabetes mellitus type 2 patients, but they did not explicitly account for the processes of cell ageing and glycation. The semi-mechanistic lifespan model by Hamrén et al.[186] was chosen as a basis for the investigations as it characterised the HbA_{1c} formation in a physiological way and allowed the investigation of the ageing process of erythrocytes similar to the maturation process of leukocyte progenitor cells in the bone marrow.

First the lifespan model by Hamrén et al.[186] was investigated but the description of HbA_{1c} profiles for some patients was not satisfactory and a second glycation pathway was introduced to the model. This idea was based on the knowledge that HbA_{1c} concentrations reflect the glycaemic control of the past 2-3 months resulting from FPG and PPG[196]. As a GLP-1 receptor agonist, lixisenatide has an influence on both pathways by - among other modes of action - enhancing beta cell function, increasing insulin secretion, suppressing glucagon and a delaying gastric emptying[195,200]. Hence, in the extended lifespan model, a second glycation pathway was taken into account. This pathway allowed for the inhibition of HbA_{1c} formation linking the second glycation rate constant of this new pathway (K_{GL2}) directly to lixisenatide concentrations via an inhibitory E_{max} model. As the inhibition of K_{GL2} was directly linked to lixisenatide concentration-time profiles the inhibitory drug effect was taken into account on a much shorter time scale for this glycation pathway, reflecting the short-term effect of PPG lowering without the need of taking actual data for this process into account. Knowing that HbA_{1c} formation depends on FPG and PPG the new, extended lifespan model allowed for the estimation of the contribution of the PPG glycation pathway without the need of data on actual insulin secretion or data from glucose challenge or tolerance tests.

Fixed-effects parameters The maximal effect describing the inhibition of K_{GL2} was fixed to 1 as an irreversible gylcation of haemoglobin can be assumed. Allowing for higher estimates for E_{max} resulted in negative values for K_{GL2} due to the way it was linked to the effect of lixisenatide ($K_{GL2} \cdot (1 - E_{\text{drug}}(t))$), reflecting a deglycation which was compensated by a higher estimate for K_{GL}. A deglycation of haemoglobin in diabetes mellitus type 2 patients with elevated glucose concentrations compared to a population not affected by diabetes mellitus is physiologically rather unlikely as the glycation process is nonenzymatic and near-proportional to the average glucose concentrations throughout the day[305]. The mechanism of the reversible or irreversible binding of glucose to haemoglobin has also been previously investigated by mathematical modelling[306–308] and was further explored by Ladyzynski et al.[309] who reported a better predictive ability of a model which described an irreversible reaction. This supports the fixation of E_{max} to 1 as for higher E_{max} the glycation got reversed as K_{GL2} became negative. The release rate K_{INH} for erythrocytes from the bone marrow was 1.1 g/L/d and the same as for the male part of the population reported by Hamrén et al. (1.1 g/L/d[186]) and comparable to the physiological value of 1.5 g/L/d reported in literature[186]. The estimated lifespan of 101 d was shorter than the previously published lifespan of 136 d[186] or the frequently cited 120 d[30]. However, in 2009 Kalicki et al.[256] analysed digitalised data from previous publi-

cations[178,186,310] with the lifespan model and estimated lifespans of 91.7, 75.4 and 91.8 d for different numbers of transit compartment which supports a lower estimate for the lifespan of erythrocytes. They reported an asymptotic curve for increasing lifespans with increasing numbers of transit compartment. For the data from Uehlinger et al.[310], the analysis by Kalicki et al. resulted in N=16 transit compartments and N=12 for the dataset previously published by Cohen et al.[178] Kalicki et al. also reanalysed the data by Hamrén et al.[186] and reported a number of 10 transit compartment and a lifespan of 87.5 d. This is in contrast to the previous findings of Hamrén et al. who reported a deterioration of the model fit for a deviation from the published four transit compartments and a lifespan of the erythrocytes of 136 d. However, Kalicki et al. introduced an additional destruction rate constant for the erythrocytes from each transit compartment which might explain the deviation.

The shorter lifespans estimated by Kalicki et al.[256] for the four studies they analysed might be explained by a reduction of the lifespan of erythrocytes due to high glucose concentrations which was previously reported in two studies[175,311] (see also section 1.6). Sayinalp et al.[312] on the other hand did not find any influence of poorly controlled diabetes on the lifespan of erythrocytes and Cohen at al. published a prolonged lifespan for patients with poorly controlled diabetes[178].

The nonlinear relation between FPG and HbA_{1c} was taken into account by introducing a power function linking FPG to K_{GL}. The exponent γ was 0.75 and very similar to the previously published 0.743[186]. This nonlinear relationship has been previously described[313] and might be due to the fact that FPG and average glucose concentrations throughout the day are not directly proportional[186], whereas average glucose and HbA_{1c} are approximately proportional to each other[305].

K_{GL} in the extended lifespan model was $1.2 \cdot 10^{-4}/(1 \cdot \text{mM})$, indicating that 0.12% of HbA_{1c} was glycated per day at FPG of 10 mmol/L. As K_{GL} characterises a chemical and not an enzymatic reaction its estimate is assumed to be more or less constant, as factors influencing this reaction are believed to vary little between patients. The estimate of K_{GL} in the lifespan model was $3.0 \cdot 10^{-4}$ /(1·mM) and higher than the previously reported $1.8 \cdot 10^{-4}/(1 \cdot \text{mM})$[186] as well as the estimated $1.2 \cdot 10^{-4}/(1 \cdot \text{mM})$ from the extended model. This might indicate that K_{GL} in the lifespan model was overestimated as it had to compensate for the lack of the second glycation pathway.

In the final model 50% (95% confidence interval: 43% - 59%) of the inhibition in glycation of haemoglobin under treatment with lixisenatide were due to the second pathway which can most probably be attributed to PPG. Previously, a contribution of PPG to the overall glycation

processes of 30% - 40% was reported[314] resembling the same order of magnitude for the contribution of this glycation pathway. Riddle et al.[315] demonstrated that targeting PPG in diabetes mellitus type 2 patients by treatment intensification with basal insulin reduced the relative contribution of basal hyperglycaemia from 76% - 80% to 32% - 42%. This finding also underlines the importance of the characterisation of the two glycation pathways in dependency of the respective drug and the adequate description of the contribution of both pathways to the overall formation of HbA_{1c} which can be done applying PK/PD modelling.
However, these findings should be discussed in context of the limitations of the model. In the final model two parameters, MRTE and γ, had to be fixed due to model stability and a correlation between K_{INH} and γ which could not be taken into account otherwise (section 3.6.2.1). Additionally, the ratio of K_{GL}:K_{GL2} changed for different initial estimates and favoured the FPG dependent pathway for decreasing values of the OFV. On the other hand, the precision of parameter estimates decreased with decreasing OFV, whereas the shrinkage increased. Hence, the final model presented in this thesis reflects a compromise between OFV and precision and shrinkage of parameter estimates.
One reason for the difficulties during parameter estimation might be that the dose of lixisenatide was constantly increased during the observed study period of 13 weeks, never reaching a steady state for a longer period of time. HbA_{1c} however changes on a much slower time scale (months instead of days). The presence of a steady state in the PK might facilitate the characterisation of the effect of lixisenatide on HbA_{1c} formation and the estimation of the parameters of the rather complex extended lifespan model.
The developed extended lifespan model is the first lifespan model which enables the differentiation and characterisation of two glycation pathways based on HbA_{1c} measurements, keeping the mentioned restrictions in parameter estimation in mind. Monnier et al.[314] and Woerle et al.[196] investigated the contribution of FPG and PPG by means of multiple linear regression and described an increasing contribution of PPG to HbA_{1c} formation with lower HbA_{1c} values. This might indicate that the contribution of FPG to the overall HbA_{1c} formation increases with progression of diabetes mellitus type 2 and most probably explains the high IIV in EC_{50} for K_{GL2}, reflecting the variable, remaining ability of the patients to secrete insulin due to different states of diabetes progression. Woerle et al.[196] reported that reduction and control of PPG was essential for achieving $HbA_{1c} < 7\%$ or $< 6.5\%$ and that the treatment and monitoring of postprandial hyperglycaemia is essential for glycaemic control. Thus, the quantification of the contribution of the additional, possibly PPG related, glycation pathway to the

overall glycation of haemoglobin under treatment with lixisenatide is of great interest when characterising the effect of antidiabetic drugs.

5 Conclusion and perspectives

The overall objective of this thesis was to contribute to the understanding and characterisation of proliferation and maturation as well as ageing processes of different blood cell lines in the bone marrow and the circulation, respectively. Semi-mechanistic population PK/PD models were used to characterise the system of leukopoiesis, to describe the adverse drug reaction of myelosuppression in a HDCT regimen as well as to investigate cell ageing of erythrocytes in the circulation and to describe the contribution of FPG and PPG to the glycation of haemoglobin. As the developed models allowed to differentiate between parameters describing the system and those associated with the drugs' effect, it was possible to investigate the implementation of the drug effect, explore possible drug-drug interactions and add to the understanding of the mode of action of the drugs. Overall, the impact of pharmacometric PK/PD modelling for the characterisation of dose-concentration-effect relations was shown, applying the approach to different therapeutic areas as well as *in vitro* data. The developed models contributed to the understanding of (patho-)physiological processes and can be used to support the planning of future clinical studies and guide the optimisation of therapy regimens in oncology as well as diabetes mellitus type 2. In the following, conclusions and perspectives for Project 1, 2 and 3 ("Leukopenia following HDCT"), Project 4 ("Characterising cytotoxic potencies") and Project 5 ("Glycation of erythrocytes throughout their lifespan") are presented:

Leukopenia following HDCT Myelosuppression is one of the most important dose-limiting adverse drug events in many anti-cancer regimens. Previously, many population PK/PD analyses described myelosuppression following conventional chemotherapy. Only one incorporated the performance of an ASCR[147], however it neglected the PK of the drugs. The final PK/PD model presented in this thesis is the first model which characterises the system of leukopoiesis in the setting of HDCT including ASCR and taking the PK of each drug of the combination regimen into account. The PK of ultrafilterable Pt, etoposide and thiotepa was successfully described by a linear two compartment models with first-order elimination from the central compartment. For carboplatin, two covariates, i.e. creatinine clearance and body weight, were identified and the delay in occurrence of thiotepa concentrations in the plasma was described by a transit compartment model. Individual PK parameters were determined and used as input for the population PK/PD model for the description of the time course

of leukopenia. The final model for myelosuppression following HDCT incorporated the retransfusion of $CD34^+$ cells and allowed for the description of the initial increase which was observed for leukocyte concentrations during the first few days of therapy. All drugs were implemented as a linear model with inhibitory effect on the proliferation rate constant of the cells in the bone marrow, assuming an additive drug effect. Although not statistically significant, the analysis indicated a possible synergistic effect of carboplatin and etoposide.
Simulations based on the final model were conducted to characterise the influence of the day on which the ASCR was performed and the amount of retransfused $CD34^+$ cells on leukocyte nadir and the duration of grade 3 leukopenia, both related to a high risk for developing serious infections. Regarding the duration of grade 3 leukopenia, the best day for the performance of an ASCR was on day 8 of the HDCT regimen. For patients receiving $\leq 0.2329 \cdot 10^9$ $CD34^+$ cells, day 8 is also favourable with respect to nadir concentrations, whereas for patients receiving higher amounts, the shorter time below grade 3 leukopenia for an ASCR on day 8 needs to be weighted against higher nadir concentrations for an ASCR on day 7 of HDCT with regard to their associated risk for infections.
To further evaluate the findings of this modelling and simulation project, analysis of more data from larger, more heterogeneous study populations with respect to inclusion criteria, dosing schedule of the chemotherapeutics and G-CSF administration would be desirable to gain further insight into the drug effects, possible interactions and the myelosupportive treatment. Additional data on retransfusion of $CD34^+$ and CFU cells as well as on different schedules for the performance of the ASCR would be very important to enable a more differentiated description and integration of the ASCR. Nevertheless, the developed model and especially the systematic investigations regarding the system describing leukopenia and the drug effects are very useful and provide a good basis for further investigations. Moreover, first systematic investigations regarding the ASCR were conducted and show that considering the entire concentration-effect relation is very important and should be preferred over the current state of the art (a pure consideration of the PK of the drugs) when planning the optimal use of myelosupportive treatment in HDCT.

Characterising cytotoxic potencies The characterisation of the influence of the supportive treatment on the impaired system of leukopoiesis was shown to be very important. However, the description of the drug effect is just as relevant. *In vitro* and *in silico* investigations can be applied to assess the desired drug effects and adverse drug reactions of combination therapies as well as different schedules for drug administration and, hence, possible schedule-

dependencies of the drug effects. Besides the desired effects of tumour destruction or inhibition of tumour growth, information on cytotoxicity and the potential severity of adverse drug reactions in human are important to guide candidate selection during drug development or make dose recommendations for first use in man.
For the description of the cytotoxic potential of compounds, data from an *in vitro* assay was analysed applying different PD models to characterise the survival index of PBMCs. A sigmoidal E_{max} model best described the data and a comparable model in the R software package was identified to provide a tool for everyday work in the experimental cell culture laboratory which is easier to handle and less cost intense than the analysis in NONMEM®. In this context the advantage of applying the population approach for analysis of blood samples from a single patient with restricted volume was discussed as the implementation of an interplate variability can support the analysis of only few drug concentrations per sample.
Additionally, an enhanced semi-mechanistic model for the description of myelosuppression was proposed which was suitable for the evaluation of clinical data and enabled the estimation of EC_{50} values which were comparable to EC_{50} values obtained from *in vitro* data. A study conducted in patients receiving docetaxel as a monotherapeutic treatment was used to exemplify the predictive performance of the new model and showed comparable EC_{50} values, whilst the overall quality of the description of the data was unchanged despite the changes introduced to the model structure. These changes comprised the introduction of a cell kill rate constant for the proliferating cells in the bone marrow and the implementation of an inhibitory and stimulatory E_{max} model for the proliferation rate constant and the new cell kill constant, respectively. To validate the predictive performance of the model and the overall approach, more myelotoxic drugs need to be investigated to prove a possible correlation between *in vitro* and model-predicted EC_{50} values. If a correlation can be established, model parameters specific for the system of haematopoiesis in combination with information from *in vitro* assays and PK profiles, e.g. scaled from animal studies or predicted applying physiological based modelling, can be used to predict entire time profiles for myelosuppression and guide dose recommendations for the first use in man.

Glycation of erythrocytes throughout their lifespan Following the principle of delay modelling by transit compartments, which was also used in this thesis to characterise maturation processes of haematopoietic progenitor cells and to describe the delay in the occurrence of thiotepa in the plasma, Hamrén et al. developed a model to investigate glycation processes of haemoglobin throughout the lifespan of erythrocytes[186]. The longer erythrocytes are in

the circulation, the higher is the degree to which haemoglobin is glycated. This knowledge and the irreversible character of the glycation process enabled the estimation of the lifespan of erythrocytes by describing the change of HbA_{1c} in a population of diabetes mellitus type 2 patients. Moreover, the extended model presented in this thesis allowed for the separation of two glycation pathways: one describing glycation due to fasting plasma glucose and one most probably reflecting the glycation of haemoglobin by postprandial plasma glucose concentrations. The inhibitory effect of lixisenatide on both pathways was assessed showing an equal inhibition of both pathways with respect to the overall glycation. Decreasing postprandial glucose concentrations was shown to be especially important to achieve HbA_{1c} values below 6.5% - 7%[196]. Hence, the possibility of characterising the inhibition of both glycation pathways as well as the quantification of the drug effect by population PK/PD modelling can add to the understanding of the mode of action of anti-diabetic drugs and might be useful in developing more effective therapy regimens.

6 Abstract / Zusammenfassung

Abstract

The objective of this thesis was to contribute to the understanding and characterisation of proliferation, maturation and ageing processes of haematopoietic progenitor and blood cells applying the population pharmacokinetic/pharmacodynamic (PK/PD) approach. Impairment and damage of proliferation and maturation of leukocyte progenitor cells in the bone marrow was investigated based on data from a clinical investigation in patients receiving a combination high-dose chemotherapy (HDCT) regimen comprising an autologuous stem cell rescue (ASCR). In Project 1, population PK models for carboplatin, etoposide and thiotepa were developed and individual PK parameter estimates for each drug were utilised to serve as input into a previously published semi-mechanistic population PK/PD model for myelosuppression[138]. This model was adjusted and further extended to account for the special setting of HDCT (Project 2). The implementation of the drugs' effects and possible drug-drug interactions were explored and the ASCR was integrated into the model. Additionally, concomitant medication influencing the time course of leukopenia was taken into account to describe all observed phases, i.e. an initial increase in leukocyte concentrations most probably attributed to the administration of dexamethasone, followed by a steep decrease caused by the high doses of the cytotoxic drugs and a fast recovery with a pronounced rebound due to ASCR and additional administration of granulocyte colony-stimulating factor.

Based on the final PK/PD model, simulations were conducted (Project 3) to investigate the optimal day for the performance of the ASCR with respect to nadir and time below (at least) grade 3 leukopenia, as both are associated with the development of serious infections. The simulations showed that not only the day on which the ASCR was performed but also the amount of retransfused $CD34^+$ cells influenced both parameters. Recommendations for planning of the myelosupportive treatment were derived.

The drug effect was further explored in Project 4, in which different PD models for the description of data from an *in vitro* cytotoxicity assay were investigated. Furthermore, a model for myelosuppression which enabled the estimation of EC_{50} values from clinical data that were comparable to those obtained from *in vitro* assays was proposed. This model might prove useful when, in return, *in vitro* data is used to predict myelosuppression in patients.

In Project 5, an existing lifespan model[186] for the description of glycated haemoglobin (HbA_{1c}),

a long-term biomarker in diabetes mellitus type 2 patients, which incorporates the ageing process of erythrocytes, was extended to describe the influence of a new drug on fasting and postprandial plasma glucose.

All developed semi-mechanistic models contributed to the deeper understanding of (patho-) physiological processes involved in cell proliferation and maturation as well as the characterisation of the systems of leukopoiesis, erythrocyte ageing and HbA_{1c} formation. In future, the models can be used to scientifically interpret clinical results, guide the planning of clinical studies and improve existing and future therapy regimens in the indications of oncology and diabetes mellitus type 2.

Zusammenfassung

Ziel dieser Arbeit war, unter Verwendung des populationsbasierten pharmakokinetischen/ pharmakodynamischen (PK/PD) Modellierungsansatzes zu einem tieferen Verständnis und der besseren Charakterisierung von Proliferations-, Reifungs- und Alterungsprozessen verschiedener Blutzelllinien beizutragen. Basierend auf Daten, die im Rahmen einer klinischen Untersuchung "Hochdosis-Chemotherapie mit anschließender autologer Stammzellretransfusion in Hodentumorpatienten" erhoben wurden, wurde die Beeinträchtigung und Schädigung der Zellproliferation und -reifung von hämatopoietischen Vorläuferzellen aus dem Knochenmark untersucht. Hierfür wurden in Projekt 1 PK Modelle für die Beschreibung der Plasmakonzentrationen von Carboplatin, Etoposid und Thiotepa entwickelt, individuelle pharmakokinetische Parameter geschätzt und diese in ein PK/PD Modell zur Beschreibung der Myelosuppression nach einer Chemotherapie[138] implementiert. Dieses Modell wurde dahingehend erweitert, dass es der besonderen Situation eines Hochdosis-Chemotherapieregimes gerecht wurde (Projekt 2). Verschiedene Möglichkeiten der Implementierung der Arzneistoffeffekte auf die proliferierenden Zellen im Knochenmark und eine mögliche Interaktion der Arzneistoffe wurden untersucht und der Prozess der autologen Retransfusion von Stammzellen erfolgreich in das Modell integriert. Des Weiteren wurde der Einfluss der verabreichten Komedikation auf den Verlauf der Leukopenie untersucht und gegebenenfalls im Modell berücksichtigt. Der typische Verlauf der Leukopenie in der untersuchten Population war durch einen initialen Anstieg der Leukozytenkonzentrationen, der wahrscheinlich auf die Applikation von Dexamethason zurückzuführen war, gekennzeichnet. Daran anschließend war ein steiler Abfall der Leukozytenkonzentration zu beobachten, welcher auf die hohe Dosis der Arzneistoffe zurückzuführen war, gefolgt von einer schnellen Erholung hin zu physiologischen Leukozytenkonzentrationen. Diese war gekennzeichnet durch ein deutliches Überschießen der Leukozytenkonzentrationen auf Grund eines Rebound-Effekts der u.a. in der autologen Stammzellretransfusion und der Applikation von Granulozyten Kolonie stimulierendem Faktor begründet war.
Basierend auf dem finalen PK/PD Modell wurden Simulationen durchgeführt, mittels derer der bestmögliche Tag für die Durchführung der autologen Stammzellretransfusion untersucht wurde (Projekt 3). Für die Bewertung wurden der Nadir und die Dauer einer Leukopenie (mindestens) dritten Grades herangezogen, da beide mit dem Auftreten von schwerwiegenden Infektionen in Zusammenhang stehen. Die Simulationen zeigten, dass nicht nur der Tag an dem die Retransfusion stattfand, sondern auch die Anzahl an retransfundierten $CD34^+$ Zellen einen Einfluss auf den Nadir und die Dauer der Leukopenie hatten und beide bei der

Planung der Durchführung einer autologen Stammzellretransfusion berücksichtigt werden sollten.
Der Effekt von zytotoxischen Wirkstoffen auf das Überleben von peripheren Mononukleären Zellen wurde in Projekt 4 anhand von *In-vitro* Daten charakterisiert. Hierfür wurden verschiedene PD Modelle für die Beschreibung des zytotoxischen Effekts untersucht. In einem weiteren Teilprojekt wurde ein Modell für die Abschätzung von EC_{50} Werten, basierend auf Neutrophilenkonzentrationen entwickelt, die im Rahmen einer klinischen Studie in Krebspatienten erhoben wurden. Dieses Modell ermöglichte die Abschätzung von EC_{50} Werten, die vergleichbar mit denen aus *In-vitro* Assays waren. Künftig könnte dieses Modell dazu genutzt werden, den Verlauf einer Myelosuppression in Patienten basierend auf *In-vitro* Daten vorherzusagen.
In Projekt 5 wurde ein Modell zur Beschreibung von glykiertem Hämoglobin (HbA_{1c}) in Patienten mit Diabetes mellitus Typ 2[186] untersucht, welches die Abschätzung der Lebensdauer von Erythrozyten in der Zirkulation ermöglicht. Das Modell wurde dahingehend erweitert, dass der Einfluss eines neuen Arzneistoffs auf Nüchtern und Postprandiale Glukosekonzentrationen im Plasma und deren Beitrag zur Inhibition der Bildung von HbA_{1c} beschrieben werden konnte.
Die Entwicklung der semi-mechanistischen Modelle konnte zu einem tieferen Verständnis von (patho-)physiologischen Vorgängen, die in der Zellproliferation und -reifung eine Rolle spielen, sowie zur Beschreibung der Lebensdauer von Zellen in der Zirkulation beitragen und die physiologischen Vorgänge der Leukopoiese unter Hochdosis-Chemotherapie und der HbA_{1c}-Bildung beschreiben. Die entwickelten Modelle können dazu beitragen, Ergebnisse klinischer Studien oder Messungen aus dem klinischen Alltag wissenschaftlich zu interpretieren, die Planung von klinischen Studien zu unterstützen und bereits bestehende oder künftige Therapieregime sowohl in der Hochdosis-Chemotherapie als auch in der Therapie von Diabetes mellitus Typ 2 zu verbessern.

7 Bibliography

[1] T. Teorell. Kinetics of distribution of substances administered to the body I. The extravascular modes of administration. *Arch Int Pharmacodyn Ther*, 57:205–225, 1937.

[2] T. Teorell. Studies on the diffusion effect upon ionic distribution: II. Experiments on ionic accumulation. *J Gen Physiol*, 21:107–22, 1937.

[3] F. H. Dost. *Der Blutspiegel - Kinetik der Konzentrationsabläufe in der Kreislaufflüssigkeit*. Thieme, Leipzig, 1953.

[4] E. Nelson. Kinetics of drug absorption, distribution, metabolism, and excretion. *J Pharm Sci*, 50:181–192, 1961.

[5] Peter L. Bonate. *Pharmacokinetic-pharmacodynamic modelling and simulation*. Springer, New York, second edi edition, 2011.

[6] P. Lees, F. M. Cunningham, and J. Elliott. Principles of pharmacodynamics and their applications in veterinary pharmacology. *J Vet Pharmacol Ther*, 27:397–414, 2004.

[7] N. H. G. Holford and L. B. Sheiner. Kinetics of pharmacologic response. *Pharmac Ther Vol*, 16:143–66, 1982.

[8] J. J. DiStefano and E. M. Landaw. Multiexponential, multicompartmental, and noncompartmental modeling. I. Methodological limitations and physiological interpretations. *Am J Physiol*, 246:R651–64, 1984.

[9] E. I. Ette and P. Williams. *Pharmacometrics: The Science of Quantitative Pharmacology*. John Wiley & Sons, 2010.

[10] S. B. Duffull, D. F. B. Wright, and H. R. Winter. Interpreting population pharmacokinetic-pharmacodynamic analyses - a clinical viewpoint. *Br J Clin Pharmacol*, 71:807–14, 2011.

[11] J. L. Steimer, A. Mallet, J. L. Golmard, and J. F. Boisvieux. Alternative approaches to estimation of population pharmacokinetic parameters: comparison with the nonlinear mixed-effect model. *Drug Metab Rev*, 15:265–92, 1984.

[12] L. B. Sheiner and S. L. Beal. Evaluation of methods for estimating population pharmacokinetics parameters. I. Michaelis-Menten model: routine clinical pharmacokinetic data. *J Pharmacokinet Biopharm*, 8:553–71, 1980.

[13] L. B. Sheiner and S. L. Beal. Evaluation of methods for estimating population pharmacokinetic parameters. II. Biexponential model and experimental pharmacokinetic data. *J Pharmacokinet Biopharm*, 9:635–51, 1981.

[14] H. Sun, E. O. Fadiran, C. D. Jones, L. Lesko, S. M. Huang, K. Higgins, C. Hu, S. Machado, S. Maldonado, R. Williams, M. Hossain, and E. I. Ette. Population pharmacokinetics. A regulatory perspective. *Clin Pharmacokinet*, 37:41–58, 1999.

[15] J. Aldrich. R.A. Fisher and the making of maximum likelihood 1912-1922. *Stat Sci*, 12: 162–176, 1997.

[16] L. B. Sheiner and S. L. Beal. Evaluation of methods for estimating population pharmacokinetic parameters. III. Monoexponential model: routine clinical pharmacokinetic data. *J Pharmacokinet Biopharm*, 11:303–19, 1983.

[17] L. Aarons. Population pharmacokinetics: theory and practice. *Br J Clin Pharmacol*, 32: 669–70, 1991.

[18] L. B. Sheiner. Learning versus confirming in clinical drug development. *Clin Pharmacol Ther*, 61:275–91, 1997.

[19] A. S. Zandvliet, J. H. M. Schellens, J. H. Beijnen, and A. D. R. Huitema. Population pharmacokinetics and pharmacodynamics for treatment optimization in clinical oncology. *Clin Pharmacokinet*, 47:487–513, 2008.

[20] L. E. Friberg and M. O. Karlsson. Mechanistic models for myelosuppression. *Invest New Drugs*, 21:183–94, 2003.

[21] A. Pessina, I. Malerba, and L. Gribaldo. Hematotoxicity testing by cell clonogenic assay in drug development and preclinical trials. *Curr Pharm Des*, 11:1055–65, 2005.

[22] M. Ogawa. Differentiation and proliferation of hematopoietic stem cells. *Blood*, 81:2844–53, 1993.

[23] S. J. Morrison, N. M. Shah, and D. J. Anderson. Regulatory mechanisms in stem cell biology. *Cell*, 88:287–98, 1997.

[24] D. J. Laird, U. H. von Andrian, and A. J. Wagers. Stem cell trafficking in tissue development, growth, and disease. *Cell*, 132:612–30, 2008.

[25] G. E. Cartwright, J. W. Athens, and Wintrobe M. M. The kinetics of granulopoiesis in normal man. *Blood*, 24:780–803, 1964.

[26] T. Suwa, J. C. Hogg, D. English, and S. F. Van Eeden. Interleukin-6 induces demargination of intravascular neutrophils and shortens their transit in marrow. *Am J Physiol Heart Circ Physiol*, 279:H2954–60, 2000.

[27] M. J. Egorin, D. A. Van Echo, M. Y. Whitacre, A. Forrest, L. M. Sigman, K. L. Engisch, and J. Aisner. Human pharmacokinetics, excretion, and metabolism of the anthracycline antibiotic menogaril (7-OMEN, NSC 269148) and their correlation with clinical toxicities. *Cancer Res*, 46:1513–20, 1986.

[28] H. Theml. *Taschenatlas der Hämatologie*. Thieme Verlag, Stuttgart - New York, 4 edition, 1998.

[29] F. Pierigè, S. Serafini, L. Rossi, and M. Magnani. Cell-based drug delivery. *Adv Drug Deliv Rev*, 60:286–95, 2008.

[30] A. Kruse, D. E. Uehlinger, F. Gotch, P. Kotanko, and N. W. Levin. Red blood cell lifespan, erythropoiesis and hemoglobin control. *Contrib Nephrol*, 161:247–54, 2008.

[31] http://www.who.int/cancer/en, last accessed: 20.08.2012.

[32] Krebs in Deutschland 2007-2008. Technical report, Robert-Koch-Institut, Gesellschaft der epidemiologischen Krebsregister in Deutschland e. V., Berlin, 2012.

[33] W Wilmanns; D Huhn; K Wilms, editor. *Internistische Onkologie*. Georg Thieme Verlag, Stuttgart, 1994.

[34] E. Frei. Curative cancer chemotherapy. *Cancer Res*, 45:6523–37, 1985.

[35] K. Wheatley, A. K. Burnett, A. H. Goldstone, R. G. Gray, I. M. Hann, C. J. Harrison, J. K. Rees, R. F. Stevens, and H. Walker. A simple, robust, validated and highly predictive index for the determination of risk-directed therapy in acute myeloid leukaemia derived from the MRC AML 10 trial. United Kingdom Medical Research Council's Adult and Childhood Leukaemia Working Parties. *Br J Haematol*, 107:69–79, 1999.

[36] D. R. Newell. Can pharmacokinetic and pharmacodynamic studies improve cancer chemotherapy? *Ann Oncol*, 5 Suppl 4:9–14; discussion 15, 1994.

[37] E. Masson and W. C. Zamboni. Pharmacokinetic optimisation of cancer chemotherapy. Effect on outcomes. *Clin Pharmacokinet*, 32:324–43, 1997.

[38] H. D. Mannuel, N. Mitikiri, M. Khan, and A. Hussain. Testicular germ cell tumors: biology and clinical update. *Curr Opin Oncol*, 24:266–71, 2012.

[39] S. D. Williams, R. Birch, L. H. Einhorn, L. Irwin, F. A. Greco, and P. J. Loehrer. Treatment of disseminated germ-cell tumors with cisplatin, bleomycin, and either vinblastine or etoposide. *N Engl J Med*, 316:1435–40, 1987.

[40] S. Hinton, P. J. Catalano, L. H. Einhorn, C. R. Nichols, E. David Crawford, N. Vogelzang, D. Trump, and P. J. Loehrer. Cisplatin, etoposide and either bleomycin or ifosfamide in the treatment of disseminated germ cell tumors: final analysis of an intergroup trial. *Cancer*, 97:1869–75, 2003.

[41] G. V. Kondagunta, J. Bacik, A. Donadio, D. Bajorin, S. Marion, J. Sheinfeld, G. J. Bosl, and R. J. Motzer. Combination of paclitaxel, ifosfamide, and cisplatin is an effective second-line therapy for patients with relapsed testicular germ cell tumors. *J Clin Oncol*, 23:6549–55, 2005.

[42] P. J. Loehrer, L. H. Einhorn, and S. D. Williams. VP-16 plus ifosfamide plus cisplatin as salvage therapy in refractory germ cell cancer. *J Clin Oncol*, 4:528–36, 1986.

[43] M. H. Voss, D. R. Feldman, and R. J. Motzer. High-dose chemotherapy and stem cell transplantation for advanced testicular cancer. *Expert Rev Anticanc*, 11:1091–103, 2011.

[44] S. Rodenhuis, A. Westermann, M. J. Holtkamp, W. J. Nooijen, J. W. Baars, E. van der Wall, I. C. Slaper-Cortenbach, and J. H. Schornagel. Feasibility of multiple courses of high-dose cyclophosphamide, thiotepa, and carboplatin for breast cancer or germ cell cancer. *J Clin Oncol*, 14:1473–83, 1996.

[45] A. D. Elias, L. J. Ayash, C. Wheeler, G. Schwartz, I. Tepler, M. McCauley, R. Mazanet, L. Schnipper, E. Frei, and K. H. Antman. High-dose ifosfamide/carboplatin/etoposide with autologous hematopoietic stem cell support: safety and future directions. *Semin Oncol*, 21:83–5, 1994.

[46] C. Kollmannsberger and C. Bokemeyer. Salvage chemotherapy after failure of first-line chemotherapy in patients with metastatic testicular cancer. *Curr Opin Support Palliat Care*, 2:167–72, 2008.

[47] Dose-intensive chemotherapy in refractory germ cell cancer–a phase I/II trial of high-dose carboplatin and etoposide with autologous bone marrow transplantation. *J Clin Oncol*, 7:932–9, 1989.

[48] A. Lorch, P. Albers, C. Winter, and J. Beyer. [High-dose chemotherapy and residual tumor resection in male germ cell tumors]. *Urologe*, 50:1047–54, 2011.

[49] J. Beyer, W. Siegert, and O. Rick. Salvage-Therapie von Patienten mit Hodentumoren und Rezidiv oder inkomplettem Ansprechen auf Primärbehandlung. *Der Onkologe*, 9: 997–1003, 2003.

[50] E. Frei and G. P. Canellos. Dose: a critical factor in cancer chemotherapy. *Am J Med*, 69: 585–94, 1980.

[51] C. Bokemeyer. Hochdosis-Chemotherapie - Neue Chancen und Risiken in der Onkologie. *Arzneimitteltherapie*, 15:237– 245, 1997.

[52] W. Brugger, R. Birken, H. Bertz, T. Hecht, K. Pressler, J. Frisch, G. Schulz, R. Mertelsmann, and L. Kanz. Peripheral blood progenitor cells mobilized by chemotherapy plus granulocyte-colony stimulating factor accelerate both neutrophil and platelet recovery after high-dose VP16, ifosfamide and cisplatin. *Br J Haematol*, 84:402–7, 1993.

[53] N. Neymark and G. Rosti. Patient management strategies and transplantation techniques in european stem cell transplantation centers offering breast cancer patients high-dose chemotherapy with peripheral blood stem cell support: a joint report from the EORTC and EBMT. *Haematologica*, 85:733–44, 2000.

[54] J. Beyer, A. Kramar, R. Mandanas, W. Linkesch, A. Greinix, J. P. Droz, J. L. Pico, a Diehl, C. Bokemeyer, H. J. Schmoll, C. R. Nichols, L. H. Einhorn, and W. Siegert. High-dose chemotherapy as salvage treatment in germ cell tumors: a multivariate analysis of prognostic variables. *J Clin Oncol*, 14:2638–45, 1996.

[55] J.-L. Pico, G. Rosti, A. Kramar, H. Wandt, V. Koza, R. Salvioni, C. Theodore, G. Lelli, W. Siegert, A. Horwich, M. Marangolo, W. Linkesch, G. Pizzocaro, H.-J. Schmoll, J. Bouzy, J.-P. Droz, and P. Biron. A randomised trial of high-dose chemotherapy in

the salvage treatment of patients failing first-line platinum chemotherapy for advanced germ cell tumours. *Ann Oncol*, 16:1152–9, 2005.

[56] C.F. Waller. Blutsatmmzellen. *Arzneimitteltherapie1*, 15:246–250, 1997.

[57] C. H. Weaver, B. Hazelton, R. Birch, P. Palmer, C. Allen, L. Schwartzberg, and W. West. An analysis of engraftment kinetics as a function of the CD34 content of peripheral blood progenitor cell collections in 692 patients after the administration of myeloablative chemotherapy. *Blood*, 86:3961–9, 1995.

[58] T. R. Klumpp, K. F. Mangan, S. L. Goldberg, E. S. Pearlman, and J. S. Macdonald. Granulocyte colony-stimulating factor accelerates neutrophil engraftment following peripheral-blood stem-cell transplantation: a prospective, randomized trial. *J Clin Oncol*, 13:1323–7, 1995.

[59] G. Morstyn, G. J. Lieschke, W. Sheridan, J. Layton, and J. Cebon. Pharmacology of the colony-stimulating factors. *Trends Pharmacol Sci*, 10:154–9, 1989.

[60] U. Dührsen, J. L. Villeval, J. Boyd, G. Kannourakis, G. Morstyn, and D. Metcalf. Effects of recombinant human granulocyte colony-stimulating factor on hematopoietic progenitor cells in cancer patients. *Blood*, 72:2074–81, 1988.

[61] W. P. Sheridan, C. G. Begley, C. A. Juttner, J. Szer, L. B. To, D. Maher, K. M. McGrath, G. Morstyn, and R. M. Fox. Effect of peripheral-blood progenitor cells mobilised by filgrastim (G-CSF) on platelet recovery after high-dose chemotherapy. *Lancet*, 339:640–4, 1992.

[62] P. Anderlini, D. Przepiorka, R. Champlin, and M. Körbling. Biologic and clinical effects of granulocyte colony-stimulating factor in normal individuals. *Blood*, 88:2819–25, 1996.

[63] B. I. Lord, L. B. Woolford, and G. Molineux. Kinetics of neutrophil production in normal and neutropenic animals during the response to filgrastim (r-metHu G-CSF) or filgrastim SD/01 (PEG-r-metHu G-CSF). *Clin Cancer Res*, 7:2085–90, 2001.

[64] T. H. Price, G. S. Chatta, and D. C. Dale. Effect of recombinant granulocyte colony-stimulating factor on neutrophil kinetics in normal young and elderly humans. *Blood*, 88:335–40, 1996.

[65] G. T. Williams, C. A. Smith, E. Spooncer, T. M. Dexter, and D. R. Taylor. Haemopoietic colony stimulating factors promote cell survival by suppressing apoptosis. *Nature*, 343 (6253):76–9, 1990.

[66] B. I. Lord, M. H. Bronchud, S. Owens, J. Chang, A. Howell, L. Souza, and T. M. Dexter. The kinetics of human granulopoiesis following treatment with granulocyte colony-stimulating factor in vivo. *Proc Natl Acad Sci USA*, 86:9499–503, 1989.

[67] Human CD34(+) bone marrow cells regulate stromal production of interleukin-6 and granulocyte colony-stimulating factor and increase the colony-stimulating activity of stroma. *Blood*, 91:3724–33, 1998.

[68] S. G. Ericson, H. Gao, G. H. Gericke, and L. D. Lewis. The role of polymorphonuclear neutrophils (PMNs) in clearance of granulocyte colony-stimulating factor (G-CSF) in vivo and in vitro. *Exp Hematol*, 25:1313–25, 1997.

[69] H. Takatani, H. Soda, M. Fukuda, M. Watanabe, A. Kinoshita, T. Nakamura, and M. Oka. Levels of recombinant human granulocyte colony-stimulating factor in serum are inversely correlated with circulating neutrophil counts. *Antimicrob Agents Chemother*, 40: 988–91, 1996.

[70] J. M. Mishler and P. M. Emerson. Development of neutrophilia by serially increasing doses of dexamethasone. *Br J Haematol*, 36:249–57, 1977.

[71] A. Ciancetta, C. Coletti, A.lessandro Marrone, and N. Re. Activation of carboplatin by chloride ions: a theoretical investigation. *Theor Chem Acc*, 129:757–769, 2011.

[72] U. Frey, J. D. Ranford, and P. J. Sadler. Ring-opening reactions of the anticancer drug carboplatin : NMR characterization of cis- [Pt (NHj) z (CBDCA-O)(5 ′ -GMP-N7)] in solution. *Inorg Chem*, 32:1333–1340, 1993.

[73] K. J. Barnham, M. I. Djuran, P. del S. Murdoch, J. D. Ranford, and P. J. Sadler. Ring-opened adducts of the anticancer drug carboplatin with sulfur amino acids. *Inorg Chem*, 35:1065–1072, 1996.

[74] O. Brett, S. Serrano, T. Macedo, D. Raimundo, H. Marques, and M. La-Scalea. Electrochemical determination of carboplatin in serum using a DNA-modified glassy carbon electrode. *Electroanalysis*, 8:992–995, 1996.

[75] R. C. Todd and S. J. Lippard. Inhibition of transcription by platinum antitumor compounds. *Metallomics*, 1:280–91, 2009.

[76] A. H. Calvert, D. R. Newell, L. A. Gumbrell, S. O'Reilly, M. Burnell, F. E. Boxall, Z. H. Siddik, I. R. Judson, M. E. Gore, and E. Wiltshaw. Carboplatin dosage: prospective evaluation of a simple formula based on renal function. *J Clin Oncol*, 7:1748–56, 1989.

[77] C. Kloft, W. Siegert, and U. Jaehde. Individualised dosing strategy for high-dose carboplatin in patients with germ cell cancer. *Br J Cancer*, 89:787–94, 2003.

[78] T. C. Shea, M. Flaherty, A. Elias, J. P. Eder, K. Antman, L. Begg, C .and Schnipper, E. Frei, and W. D. Henner. A phase I clinical and pharmacokinetic study of carboplatin and autologous bone marrow support. *J Clin Oncol*, 7:651–61, 1989.

[79] C. Kloft. *Klinisch-pharmakokinetische und pharmakodynamische Untersuchungen zur Dosierungsoptimierung von Platinkomplexen*. Dissertation, Freie Universität Berlin, 1997.

[80] A. K. Holzer, G. Samimi, K. Katano, W. Naerdemann, X. Lin, R. Safaei, and S. B. Howell. The copper influx transporter human copper transport protein 1 regulates the uptake of cisplatin in human ovarian carcinoma cells. 66:817–823, 2004.

[81] A. Láznícková, M. Láznícek, J. Květina, and J. Drobník. Pharmacokinetics and plasma protein binding of two platinum cytostatics CHIP and CBDCA in rats. *Cancer Chemother and Pharmacol*, 17:133–6, 1986.

[82] W. J. van der Vijgh and I. Klein. Protein binding of five platinum compounds. Comparison of two ultrafiltration systems. *Cancer Chemother Pharmacol*, 18(2):129–32, 1986.

[83] D. R. Newell, Z. H. Siddik, L. A. Gumbrell, F. E. Boxall, M. E. Gore, I. E. Smith, and A. H. Calvert. Plasma free platinum pharmacokinetics in patients treated with high dose carboplatin. *Eur J Canc Clin Oncol*, 23:1399–405, 1987.

[84] H. Calvert, I. Judson, and W. J. van der Vijgh. Platinum complexes in cancer medicine: pharmacokinetics and pharmacodynamics in relation to toxicity and therapeutic activity. *Cancer Surv*, 17:189–217, 1993.

[85] K. K. Fields, G. J. Elfenbein, H. M. Lazarus, B. W. Cooper, J. B. Perkins, R. J. Creger, O. F. Ballester, J. H. Hiemenz, W. E. Janssen, and P. E. Zorsky. Maximum-tolerated doses of ifosfamide , carboplatin , and etoposide given over 6 days followed by autologous stem-cell Rescue: toxicity profile high-dose. *J Clin Oncol*, 13:323–332, 1995.

[86] N. J. Vogelzang, D. Raghavan, and B. J. Kennedy. VP-16-213 (etoposide): the mandrake root from Issyk-Kul. *Am J Med*, 72:136–44, 1982.

[87] S. Joel. The clinical pharmacology of etoposide: an update. *Cancer Treat Rev*, 22:179–221, 1996.

[88] B. K. Sinha. Topoisomerase inhibitors. A review of their therapeutic potential in cancer. *Drugs*, 49:11–9, 1995.

[89] S. P. Joel and M. L. Slevin. Schedule-dependent topoisomerase II-inhibiting drugs. *Cancer Chemother Pharmacol*, 34 Suppl:S84–8, 1994.

[90] J. M. van Maanen, J. Retèl, J. de Vries, and H. M. Pinedo. Mechansim of action of antitumor drug etoposide: a review. *J Natl Cancer Inst*, 80:1526–33, 1988.

[91] L. M. Allen and P. J. Creaven. Comparison of the human pharmacokinetics of VM-26 and VP-16, two antineoplastic epipodophyllotixin glucopyranoside derivatives. *Eur J Cancer*, 11:697–707, 1975.

[92] A. Gouyette, A. Deniel, J. L. Pico, J. P. Droz, D. Baume, M. Ostronoff, N. le Bail, and M. Hayat. Clinical pharmacology of high-dose etoposide associated with cisplatin. Pharmacokinetic and metabolic studies. *Eur J Canc Clin Oncol*, 23:1627–32, 1987.

[93] C. F. Stewart, J. A. Pieper, S. G. Arbuck, and W. E. Evans. Altered protein binding of etoposide in patients with cancer. *Clin Pharmacol Ther*, 45:49–55, 1989.

[94] P. Aita, I. Robieux, R. Sorio, S. Tumolo, G. Corona, R. Cannizzaro, a M. Colussi, M. Boiocchi, and G. Toffoli. Pharmacokinetics of oral etoposide in patients with hepatocellular carcinoma. *Cancer Chemother Pharmacol*, 43:287–94, 1999.

[95] T. L. Schwinghammer, R. A. Fleming, C. S. Rosenfeld, D. Przepiorka, R. K. Shadduck, E. J. Bloom, and C. F. Stewart. Disposition of total and unbound etoposide following high-dose therapy. *Cancer Chemother Pharmacol*, 32:273–8, 1993.

[96] W. E. Evans, J. A. Sinkule, W. R. Crom, L. Dow, A. T. Look, and G. Rivera. Pharmacokinetics of teniposide (VM26) and etoposide (VP16-213) in children with cancer. *Cancer Chemother Pharmacol*, 7:147–50, 1982.

[97] S. Stremetzne. *Entwicklung bioanalytischer Methoden für die Anwendung in pharmakokinetischen Untersuchungen an Tumorpatienten.* PhD thesis, Freie Universität Berlin, 1997.

[98] K. R. Hande, P. J. Wedlund, R. M. Noone, K. R. Hã, J. Wedlund, G. R. Wilkinson, F. A. Greco, and S. N. Wolff. Pharmacokinetics of high-dose etoposide (VP-16-213) administered to cancer patients pharmacokinetics of high-dose etoposide (VP-16-213) administered to cancer patients. *Cancer Res*, 44:379–382, 1984.

[99] N. Haim, J. Nemec, J. Roman, and B. K. Sinha. Peroxidase-catalyzed metabolism of etoposide (VP-16-213) and covalent binding of reactive intermediates to cellular macromolecules. *Cancer Res*, 47:5835–40, 1987.

[100] K. Hande, L. Anthony, R. Hamilton, R. Bennett, B. Sweetman, and R. Branch. Identification of etoposide glucuronide as a major metabolite of etoposide in the rat and rabbit. *Cancer research*, 48:1829–34, 1988.

[101] P. E. Postmus, E. G. de Vries, H. G. De Vries-Hospers, R. Vriesendorp, G. W. van Imhoff, J. J. Holthuis, C. T. Sibinga, D. T. Sleijfer, and N. H. Mulder. Cyclophosphamide and VP 16-213 with autologous bone marrow transplantation. A dose escalation study. *Eur J Canc Clin Oncol*, 20:777–82, 1984.

[102] Fachinformation. Vepesid J., 1998.

[103] M. L. Slevin, P. I. Clark, S. P. Joel, S. Malik, R. J. Osborne, W. M. Gregory, D. G. Lowe, R. H. Reznek, and P. F. Wrigley. A randomized trial to evaluate the effect of schedule on the activity of etoposide in small-cell lung cancer. *J Clin Oncol*, 7:1333–40, 1989.

[104] S. N. Wolff, D. H. Johnson, J. D. Hainsworth, and F. A. Greco. High-dose VP-16-213 monotherapy for refractory germinal malignancies: a phase II study. *J Clin Oncol*, 2: 271–4, 1984.

[105]

[106] M. M. Hudson, H. J. Weinstein, S. S. Donaldson, C. Greenwald, L. Kun, N. J. Tarbell, W. A. Humphrey, C. Rupp, N. M. Marina, J. Wilimos, and M. P. Link. Acute Hypersensitivity Reactions to Etoposide in a VEPA Regimen for Hodgkin ' s Disease. *J Clin Oncol*, 11:1080–1084, 1993.

[107] S. J. Kellie, W. M. Crist, C. H. Pui, M. E. Crone, D. L. Fairclough, J. H. Rodman, and G. K. Rivera. Hypersensitivity reactions to epipodophyllotoxins in children with acute lymphoblastic leukemia. *Cancer*, 67:1070–5, 1991.

[108] E. Tucci and L. Pirtoli. Etoposide-induced hypersensitivity reactions. Report of two cases. *Chemioterapia*, 4:460–2, 1985.

[109] G. Ehninger, B. Proksch, H. Schmidt, P. Waidelich, B. Eichel, and R. Dopfer. Unaltered pharmacokinetics after the administration of high-dose etoposide without prior dilution. *Cancer Chemother Pharmacol*, 28:214–6, 1991.

[110] K. Mross, P. Bewermeier, J. Reifke, W. Krüger, M. Stockschläder, A. Zander, and D. K. Hossfeld. Pharmacokinetics of high-dose VP-16: 6-hour infusion versus 34-hour infusion. *Bone Marrow Transplant*, 13:423–30, 1994.

[111] H. Yokoyama, T. Aoyama, T. Matsuyama, Y. Yamamura, K. Nakajima, K. Nakamura, H. Sato, H. Kotaki, S. Chiba, H. Hirai, Y. Yazaki, and T. Iga. The cause of polyurethane catheter cracking during constant infusion of etoposide (VP-16) injection. *Yakugaku Zasshi*, 118:581–8, 1998.

[112] B. Hagen, R. A. Walstad, and O. G. Nilsen. Pharmacokinetics of thio-TEPA at two different doses. *Cancer Chemother Pharmacol*, 22:356–8, 1988.

[113] M. J. Maanen, C. J. Smeets, and J. H. Beijnen. Chemistry, pharmacology and pharmacokinetics of N,N′,N" -triethylenethiophosphoramide (ThioTEPA). *Cancer Treat Rev*, 26: 257–68, 2000.

[114] M. J. Egorin, S. R. Akman, and P. L. Gutierrez. Plasma pharmacokinetics and tissue distribution of thiotepa in mice. *Canc Treat Rep*, 68:1265–8, 1984.

[115] A. Ruggiero, V. Conter, M. Milani, E. Biagi, I. Lazzareschi, P. Sparano, and R. Riccardi. Intrathecal chemotherapy with antineoplastic agents in children. *Paediatr Drugs*, 3:237–46, 2001.

[116] M. J. van Maanen, I. M. Tijhof, J. M. Damen, C. Versluis, J. J. van den Bosch, A. J. Heck, S. Rodenhuis, and J. H. Beijnen. A search for new metabolites of N,N′,N″-triethylenethiophosphoramide. *Cancer Res*, 59:4720–4, 1999.

[117] S. K. Srivastava, S. S. Singhal, X. Hu, Y. C. Awasthi, P. Zimniak, and S. V. Singh. Differential catalytic efficiency of allelic variants of human glutathione S-transferase Pi in catalyzing the glutathione conjugation of thiotepa. *Arch Biochem Biophys*, 366:89–94, 1999.

[118] M. J. Lind and C. Ardiet. Pharmacokinetics of alkylating agents. *Cancer Surv*, 17:157–88, 1993.

[119] B. E. Cohen, M. J. Egorin, E. A. Kohlhepp, J. Aisner, and P. L. Gutierrez. Human plasma pharmacokinetics and urinary excretion of thiotepa and its metabolites. *Canc Treat Rep*, 70:859–64, 1986.

[120] P. J. O'Dwyer, F. LaCreta, S. Nash, P. W. Tinsley, R. Schilder, M. L. Clapper, K. D. Tew, L. Panting, S. Litwin, and R. L. Comis. Phase I study of thiotepa in combination with the glutathione transferase inhibitor ethacrynic acid. *Cancer Res*, 51:6059–65, 1991.

[121] A. M. Hussein, W. P. Petros, M. Ross, J. J. Vredenburgh, M. L. Affrontil, R. B. Jones, E. J. Shpall, P. Rubin, M. Elkordy, C. Gilbert, C. Gupton, M. J. Egorin, J. Soper, A. Berchuck, D. Clarke-Person, D. A. Berry, and W. P. Peters. A phase I/II study of high-dose cyclophosphamide, cisplatin, and thioTEPA followed by autologous bone marrow and granulocyte colony-stimulating factor-primed peripheral-blood progenitor cells in patients with advanced malignancies. *Cancer Chemother Pharmacol*, 37:561–8, 1996.

[122] B. Hagen. Pharmacokinetics of thio-TEPA and TEPA in the conventional dose-range and its correlation to myelosuppressive effects. *Cancer Chemother Pharmacol*, 27:373–8, 1991.

[123] http://www.ema.europa.eu/docs/de_DE/document_library/EPAR_-_Product_Information/human/001046/WC500090252.pdf, last accessed: 20.08.2012.

[124] S. P. Ackland, K. E. Choi, M. J. Ratain, M. J. Egorin, S. F. Williams, J. A. Sinkule, and J. D. Bitran. Human plasma pharmacokinetics of thiotepa following administration of high-dose thiotepa and cyclophosphamide. *J Clin Oncol*, 6:1192–6, 1988.

[125] A. Pession, A. Prete, F. Locatelli, S. Bella, F. Melchionda, A. Garaventa, R. Burnelli, and G. Paolucci. Phase I study of high-dose thiotepa with busulfan, etoposide, and autologous stem cell support in children with disseminated solid tumors. *Med Pediatr Oncol*, 33:450–4, 1999.

[126] B. Chen, T. Ahmed, A. Mannancheril, M. Gruber, and D. L. Benzil. Safety and efficacy of high-dose chemotherapy with autologous stem cell transplantation for patients with malignant astrocytomas. *Cancer*, 100:2201–7, 2004.

[127] L. E. Friberg, A. Freijs, M. Sandström, and M. O. Karlsson. Semiphysiological model for the time course of leukocytes after varying schedules of 5-fluorouracil in rats. *J Pharmacol Exp Ther*, 295:734–40, 2000.

[128] R. E. Parchment, M. Gordon, C. K. Grieshaber, C. Sessa, D. Volpe, and M. Ghielmini. Predicting hematological toxicity (myelosuppression) of cytotoxic drug therapy from in vitro tests. *Ann Oncol*, 9:357–64, 1998.

[129] C. Kloft, J. Wallin, A. Henningsson, E. Chatelut, and M. O. Karlsson. Population pharmacokinetic-pharmacodynamic model for neutropenia with patient subgroup identification: comparison across anticancer drugs. *Clin Cancer Res*, 12:5481–90, 2006.

[130] U.S. Department of health and human services. Common Terminology Criteria for Adverse Events (CTCAE) Version 4, 2009.

[131] G. P. Bodey, M. Buckley, Y. S. Sathe, and E. Freireich. Quantitative relationships between circulating leukocytes and infection in patients with acute leukemia. *Ann Intern Med*, 64: 328–340, 1966.

[132] G. L. Rosner and P. Müller. Pharmacodynamic analysis of hematologic profiles. *J Pharmacokinet Biopharm*, 22:499–524, 1994.

[133] M. O. Karlsson, R. E. Port, M. J. Ratain, and L. B. Sheiner. A population model for the leukopenic effect of etoposide. *Clin Pharmacol Ther*, 57:325–34, 1995.

[134] M. O. Karlsson, V. Molnar, J. Bergh, A. Freijs, and R. Larsson. A general model for time-dissociated pharmacokinetic-pharmacodynamic relationship exemplified by paclitaxel myelosuppression. *Clin Pharmacol Ther*, 63:11–25, 1998.

[135] H. Minami, Y. Sasaki, N. Saijo, T. Ohtsu, H. Fujii, T. Igarashi, and K. Itoh. Indirect-response model for the time course of leukopenia with anticancer drugs. *Clin Pharmacol Ther*, 64:511–21, 1998.

[136] W. C. Zamboni, D. Z. D. Argenio, C. F. Stewart, T. Macvittie, B. J. Delauter, A. M. Farese, D. M. Potter, N. M. Kubat, D. Tubergen, and M. J. Egorin. Pharmacodynamic Model of Topotecan-induced Time Course. *Clin Cancer Res*, 7:2301–2308, 2001.

[137] L. E. Friberg, C. J. Brindley, M. O. Karlsson, and A. J. Devlin. Models of schedule dependent haematological toxicity of 2'-deoxy-2'-methylidenecytidine (DMDC). *Eur J Clin Pharmacol*, 56:567–74, 2000.

[138] L. E. Friberg, A. Henningsson, H. Maas, L. Nguyen, and M. O. Karlsson. Model of chemotherapy-induced myelosuppression with parameter consistency across drugs. *J Clin Oncol*, 20:4713–4721, 2002.

[139] J. C. Panetta, M. N. Kirstein, A. J. Gajjar, G. Nair, M. Fouladi, and C. F. Stewart. A mechanistic mathematical model of temozolomide myelosuppression in children with high-grade gliomas. *Math Biosci*, 186:29–41, 2003.

[140] J. B. Bulitta, P. Zhao, R. D. Arnold, D. R. Kessler, R. Daifuku, J. Pratt, G. Luciano, A.-R. Hanauske, H. Gelderblom, A. Awada, and W. J. Jusko. Multiple-pool cell lifespan models for neutropenia to assess the population pharmacodynamics of unbound paclitaxel from two formulations in cancer patients. *Cancer Chemother Pharmacol*, 63:1035–48, 2009.

[141] E. Soto, A. Staab, C. Doege, M. Freiwald, G. Munzert, and I. F. Trocóniz. Comparison of different semi-mechanistic models for chemotherapy-related neutropenia: application to BI 2536 a Plk-1 inhibitor. *Cancer Chemother Pharmacol*, 68:1517–27, 2011.

[142] W. Krzyzanski and W. J. Jusko. Multiple-pool cell lifespan model of hematologic effects of anticancer agents. *J Pharmacokinet Pharmacodyn*, 29:311–37, 2002.

[143] F. Léger, W. J. Loos, R. Bugat, R. H. J. Mathijssen, M. Goffinet, J. Verweij, A. Sparreboom, and E. Chatelut. Mechanism-based models for topotecan-induced neutropenia. *Cancer Chemother and Pharmacol*, 76:567–78, 2004.

[144] M. Joerger, A. D. R. Huitema, M. T. Huizing, P. H. B. Willemse, A. de Graeff, H. Rosing, J. H. M. Schellens, J. H. Beijnen, and J. B. Vermorken. Safety and pharmacology of paclitaxel in patients with impaired liver function: a population pharmacokinetic-pharmacodynamic study. *Br J Clin Pharmacol*, 64:622–33, 2007.

[145] J. E. Latz, M. O. Karlsson, J. J. Rusthoven, A. Ghosh, and R. D. Johnson. A semimechanistic-physiologic population pharmacokinetic/pharmacodynamic model for neutropenia following pemetrexed therapy. *Cancer Chemother and Pharmacol*, 57:412–26, 2006.

[146] J. E. Latz, K. L. Schneck, K. Nakagawa, M. A. Miller, and C. H. Takimoto. Population pharmacokinetic/pharmacodynamic analyses of pemetrexed and neutropenia: effect of vitamin supplementation and differences between Japanese and Western patients. *Clin Cancer Res*, 15:346–54, 2009.

[147] A. Ramon-Lopez, R. Nalda-Molina, B. Valenzuela, and J. J. Perez-Ruixo. Semi-mechanistic model for neutropenia after high dose of chemotherapy in breast cancer patients. *Pharm Res*, 26:1952–62, 2009.

[148] K. Ozawa, H. Minami, and H. Sato. Population pharmacokinetic and pharmacodynamic analysis for time courses of docetaxel-induced neutropenia in Japanese cancer patients. *Cancer Sci*, 98:1985–1992, 2007.

[149] F. Puisset, J. Alexandre, J.-M. Treluyer, V. Raoul, H. Roché, F. Goldwasser, and E. Chatelut. Clinical pharmacodynamic factors in docetaxel toxicity. *Br J Cancer*, 97:290–6, 2007.

[150] A. Schmitt, L. Gladieff, C. M. Laffont, A. Evrard, J.-C. Boyer, A. Lansiaux, C. Bobin-Dubigeon, M.-C. Etienne-Grimaldi, M. Boisdron-Celle, M. Mousseau, F. Pinguet, A. Floquet, E. M. Billaud, C. Durdux, C. Le Guellec, J. Mazières, T. Lafont, F. Ollivier, D. Concordet, and E. Chatelut. Factors for hematopoietic toxicity of carboplatin: refining the targeting of carboplatin systemic exposure. *J Clin Oncol*, 28:4568–74, 2010.

[151] E. Soto, A. Staab, M. Freiwald, G. Munzert, H. Fritsch, C. Döge, and I. F. Trocóniz. Prediction of neutropenia-related effects of a new combination therapy with the anticancer drugs BI 2536 (a Plk1 inhibitor) and pemetrexed. *Clin Pharmacol Ther*, 88:660–7, 2010.

[152] A. S. Zandvliet, J. H. M. Schellens, W. Copalu, J. H. Beijnen, and A. D. R. Huitema. Covariate-based dose individualization of the cytotoxic drug indisulam to reduce the risk of severe myelosuppression. *J Pharmacokinet Pharmacodyn*, 36:39–62, 2009.

[153] A. L. Quartino, L. E. Friberg, and M. O. Karlsson. A simultaneous analysis of the time-course of leukocytes and neutrophils following docetaxel administration using a semi-mechanistic myelosuppression model. *Invest New Drugs*, 30:833–45, 2012.

[154] I. F. Trocòniz, M. J. Garrido, C. Segura, J.-M. Cendrós, P. Principe, C. Peraire, and R. Obach. Phase I dose-finding study and a pharmacokinetic/pharmacodynamic analysis of the neutropenic response of intravenous diflomotecan in patients with advanced malignant tumours. *Cancer Chemother Pharmacol*, 57:727–35, 2006.

[155] C. van Kesteren, A. S. Zandvliet, M. O. Karlsson, R. A. A. Mathôt, C. J. A. Punt, J.-P. Armand, E. Raymond, A. D. R. Huitema, C. Dittrich, H. Dumez, H. H. Roché, J.-P. Droz, M. Ravic, S. M. Yule, J. Wanders, J. H. Beijnen, P. Fumoleau, and J. H. M. Schellens. Semi-physiological model describing the hematological toxicity of the anti-cancer agent indisulam. *Invest New Drugs*, 23:225–34, 2005.

[156] M. Sandström, H. Lindman, P. Nygren, E. Lidbrink, J. Bergh, and M. O. Karlsson. Model describing the relationship between pharmacokinetics and hematologic toxicity of the epirubicin-docetaxel regimen in breast cancer patients. *J Clin Oncol*, 23:413–21, 2005.

[157] M. Sandström, H. Lindman, P. Nygren, M. Johansson, J. Bergh, and M. O. Karlsson. Population analysis of the pharmacokinetics and the haematological toxicity of the fluorouracil-epirubicin-cyclophosphamide regimen in breast cancer patients. *Cancer Chemother Pharmacol*, 58:143–56, 2006.

[158] Iris Minichmayr, Valerie Nock, Ulrich Jaehde, and Charlotte Kloft. Thrombocytopenia following high-dose chemotherapy with carboplatin, etoposide and thiotepa in patients with testicular germ cell cancer. *Int J Clin Pharmacol Ther*, 51:74–6, 2013.

[159] L. E. Friberg, M. Sandström, and M. O. Karlsson. Scaling the time-course of myelosuppression from rats to patients with a semi-physiological model. *Invest New Drugs*, 28: 744–53, 2010.

[160] A. Pessina, B. Albella, J. Bueren, P. Brantom, S. Casati, L. Gribaldo, C. Croera, G. Gagliardi, P. Foti, R. Parchment, D. Parent-Massin, Y. Sibiril, and R. Van Den Heuvel. Prevalidation of a model for predicting acute neutropenia by colony forming unit granulocyte/macrophage (CFU-GM) assay. *Toxicol In Vitro*, 15:729–40, 2001.

[161] C. Haglund, A. Aleskog, L. D. Hå kansson, M. Höglund, S. Jacobsson, R. Larsson, and E. Lindhagen. The FMCA-GM assays, high throughput non-clonogenic alternatives to CFU-GM in preclinical hematotoxicity testing. *Toxicol Lett*, 194:102–7, 2010.

[162] T. Mosmann. Rapid colorimetric assay for cellular growth and survival: application to proliferation and cytotoxicity assays. *J Immunol Methods*, 65:55–63, 1983.

[163] G. Dal Negro, L. Vandin, M. Bonato, P. Repeto, and D. Sciuscio. A new experimental protocol as an alternative to the colony-forming unit-granulocyte/macrophage (CFU-GM) clonogenic assay to assess the haematotoxic potential of new drugs. *Toxicol In Vitro*, 20:750–6, 2006.

[164] C. Ferlini, M. Distefano, L. Pierelli, G. Bonanno, A. Fattorossi, A. Battaglia, S. Mancuso, and G. Scambia. A new method to evaluate in vitro myelotoxicity of antitumour agents in the first steps of drug development. *Pharmacol Toxicol*, 89:231–6, 2001.

[165] R. Larsson and P. Nygren. Prediction of individual patient response to chemotherapy by the fluorometric microculture cytotoxicity assay (FMCA) using drug specific cut-off limits and a Bayesian model. *Anticancer Res*, 13:1825–9, 1993.

[166] A. L. Quartino, M. O. Karlsson, A. Freijs, N. Jonsson, P. Nygren, J. Kristensen, E. Lindhagen, and R. Larsson. Modeling of in vitro drug activity and prediction of clinical outcome in acute myeloid leukemia. *J Clin Pharmacol*, 47:1014–21, 2007.

[167] http://www.taxotere.com, last accessed: 11.10.2012.

[168] J. J. Manfredi and S. B. Horwitz. Taxol: an antimitotic agent with a new mechanism of action. *Pharmacol Ther*, 25:83–125, 1984.

[169] I. Ringel and S. B. Horwitz. Studies with RP 56976 (taxotere): a semisynthetic analogue of taxol. *J Natl Cancer Inst*, 83:288–91, 1991.

[170] J. F. Díaz and J. M. Andreu. Assembly of purified GDP-tubulin into microtubules induced by taxol and taxotere: reversibility, ligand stoichiometry, and competition. *Biochemistry*, 32:2747–55, 1993.

[171] http://www.fachinfo.de, last accessed: 11.10.2012.

[172] S. Urien, J. Barré, C. Morin, A. Paccaly, G. Montay, and J. P. Tillement. Docetaxel serum protein binding with high affinity to alpha 1-acid glycoprotein. *Invest New Drugs*, 14: 147–51, 1996.

[173] H. L. McLeod, C. M. Kearns, J. G. Kuhn, and R. Bruno. Evaluation of the linearity of docetaxel pharmacokinetics. *Cancer Chemother Pharmacol*, 42:155–9, 1998.

[174] E. Ponder. Red Cell Cytochemistry. *Ann N Y Acad Sci*, 48:579–614, 1947.

[175] M. A. Virtue, J. K. Furne, F. Q. Nuttall, and M. D. Levitt. Relationship between GHb concentration and erythrocyte survival determined from breath carbon monoxide concentration. *Diabetes Care*, 27:931–5, 2004.

[176] V. Rattan, Y. Shen, C. Sultana, D. Kumar, and V. K. Kalra. Diabetic RBC-induced oxidant stress leads to transendothelial migration of monocyte-like HL-60 cells. *Am J Physiol*, 273:E369–75, 1997.

[177] T. Kamada, D. E. McMillan, T. Yamashita, and S. Otsuji. Lowered membrane fluidity of younger erythrocytes in diabetes. *Diabetes Res Clin Pract*, 16:1–6, 1992.

[178] R. M. Cohen, R. S. Franco, P. K. Khera, E. P. Smith, C. J. Lindsell, P. J. Ciraolo, M. B. Palascak, and C. H. Joiner. Red cell life span heterogeneity in hematologically normal people is sufficient to alter HbA1c. *Blood*, 112:4284–91, 2008.

[179] C. M. Peterson, R. L. Jones, R. J. Koenig, E. T. Melvin, and M. L. Lehrman. Reversible hematologic sequelae of diabetes mellitus. *Ann Intern Med*, 86:425–9, 1977.

[180] P. M. Jauslin, N. Frey, and M. O. Karlsson. Modeling of 24-hour glucose and insulin profiles of patients with type 2 diabetes. *J Clin Pharmacol*, 51:153–64, 2011.

[181] H. E. Silber, P. M. Jauslin, N. Frey, R. Gieschke, U. S. H. Simonsson, and M. O. Karlsson. An integrated model for glucose and insulin regulation in healthy volunteers and type 2 diabetic patients following intravenous glucose provocations. *J Clin Pharmacol*, 47: 1159–71, 2007.

[182] H. E. Silber, P. M. Jauslin, N. Frey, and M. O. Karlsson. An integrated model for the glucose-insulin system. *Basic clin pharmacol*, 106:189–94, 2010.

[183] J. Ribbing, B. Hamrén, M. K. Svensson, and M. O. Karlsson. A model for glucose, insulin, and beta-cell dynamics in subjects with insulin resistance and patients with type 2 diabetes. *J Clin Pharmacol*, 50:861–72, 2010.

[184] N. Frey, C. Laveille, M. Paraire, M. Francillard, N. H. G. Holford, and R. Jochemsen. Population PKPD modelling of the long-term hypoglycaemic effect of gliclazide given as a once-a-day modified release (MR) formulation. *Br J Clin Pharmacol*, 55:147–57, 2003.

[185] W. de Winter, J. DeJongh, T. Post, B. Ploeger, R. Urquhart, I. Moules, D. Eckland, and M. Danhof. A mechanism-based disease progression model for comparison of long-term effects of pioglitazone, metformin and gliclazide on disease processes underlying type 2 diabetes mellitus. *J Pharmacokinet Pharmacodyn*, 33:313–43, 2006.

[186] B. Hamrén, E. Björk, M Sunzel, and M. O. Karlsson. Models for plasma glucose, HbA1c, and hemoglobin interrelationships in patients with type 2 diabetes following tesaglitazar treatment. *Clin Pharmacol Ther*, 84:228–35, 2008.

[187] G. Danaei, M. M. Finucane, Y. Lu, G. M. Singh, M. J. Cowan, C. J. Paciorek, J. K. Lin, F. Farzadfar, Y.-H. Khang, G. a Stevens, M. Rao, M. K. Ali, L. M. Riley, C. A. Robinson, and M. Ezzati. National, regional, and global trends in fasting plasma glucose and diabetes prevalence since 1980: systematic analysis of health examination surveys and

epidemiological studies with 370 country-years and 2·7 million participants. *Lancet*, 378: 31–40, 2011.

[188] *IDF Diabetes Atlas*. International Diabetes Federation, 4 edition, 2009.

[189] publisher = Wissenschaftliche Verlagsgesellschaft mgH Stuttgart title = Mutscher Arzneimittelwirkungen year = 2008 Mutschler, E. G. and Kroemer, G. and Heyo, K. and Ruth, P. and Schäfer-Korting, M., edition = 9. Stuttgart.

[190] Guideline for management of postmeal glucose, 2007. Last accessed: 20.08.2012. URL http://www.idf.org/.

[191] K. H. Gabbay, K. Hasty, J. L. Breslow, R. C. Ellison, H. F. Bunn, and P. M. Gallop. Glycosylated hemoglobins and long-term blood glucose control in diabetes mellitus. *J Clin Endocrinol Metab*, 44:859–64, 1977.

[192] J. F. Fitzgibbons, R. D. Koler, and R. T. Jones. Red cell age-related changes of hemoglobins AIa + b and A , C in normal and diabetic subjects. *J Clin Invest*, 58:820–824, 1976.

[193] C. Krzisnik and J. Lukac-Bajalo. Glycosylated hemoglobin in fractions of erythrocytes of different ages. *J Endocrinol Invest*, 16:495–8, 1993.

[194] M. M. Elseweidy, M. Stallings, and E. C. Abraham. Changes in glycosylated hemoglobins with red cell aging in normal and diabetic subjects and in newborn infants of normal and diabetic mothers. *J Lab Clin Med*, 102:628–36, 1983.

[195] R. E. Ratner, J. Rosenstock, and G. Boka. Dose-dependent effects of the once-daily GLP-1 receptor agonist lixisenatide in patients with Type 2 diabetes inadequately controlled with metformin: a randomized, double-blind, placebo-controlled trial. *Diabet Med*, 27: 1024–32, 2010.

[196] H. J. Woerle, C. Neumann, S. Zschau, S. Tenner, A. Irsigler, J. Schirra, J. E. Gerich, and B. Göke. Impact of fasting and postprandial glycemia on overall glycemic control in type 2 diabetes Importance of postprandial glycemia to achieve target HbA1c levels. *Diabetes Res Clin Pract*, 77:280–5, 2007.

[197] M. Christensen, F. K. Knop, T. Vilsbø ll, and J. J. Holst. Lixisenatide for type 2 diabetes mellitus. *Expert Opin Investig Drugs*, 20:549–57, 2011.

[198] Summary of opinion (initial authorisation): Lyxumia - lixisenatide , 2012. Last accessed: 24.02.2013. URL http://www.ema.europa.eu.

[199] D. J. Drucker. Enhancing incretin action for the treatment of type 2 diabetes. *Diabetes care*, 26:2929–40, 2003.

[200] A. H. Barnett. Lixisenatide: evidence for its potential use in the treatment of type 2 diabetes. *Core Evid*, 6:67–79, 2011.

[201] S. L. Beal. Population pharmacokinetic data and parameter estimation based on their first two statistical moments. *Drug Metab Rev*, 15:173–93, 1984.

[202] C. W. Tornøe, H. Agersø, E. N. Jonsson, H. Madsen, and H. A. Nielsen. Non-linear mixed-effects pharmacokinetic/pharmacodynamic modelling in NLME using differential equations. *Comput Methods Programs Biomed*, 76:31–40, 2004.

[203] G. Colin Pillai, F. Mentré, and J.-L. Steimer. Non-linear mixed effects modeling - from methodology and software development to driving implementation in drug development science. *J Pharmacokinet Pharmacodyn*, 32:161–83, 2005.

[204] M. L. Lindstrom and D. M. Bates. Nonlinear mixed effects models for repeated measures data. *Biometrics*, 46:673–87, 1990.

[205] M. Frank. *Population pharmacokinetic modelling and simulation of nevirapine in pregnant women and newborns for dosing strategies to prevent HIV-1 transmission in resource-constrained countries*. Dissertation, Freie Universität Berlin, 2011.

[206] S. L. Beal and L. B. Sheiner. *NONMEM Users Guides*. Universtity of California, 1988.

[207] R. J. Bauer and T. M. Ludden. Improvements and New Estimation Methods in NONMEM 7 for PK/PD Population Analysis. *PAGE*, 18, 2009. URL www.page-meeting.org/?abstract=1516.

[208] J. Ribbing, J. Nyberg, O. Caster, and E. N. Jonsson. The lasso - a novel method for predictive covariate model building in nonlinear mixed effects models. *J Pharmacokinet Pharmacodyn*, 34:485–517, 2007.

[209] E. N. Jonsson and M. O. Karlsson. Automated covariate model building within NONMEM. *Pharm Res*, 15:1463–8, 1998.

[210] A. Khandelwal, K. Harling, E. N. Jonsson, A. C. Hooker, and M. O. Karlsson. A fast method for testing covariates in population PK/PD Models. *AAPS J*, 13:464–72, 2011.

[211] http://www.wright-dose.com/tip1.php, last accessed: 22.10.2012.

[212] G. W. Oehlert. A Note on the Delta Method. *Am Stat*, 46:27–29, 1992.

[213] R. M. Savic and M. O. Karlsson. Importance of shrinkage in empirical bayes estimates for diagnostics: problems and solutions. *AAPS J*, 11:558–69, 2009.

[214] http://psn.sourceforge.net/docs.php, last accessed: 11.10.2012.

[215] A.C. Hooker, C. E. Staatz, and M. O. Karlsson. Conditional weighted residuals (CWRES): a model diagnostic for the FOCE method. *Pharm Res*, 24:2187–97, 2007.

[216] K. Brendel, C. Dartois, E. Comets, A. Lemenuel-Diot, C. Laveille, Br. Tranchand, P. Girard, C. M. Laffont, and F. Mentré. Are population pharmacokinetic and/or pharmacodynamic models adequately evaluated? A survey of the literature from 2002 to 2004. *Clin Pharmacokinet*, 46:221–34, 2007.

[217] *FDA Guidance for industry: Population Pharmacokinetics*, 1999.

[218] M. Biertümpel. Untersuchung zellbasierter Assays zur Bestimmung der Zytotoxizität von Zytostatika auf periphere mononucleäre Zellen. Diplomarbeit, Martin-Luther Universität Halle-Wittenberg, in preparation.

[219] R. Bruno, D. Hille, A. Riva, N. Vivier, W. W. ten Bokkel Huinnink, A. T. van Oosterom, S. B. Kaye, J. Verweij, F. V. Fossella, V. Valero, J. R. Rigas, A. D. Seidman, B. Chevallier, P. Fumoleau, H. A. Burris, P. M. Ravdin, and L. B. Sheiner. Population pharmacokinetics/pharmacodynamics of docetaxel in phase II studies in patients with cancer. *J Clin Oncol*, 16:187–96, 1998.

[220] V. Nock, D. Rüppel, and C. Kloft. Comparison of three PK/PD models for glycated haemoglobin in diabetes type 2 patients treated with lixisenatide. *PAGE*, 21, 2012. URL www.page-meeting.org/?abstract=2335.

[221] D. Du Bois and E. F. Du Bois. A formula to estimate the approximate surface area if height and weight be known. *Arch Int Med*, 17:863–871, 1916.

[222] D. W. Cockcroft and M. H. Gault. Prediction of creatinine clearance from serum creatinine. *Nephron*, 16:31–41, 1976.

[223] S. B. Duffull, M. J. Dooley, B. Green, S. G. Poole, and C. M. J. Kirkpatrick. A standard weight descriptor for dose adjustment in the obese patient. *Clin Pharmacokinet*, 43:1167–78, 2004.

[224] S. L. Beal. Ways to fit a PK model with some data below the quantification limit. *J Pharmacokinet Pharmacodyn*, 28:481–504, 2001.

[225] L. Lindbom, J. Ribbing, and E. N. Jonsson. Perl-speaks-NONMEM (PsN)–a Perl module for NONMEM related programming. *Comput Methods Programs Biomed*, 75:85–94, 2004.

[226] R Development Core Team. *R: A Language and Environment for Statistical Computing*. R Foundation for Statistical Computing, Vienna, Austria, 2008.

[227] E.N. Jonsson and M. O. Karlsson. Xpose - and s-plus based population pharmacokinetic/pharmacodynamic model building aid for nonmem. *Computer Methods and Programs in Biomedicine*, 58(1):51–64, 1999.

[228] H. Wickham. *ggplot2: elegant graphics for data analysis.* Springer New York, 2009.

[229] C. Ritz and J. C. Streibig. Bioassay analysis using r. *Journal of Statistical Software*, 12, 2005.

[230] D. A. Karnofsky, W. H. Abelmann, L. F. Craver, and J. H. Burchenal. The use of the nitrogen mustards in the palliative treatment of carcinoma. *Cancer*, 1(4):634–656, 1948.

[231] C. Kloft, H. Appelius, W. Siegert, W. Schunack, and U. Jaehde. Determination of platinum complexes in clinical samples by a rapid flameless atomic absorption spectrometry assay. *Ther Drug Monit*, 21:631–7, 1999.

[232] S. Reif, D. Kingreen, C. Kloft, J. Grimm, W. Siegert, W. Schunack, and U. Jaehde. Bioequivalence investigation of high-dose etoposide and etoposide phosphate in lymphoma patients. *Cancer Chemother Pharmacol*, 48:134–140, 2001.

[233] U. Geisler. Analytik und Pharmakokinetic als Grundlage für ein Therapeutisches Drug Monitoring von Thiotepa. Diplomarbeit, Pharmazeutisches Institut Rheinische Friedrich-Wilhelms-Universitaet Bonn, 2002.

[234] B. Wolkewitz. *Pharmakokinetische Untersuchungen der Kombination von Thiotepa und Mitoxantron in der Hochdosistherapie des Mammakarzinoms*. Dissertation, Universität Essen, 2001.

[235] B. Jilma. Glucocorticoids dose-dependently increase plasma levels of granulocyte colony stimulating factor in man. *J Clin Endocrinol Metab*, 83:1037–1040, 1998.

[236] A. Lindauer, C. Eickhoff, C. Kloft, and U. Jaehde. Population pharmacokinetics of high-dose carboplatin in children and adults. *Ther Drug Monit*, 32:159–68, 2010.

[237] L. Nguyen, E. Chatelut, C. Chevreau, B. Tranchand, I. Lochon, J. M. Bachaud, A. Pujol, G. Houin, R. Bugat, and P. Canal. Population pharmacokinetics of total and unbound etoposide. *Cancer Chemother Pharmacol*, 41:125–32, 1998.

[238] B. You, B. Tranchand, P.l Girard, C. Falandry, B. Ribba, S. Chabaud, P.-J. Souquet, I. Court-Fortune, V. Trillet-Lenoir, C. Fournel, M. Tod, and G. Freyer. Etoposide pharmacokinetics and survival in patients with small cell lung cancer: a multicentre study. *Lung Cancer*, 62:261–72, 2008.

[239] M. O. Karlsson and N. H. G. Holford. A Tutorial on Visual Predicitve Checks. *PAGE*, 17, 2008. URL www.page-meeting.org/?abstract=1434.

[240] R. M. Savic, D. M. Jonker, T. Kerbusch, and M. O. Karlsson. Implementation of a transit compartment model for describing drug absorption in pharmacokinetic studies. *J Pharmacokinet Pharmacodyn*, 34:711–26, 2007.

[241] C. F. Minto, T. W. Schnider, T. G. Short, K. M. Gregg, A. Gentilini, and S. L. Shafer. Response surface model for anesthetic drug interactions. *Anesthesiology*, 92:1603–16, 2000.

[242] C. Dansirikul, H. E. Silber, and M. O. Karlsson. Approaches to handling pharmacodynamic baseline responses. *J Pharmacokinet Pharmacodyn*, 35:269–83, 2008.

[243] Y. N. Sun and W. J. Jusko. Transit compartments versus gamma distribution function to model signal transduction processes in pharmacodynamics. *J Pharm Sci*, 87:732–7, 1998.

[244] C. Nissen, Y. Moser, B. Speck, M. Bürgin, and H. Bendy. Dexamethasone enhances 'CSA' release and depresses 'BPA' release. *Br J Haematol*, 53:301–10, 1983.

[245] H.B. Mann and D.R. Whitney. On a test of whether one of two random variables is stochastically larger than the other. *Ann Math Statist*, 18:50–60, 1947.

[246] F. E. Grubbs. Sample criteria for testing outlying observations. *Ann Math Statist*, 21(1): 27–58, 1950.

[247] F. J. Richards. A flexible growth function for empirical use. *J Exp Bot*, 10:290–300, 1959.

[248] P. H. Van der Graaf and R. C. Schoemaker. Analysis of asymmetry of agonist concentration-effect curves. *J Pharmacol Toxicol Methods*, 41:107–15.

[249] UPSS. Uppsala Summer School 2011 Course Material, 2011.

[250] A. Pessina, B. Albella, M. Bayo, J. Bueren, P. Brantom, S. Casati, C. Croera, R. Parchment, D. Parent-Massin, G. Schoeters, Y. Sibiri, R. Van Den Heuvel, and L. Gribaldo. In vitro tests for haematotoxicity: prediction of drug-induced myelosuppression by the CFU-GM assay. *Altern Lab Anim*, 30 Suppl 2:75–9, 2002.

[251] M. de Graaff, M. Maliepaard, D. Pluim, B. J. Floot, I. C. Slpaer-Cortenbach, and J. H. Schellens. In vitro antagonistic cytotoxic interactions between platinum drugs and taxanes on bone marrow progenitro cell CFU-GM. *Anticancer Drugs*, 10:213–8, 1999.

[252] D. Rüppel, W. Weber, Y. H. Liu, and Steinsträsser, A. Modelling of Lixisenatide in Diabetes Type 2. *Symposium on Measurement and Kinetics of in Vivo Drug Effects*, pages 227–228, 2010.

[253] T. Frank. Population pharmacokinetics of lixisenatide, a once-daily human glucagon-like peptide-1 reseptor agonist, in healthy subjects and in patients with type 2 diabetes. *J Pharm Drug Deliv Res*, 2013. In press.

[254] N. L. Dayneka, V. Garg, and W. J. Jusko. Comparison of four basic models of indirect pharmacodynamic responses. *J Pharmacokinet Biopharm*, 21:457–78, 1993.

[255] B. Hamrén, E. Björk, and M. O. Karlsson. Mechanism-based pharmacokinetic and pharmacodynamic modelling of tesaglitazar in type 2 diabetes patients. *PAGE*, 15, 2006. URL www.page-meeting.org/?abstract=961.

[256] R. M. Kalicki, R. Lledó-García, and M. O. Karlsson. Modeling of Red Blood Cell (RBC) Lifespan (LS) in a Hematologically Normal Population. *PAGE*, 18, 2009. URL www.page-meeting.org/?abstract=1677.

[257] S. Reif. *Ansätze zur Optimierung der Chemotherapie mit Etoposid auf der Grundlage pharmakokinetischer Untersuchungen*. Dissertation, Freie Universität Berlin, 2002.

[258] A. L. Quartino. *Pharmacometric models for improved prediction of myelosuppression and treatment response in oncology*. PhD thesis, Uppsala Universitet, 2011.

[259] C. Ekhart, V. D. Doodeman, S. Rodenhuis, P. H. M. Smits, J. H. Beijnen, and A. D. R. Huitema. Polymorphisms of drug-metabolizing enzymes (GST, CYP2B6 and CYP3A) affect the pharmacokinetics of thiotepa and tepa. *Br J Clin Pharmacol*, 67:50–60, 2009.

[260] K. K. Fields, G. J. Elfenbein, J. B. Perkins, J. W. Hiemenz, W. E. Janssen, P. E. Zorsky, O. F. Ballester, L. E. Kronish, and M. C. Foody. Two novel high-dose treatment regimens for metastatic breast cancer-ifosfamide, carboplatin, plus etoposide and mitoxantrone plus thiotepa: outcomes and toxicities. *Semin Oncol*, 20:59–66, 1993.

[261] M. Shen, R. J. Schilder, C. Obasaju, and J. M. Gallo. Population pharmacokinetic and limited sampling models for carboplatin administered in high-dose combination regimens with peripheral blood stem cell support. *Cancer Chemother Pharmacol*, 50:243–50, 2002.

[262] S. B. Duffull, E. J. Begg, B. A. Robinson, and J. J. Deely. A sequential bayesian algorithm for dose individualisation of carboplatin. *Cancer Chemother Pharmacol*, 39:317–26, 1997.

[263] E. Chatelut, P. Canal, V. Brunner, C. Chevreau, A. Pujol, A. Boneu, H. Roché, G. Houin, and R. Bugat. Prediction of carboplatin clearance from standard morphological and biological patient characteristics. *J Natl Cancer Inst*, 87:573–80, 1995.

[264] D. M. Woloschuk, J. M. Pruemer, and R. J. Cluxton. Carboplatin: a new cisplatin analog. *Drug Intel Clin Phar*, 22:843–9, 1988.

[265] F. Elferink, W. J. van der Vijgh, I. Klein, J. B. Vermorken, H. E. Gall, and H. M. Pinedo. Pharmacokinetics of carboplatin after i.v. administration. *Canc Treat Rep*, 71:1231–7, 1987.

[266] P. O. Mulder, E. G. de Vries, D. R. Uges, A. H. Scaf, D. T. Sleijfer, and N. H. Mulder. Pharmacokinetics of carboplatin at a dose of 750 mg m-2 divided over three consecutive days. *Br J Cancer*, 61:460–4, 1990.

[267] E. Chatelut, A. Dezeuze, M. Lavit, C. Chevreau, A. Pujol, A. Boneu, H. Roché, G. Houin, R. Bugat, and P. Canal. Prediction of carboplatin clearance from morphological and biological patient characteristics. *Bull Cancer*, 82:946–53, 1995.

[268] J. G. Wright, A. V. Boddy, M. Highley, J. Fenwick, A. McGill, and A. H. Calvert. Estimation of glomerular filtration rate in cancer patients. *Br J Cancer*, 84:452–9, 2001.

[269] B. J. Anderson and N. H. G. Holford. Mechanism-based concepts of size and maturity in pharmacokinetics. *Annu Rev Pharmacol Toxicol*, 48:303–32, 2008.

[270] W. C. Su, S. L. Chang, T. Y. Chen, J. S. Chen, and C. J. Tsao. Comparison of in vitro growth-inhibitory activity of carboplatin and cisplatin on leukemic cells and hematopoietic progenitors: the myelosuppressive activity of carboplatin may be greater than its antileukemic effect. *Jpn J Clin Oncol*, 30:562–7, 2000.

[271] J. Ciccolini, S. Monjanel-Mouterde, S.-S. Bun, C. Blanc, F. Duffaud, R. Favre, and A. Durand. Population pharmacokinetics of etoposide: application to therapeutic drug monitoring. *Ther Drug Monit*, 24:709–14, 2002.

[272] G. Freyer, B. Tranchand, B. Ligneau, C. Ardiet, P. J. Souquet, I. Court-Fortune, R. Riou, P. Rebattu, J. P. Boissel, V. Trillet-Lenoir, and P. Girard. Population pharmacokinetics of doxorubicin, etoposide and ifosfamide in small cell lung cancer patients: results of a multicentre study. *Br J Clin Pharmacol*, 50:315–24, 2000.

[273] J. M. Henwood and R. N. Brogden. Etoposide. A review of its pharmacodynamic and pharmacokinetic properties, and therapeutic potential in combination chemotherapy of cancer. *Drugs*, 39:438–90, 1990.

[274] G. Würthwein, T. Klingebiel, S. Krümpelmann, M. Metz, K. Schwenker, K. Kranz, C. Lanvers, and J. Boos. Population pharmacokinetics of high-dose etoposide in children receiving different conditioning regimens. *Anticancer Drugs*, 13:101–10, 2002.

[275] J. J. Holthuis, P. E. Postmus, W. J. Van Oort, B. Hulshoff, H. Verleun, D. T. Sleijfer, and N. H. Mulder. Pharmacokinetics of high dose etoposide (VP 16-213). *Eur J Canc Clin Oncol*, 22:1149–55, 1986.

[276] B. Tranchand, C. Amsellem, E. Chatelut, G. Freyer, A. Iliadis, B. Ligneau, V. Trillet-Lenoir, P. Canal, I. Lochon, and C. J. Ardiet. A limited-sampling strategy for estimation of etoposide pharmacokinetics in cancer patients. *Cancer Chemother Pharmacol*, 43:316–22, 1999.

[277] M. D'Incalci, P. Farina, C. Sessa, C. Mangioni, V. Conter, G. Masera, M. Rocchetti, M. B. Pisoni, E. Piazza, M. Beer, and F. Cavalli. Pharmacokinetics of VP16-213 given by different administration methods. *Cancer Chemother Pharmacol*, 7:141–5, 1982.

[278] W. Blaschek. *Hagers Enzyklopädie der Arzneistoffe und Drogen*. Springer, Berlin.

[279] C. Tagesson and C. Edling. Influence of surface-active food additives on the integrity and permeability of rat intestinal mucosa. *Food Chem Toxicol*, 22:861–4, 1984.

[280] I. Tsujino, T. Yamazaki, M. Masutani, U. Sawada, and T. Horie. Effect of Tween-80 on cell killing by etoposide in human lung adenocarcinoma cells. *Cancer Chemother Pharmacol*, 43:29–34, 1999.

[281] C. F. Stewart. Use of etoposide in patients with organ dysfunction: pharmacokinetic and pharmacodynamic considerations. *Cancer Chemother Pharmacol*, 34 Suppl, 1994.

[282] T. Kerbusch, J. de Kraker, H. J. Keizer, J. W. van Putten, H. J. Groen, R. L. Jansen, J. H. Schellens, and J. H. Beijnen. Clinical pharmacokinetics and pharmacodynamics of ifosfamide and its metabolites. *Clin Pharmacokinet*, 40:41–62, 2001.

[283] Plasma etoposide catechol increases in pediatric patients undergoing multiple-day chemotherapy with etoposide. *Clin Cancer Res*, 10:2977–85, 2004.

[284] A. Pessina, B. Albella, M. Bayo, J. Bueren, P. Brantom, S. Casati, C. Croera, G. Gagliardi, P. Foti, R. Parchment, D. Parent-Massin, G. Schoeters, Y. Sibiril, R. Van Den Heuvel, and L. Gribaldo. Application of the CFU-GM assay to predict acute drug-induced neutropenia: an international blind trial to validate a prediction model for the maximum tolerated dose (MTD) of myelosuppressive xenobiotics. *Toxicol Sci*, 75:355–67, 2003.

[285] A. D. R. Huitema, R. A. Mathôt, M. M. Tibben, J. H. Schellens, S. Rodenhuis, and J. H. Beijnen. Population pharmacokinetics of thioTEPA and its active metabolite TEPA in patients undergoing high-dose chemotherapy. *Br J Clin Pharmacol*, 51:61–70, 2001.

[286] M. E. de Jonge, A. D. R. Huitema, S. Rodenhuis, and J. H. Beijnen. Sparse sampling design for therapeutic drug monitoring of sequentially administered cyclophosphamide, thiotepa, and carboplatin (CTC). *Ther Drug Monit*, 27:393–402, 2005.

[287] D. Przepiorka, T. Madden, C. Ippoliti, Z. Estrov, and M. Dimopoulos. Dosing of thioTEPA for myeloablative therapy. *Cancer Chemother Pharmacol*, 37:155–60, 1995.

[288] M. J. Moore. Clinical pharmacokinetics of cyclophosphamide. *Clin Pharmacokinet*, 20: 194–208, 1991.

[289] M. J. van Maanen and J. H. Beijnen. Liquid chromatographic-mass spectrometric determination of the novel, recently identified thioTEPA metabolite, thioTEPA-mercapturate, in urine. *J Chromatogr B Analyt Technol Biomed Life Sci*, 732:73–9, 1999.

[290] A Bayesian population PK-PD model for ispinesib/docetaxel combination-induced myelosuppression. *Cancer Chemother Pharmacol*, 63:469–76, 2009.

[291] A. S. Zandvliet, J. H. M. Schellens, C. Dittrich, J. Wanders, J. H. Beijnen, and A. D. R. Huitema. Population pharmacokinetic and pharmacodynamic analysis to support treatment optimization of combination chemotherapy with indisulam and carboplatin. *Br J Clin Pharmacol*, 66:485–97, 2008.

[292] P. Jacqmin, E. Snoeck, E. A. Van Schaick, R. Gieschke, P. Pillai, J. Steimer, and P. Girard. Modelling response time profiles in the absence of drug concentrations: definition and performance evaluation of the K-PD model. *J Pharmacokinet Pharmacodyn*, 34, 2007.

[293] Y. Kano, M. Akutsu, K. Suzuki, and M. Yoshida. Effects of carboplatin in combination with other anticancer agents on human leukemia cell lines. *Leuk Res*, 17:113–9, 1993.

[294] R. A. Fleming, A. A. Miller, and C. F. Stewart. Etoposide: an update. *Clin Pharm*, 8: 274–93, 1989.

[295] A. L. Quartino, M. O. Karlsson, H. Lindman, and L. E. Friberg. An integrated G-CSF-myelosuppression model characterizing the target mediated disposition of endogenous G-CSF in breast cancer patients following chemotherapy. *PAGE*, 20, 2011. URL www.page-meeting.org/?abstract=2255.

[296] M. L. Pastor, C. M. Laffont, A. Schmitt, E. Chatelut, and D. Concordet. Modeling of the effect of G-CSF in limiting the neutropenic toxicity of carboplatin. *PAGE*, 21, 2012. URL www.page-meeting.org/?abstract=2511.

[297] J. L. Kadish and R. S. Basch. Hematopoietic thymocyte precursors. III. A population of thymocytes with the capacity to return ("home") to the thymus. *Cell Immunol*, 30:12–24, 1977.

[298] L. K. Roskos, P. Lum, P. Lockbaum, G. Schwab, and B.-B. Yang. Pharmacokinetic/pharmacodynamic modeling of pegfilgrastim in healthy subjects. *J Clin Pharmacol*, 46:747–57, 2006.

[299] J. Hing, J. J. Perez-Ruixo, K. Stuyckens, A. Soto-Matos, L. Lopez-Lazaro, and P. Zannikos. Mechanism-based pharmacokinetic/pharmacodynamic meta-analysis of trabectedin (ET-743, Yondelis) induced neutropenia. *Clin Pharmacol Ther*, 83:130–43, 2008.

[300] Dexamethasone-induced leucocytosis in pregnancy. *Br J Obstet Gynaecol*, 104:851–3, 1997.

[301] J. Crawford, D. C. Dale, and G. H. Lyman. Chemotherapy-induced neutropenia: risks, consequences, and new directions for its management. *Cancer*, 100:228–37, 2004.

[302] Richtlinie zur Transplantation peripherer Blutstammzellen. *Deutsches Ärzteblatt*, 94(23): 1584–1592, 1997.

[303] W. E. Scales, A. J. Vander, M. B. Brown, and M. J. Kluger. Human circadian rhythms in temperature, trace metals, and blood variables. *J Appl Physiol*, 65:1840–6, 1988.

[304] K. Nakashima, O. Nishizaki, Y. Andoh, H. Takei, A. Itai, and Y. Yoshida. Glycated hemoglobin in fractionated erythrocytes. *Clin Chem*, 35:958–62, 1989.

[305] H. F. Bunn, K. H. Gabbay, and P. M. Gallop. The glycosylation of hemoglobin: relevance to diabetes mellitus. *Science*, 200:21–7, 1978.

[306] H. B. Mortensen, A. Vø lund, and C. Christophersen. Glucosylation of human haemoglobin A. Dynamic variation in HbA1c described by a biokinetic model. *Clin Chim Acta*, 136:75–81, 1984.

[307] K. W. Beach. A theoretical model to predict the behavior of glycosylated hemoglobin levels. *J Theor Biol*, 81:547–61, 1979.

[308] Y. Tahara and K. Shima. The response of GHb to stepwise plasma glucose change over time in diabetic patients. *Diabetes Care*, 16:1313–4, 1993.

[309] P. Ladyzyński, J. M. Wójcicki, M. Bak, S. Sabalińska, J. Kawiak, P. Foltyński, J. Krzymień, and W. Karnafel. Validation of hemoglobin glycation models using glycemia monitoring in vivo and culturing of erythrocytes in vitro. *Ann Biomed Eng*, 36:1188–202, 2008.

[310] D. E. Uehlinger, F. A. Gotch, and L. B. Sheiner. A pharmacodynamic model of erythropoietin therapy for uremic anemia. *Clin Pharmacol Ther*, 51:76–89, 1992.

[311] A. Strocchi, S. Schwartz, M. Ellefson, R. R. Engel, A. Medina, and M. D. Levitt. A simple carbon monoxide breath test to estimate erythrocyte turnover. *J Lab Clin Med*, 120:392–9, 1992.

[312] S. Sayinalp, T. Sözen, A. Usman, and S. Dündar. Investigation of the effect of poorly controlled diabetes mellitus on erythrocyte life. *J Diabetes Complications*, 9, 1995.

[313] J. Chou, C. A. Robinson, and A. L. Siegel. Simple method for estimating glycosylated hemoglobins, and its application to evaluation of diabetic patients. *Clin Chem*, 24:1708–10, 1978.

[314] L. Monnier, H. Lapinski, and C. Colette. Contributions of fasting and postprandial plasma glucose increments to the overall diurnal hyperglycemia of type 2 diabetic patients: variations with increasing levels of HbA(1c). *Diabetes Care*, 26:881–5, 2003.

[315] M. Riddle, G. Umpierrez, A. DiGenio, R. Zhou, and J. Rosenstock. Contributions of basal and postprandial hyperglycemia over a wide range of A1C levels before and after treatment intensification in type 2 diabetes. *Diabetes Care*, 34:2508–14, 2011.

7.1 Publications

Original Papers

V. Nock, A. Lindauer, U. Jaehde, C. Kloft
Prediction of cytotoxic drug concentrations at the day of autologous stem cell rescue in a high-dose chemotherapy regimen.
International Journal of Clinical Pharmacology and Therapeutics (51), 2013

I. Minichmayr, V. Nock, U. Jaehde, C. Kloft
Thrombocytopenia following high-dose chemotherapy with carboplatin, etoposide and thiotepa in patients with testicular germ cell cancer.
International Journal of Clinical Pharmacology and Therapeutics (51), 2013

Presentations

V. Nock, A. Lindauer, U. Jaehde, C. Kloft
Optimal day for autologous stem cell rescue in a combination high-dose chemotherapy regimen in patients with testicular cancer.
CESAR Annual Meeting, Essen, Germany, 28.-30. 06.2012.
[http://www.cesar.or.at/download/text/2053/Annual Meeting 2012 Abstract Book_2012-08-07.pdf, V04]

Conference Abstracts

I. Minichmayr, V. Nock , U. Jaehde, C. Kloft
Thrombocytopenia following high-dose chemotherapy with autologous stem cell retransfusion in patients with testicular cell cancer
CESAR Annual Meeting, Essen, Germany, 28. - 30. 06.2012.
[http://www.cesar.or.at/download/text/2053/Annual Meeting 2012 Abstract Book_2012-08-07.pdf, abstract P26]).

V. Nock, D. Rüppel, C. Kloft
Comparison of three PK/PD models for glycated haemoglobin in diabetes type 2 patients treated with lixisenatide.
21^{st} Population Approach Group Europe (PAGE), Venice, Italy, 05. - 08.06.2012.
PAGE 21 (2012) Abstr 2335 [www.page-meeting.org/?abstract=2335].

V. Nock, A. Lindauer, U. Jaehde, C. Kloft
Understanding the time course of leukopenia in patients undergoing high-dose chemotherapy.
CESAR Annual Meeting, Greifswald, Germany, 16. - 18. 06. 2011.
http://www.cesar.or.at/download/text/2032/CESAR Annual Meeting 2011 Abstract Book Druckvorlage.pdf (2011).

V. Nock, A. Lindauer, U. Jaehde, C. Kloft
Leukopenia following triple high-dose chemotherapy and stem cell rescue.
20^{th} Population Approach Group Europe (PAGE), Athens, Greece, 07. - 10.06.2011.
PAGE 20 (2011) Abstr 2156 [www.page-meeting.org/?abstract=2156].

V. Nock, A. Lindauer, U. Jaehde, C. Kloft
Leukopenia in cancer patients receiving high-dose chemotherapy and myelosupportive treatment.
Jahrestagung der Deutschen Pharmazeutischen Gesellschaft (DPhG) 2010, Braunschweig, 04. - 07.10.2010. Proceedings, 132 (2010).

V. Nock, A. Lindauer, U. Jaehde, C. Kloft
Leukopenia following high-dose chemotherapy with autologuos stem cell retransfusion in patients with testicular cell cancer.
19^{th} Population Approach Group Europe (PAGE), Berlin, Germany, 08. - 11.06.2010.
PAGE 19 (2010) Abstr 1826 [www.page-meeting.org/?abstract=1826].

7.2 Curriculum Vitae

Der Lebenslauf ist in der Online-Version
aus Gründen des Datenschutzes nicht enthalten

8 Appendix

8.1 Tables

Table 8.1 Model development summary - key models of the model development for carboplatin (platinum)

Model number	Model description	Random effects (IIV)	Number of parameters	OFV
306	IIV on all parameters	CL, V_{cen}, Q, V_{per}	10	-857.4
309	Base model	CL, V_{cen}	8	-856.2
313	Full covariate model: CL_CLCR, CL_HT Q_AGE, Q_HT V_{cen}_WT	CL, V_{cen}, V_{per}	15	-891.9
311	Final, reduced covariate model CL_CLCR V_{cen}_WT	CL, V_{cen}	11	-885.4
321	Final model long infusion duration	CL	9	-872.1
327	Final model short infusion duration	CL	9	-895.3

OFV: objective function value; IIV: interindividual variability; CL: clearance

V_{cen}: central volume of distribution ; Q: intercompartmental CL;V_{per}: peripheral volume of distribution

Table 8.2 Model development summary - key models of the model development for etoposide

Model number	Model description	Random effects (IIV)	Number of parameters	OFV
072	1 CMT	CL, V_{cen}	5	1789.1
074	2 CMT	CL, V_{cen}, Q, V_{per}	9	1259.7
073	3 CMT	CL, V_{cen}, Q	10	1267.8
2 CMT model				
153.1	Additive residual variability	CL, V_{cen}, Q	8	41594.0
153	proportional residual variability	CL, V_{cen}, Q	8	1207.0
168	Base model combined residual variability	CL, V_{cen}	8	1057.3
172	Full covariate model CL_AST, hockey stick (2 slopes)	CL, V_{cen}	10	1038.0
200	Combined residual variability, IIV on all parameters, correlation CL and V_{cen}	CL, V_{cen}, Q, V_{per}	11	1004.3
174	Final model, short infusion time correlation CL and V_{cen}	CL and V_{cen}	9	1007.0
204	Final model, long infusion time correlation CL and V_{cen}	CL and V_{cen}	9	1002.0

OFV: objective function value; CMT:compartment; IIV: interindividual variability

CL: clearance; V_{cen}: central volume of distribution ; Q: intercompartmental CL

V_{per}: peripheral volume of distribution

CL_AST: covariate influence of AST on CL

Table 8.3 Model development summary - key models of the model development for thiotepa concentrations

Model number	Model description	Random effects (IIV)	Number of parameters	OFV
041	1 CMT	CL, V	4	57.4
042	2 CMT	CL, V_{cen}, Q, V_{per}	8	-32.6
2 CMT model with LAG time model				
063	No variability on ALAG	CL, V_{cen}, Q, V_{per}	9	-61.1
183	IIV on ALAG	CL, V_{cen}, ALAG	10	-115.6
2 CMT model with transit delay model				
286	additive residual variability on ln scale, FIX V_{per}	V_{cen}, TT	8	90.0
289	Combined residual variability on ln scale, FIX N and V_{per}	V_{cen}, TT	8	72.5
282	FIX N and V_{per}, additive residual variability on ln scale	CL, V_{cen}, Q, V_{per}, TT, N	9 9	74.7 74.7
281_r2	Final model, additive residual variability on ln scale, FIX N and V_{per}	V_{cen}, TT	7	72.6

OFV: objective function value; CMT: compartment; ALAG: parameter for estimation of lag time

IIV: interindividual variability; CL: clearance; V_{cen}: central volume of distribution

Q: intercompartmental CL ; V_{per}: peripheral volume of distribution

TT: mean transition time; N: number of transit compartments

ln scale: logarithmic scale

Table 8.4 Model development summary - key models for the PK/PD model for myelosuppression 1

Model number	Reference model	Model description	Number of parameters	ΔOFV	OFV
Drug effect					
704	696	E_{max} model for C	15	-16.5	30.4
705	696	E_{max} model for E	15	-4.5	42.0
706	696	E_{max} model for T	15	0	46.6
680	696	Drug-drug interaction between C and E	15	-4.5	42.1
Baseline estimation methods					
622	-	B1 method	15	-	42.6
661	-	B2 method	13	-	59.9
662	-	B3 method	15	-	41.4
Number of transit compartments					
649	-	3 transit compartments	14	-	83.5
648	649	4 transit compartments	14	-23.1	60.4
647	649	5 transit compartments	14	-35.7	47.8
622	649	6 transit compartments	14	-40.9	42.6
646	649	7 transit compartments	14	-35.5	48.0
Initial increase					
420.1	-	Single initialisation of INI_{DEXA}	13	-	15.0
424a	420.1	Multiple initialisation of INI_{DEXA}	13	21.5	36.5
677	671_r2	No INI_{DEXA}	12	61.7	106.6
Integration of stem cell rescue					
3 transit compartments (scenario A)					
293_FO	-	All $CD34^+$ cells (i) entering Prol (A-i-Prol)	11	-	95.2
301	-	CFU cells only (ii) entering Prol via one transit compartment (A-ii-Prol)	11	-	80.6
310	-	CFU cells (ii) entering Prol via a transit compartment; remaining $CD34^+$ cells (iii) enter T1 (A-ii-Prol + A-iii-T1)	12	-	75.2

continued...

Table 8.5 Model development summary - key models for the PK/PD model for myelosuppression 2

Model number	Reference model	Model description	Number of parameters	ΔOFV	OFV
6 transit compartments (scenario B)					
353a	-	CFU-cells (ii) entering Prol via one transit compartment, remaining $CD34^+$ cells (iii) enter T1 (B-ii-Prol + B-iii-T1)	15	-	49.4
394	-	All $CD34^+$-cells (i) enter Prol via one transit compartment, (B-i-Prol)	13	-	49.7
Additional feedback					
639	-	Single feedback on k_{prol}	14	-	42.6
640	639	Two feedbacks on k_{prol} and k_{tr}, including INI	15	0.2	42.4
Covariate analysis					
707	696	G-CSF_γ	15	-10.8	35.7
644	640	G-CSF_β	17	-7.55	34.8
117	105	DEXA_k_{prol} and _MMT	10	-6.7	236.0
Final model					
711	-	Final model	14	-	46.6

...end

OFV: objective function value; IIV: interindividual variability; CMT: compartment

C: carboplatin; E: etoposide; T: thiotepa

Prol: compartment of proliferating cells; CFU: colony forming unit

k_{prol} and k_{tr}: proliferation and transition rate constant; T1: first transit compartment

INI: compartment for the description of the initial increase in leukocyte concentrations; DEXA: dexamethasone

MMT: Mean maturation time; γ and β: exponents of the two feedback mechanisms

G-CSF: granulocyte colony stimulating factor

8.2 Figures

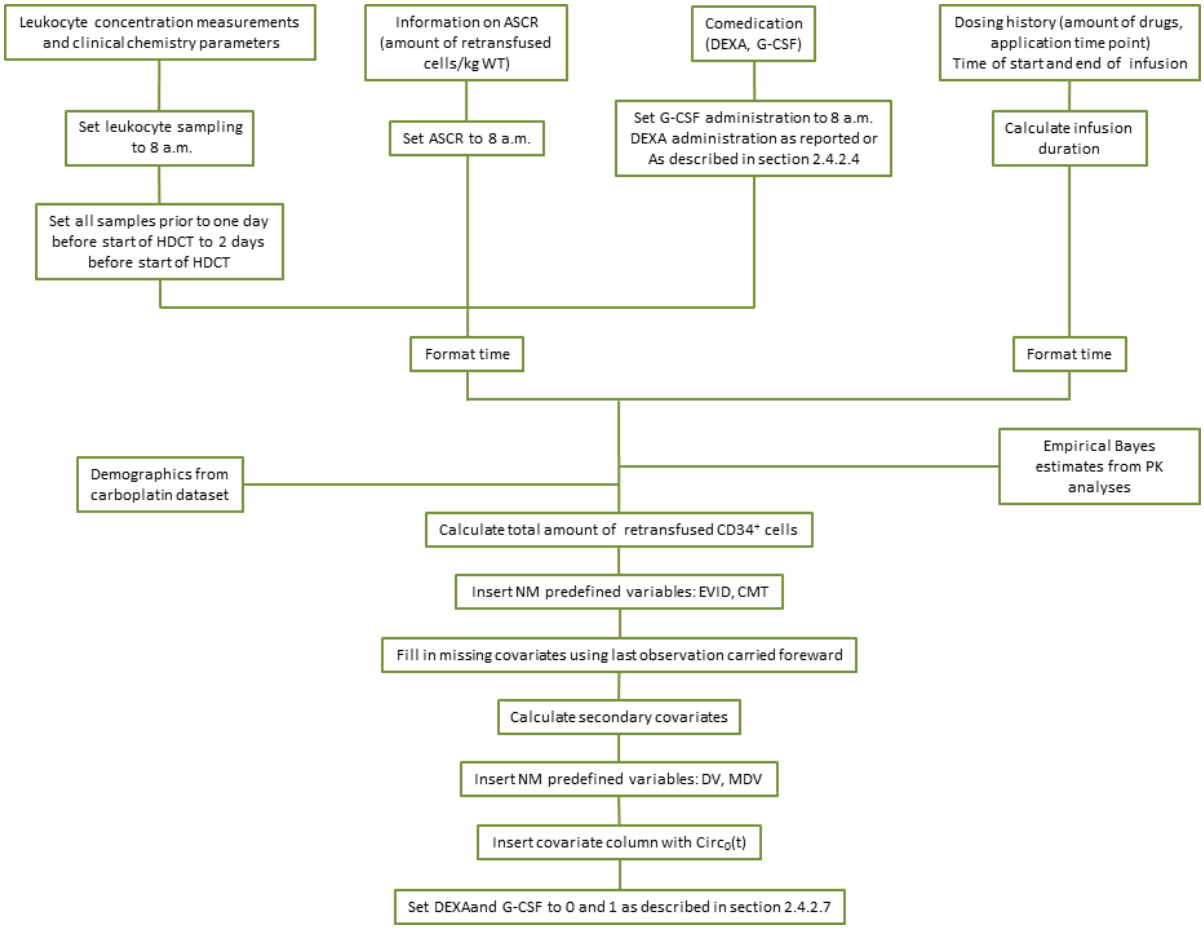

Figure 8.1 Schematic depiction of the dataset building procedure for the dataset for the PK/PD model for leukopoiesis

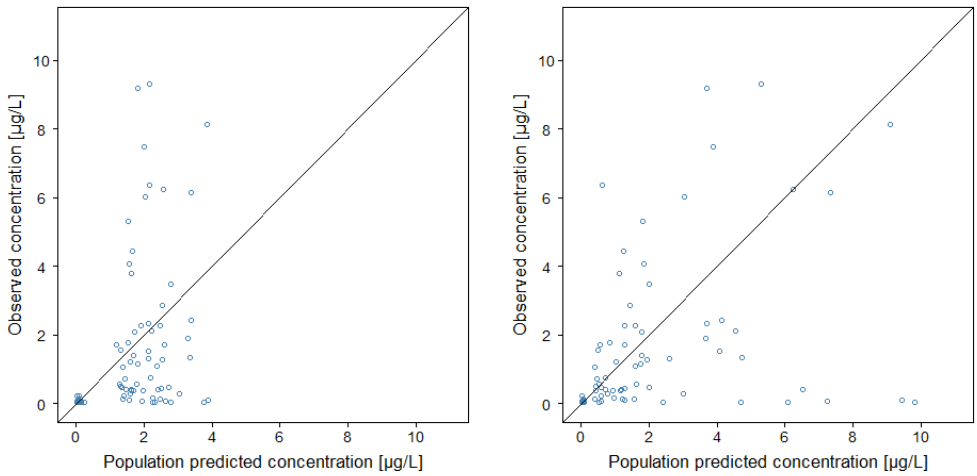

Figure 8.2 Goodness of fit plots for the one (left) and two (right) compartment model for thiotepa concentrations.

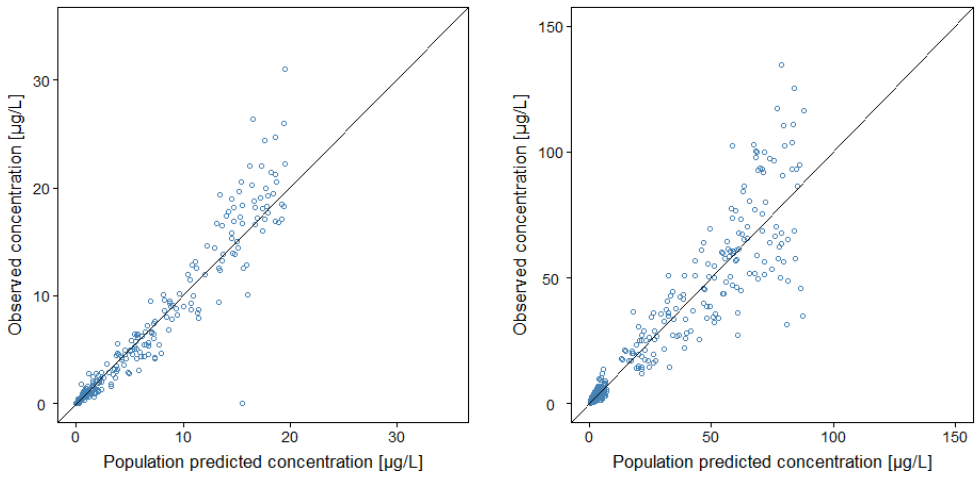

Figure 8.3 Goodness of fit plots for the final model for carboplatin fitted to a dataset comprising the long infusion durations (left).Goodness of fit plots for the final model for etoposide fitted to a dataset comprising the long infusion durations (right).

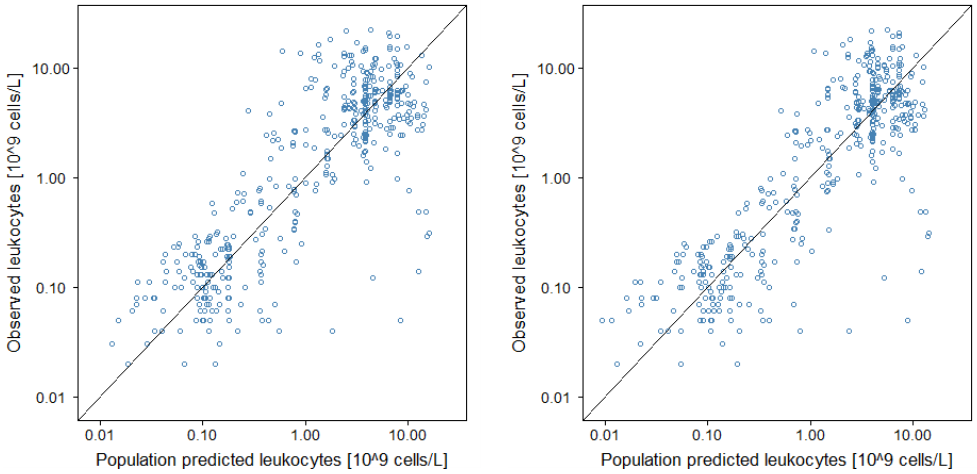

Figure 8.4 Goodness of fit plot for the model for myelosuppression with an E_{max} model (left) and a linear slope model (right) characterising the drug effect of carboplatin.

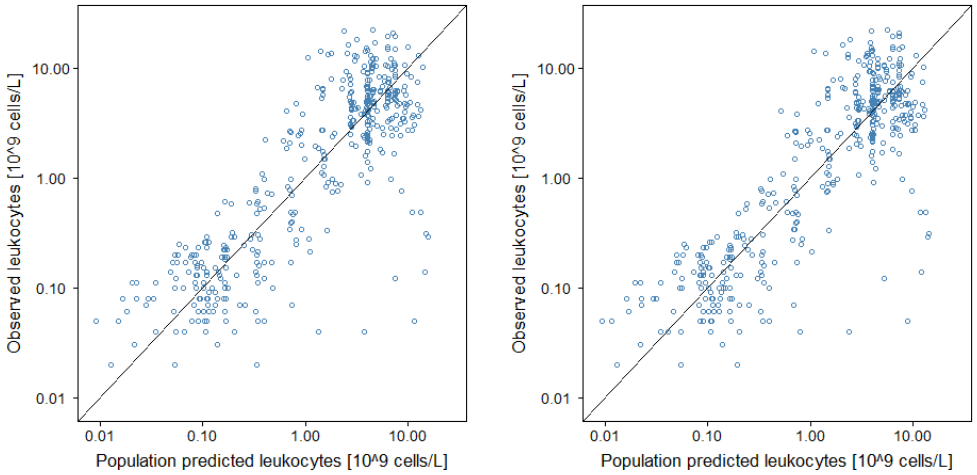

Figure 8.5 Goodness of fit plot for the model for the description of leukopenia including a drug-drug interaction between carboplatin and etoposide (left) and the model with an additive effect for all drugs (right).

8.3 Equations

$$E(t) = \frac{E_{max}}{(1 + ASSY \cdot e^{SLOPE \cdot ln \frac{ED_i}{C(t)}})^{\frac{1}{ASSY}}} \tag{8.1}$$

for ASSY=1

$$E(t) = \frac{E_{max}}{(1 + e^{SLOPE \cdot ln \frac{ED_i}{C(t)}})} \tag{8.2}$$

as $e^{a \cdot b} = e^{b^a}$

$$E(t) = \frac{E_{max}}{(1 + e^{ln \frac{ED_i}{C(t)}^{SLOPE}})} \tag{8.3}$$

$$E(t) = \frac{E_{max}}{1 + \frac{ED_i}{C(t)}^{SLOPE}} \tag{8.4}$$

$$E(t) = \frac{E_{max} \cdot C(t)^{SLOPE}}{C(t)^{SLOPE} + ED_i^{SLOPE}} \tag{8.5}$$

Acknowledgements

The Graduate Research Training Program PharMetrX - Pharmacometrics and computational disease modelling is gratefully acknowledged for the financial support and the unique opportunity to experience the field of pharmacometric modelling and simulation jointly within academia and industry.

I would like to express my sincere gratitude to:

My supervisor Professor Charlotte Kloft for the very interesting and exciting projects, her support and encouragement at any time, her valuable input, thoughts, ideas and comments, the good discussions, her motivation and enthusiasm for all projects and beyond,

Professor Wilhelm Huisinga for opening new perspectives, his curiosity and his interest in my work and the valuable discussions,

The participants of the study and Professor Jörg Beyer for his contribution to the clinical part of the investigation,

Professor Ulrich Jaehde for his interest and comments as well as providing parts of the data,

My Mentor Diether Rüppel for his constant support and ideas, for challenging me and my work, for making my stay at Sanofi possible and providing a very interesting project,

Sanofi Aventis GmbH Deutschland for the opportunity to gain insights into Pharmacometrics in industry and the permission to use the data. Hilde Nimmesgern for organising and Axel Steinsträßer for supporting this internship and thank you to all the colleagues at Sanofi,

Mrs. Thüring and Mr. Proppe for the cluster support at the URZ at the Martin-Luther-Universität in Halle and the Zedat at the Freie Universität Berlin,

Professor Rainer Paschke, Goran Kaluderovic and Valentina Tayurskaya from Biosolutions Halle GmbH for their input and support of the *in vitro* investigations; Petra Schwarz for her guidance and time and Marcus Biertümpel for his interest in the topic and his work on the cytotoxicity assay,

Above all I would like to thank my family, friends and flatmates for their support, patients, phone calls, visits and vacations spent with me, their friendship, lifting my spirits, being there for me and cooking when I needed it most,

Last but not least I would like to thank my colleagues and friends especially in Halle, Berlin and Potsdam but also Bonn, not only for the scientific discussions, problem solving, questioning, challenging and supporting my work, but the coffee breaks, hot chocolates, "Döner-Man" errands, movie nights, cooking, parties, going out for drinks, talking, shopping, relaxing,. . . and overall their friendship - thank you for the past 3.5 years and hopefully more to come!